Sphagnum Desiccation Responses

Willem Q.M. van de Koot

PhD thesis
Aberystwyth University
2022

Mandatory Layout of Declaration/Statements

Word Count of thesis: DECLARATION	49682
This work has not previously been accepted in substance for any degree and is not being concur submitted in candidature for any degree.	
Candidate name	Willem van de Koot
Signature:	
Date	23/09/2022

STATEMENT 1

This thesis is the result of my own investigations, except where otherwise stated. Where ***correction services** have been used, the extent and nature of the correction is clearly marked in a footnote(s).

Other sources are acknowledged by footnotes giving explicit references. A bibliography is appended.

Signature:	
Date	23/09/2022

[*this refers to the extent to which the text has been corrected by others]

STATEMENT 2

I hereby give consent for my thesis, if accepted, to be available for photocopying and for inter-library loan, and for the title and summary to be made available to outside organisations.

Signature:	
Date	23/09/2022

NB: *Candidates on whose behalf a bar on access (hard copy) has been approved by the University should use the following version of Statement 2:*

I hereby give consent for my thesis, if accepted, to be available for photocopying and for inter-library loans after expiry of a bar on access approved by Aberystwyth University.

Signature:	
Date	

Please sign Section A or Section B

Author Name:	Willem van de Koot
Title of work:	*Sphagnum Desiccation Responses*
Supervisor/Department:	John H. Doonan/IBERS
Research Grant if any	Leverhulme Trust
Qualification/Degree obtained	PhD

Section A (for candidates agreeing to open access now or following an embargo period).
Details of the Work

I hereby authorise deposit of the above item in the digital repository maintained by Aberystwyth University, and/or in any other repository authorised for use by Aberystwyth University.

This item is a product of my own research endeavours and is covered by the agreement below in which the item is referred to as "the Work". It is identical in content to that deposited in the Library, subject to point 4 below.

Non-exclusive Rights

Rights granted to the digital repository through this agreement are entirely non-exclusive. I am free to publish the Work in its present version or future versions elsewhere.

I agree that Aberystwyth University may electronically store, copy or translate the Work to any approved medium or format for the purpose of future preservation and accessibility.

Aberystwyth University is not under any obligation to reproduce or display the Work in the same formats or resolutions in which it was originally deposited.

AU Digital Repository

I understand that works deposited in the digital repository will be accessible to a wide variety of people and institutions, including automated agents and search engines via the World Wide Web.

I understand that once the Work is deposited, the item and its metadata may be incorporated into public access catalogues or services, national databases of electronic theses and dissertations such as the British Library's EThOS or any service provided by the National Library of Wales.

I understand that the Work may be made available via the National Library of Wales Online Electronic Theses Service under the declared terms and conditions of use. I agree that as part of this service the National Library of Wales may electronically store, copy or convert the Work to any approved medium or format for the purpose of future preservation and accessibility. The National Library of Wales is not under any obligation to reproduce or display the Work in the same formats or resolutions in which it was originally deposited.

I declare/agree:

1. That I am the author or have the authority of the author/s to make this agreement and do hereby give Aberystwyth University the right to make available the Work in the way described above.

2. That the electronic copy of the Work deposited in the digital repository and covered by this agreement, is identical in content to the paper copy of the Work deposited in the Library of Aberystwyth University and the National Library of Wales, subject to point 4 below.

3. That I have exercised reasonable care to ensure that the Work is original and, to the best of my knowledge, does not breach any laws including those relating to defamation, libel and copyright.

4. That, in instances where the intellectual property of other authors or copyright-holders is included in the work, and as appropriate, I have either:

- gained explicit permission for the inclusion of that material in the electronic form of the Work as accessed through the open access digital repository OR
- limited it to amounts allowed for by current legislation OR
- established that the material is out of copyright OR
- removed that material from the electronic version to be deposited OR
- highlighted that material which needs to be removed from the electronic version and informed Information Services

5. That Aberystwyth University does not hold any obligation to take legal action on behalf of the Depositor, or other rights holders, in the event of a breach of intellectual property rights, or any other right, in the material deposited.

6. That Aberystwyth University reserves the right to impose an indefinite embargo on the thesis should it see fit.

7. That if, as a result of my having knowingly or recklessly given a false statement at points 1, 2, 3 or 4 above, the University or the National Library of Wales suffers loss, I will make good that loss and indemnify Aberystwyth University and the National Library of Wales for all actions, suits, proceedings, claims, demands and costs occasioned in consequence of my false statement.

I agree to my thesis being made available immediately

Signature	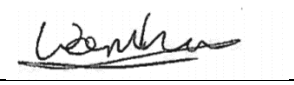	Date	23/09/2022

Section B (for candidates whose thesis cannot be made electronically accessible)
I declare/agree: That I am the author or have the authority of the author/s to make this agreement

That Aberystwyth University may hold an electronic copy of this work and translate it to any approved medium or format for the purpose of future preservation.

That the electronic copy of the Work is identical in content to the paper copy of the Work deposited in the Library of Aberystwyth University

That Aberystwyth University may make the bibliographic data and abstract of this work available in the digital repository maintained by Aberystwyth University, and/or in any other repository authorised for use by Aberystwyth University.

This thesis requires an **indefinite embargo** on full text open access in the digital repository maintained by Aberystwyth University, and/or in any other repository authorised for use by Aberystwyth University due to:

Extensive third party copyright included	☐
Confidentiality	☐
Long term commercial sensitivity	☐
Other [please specify]	☐

Signature		Date	Click here to enter text.

Authorisation of indefinite embargo

An embargo on open access has been agreed for this work **(to be signed by Institute Director or designated nominee)**

Print Name	Click here to enter text.

This summary sheet should be completed after you have read the guidance notes. The completed sheet should be submitted by you to your Department/School/Institute at the time of submission of your work and the supporting documentation.

Candidate's Surname/Family Name:	van de Koot
Candidate's Forenames:	Wilhelmus Quirinus Maria
Candidate for the Degree of (PhD, MPhili, LLM (Res)	PhD
Academic year the work submitted for examination	2022
Full title of thesis:	*Sphagnum Desiccation Responses*

Summary:

Peatmosses (*Sphagnum*) perform important roles in water management in peatlands ensuring that these ecosystems function as carbon sinks rather than carbon sources. By keeping the ecosystem wet, they prevent the breakdown of organic matter into greenhouse gases. Drought and desiccation are becoming increasingly prevalent, and many peatlands have been previously damaged for agriculture or fuel. In this thesis, *Sphagnum* desiccation responses were evaluated on multiple levels, including the molecular and physiological responses of individual plants and colonies. Furthermore, novel image-based quantification techniques were developed using computer vision and deep learning that provide a framework for high throughput field-based measurements. The main findings of this work are that desiccation tolerance pathways are conserved in *Sphagnum* including the role of ABA and ABA-responsive genes., The effect of colony density on water holding capacity showed that a larger stem density resulted in increased gravimetric water content, allowing denser colonies to maintain photosynthetic functioning for longer and mitigating physiological debilitation. In addition, a computer vision pipeline was developed that could rapidly quantify the number of plants in a colony and calculate the stem density. This computer vision pipeline was subsequently used as a base to develop a deep learning model using YOLOv5 architecture, which removed the practical constraints of computer vision while improving performance. Further development of computer vision techniques focussed on the quantifiable colour change *Sphagnum* plants undergo when drying, as they take on a white hue. Combining measurements of capitulum water content with RGB- and multispectral indices, the desiccation status of *Sphagnum* plants can be measured using standard camera images. Ultimately, the research presented in this thesis provides novel insights into the desiccation tolerance mechanisms of *Sphagnum* peatmosses, which are present on the molecular and structural level, whilst also providing new tools for conservationists to monitor plant health *in situ*.

Acknowledgements

I would first like to express my deepest thanks and gratitude to Prof. John Doonan and Dr. Candida Nibau. Their continuous support, endless ideas and sharp, critical view helped shape this thesis into a work that I am genuinely proud of. I'm grateful for having had the opportunity to work and learn with both of them and their trust in my work.

Secondly, I would like to extend my thanks to all the people who I've had pleasure to work with over these last four years. These include, but are not limited to the two most 'enthusiastic-about-moss' undergraduates I have ever met, Dominic Spiliotis and Olga Olver. It's rare to find students with their amount of interest and curiosity for all things *Sphagnum*, and I wish them the best for their futures, academic or otherwise. Further thanks go to the National Plant Phenomics Centre's Jason Brook, Fiona Corke, Karen Askew and Kevin Williams, and the European Plant Phenotyping Network's Henrik Buschmann. Without their efforts to keep everything running, especially on the Gravimetrics platform and the associated imaging equipment, a lot of the work in this thesis would have been impossible. Additional thanks go out to Andrew Lloyd, Alan Gay, Gabi Clifton-Brown and Agnieszka Gladala-Kostarz, whose criticisms, contributions and collegiality have been much appreciated.

Furthermore, I would like to thank all the co-authors of the two published chapters who haven't been mentioned yet, namely Weilun Chen, Larissa van Vliet, Tina Kramaric, Manfred Beckmann, Luis Mur and Yuji Hiwatashi. A special acknowledgment goes out to Jinle Lin for his work on the deep learning algorithm during the Super-Sprint Project, for whom I wish much success with the remainder of his PhD. I would also like to express my gratitude to Justin Lyons, Mariecia Fraser, Hannah Vallin and Ann Mc Cann, for permitting me to conduct research on the Cors Fochno, Pwllpeiran and Sluggan Moss sites respectively.

My sincere thanks go to the main funding body, Leverhulme Trust, for not only funding this project but also providing an additional year's worth of funding in the aftermath of the coronavirus pandemic. Additionally, I would like to thank the Welsh Government for providing funding for the work undertaken in Chapter 6, as part of their Super-Sprint Projects, organised by the Wales Data Nation Accelerator

(WDNA), as well as the Irish Peatland Conservation Council who funded the fieldwork undertaken in Northern Ireland.
A warm thanks goes out to all my friends and family in the Netherlands, especially my parents and brothers (including René Vermond-van der Meij, the unofficial 4th), for their unconditional support and interest in my work. A special thanks goes out to fellow PhD candidates Werner de Gier, for always being up for a chat about all things biology, and Jerry Kamer for his great understanding of physics and formulae. Lastly, I would like to thank the most important person in my life, Larissa van Vliet. Without her love and support I would never have begun in the first place.

Table of Contents

List of Figures

List of Tables

Abbreviations

Abbreviation	Meaning
°C	Degrees Celsius
µ	Micro
µg	Microgram
µL	Microliter
µM	Micromolar
ABA	Abscisic acid
ABI	Abscisic acid Insensitive
AC_{CB}	Anthocyanin content-chroma basic
AC_{CR}	Anthocyanin content-chroma ratio
AIC	Akaike Index Criterion
ARI	Anthocyanin Reflectance Index
BGR	Blue to Green ratio
cDNA	Complementary DNA
CF	Chlorophyll Fluorescence
cm	Centimeter
CO_2	Carbon dioxide
CRI	Carotenoid Reflectance Index
csv	comma separated value
CV	Computer Vision
d	day
Df	Degrees of Freedom
DNA	Deoxyribonucleic acid
DOE-JGI	Department of Energy's Joint Genome Institute
DoG	Difference of Gaussian
DOI	Digital Object Identifier
DPI	Dots Per Inch
DT	Desiccation tolerance
ESA	European Space Agency
ExG	Excessive Green

FI-ESI-M	Flow infusion electro-spray ionisation high resolution mass spectrometry
Fm	Maximum fluorescence
FN	False Negative
Fo	Minimum fluorescence
FOV	Field of View
FP	False Positive
Fv	Variable fluorescence
Fv/Fm	Quantum efficiency of photosystem II
Fw	Forward
g	Gram
GBIF	Global Biodiversity Information Facility
GLI	Green Leaf Index
GUI	Graphical User Interface
h	Hour
H_2O	Water
HPLC-grade	High Performance Liquid Chromatography-grade
HSV	Hue, Saturation, Value
kg	kilogram
LAB	Lightness, Green/Red chromatic axis, Blue/Yellow chromatic axis
LEA	Late Embryogenic Active
LiCl	Lithium Chloride
mAP	mean Average Precision
MeOH	Methanol
mg	Milligram
min	minute
ML	Maximum Likelihood
mm	Millimeter
MSI	Multispectral Index
mSoG	modified Strength of Green
mSoR	modified Strength of Red
n	number
NDVI	Normalised Difference Vegetation Index

ng	nanogram
nm	Nanometer
NPPC	National Plant Phenomics Centre
NPQ	Non Photochemical Quenching
NTC	nourseothricin
OS	Ordnance Survey
PAR	Photosynthetic Active Radiation
PCR	Polymerase Chain Reaction
Pers. Comm.	Personal communication
PP2C	Protein Phosphate 2C
PPFD	Photosynthetic Photon Flux Density
PRI	Photochemical Reflectance Index
PSII	Photosystem II
px	pixel
qPCR	Quantitative polymerase chain reaction
RGB	Red, Green, Blue
RH	Relative Humidity
RNA	Ribonucleic acid
ROI	Region of Interest
RSS	Residual Sum of Squares
Rv	Reverse
RWC	Relative Water Content
s	Second
SD	Standard Deviation
UAV	Unmanned Aerial Vehicle
v/v	Volume concentration of the solute in solution
VIF	Variation Inflation Factor
VMC	Volumetric Moisture Content
WC	Water content
YCrCb	Luma, Chroma blue, Chroma red
YOLO	You Only Look Once

CHAPTER 1 – GENERAL INTRODUCTION

Chapter summary

Peatmosses of the genus *Sphagnum* have an important function in the formation of peatlands and their capacity for carbon storage, water storage and biodiversity. Through special morphological adaptations for the uptake and retention of water, these mosses engineer the ecosystem. Where the rate of vegetational growth exceeds that of decay of dead organic matter, peat forms and accumulates, allowing the peatland to function as a carbon sink. Due to increasing global temperatures and extreme weather events, in combination with anthropogenic alteration of the ecosystem, peatlands are increasingly exposed to oxygen which causes the peat to deteriorate and releases large amounts of greenhouse gases. Understanding the adaptations that *Sphagnum* mosses have for avoiding or coping with desiccation is essential to be able to successfully protect these ecosystems. Historically, *Sphagnum* species have been separated into two main groups based on their ecology, the hollow and hummock groups. Hollow species inhabit wet pools and are regarded as more desiccation tolerant because these habitats are more prone to drying, whilst the hummock group delays drying by forming a tight water holding cushion. Although the relationship between different species and their desiccation tolerance has been previously investigated, several key questions remain unanswered. One such question relates to how plant density affects the rate of water loss and collective desiccation tolerance, despite the observation that density can be a crucial distinction between hummock and hollow. Another question relates to the underlying molecular responses to desiccation that may be homologous to those of higher plants. Finally, the potential of image-based measurement techniques for the quantification of *Sphagnum* water content is considered, and computer vision and deep learning algorithms for high-throughput data analyses have been developed.

The findings presented in this thesis elucidate some of the molecular and physiological responses in *Sphagnum* to drought, using a recurring cast of species to show how responses vary depending on habitat and niche preferences, between and within species, and highlight the role of colony density as a desiccation avoidance mechanism whilst providing new methodologies to measure density and desiccation.

1.1 - Introduction

The ecological importance of peatlands has been widely recognised in recent years and their function as a carbon storage and provision of important ecosystem services for agriculture, flood mitigation and water supply has received increased attention. Historically, peat has been used as a fuel (Figure 1.1) and is to this day a popular horticultural product. Recent estimates suggest that up to 25% of all soil-sequestered carbon globally is stored in peatlands (Loisel et al., 2021; Yu et al., 2010). This would make peatlands the largest terrestrial carbon stores, even larger than the rainforests.

Figure 1.1. Small scale peat harvesting operation in Northern Ireland.
Traditionally, peat has been used as fuel in the northern hemisphere, and extraction continues to this day in some parts of the world including Scotland and Northern Ireland.

Peatlands, more specifically 'raised bogs', store vast amounts of carbon due to their high water tables (Figure 1.2) (Clymo and Hayward, 1982; Page and Baird, 2016; Stivrins et al., 2017). These high water tables, combined with acidification of the water caused by the peatmosses from the genus *Sphagnum* L., create an anaerobic environment in which dead plant matter cannot be broken down faster than new growth is generated by the plants on top of the peat bog, reducing the release of greenhouse gasses associated with decaying organic matter and effectively functioning as a carbon sink (Figure 1.2) (Clymo and Hayward, 1982; Gorham, 1957). This built up dead organic matter has been used by mankind for centuries in medicine (Drobnik and Stebel, 2020), as a fuel source (Figure 1.1) (Hausding, 1921), and also became a popular growing substrate in commercial horticulture during the 20th century (Alexander et al., 2008; Hausding, 1921).

Although anthropogenic activity continues to have a significant impact on peatland health, the main threat to which peatlands are now exposed is desiccation. This can be the result of climate change as exemplified by the exceptionally dry summer of 2018, or the result of artificial lowering of the water table by anthropogenic activity such as peat harvesting or drainage for agriculture. Draining the peat and exposing it to oxygen causes decomposition of the organic matter, which releases large quantities of carbon into the atmosphere, commonly as carbon dioxide (CO_2) from peat exposed to oxygen but also as methane (CH_4), an even more potent greenhouse gas, from dissolved organic carbon seeping into the water table from the still submerged peat and from burned peat (Leifeld and Menichetti, 2018; Wang et al., 2013). Furthermore, the eroded peat soils lose their capacity as water stores, leaving adjacent areas susceptible to flooding in the event of heavy precipitation (Gauthier et al., 2022; Shuttleworth et al., 2019) and, last but not least, an important and unique biodiversity area is lost, as the peatbogs, uplands and hollows are key habitats for many birds, insects and plants (Andrews et al., 2022; Carrell et al., 2019).

Figure 1.2. The raised bog Cors Fochno in Wales (United Kingdom).
This habitat is dominated by *Sphagnum* mosses, ericaceous shrubs and *Molinia* grasses. Below this vegetation layer, peat has accumulated as the decay of dead organic matter is hindered by the anaerobic and acidic environment created by the *Sphagnum* mosses. Photo by Olga Olver.

1.2 - *Sphagnum* and water retention

The high water table in raised bogs can be considered to be “engineered”, or enhanced, due to the presence of *Sphagnum* mosses and their presence can thus establish and maintain a favourable environment for their continued growth, while suppressing the growth of many higher plants. This section introduces some of their features that might contribute to water retention, including plant structure, cellular adaptations and colony morphology.

Sphagnum is a cosmopolitan genus of bryophytes belonging to the *Sphagnopsida*. Mosses belonging to this genus are most common in the temperate areas of the northern hemisphere, where they are often found as a main component in peatbogs, mires, wetlands and other nutrient-poor habitats. The actual groundwater level in the surrounding landscape can be significantly lower than the water table in the raised bog. Most bogs can be referred to as being ‘ombrotrophic’, which means their main or often only source of water is through precipitation. Cellular adaptations of *Sphagnum* (which set it apart from any other moss) allow them to retain much of the precipitation, creating a very wet ecosystem which they will eventually dominate as higher plants lose access to nutrients and their roots get waterlogged.

Compared to most other bryophytes, *Sphagnum* plants have a unique structural morphology (Clymo and Hayward, 1982; Ligrone and Duckett, 1998). The plant consists of a single stem, topped by a head, referred to as the capitulum, which is the main area of growth (Figure 1.3). This capitulum is an arrangement of young branches and leaves, which are ordered into small groups known as fascicles. As the plants grow upwards, the fascicles in the capitulum develop laterally and, within each fascicle, diverge into either spreading or pendent branches. The former spread out laterally, whilst the latter are appressed along the main stem. Within a colony, the plants are arranged with the capitulum upwards, forming dense cushions or mats. As they grow upwards, the lower sections of the plants receive less light and eventually die.

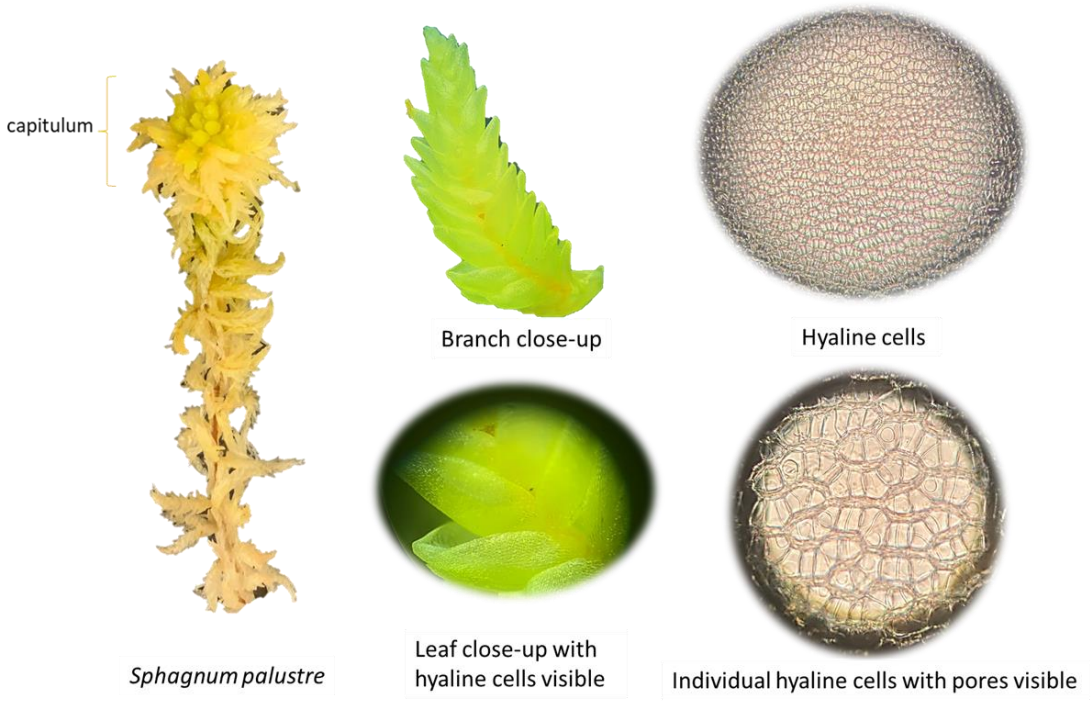

Figure 1.3. Whole plant structure of *Sphagnum palustre*.
The general morphology of *Sphagnum* plants consists of a stem with two types of branches – spreading and pendent – and a capitulum or 'head' at the apex. This capitulum is the main area of growth in the plants. In close up, the branches and leaflets form small capillary spaces which are enhanced by the presence of hyaline cells. These cells are devoid of contents and serve as water storage and retention mechanism.

1.2.1 – Hyaline cell function and formation

The leaves contain specialised cells known as hyaline cells. Although other bryophytes also have hyaline cells, commonly in the form of white hair points protruding from the tips of leaflets, the hyaline cells in *Sphagnum* are structurally unique. Mature hyaline cells. are elongated and hollow (dead) with one or several pores that allow water to enter and exit (Clymo and Hayward, 1982). Hyaline cells identity seems to be defined at an early stage of leaf development where, through a series of unequal divisions, 2 chlorocysts and 1 hyaline cell are formed from a parent cell (Kremer & Drinnan, 2004, Figure 1.4A & B). The hyaline cell then begins to elongate (Figure 1.3C) and the secondary wall structures are formed (Figure 1.4D).

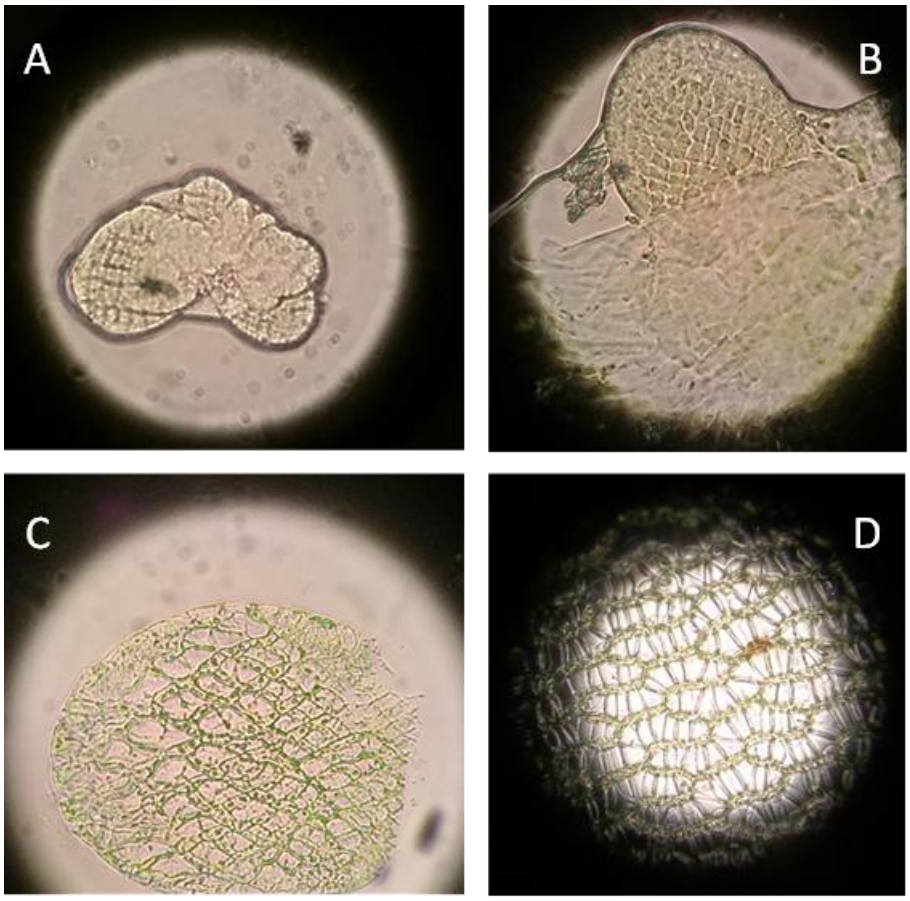

Figure 1.4. The formation of hyaline cells in different stages of leaf development. Unspecialised diamond-shaped cells in developing leaflets (A, B); Initial elongation and specialisation at the distal end of the leaflet (C); Mature hyaline cells and chlorocysts in a *Sphagnum* leaf (D).

Ultimately pores, after their formation on the outer secondary cell wall, are formed by rupturing of the inner cell membrane, after which the cellular contents disappear and the cell dies (Kremer and Drinnan, 2004). The porous, hollow hyaline cells in the leaves are unique to *Sphagnum*, but bear striking similarities to the vessels in the xylem of higher plants in terms both of function and of ontogeny (Iakimova and Woltering, 2017). Particularly the fact that they are dead and hollow makes them very similar in form and function to xylem, but also the way the microtubules behave during the cellular development is also similar (Kremer and Drinnan, 2004; Pesquet et al., 2010; Schnepf, 1973). Other than their proposed function in water retention and transport, hyaline cells host a variety of organisms, ranging from monocellular algae to nematodes and fungi (Kostka et al., 2016; Rimington et al., 2018). Hyaline cells are also found on the stem although, in most species, these are without pores.

1.2.2 – Stem and branch structural adaptions

Another feature that could be related to water conductivity is the presence of two different branch types. Alongside the 'regular' spreading branches are elongated, sometimes whip-like branches, known as the 'pendent' branches, which tend to droop down closely around the main stem (Figure 1.3). These could function as a wick, allowing water to move up towards the capitulum, which contains the main meristem for apical growth as well as being the area where new branches are formed (Clymo and Hayward, 1982; Kremer and Drinnan, 2004; Ligrone and Duckett, 1998).

As all of *Sphagnum*'s water uptake traits, namely the branch structure and hyaline cell positions, are external, this has led to the claim that up to 90% of *Sphagnum* water content may be external (Clymo and Hayward, 1982). Interestingly, this also has some negative impacts on the plants. This external water increases the barriers to gas exchange, consequently reducing *Sphagnum*'s photosynthetic capacities at full saturation. Experiments revealed that the optimum water content for *Sphagnum* gas exchange and photosynthesis was at of 7 g g^{-1} water per dry mass (Williams and Flanagan, 1996). Water content values in *Sphagnum* in many of their preferred habitats regularly exceed that value however, suggesting the plants may prioritise waterlogging over photosynthetic capacity.

Clymo and Hayward (1982) used a chromatography-like experiment to track the movement of water through a plant and found that water was exchanged between plants in a colony, and that the spreading branches in particular facilitate the exchange between plants, whilst pendent branches retain water to the individual plant. This idea of within-colony water movement has implications for the importance of colony density on water retention: a higher stem density could support a higher exchange rate between plants and, perhaps, a lower loss rate (evaporation) to the atmosphere. However, this has not been experimentally tested, and could present important information for conservationists, particularly if there are genetic differences between species.

The adaptations for water retention and upwards movement of water through the wicking pendent branches then raises the water table in the bog as the height increases by the growth of *Sphagnum*. As this process has been going on for several millennia, the height of a raised bog may be upwards of several meters, despite the

slow accumulation rate of the peat itself, which is generally considered to be only a few millimetres a year (Stivrins et al., 2017).

1.2.3 – Colony morphology adaptions

Sphagnum plants rarely grow as individual plants, and typically form complex (and often multi-species) communities. Although the role of the *Sphagnum* colony structure has not been fully investigated, its potential significance has been recognised and mentioned as a contributory factor in discussions (Bengtsson et al., 2020; Elumeeva et al., 2011), and used as a descriptive trait to separate hummock and hollow assemblages (Hájek and Vicherová, 2014; Johnson et al., 2015; Schipperges and Rydin, 1998).

Between different habitats, there can be significant differences between the stem density (herein defined as the number of stems per unit area) of the *Sphagnum* colonies, and environmental variation is suggested to be a more likely factor in determining colony density than species or genetic differences (Piatkowski and Shaw, 2019). Different levels of nutrients can significantly alter the behaviour and growth (including stem density) of axenic culture-grown *Sphagnum* (Anderson et al., 1992; Beike et al., 2015; Boquete et al., 2016; Limpens et al., 2017; Stenøien et al., 1997; Sundberg and Rydin, 2002).

In other bryophytes, colony structure significantly affected desiccation resilience by slowing the drying process (Cruz de Carvalho et al., 2019). A similar advantage was hypothesised for *Sphagnum* (Elumeeva et al., 2011). However, the complexity of this trait was highlighted in a model where increased canopy ‘roughness’, i.e. less homogeneous structure, reduced evaporation due to emergent plants shielding the rest of the colony despite desiccating themselves (Elumeeva et al., 2011).

Colony density is often mentioned as a variable in *Sphagnum* literature, and often in its most crude distinction, namely the hummock/hollow distinction with hummocks growing dense above the water table and hollows having plants loosely growing in niches closer to the water table. Despite this, little data exist on the evolutionary advantages of colony structures and why density variation between environments and species. It is likely that the lack of data regarding colony density is

caused by the labour-intensive nature of counting *Sphagnum* plants, as an area of 100 cm^2 may contain as many as 200 plants.

Colony structure and particularly stem density may provide novel insights for *Sphagnum* conservation programmes, especially recolonisation projects where plants are transplanted onto previously damaged peatlands. Increased colony density in *Sphagnum* plugs could theoretically significantly increase the desiccation resilience of the newly planted material, boosting conservation efforts.

1.3 - Desiccation tolerance of *Sphagnum*

Sphagnum is considered to be intolerant of desiccation (Abel, 1956) as might be expected from its ecological preferences. Desiccation tolerance, in this case, refers to being able to completely resurrect after prolonged periods of low water content with minimal cellular or physiological damage. Highly desiccation tolerant mosses such as *Tortula* Hedw. live on exposed substrates, such as rock, with very limited or intermittent water availability and have evolved specific mechanisms to deal with these environments (Melvin J Oliver et al., 2000; Oliver et al., 2009).

On the contrary, *Sphagnum* has been described as 'desiccation avoidant' (Hájek and Vicherová, 2014), preferring perpetually wet environments such as bogs and high humidity woodlands where desiccation can be avoided for the majority of the year. When used in restoration projects however, *Sphagnum* plants may be transferred to ecosystems where a solely desiccation avoidance strategy is less successful due to the damaged nature of the habitat, such as previously drained wetlands. Furthermore, as global climate warming affects precipitation patterns, even previously functioning peatlands may become more susceptible to prolonged periods of drought. In this context, understanding the desiccation tolerance of *Sphagnum* and how to promote its desiccation avoidance strategies is critical.

The effects of desiccation on *Sphagnum* have been previously investigated. Historically these studies tended to focus on one or several species from two somewhat artificial groupings: the hummock group and the hollow group (Figure 1.5) (Clymo, 1973). The ecology of hummock species involves forming thick cushions above the water table, whilst habit of the hollow species is living submerged in pools or close to water in a very wet environment.

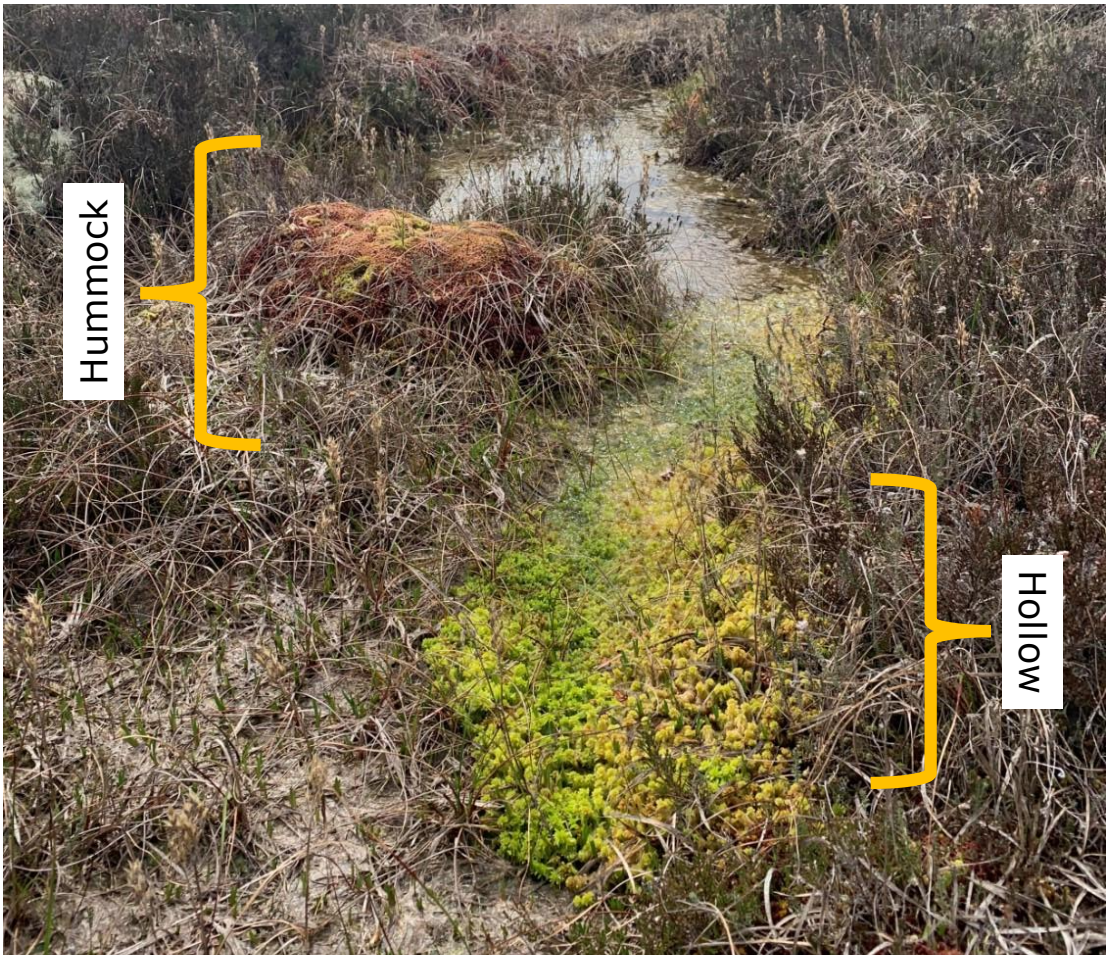

Figure 1.5. Contrasting microhabitats within a bog in Northern Ireland.
The hollow habitat, in this figure inhabited by *S. cuspidatum*, is more prone to drying out than the hummock habitat, in which the *S. capillifolium* mosses prevent the evaporation of water by forming dense cushions.

The general consensus has been that the hollow inhabiting species tend to have a higher desiccation tolerance than their hummock inhabiting relatives. Although this may seem paradoxical, as hollow inhabiting species tend to be either submerged or very wet most of the time, it is actually quite logical as these habitats are also prone to intermittent drying out, sometimes completely several times annually. The hummock species, on the other hand, tend to avoid total desiccation by associating closely together, which minimises the surface of each individual stem exposed to the flow of air on their capitulum to reduce evaporation, and therefore do not normally need to be so tolerant of desiccation as it is a relatively less common condition for them.

1.3.1 – Photo-physiological measurements of *Sphagnum* drought stress

The effect of desiccation is typically be quantified by the photosynthetic performance (Bengtsson et al., 2016; Korrensalo et al., 2016; Schipperges and Rydin, 1998; Williams and Flanagan, 1996). As water is essential for photosynthesis, desiccation directly affects physiology. More recently, the molecular mechanisms drought responses have also become a research focus (Winnicka and Melosik, 2019). Typical parameters measured included photosynthetic capacity through the measurement of CO_2 concentrations, water content and survival (Bengtsson et al., 2016; Hájek and Vicherová, 2014; Kangas et al., 2014; Van Gaalen et al., 2007; Wagner and Titus, 1984; Wang and Bader, 2018). However, with respect to the recovery of photosynthetic ability after desiccation, there was no relationship to the wetness of the habitat of the respective species (Hájek and Vicherová, 2014).

Although several studies have looked at desiccation tolerance in *Sphagnum*, some questions remain. Firstly, there is a large amount of variation in responses to treatments in wild collected material. This may be induced by seasonal events that happened before the collection of the samples (Gaberščik and Martinčič, 1987). A study on several *Sphagnum* species showed significant differences between two years within the same species, most likely due to weather conditions that induced an increase or decrease in desiccation tolerance.

Furthermore, studies using only the CO_2 gas exchange as a proxy for photosynthetic activity do not take into account the amount of gas exchange that might be the result of microorganisms living on the *Sphagnum* itself (Schipperges and Rydin, 1998). In a large-scale experimental study, the complex nature of the inducible desiccation tolerance was untangled (Hájek and Vicherová, 2014). This study suggested that desiccation tolerance is induced several times annually depending on the seasons, but is more pronounced in hollow species than in hummock species. Furthermore, desiccation tolerance could also be induced in the lab by slow drying and through application of Abscisic Acid (ABA). This ABA-induced desiccation tolerance has also been found in a different bryophyte model organism, *Physcomitrium patens* (Hedw.) Mitt. (Rathnayake et al., 2018; Stevenson et al., 2016), where there is now a molecular model.

1.3.2 – Molecular responses to desiccation

Acquisition of desiccation tolerance has been one of the most significant developments in plant evolution, as it enabled plants to grow on land (Melvin J. Oliver et al., 2000). While structural traits such as roots, cuticles and vascular systems have been essential for the transition to land in plants, *Sphagnum* lacks these characteristics (Figure 1.6). Although *Sphagnum*'s hyaline cells fulfil a water uptake and retention function, they are far more susceptible to desiccation due to their external position on the plant, leaving them exposed to evaporation. To make up for their lack of structural traits, bryophytes have developed complex molecular pathways to overcome desiccation (Charron and Quatrano, 2009; Proctor et al., 2007).

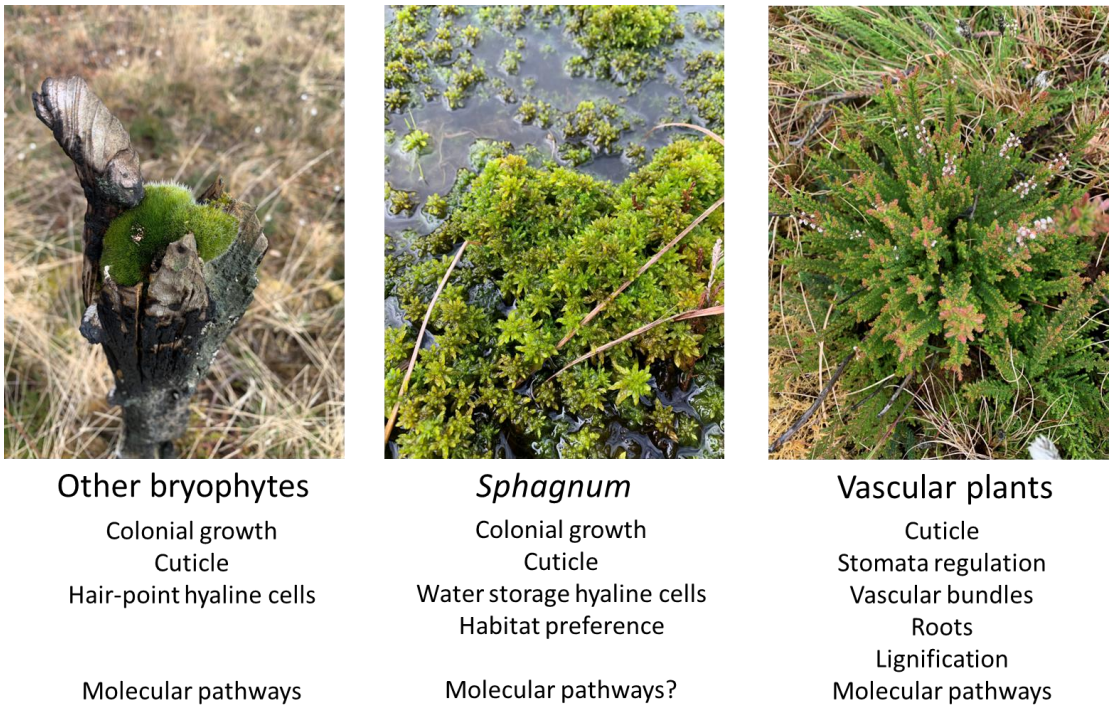

Figure 1.6. Desiccation tolerance innovations between other bryophytes, *Sphagnum* and vascular plants.
While vascular plants have developed a large number of desiccation tolerance mechanisms involving plant structure, such as vascular bundles, rots and lignification, bryophytes rely on colony structure for water retention. Hyaline cells are present in different genera with different functions, but in other bryophytes are usually white hair points extruding from the leaves, which increase the boundary layer as desiccation tolerance mechanisms. *Sphagnum* hyaline cells however are unique in structure. While some molecular pathways are known to be conserved in land plants, their full extent and diversity in bryophytes is not fully understood and has only recently been investigated in *Sphagnum*. Figure adapted from (Glime, 2017).

These molecular mechanisms can be traced back to primitive plants, which lacked the previously mentioned structural characteristics and developed these molecular mechanisms for desiccation tolerance in the transition to land (Cuming, 2019). Although the evolutionary relationship of molecular pathways between higher plants and basal land plant groups, such as bryophytes, is poorly understood, it is assumed that the base genes for these functions are highly conserved (Vanburen et al., 2018), and a recent investigation on *P. patens* suggested that NAC (No apical meristem (NAM), Arabidopsis transcription activation factor (ATAF1/2), Cup-shaped cotyledon (CUC)) domain transcription factors, which are essential in the formation of water conducting structures in higher plants (Fukuda, 2016; Heo et al., 2017), also contributed to the formation of water conducting tissues in *P. patens* (Xu et al., 2014).

In the same publication, *Selaginella moellendorffii* Hieron. is also reported as having many genes related to the NAC domain. *S. moellendorffii* is a highly desiccation tolerant clubmoss, and also known as a resurrection plant. *Sphagnum*, however, is not a desiccation tolerant plant, as it experiences some degree of damage when subjected to desiccation. Nevertheless, as these NAC domain transcription factors are highly conserved, they were also found also be present in *Sphagnum* and their function was maintained (Terada et al., 2021).

Vanburen *et al.* (2018) did extensive molecular research on *Selaginella lepidophylla*, and found that the changes in gene expression of this plant under drought stress follows a similar pattern to that of higher plants, such as *Boea* Comm. Ex. Lamm. (Wang et al., 2017; Xiao et al., 2015). The investigations into the molecular basis of the mechanisms that provide plants with desiccation tolerance have important economic potential, such as the application of desiccation tolerance in crop breeding.

Another plant hormone involved in the regulation of desiccation tolerance molecular responses is ABA (Ali et al., 2020; Chaves et al., 2003). ABA is a carotenoid synthesised in the plastids and essential for the activation of several physiological processes in higher plants, including seed germination and stomata closure, but also regulates molecular responses to drought stress (Song et al., 2016). In non-vascular plants, such as the bryophyte *Physcomitrium patens*, ABA was found to have a similar function (Johri, 2008). Deletion of ABA-related genes such as

ABSICISIC ACID INSENSITVE 3 (ABI3) from *P. patens* significantly reduced the plants' desiccation tolerance (Khandelwal et al., 2010).

In *Sphagnum*, pre-treatment with ABA has been shown to increase desiccation tolerance (Hájek and Vicherová, 2014; Marschall and Borbély, 2011). It would be interesting to see if these molecular responses are also present in *Sphagnum* or whether they have been lost in or differently regulated in the desiccation avoidant hummock species. *Sphagnum* may have developed a unique strategy to cope with desiccation, particularly the species in habitats that are regularly exposed to desiccation, and understanding this could help in the protection of peatland ecosystems.

1.4 – Peatland measurements and remote sensing approaches

Although *in vitro* or controlled environment research provides a foundation for our understanding of physiological and molecular responses to desiccation, there is a strong case for translating any findings to the field. As *Sphagnum* is a cornerstone species of many peatland ecosystems, the development of methods that translate laboratory-based concepts to natural habitats is essential and could provide significant tools and/or information for conservationists.

While many research sites on peatlands have dedicated water table monitoring systems such as dip wells, and keep *Sphagnum* cover and diversity records, the use of *Sphagnum* itself as a reporter of its environment within peatlands is a relatively novel concept. Biomonitoring, the use of biota for the measurement of environmental variables, has seen use of *Sphagnum* previously in air pollution monitoring, but not directly related to peatland ecosystems.

1.4.1 – Traditional biomonitoring

Historically, bryophytes have been widely used to make inferences about their natural environment. Especially since the increased awareness of environmental pollution in the early 70's the monitoring of lichens and bryophytes saw an increase in popularity (Burton and Peterson, 1979; Goodman and Roberts, 1971; Say et al., 1981). One of the advantages of the use of biota for this 'biomonitoring', where organisms are used for the quantification of environmental variables, is the cost-efficiency and its potential for longer-term monitoring, making biomonitoring approaches less susceptible to transient effects compared to single timepoint measurements (Goodman and Roberts, 1971).

Bryophytes fulfil many of the desirable traits for biomonitoring (Ares et al., 2012). They are abundant, reproduce in high quantities both sexually and asexually, have high element uptake capacity (Carter and Porter, 1997; Wehr et al., 1983) and, most importantly, are very sensitive to changes in the environment. This is, in part, because bryophytes lack roots, meaning they are nearly entirely dependent on precipitation for water and nutrients. Changes in air and water quality therefore directly impact bryophytes.

Typically, two types of biomonitoring are recognised, namely passive and active biomonitoring. The distinction between the two is the use of transplanted

bryophytes (which may be obtained from sterile culture or a different environment) or the use of locally occurring bryophytes. While active biomonitoring, which uses transplanted bryophytes, has been perceived as a powerful method due to its known exposure times, passive biomonitoring using the species already present in the environment can be used to set up a network of sampling points that can be measured over longer periods of time. This section outlines the potential of *Sphagnum* for passive biomonitoring of peatland ecosystem health.

1.4.2 – The potential of *Sphagnum* in peatland biomonitoring

Within peatlands, *Sphagnum* peatmosses fulfil several of the desired traits for biomonitoring. As a cornerstone species of many peatlands, they are abundant. Their sporophytes are known to carry several thousands of potential progeny and they can also regenerate vegetatively from fragments. And, most importantly, they rely on surface water and precipitation for water access, making them very sensitive to changes in the local water regime.

Usually, the water table in peatlands is measured with dip wells, which consist of porous tubes driven down into the peat. Measuring sticks or other height measurement tools can then be lowered into the tube to measure the height of the water table. These measurements are intensive, requiring specialists with appropriate equipment to record the height of the water table. Furthermore, they are not directly informative of the health of the vegetation on the peatland. Measurements based on *Sphagnum* water content could potentially provide an alternative solution to these measurements, as *Sphagnum* directly reflects the peatland near surface hydrology. *Sphagnum* plants exhibit signs of desiccation long before associated peatland vegetation (such as ericaceous shrubs or *Molinia* grasses) do. Their abundance on the peatlands and independence of dip well equipment also increases the potential area available for measurement.

When *Sphagnum* dries out, it undergoes a remarkable visual change. The hyaline cells, which normally are filled with water, when empty, give the plant a whitish hue (Figure 1.7). Other bryophytes that have different types of hyaline cells, such as the hair points extruding from the leaves of *Grimmia* and *Syntrichia* species, exhibit a similar change in colour (Glime, 2017). This effect has been hypothesised to increase the reflectance or ‘albedo’ of the moss, potentially reducing photodamage

when drying (Bowker et al., 2010; Giordano et al., 2009; Hanson and Rice, 2014), whilst it has also been shown to increase the boundary layer, which may affect drying and rewetting dynamics (Proctor, 1982).

While this reduction in photodamage may be present to an extent in *Sphagnum*, the other two mentioned bryophyte genera include true desiccation tolerant mosses, able to survive and fully resurrect after extensive desiccation while *Sphagnum* is known to sustain cellular damage after a long drought period (Gerdol et al., 1996; Schipperges and Rydin, 1998). *Sphagnum'*s dependence on the water table makes it a direct and dynamic reporter of the hydrology and, by quantifying the colour change through image based biomonitoring it should be possible to monitor the extent of peatland hydration.

Figure 1.7. The contrast between wet and dry *Sphagnum fallax* plants.
As the plants dry out, the hyaline cells give *S. fallax* a white appearance. The plants on the right are dry, whilst the plants on the left are saturated and healthy.

1.4.3 – Remote sensing methodologies

Image based quantification techniques have long been used in agronomy and ecosystem monitoring, where they are commonly referred to as 'remote sensing'. The advantage of these techniques is that, when fully calibrated with traditional field data, the need for destructive or manual sampling is much reduced. Instead, these techniques can be scaled to provide high-throughput, non-invasive measurements

(del Valle et al., 2018). Typically, spectral waveband images are used that are collected by satellite or drone cameras (Xue and Su, 2017).
Calculations combining data collected at various wavebands has resulted in the development of so-called (multispectral) vegetational indices (Rahimzadeh-Bajgiran et al., 2012), which can be used to estimate a number of biological variables usually related to plant health from image data (Gitelson & Merzlyak, 1997; Anatoly A. Gitelson, Keydan, & Merzlyak, 2006; Sims & Gamon, 2002). Common indices include Normalised Difference Vegetation Index (NDVI), which is used to quantify chlorophyll content, Carotenoid Reflectance Index (CRI) and Anthocyanin Reflectance Index (ARI) (Rahimzadeh-Bajgiran et al., 2012), which are used to quantify carotenoids and anthocyanins respectively, and Photochemical Reflectance Index (PRI) which estimates the performance of photosynthesis (Gamon et al., 1992). The disadvantage of these techniques is their requirement for expensive imaging equipment capable of restricting the wavelengths measured.

With the increasing ubiquity of regular high-resolution cameras, normal colour photography or 'RGB-based' imaging techniques (after the three colour channels used to generate an image, namely Red, Green and Blue) has become increasingly of interest. RGB-based vegetational indices have been developed, which aim to quantify similar variables as their multispectral counterparts. As such, there are for example RGB-based indices to estimate chlorophyll and anthocyanin content (del Valle et al., 2018; Kawashima and Nakatani, 1998; Sánchez-Sastre et al., 2020), but also moisture content (Elshikha et al., 2016) and plant cover (Louhaichi et al., 2001; Sánchez-Sastre et al., 2020). There exists potential for such RGB-based indices to increase the quantity of data acquired due to their relative low cost and accessibility, especially when citizen science programmes take advantage of the ubiquity of smartphone imaging.

Another use of RGB-based indices has been their applicability in computer vision and deep learning methods. As these indices may highlight or reduce certain aspects of an image, they can potentially be used for automated detection algorithms. For example, the index Excessive Green, which increases the contrast between green plants and the background (typically soil), and was used for the detection of weeds (Wenhua Mao et al., 2013; Woebbecke et al., 1995). Object detection, such as the detection of fruits or weeds, is becoming more important and commonplace in agriculture (Robb et al., 2020), and traditional computer vision techniques are

increasingly replaced by more accurate deep learning and machine learning driven algorithms (Chowdhury et al., 2022; Feng et al., 2019; Hüther et al., 2020; Lyu et al., 2022).

Bryophytes are generally much smaller than most plants that are imaged by drones or satellites, and the resolution provided by these may be inadequate for plant or even colony-level assessment of moss plant traits. The European Space Agency (ESA) tested a system through which remote sensing was applied to measure the Moisture Stress Index (MSI) of a raised bog near Borth in Wales (Harris et al., 2006). They took patches of two *Sphagnum* species (*S. magellanicum* Bridel and *S. pulchrum* Warnstorf) with approximately 10 cm of underlying litter and conducted drying and rewetting experiments, measuring the Volumetric Moisture Content (VMC) and spectral response. Using these data in a model and then taking measurements by drone allowed them to assess near-surface hydrological conditions. However, their results were mixed and potentially not applicable to drier conditions, as the method preferentially detected wetter areas. Unfortunately, there have been no further developments of their methodology since.

Other image-based approaches to bryophyte health typically used regular consumer-grade cameras from close range (between 1 and several meters), and measured a range of variables including photosynthesis and general plant health, but have also been used to estimate vegetation change over time (Benavides and Jesús, 2009; Robinson et al., 2018). The potential to use integrated computer vision methods to produce a system for high-throughput water content quantification in *Sphagnum* by measuring the colour change as the plants whiten from desiccation could provide a significant source of data. Taking advantage of the ubiquity of smartphone cameras and online repositories such as iNaturalist (https://www.inaturalist.org) and GBIF (GBIF, n.d.) there is the potential to increase the monitoring capacity of conservationists and associated agencies significantly.

1.5 - Restoration projects and rewetting of peatlands

Although there is an increased demand for peat in the horticultural market, industrial scale peat extraction as a fossil fuel is coming to an end in many countries, as more energy efficient fuel sources are coming into use. However, centuries of peat harvesting have taken a toll on peatlands and bare, exposed peat is found in many old harvesting claims.

In Ireland, large horticultural peat mining companies such as Bullrush already employ the tactic of sculpting previously harvested peatland to promote flooding followed by spreading wild-collected *Sphagnum* species. The results resemble a functional hollow type ecosystem. Although the rewetting and revegetation of *Sphagnum* most likely prevents the bare peat soil from eroding and emitting large quantities of greenhouse gases, the ecosystem that is restored is not the same as that from which the peat was harvested. This would have been a raised bog occupied by hummock forming *Sphagnum* species, which is an ecosystem that was formed after the last ice age over the course of several thousands of years. As peat accumulation is estimated to be only 1 mm annually, each 1 meter deep section of peat can be assumed to be around 1000 years old. Cors Fochno, a near intact raised bog in West Wales, was measured to be around 7 meters deep in some areas, representing an ecosystem of potentially well over 7000 years in age (M. Bailey, 2019 pers. comm.).

There have been several investigations into the rewetting of peatlands and to what extent diversity and ecosystem functions are restored (Gaudig et al., 2013; González et al., 2014; Schröder et al., 2015). After the *Sphagnum* had established properly, the conservation value in terms of, for example biodiversity and resilience, was similar to that of an undisturbed reference site (Muster et al., 2015). The initial recovery of *Sphagnum* can be hindered by the growth of woody plants for which the acidic nutrient poor soil is ideal, although they are overcome eventually (González et al., 2014; Potvin et al., 2014), and flooding of peatlands as a restoration method can also negatively impact *Sphagnum*. While some species such as *S. cuspidatum* and *S. inundatum* tolerate prolonged periods of submergence, species that occupy niches above the water table are not tolerant of flooding (Borkenhagen and Cooper, 2018). Despite this, restored peatlands may eventually become carbon sinks again (Brown et al., 2017), and even become a *Sphagnum* farming resource (Gaudig et al., 2013; Muster et al., 2015; Temmink et al., 2017).

1.6 - Aims

The main aim of this thesis is to expand the current knowledge on *Sphagnum* desiccation responses, ultimately for the benefit of ecosystem restoration programmes.

The research objectives were:

- To elucidate the molecular response of *Sphagnum* to desiccation events.
- To understand how colony density affects water content dynamics.
- To assess how the relative humidity-induced desiccation affects individual plants.
- To develop image-based tools for the measurement of *Sphagnum* colony variables in the field.
- To establish the relationship between image-based measurement techniques and measured plant traits.

Desiccation responses were investigated on multiple levels: the environmental level, the colony level, the individual plant level and the molecular level. A recurring cast of species was used for these experiments, covering a wide range of niches, colours and shapes found in the genus *Sphagnum*. Computer-based imaging pipelines were developed that can quantify Sphagnum densities in the field and extract water content data from simple RGB images. Ultimately, taken together, the data generated in this thesis will provide conservationists and peatland researchers with tools to aid the quantification of colony density and *Sphagnum* water content and, ultimately, better understand the role of colony density in the desiccation responses of *Sphagnum*.

1.7 - References

Abel, W.O., 1956. Die Austrocknungsresistenz der Laubmoose. Österreichische Akad. der Wissens- chaften, Math. Klasse, Sitzungsberichte, Abteilung I 165, 619–707.

Alexander, P.D., Bragg, N.C., Meade, R., Padelopoulos, G., Watts, O., 2008. Peat in Horticulture and Conservation: the UK Response to a Changing World. Mires Peat 3, 1–10.

Ali, S., Hayat, K., Iqbal, A., Xie, L., 2020. Implications of abscisic acid in the drought stress tolerance of plants. Agronomy 10, 1–28. https://doi.org/10.3390/agronomy10091323

Anderson, L.E., Basile, M.R., Basile, D. V, 1992. Common garden experiments with Sphagnum in axenic culture. J. Bryol. 17, 15–25. https://doi.org/none

Andrews, L.O., Rowson, J.G., Caporn, S.J.M., Dise, N.B., Barton, E., Garrett, E., Gehrels, W.R., Gehrels, M., Kay, M., Payne, R.J., 2022. Plant community responses to experimental climate manipulation in a Welsh ombrotrophic peatland and their palaeoenvironmental context. Glob. Chang. Biol. 28, 1596–1617. https://doi.org/10.1111/gcb.16003

Ares, A., Aboal, J.R., Carballeira, A., Giordano, S., Adamo, P., Fernández, J.A., 2012. Moss bag biomonitoring: A methodological review. Sci. Total Environ. 432, 143–158. https://doi.org/10.1016/j.scitotenv.2012.05.087

Beike, A.K., Spagnuolo, V., Lüth, V., Steinhart, F., Ramos-Gómez, J., Krebs, M., Adamo, P., Rey-Asensio, A.I., Fernández, J.A., Giordano, S., Decker, E.L., Reski, R., 2015. Clonal in vitro propagation of peat mosses (Sphagnum L.) as novel green resources for basic and applied research. Plant Cell. Tissue Organ Cult. 120, 1037–1049. https://doi.org/10.1007/s11240-014-0658-2

Benavides, J.C., Jesús, I.S., 2009. Digitized Images Provide More Accuracy and Efficiency to Estimate Bryophyte Cover. Bryologist 112, 12–18.

Bengtsson, F., Granath, G., Cronberg, N., Rydin, H., 2020. Mechanisms behind species-specific water economy responses to water level drawdown in peat mosses. Ann. Bot. 126, 219–230. https://doi.org/10.1093/aob/mcaa033

Bengtsson, F., Granath, G., Rydin, H., 2016. Photosynthesis, growth, and decay traits in Sphagnum - a multispecies comparison. Ecol. Evol. 6, 3325–3341. https://doi.org/10.1002/ece3.2119

Boquete, M.T., Fernández, J.A., Aboal, J.R., Shaw, A.J., 2016. Significance of the intraspecific morphological variability in biomonitoring studies with mosses: Among-populations and between-sexes approach. Environ. Exp. Bot. 130, 106–112. https://doi.org/10.1016/j.envexpbot.2016.05.013

Borkenhagen, A., Cooper, D.J., 2018. Tolerance of fen mosses to submergence, and the influence on moss community composition and ecosystem resilience. J. Veg. Sci. 29, 127–135. https://doi.org/10.1111/jvs.12610

Bowker, M.A., Maestre, F.T., Escolar, C., 2010. Biological crusts as a model system for examining the biodiversity-ecosystem function relationship in soils. Soil Biol. Biochem. 42, 405–417. https://doi.org/10.1016/j.soilbio.2009.10.025

Brown, C.M., Strack, M., Price, J.S., 2017. The effects of water management on the CO2 uptake of Sphagnum moss in a reclaimed peatland. Mires Peat 20, 1–15. https://doi.org/10.19189/MaP.2016.OMB.258

Burton, M.A.S., Peterson, P.J., 1979. Metal accumulation by aquatic bryophytes from polluted mine streams. Environ. Pollut. 19, 39–46. https://doi.org/10.1016/0013-9327(79)90111-3

Carrell, A.A., Kolton, M., Glass, J.B., Pelletier, D.A., Warren, M.J., Kostka, J.E., Iversen, C.M., Hanson, P.J., Weston, D.J., 2019. Experimental warming alters the community composition, diversity, and N2 fixation activity of peat moss (Sphagnum fallax) microbiomes. Glob. Chang. Biol. 2993–3004. https://doi.org/10.1111/gcb.14715

Carter, L.F., Porter, S.D., 1997. Trace-element accumulation by Hygrohypnum ochraceum in the upper Rio Grande basin, Colorado and New Mexico, USA. Environ. Toxicol. Chem. 16, 2521–2528. https://doi.org/10.1002/etc.5620161213

Charron, A.J., Quatrano, R.S., 2009. Between a rock and a dry place: The water-stressed moss. Mol. Plant 2, 478–486. https://doi.org/10.1093/mp/ssp018

Chaves, M.M., Maroco, J.P., Pereira, J.S., 2003. Understanding plant responses to drought - From genes to the whole plant. Funct. Plant Biol. 30, 239–264. https://doi.org/10.1071/FP02076

Chowdhury, P.N., Shivakumara, P., Nandanwar, L., Samiron, F., Pal, U., Lu, T., 2022. Oil palm tree counting in drone images. Pattern Recognit. Lett. 153, 1–9. https://doi.org/10.1016/j.patrec.2021.11.016

Clymo, R.S., 1973. The Growth of Sphagnum: Some Effects of Environment. J. Ecol. 61, 849. https://doi.org/10.2307/2258654

Clymo, R.S., Hayward, P.M., 1982. The Ecology of Sphagnum, in: Bryophyte Ecology. Springer Netherlands, Dordrecht, pp. 229–289. https://doi.org/10.1007/978-94-009-5891-3_8

Cruz de Carvalho, R., Maurício, A., Pereira, M.F., Marques da Silva, J., Branquinho, C., 2019. All for One: The Role of Colony Morphology in Bryophyte Desiccation Tolerance. Front. Plant Sci. 10, 1–12. https://doi.org/10.3389/fpls.2019.01360

Cuming, A.C., 2019. Evolution of ABA signaling pathways, Advances in Botanical Research. Elsevier Ltd. https://doi.org/10.1016/bs.abr.2019.06.003

del Valle, J.C., Gallardo-López, A., Buide, M.L., Whittall, J.B., Narbona, E., 2018. Digital photography provides a fast, reliable, and noninvasive method to estimate anthocyanin pigment concentration in reproductive and vegetative plant tissues. Ecol. Evol. 8, 3064–3076. https://doi.org/10.1002/ece3.3804

Drobnik, J., Stebel, A., 2020. Central European ethnomedical and officinal uses of peat, with special emphasis on the Tołpa peat preparation (TPP): An historical review. J. Ethnopharmacol. 246, 112248. https://doi.org/10.1016/j.jep.2019.112248

Elshikha, D.M., Hunsaker, D.J., Bronson, K.F., Sanchez, P.L., 2016. Using RGB-based vegetation indices for monitoring guayule biomass, moisture content and rubber. 2016 Am. Soc. Agric. Biol. Eng. Annu. Int. Meet. ASABE 2016. https://doi.org/10.13031/aim.20162380922

Elumeeva, T.G., Soudzilovskaia, N.A., During, H.J., Cornelissen, J.H.C., 2011. The importance of colony structure versus shoot morphology for the water balance of 22 subarctic bryophyte species. J. Veg. Sci. 22, 152–164. https://doi.org/10.1111/j.1654-1103.2010.01237.x

Feng, X., Zhan, Y., Wang, Q., Yang, X., Yu, C., Wang, H., Tang, Z.Y., Jiang, D., Peng, C., He, Y., 2019. Hyperspectral imaging combined with machine learning as a tool to obtain high-throughput plant salt-stress phenotyping. Plant J. 1448–1461. https://doi.org/10.1111/tpj.14597

Fukuda, H., 2016. Signaling, transcriptional regulation, and asynchronous pattern formation governing plant xylem development. Proc. Japan Acad. Ser. B 92,

98–107. https://doi.org/10.2183/pjab.92.98
Gaberščik, A., Martinčič, A., 1987. Seasonal dynamics of net photosynthesis and productivity of Sphagnum papillosum. Lindbergia 13, 105–110.
Gamon, J.A., Peñuelas, J., Field, C.B., 1992. A Narrow-Waveband Spectral Index That Tracks Diurnal Changes in Photosynthetic Efficiency. Remote Sens. Environ. 41, 35–44. https://doi.org/10.1016/0034-4257(92)90059-S
Gaudig, G., Fengler, F., Krebs, M., Prager, A., Schulz, J., Wichmann, S., Joosten, H., 2013. Sphagnum farming in Germany – a review of progress. Mires Peat 13, 1–11.
Gauthier, T.J., Elliott, J.B., Mccarter, C.P.R., Price, J.S., 2022. Field-scale compression of Sphagnum moss to improve water retention in a restored bog. J. Hydrol. 612, 128160. https://doi.org/10.1016/j.jhydrol.2022.128160
GBIF, n.d. GBIF Secretariat: GBIF Backbone Taxonomy. https://doi.org/10.15468/39omei
Gerdol, R., Bonora, A., Gualandri, R., Pancaldi, S., 1996. CO2 exchange, photosynthetic pigment composition, and cell ultrastructure of Sphagnum mosses during dehydration and subsequent rehydration. Can. J. Bot. 74, 726–734. https://doi.org/10.1139/b96-091
Giordano, S., Colacino, C., Basile, A., Esposito, A., Castaldo-cobianchi, R., 2009. Morphological adaptation to water uptake and transport in the poikilohydric moss Tortula ruralis. G. Bot. Ital. 127, 1123–1132.
Gitelson, A.A., Keydan, G.P., Merzlyak, M.N., 2006. Three-band model for noninvasive estimation of chlorophyll, carotenoids, and anthocyanin contents in higher plant leaves. Geophys. Res. Lett. 33. https://doi.org/10.1029/2006GL026457
Gitelson, A.A., Merzlyak, M.N., 1997. Remote estimation of chlorophyll content in higher plant leaves. Int. J. Remote Sens. 18, 2691–2697. https://doi.org/10.1080/014311697217558
Glime, J.M., 2017. Chapter 7-4a Water Relations: Leaf Strategies – Structural, in: Bryophyte Ecology. Michigan Technological University, pp. 1–42.
González, E., Henstra, S.W., Rochefort, L., Bradfield, G.E., Poulin, M., 2014. Is rewetting enough to recover Sphagnum and associated peat-accumulating species in traditionally exploited bogs? Wetl. Ecol. Manag. 22, 49–62. https://doi.org/10.1007/s11273-013-9322-6
Goodman, G., Roberts, T., 1971. Plants and soils as indicators of metals in the air. Nature 231, 287–292. https://doi.org/10.1038/231287a0
Gorham, E., 1957. The Development of Peat Lands. Q. Rev. Biol. 32, 145–166. https://doi.org/10.1007/s13398-014-0173-7.2
Hájek, T., Vicherová, E., 2014. Desiccation tolerance of Sphagnum revisited: a puzzle resolved. Plant Biol. 16, 665–773. https://doi.org/10.1111/plb.12126
Hanson, D.T., Rice, S.K., 2014. Photosynthesis in Bryophytes and Early Land Plants, in: Advances in Photosynthesis and Respiration. Springer Science, Dordrecht, pp. 291–308. https://doi.org/10.1007/978-94-007-6988-5
Harris, A., Bryant, R.G., Baird, A.J., 2006. Remote sensing of Sphagnum stress: A proxy for near-surface wetness conditions in northern peatlands? Eur. Sp. Agency, (Special Publ. ESA SP.
Hausding, A., 1921. A Handbook on The Winning and the Utilization of Peat, 3rd, English ed. His Majesty's Stationery Office, London.
Heo, J. ok, Blob, B., Helariutta, Y., 2017. Differentiation of conductive cells: a matter of life and death. Curr. Opin. Plant Biol. 35, 23–29.

https://doi.org/10.1016/j.pbi.2016.10.007
Hüther, P., Schandry, N., Jandrasits, K., Bezrukov, I., Becker, C., 2020. ARADEEPOPSIS, an automated workflow for top-view plant phenomics using semantic segmentation of leaf States. Plant Cell 32, 3674–3688. https://doi.org/10.1105/tpc.20.00318
Iakimova, E.T., Woltering, E.J., 2017. Xylogenesis in zinnia (Zinnia elegans) cell cultures: unravelling the regulatory steps in a complex developmental programmed cell death event. Planta 245, 681–705. https://doi.org/10.1007/s00425-017-2656-1
Johnson, M.G., Granath, G., Tahvanainen, T., Pouliot, R., Stenøien, H.K., Rochefort, L., Rydin, H., Shaw, A.J., 2015. Evolution of niche preference in Sphagnum peat mosses. Evolution (N. Y). 69, 90–103. https://doi.org/10.1111/evo.12547
Johri, M.M., 2008. Hormonal regulation in green plant lineage families. Physiol. Mol. Biol. Plants 14, 23–38. https://doi.org/10.1007/s12298-008-0003-5
Kangas, L., Maanavilja, L., Hájek, T., Juurola, E., Chimner, R.A., Mehtätalo, L., Tuittila, E.S., 2014. Photosynthetic traits of Sphagnum and feather moss species in undrained, drained and rewetted boreal spruce swamp forests. Ecol. Evol. 4, 381–396. https://doi.org/10.1002/ece3.939
Kawashima, S., Nakatani, M., 1998. An algorithm for estimating chlorophyll content in leaves using a video camera. Ann. Bot. 81, 49–54. https://doi.org/10.1006/anbo.1997.0544
Khandelwal, A., Cho, S.H., Marella, H., Sakata, Y., Perroud, P.F., Pan, A., Quatrano, R.S., 2010. Role of ABA and ABI3 in desiccation tolerance. Science (80-.). 327, 546. https://doi.org/10.1126/science.1183672
Korrensalo, A., Hájek, T., Vesala, T., Mehtätalo, L., Tuittila, E.S., 2016. Variation in photosynthetic properties among bog plants. Botany 94, 1127–1139. https://doi.org/10.1139/cjb-2016-0117
Kostka, J.E., Weston, D.J., Glass, J.B., Lilleskov, E.A., Shaw, A.J., Turetsky, M.R., 2016. The Sphagnum microbiome: new insights from an ancient plant lineage. New Phytol. 211, 57–64. https://doi.org/10.1111/nph.14137
Kremer, C.L., Drinnan, A.N., 2004. Secondary walls in hyaline cells of Sphagnum. Aust. J. Bot. 52, 243–256. https://doi.org/10.1071/BT03010
Leifeld, J., Menichetti, L., 2018. The underappreciated potential of peatlands in global climate change mitigation strategies. Nat. Commun. 9, 1–7. https://doi.org/10.1038/s41467-018-03406-6
Ligrone, R., Duckett, J.G., 1998. Development of the leafy shoot in Sphagnum (Bryophyta) involves the activity of both apical and subapical meristems. New Phytol. 140, 581–595.
Limpens, J., Bohlin, E., Nilsson, M.B., 2017. Phylogenetic or environmental control on the elemental and organo-chemical composition of Sphagnum mosses? Plant Soil 417, 69–85. https://doi.org/10.1007/s11104-017-3239-4
Loisel, J., Gallego-Sala, A. V., Amesbury, M.J., Magnan, G., Anshari, G., Beilman, D.W., Benavides, J.C., Blewett, J., Camill, P., Charman, D.J., Chawchai, S., Hedgpeth, A., Kleinen, T., Korhola, A., Large, D., Mansilla, C.A., Müller, J., van Bellen, S., West, J.B., Yu, Z., Bubier, J.L., Garneau, M., Moore, T., Sannel, A.B.K., Page, S., Väliranta, M., Bechtold, M., Brovkin, V., Cole, L.E.S., Chanton, J.P., Christensen, T.R., Davies, M.A., De Vleeschouwer, F., Finkelstein, S.A., Frolking, S., Gałka, M., Gandois, L., Girkin, N., Harris, L.I., Heinemeyer, A., Hoyt, A.M., Jones, M.C., Joos, F., Juutinen, S., Kaiser, K., Lacourse, T., Lamentowicz, M., Larmola, T., Leifeld, J., Lohila, A., Milner,

A.M., Minkkinen, K., Moss, P., Naafs, B.D.A., Nichols, J., O'Donnell, J., Payne, R., Philben, M., Piilo, S., Quillet, A., Ratnayake, A.S., Roland, T.P., Sjögersten, S., Sonnentag, O., Swindles, G.T., Swinnen, W., Talbot, J., Treat, C., Valach, A.C., Wu, J., 2021. Expert assessment of future vulnerability of the global peatland carbon sink. Nat. Clim. Chang. 11, 70–77. https://doi.org/10.1038/s41558-020-00944-0

Louhaichi, M., Borman, M.M., Johnson, D.E., 2001. Spatially located platform and aerial photography for documentation of grazing impacts on wheat. Geocarto Int. 16, 65–70. https://doi.org/10.1080/10106040108542184

Lyu, S., Li, R., Zhao, Y., Li, Z., Fan, R., Liu, S., 2022. Green Citrus Detection and Counting in Orchards Based on YOLOv5-CS and AI Edge System. Sensors 22, 1–20. https://doi.org/10.3390/s22020576

Marschall, M., Borbély, P., 2011. Photosynthetic responses of the desiccation intolerant Sphagnum angustifolium in relation to increasing its desiccation tolerance by exogenous ABA. Acta Biol. Szeged. 55, 119–121.

Muster, C., Gaudig, G., Krebs, M., Joosten, H., 2015. Sphagnum farming: the promised land for peat bog species? Biodivers. Conserv. 24, 1989–2009. https://doi.org/10.1007/s10531-015-0922-8

Oliver, M.J., Hudgeons, J., Dowd, S.E., Payton, P.R., 2009. A combined subtractive suppression hybridization and expression profiling strategy to identify novel desiccation response transcripts from Tortula ruralis gametophytes. Physiol. Plant. 136, 437–460. https://doi.org/10.1111/j.1399-3054.2009.01245.x

Oliver, Melvin J., Tuba, Z., Mishler, B.D., 2000. The evolution of vegetative desiccation tolerance in land plants. Plant Ecol. 151, 85–100. https://doi.org/10.1023/A:1026550808557

Oliver, Melvin J, Velten, J., Wood, A.J., 2000. Bryophytes as experimental models for the study of environmental stress tolerance: Tortula ruralis and desiccation-tolerance in mosses. Plant Ecol. 151, 73–84. https://doi.org/10.1023/A:1026598724487

Page, S.E., Baird, A.J., 2016. Peatlands and Global Change: Response and Resilience. Annu. Rev. Environ. Resour. 41, 35–57. https://doi.org/10.1146/annurev-environ-110615-085520

Pesquet, E., Korolev, A. V., Calder, G., Lloyd, C.W., 2010. The Microtubule-Associated Protein AtMAP70-5 Regulates Secondary Wall Patterning in Arabidopsis Wood Cells. Curr. Biol. 20, 744–749. https://doi.org/10.1016/j.cub.2010.02.057

Piatkowski, B.T., Shaw, A.J., 2019. Functional trait evolution in Sphagnum peat mosses and its relationship to niche construction. New Phytol. 223, 939–949. https://doi.org/10.1111/nph.15825

Potvin, L.R., Kane, E.S., Chimner, R.A., Kolka, R.K., Lilleskov, E.A., 2014. Effects of water table position and plant functional group on plant community, aboveground production, and peat properties in a peatland mesocosm experiment (PEATcosm). Plant Soil 387, 277–294. https://doi.org/10.1007/s11104-014-2301-8

Proctor, M.C.F. (1982). Physiological Ecology: Water Relations, Light and Temperature Responses, Carbon Balance. In: Smith, A.J.E. (eds) Bryophyte Ecology. Springer, Dordrecht. https://doi.org/10.1007/978-94-009-5891-3_10

Proctor, M.C.F., Oliver, M.J., Wood, A.J., Alpert, P., Stark, L.R., Cleavitt, N.L., Mishler, B.D., 2007. Desiccation-tolerance in bryophytes: A review. Bryologist 110, 595–621. https://doi.org/10.1639/0007-

2745(2007)110[595:DIBAR]2.0.CO;2
Rahimzadeh-Bajgiran, P., Munehiro, M., Omasa, K., 2012. Relationships between the photochemical reflectance index (PRI) and chlorophyll fluorescence parameters and plant pigment indices at different leaf growth stages. Photosynth. Res. 113, 261–271. https://doi.org/10.1007/s11120-012-9747-4
Rathnayake, K.N., Nelson, S., Seeve, C., Oliver, M.J., Koster, K.L., 2018. Acclimation and endogenous abscisic acid in the moss Physcomitrella patens during acquisition of desiccation tolerance. Physiol. Plant. https://doi.org/10.1111/ppl.12892
Rimington, W.R., Pressel, S., Duckett, J.G., Field, K.J., Read, D.J., Bidartondo, M.I., 2018. Ancient plants with ancient fungi: liverworts associate with early-diverging arbuscular mycorrhizal fungi. Proc. R. Soc. B Biol. Sci. 285. https://doi.org/10.1098/rspb.2018.1600
Robb, C., Hardy, A., Doonan, J.H., Brook, J., 2020. Semi-Automated Field Plot Segmentation From UAS Imagery for Experimental Agriculture. Front. Plant Sci. 11, 1–13. https://doi.org/10.3389/fpls.2020.591886
Robinson, S.A., King, D.H., Bramley-Alves, J., Waterman, M.J., Ashcroft, M.B., Wasley, J., Turnbull, J.D., Miller, R.E., Ryan-Colton, E., Benny, T., Mullany, K., Clarke, L.J., Barry, L.A., Hua, Q., 2018. Rapid change in East Antarctic terrestrial vegetation in response to regional drying. Nat. Clim. Chang. 8, 879–884. https://doi.org/10.1038/s41558-018-0280-0
Sánchez-Sastre, L.F., Alte da Veiga, N.M.S., Ruiz-Potosme, N.M., Carrión-Prieto, P., Marcos-Robles, J.L., Navas-Gracia, L.M., Martín-Ramos, P., 2020. Assessment of RGB Vegetation Indices to Estimate Chlorophyll Content in Sugar Beet Leaves in the Final Cultivation Stage. AgriEngineering 2, 128–149. https://doi.org/10.3390/agriengineering2010009
Say, P.J., Harding, J.P.C., Whitton, B.A., 1981. Aquatic mosses as monitors of heavy metal contamination in the river etherow, great britain. Environ. Pollution. Ser. B, Chem. Phys. 2, 295–307. https://doi.org/10.1016/0143-148X(81)90026-4
Schipperges, B., Rydin, H., 1998. Response of photosynthesis of Sphagnum species from contrasting microhabitats to tissue water content and repeated desiccation. New Phytol. 140, 677–684.
Schnepf, E., 1973. Mikrotubulus-Anordnung und -Umordnung, Wanbildung und Zellmorphogenese in jungen Sphagnum-Blättchen. Protoplasma 78, 145–173.
Schröder, C., Dahms, T., Paulitz, J., Wichtmann, W., Wichmann, S., 2015. Towards large-scale paludiculture: addressing the challenges of biomass harvesting in wet and rewetted peatlands. Mires Peat 16, 1–18.
Shuttleworth, E.L., Evans, M.G., Pilkington, M., Spencer, T., Walker, J., Milledge, D., Allott, T.E.H., 2019. Restoration of blanket peat moorland delays stormflow from hillslopes and reduces peak discharge. J. Hydrol. X 2, 1–14. https://doi.org/10.1016/j.hydroa.2018.100006
Sims, D.A., Gamon, J.A., 2002. Relationships between leaf pigment content and spectral reflectance across a wide range of species, leaf structures and developmental stages. Remote Sens. Environ. 81, 337–354. https://doi.org/10.1016/S0034-4257(02)00010-X
Song, L., Huang, S.S.C., Wise, A., Castanoz, R., Nery, J.R., Chen, H., Watanabe, M., Thomas, J., Bar-Joseph, Z., Ecker, J.R., 2016. A transcription factor hierarchy defines an environmental stress response network. Science (80-.). 354. https://doi.org/10.1126/science.aag1550
Stenøien, H.K., Bakken, S., Flatberg, K.I., 1997. Phenotypic Variation in the

Sphagnum Recurvum Complex: a Cultivation Experiment. J. Bryol. 19, 731–750. https://doi.org/10.1179/jbr.1997.19.4.731
Stevenson, S.R., Kamisugi, Y., Trinh, C.H., Schmutz, J., Jenkins, J.W., Grimwood, J., Muchero, W., Tuskan, G.A., Rensing, S.A., Lang, D., Reski, R., Melkonian, M., Rothfels, C.J., Li, F.-W., Larsson, A., Wong, G.K.-S., Edwards, T.A., Cuming, A.C., 2016. Genetic analysis of Physcomitrella patens identifies ABSCISIC ACID NON-RESPONSIVE (ANR), a regulator of ABA responses unique to basal land plants and required for desiccation tolerance. Plant Cell tpc.00091.2016. https://doi.org/10.1105/tpc.16.00091
Stivrins, N., Ozola, I., Gałka, M., Kuske, E., Alliksaar, T., Andersen, T.J., Lamentowicz, M., Wulf, S., Reitalu, T., 2017. Drivers of peat accumulation rate in a raised bog: impact of drainage, climate, and local vegetation composition. Mires Peat 19, UNSP 08. https://doi.org/10.19189/MaP.2016.OMB.262
Sundberg, S., Rydin, H., 2002. Habitat requirements for establishment of Sphagnum from spores. J. Ecol. 90, 268–278. https://doi.org/10.1046/j.1365-2745.2001.00653.x
Temmink, R.J.M., Fritz, C., van Dijk, G., Hensgens, G., Lamers, L.P.M., Krebs, M., Gaudig, G., Joosten, H., 2017. Sphagnum farming in a eutrophic world: The importance of optimal nutrient stoichiometry. Ecol. Eng. 98, 196–205. https://doi.org/10.1016/j.ecoleng.2016.10.069
Terada, S., Kubo, M., Akiyoshi, N., Sano, R., Nomura, T., Sawa, S., Ohtani, M., Demura, T., 2021. Expression of peat moss VASCULAR RELATED NAC-DOMAIN homologs in Nicotiana benthamiana leaf cells induces ectopic secondary wall formation. Plant Mol. Biol. 106, 309–317. https://doi.org/10.1007/s11103-021-01148-6
Van Gaalen, K.E., Flanagan, L.B., Peddle, D.R., 2007. Photosynthesis, Chlorophyll Fluorescence and Spectral Reflectance in Sphagnum Moss at Varying Water Contents. Oecologia 153, 19–28. https://doi.org/10.1007/s00442-007-0718-y
Vanburen, R., Wai, C.M., Ou, S., Pardo, J., Bryant, D., Jiang, N., Mockler, T.C., Edger, P., Michael, T.P., 2018. Extreme haplotype variation in the desiccation-tolerant clubmoss Selaginella lepidophylla. Nat. Commun. 9, 1–8. https://doi.org/10.1038/s41467-017-02546-5
Wagner, D.J., Titus, J.E., 1984. Comparative desiccation tolerance of two Sphagnum mosses. Oecologia 62, 182–187.
Wang, X., Song, C., Wang, J., Miao, Y., Mao, R., Song, Y., 2013. Carbon release from Sphagnum peat during thawing in a montane area in China. Atmos. Environ. 75, 77–82. https://doi.org/10.1016/j.atmosenv.2013.04.056
Wang, Y., Liu, K., Bi, D., Zhou, S., Shao, J., 2017. Characterization of the transcriptome and EST-SSR development in *Boea clarkeana* , a desiccation-tolerant plant endemic to China. PeerJ 5, e3422. https://doi.org/10.7717/peerj.3422
Wang, Z., Bader, M.Y., 2018. Associations between shoot-level water relations and photosynthetic responses to water and light in 12 moss species. AoB Plants 10, 1–14. https://doi.org/10.1093/aobpla/ply034
Wehr, J.D., Empain, A., Mouvet, C., Say, P.J., Whitton, B.A., 1983. Methods for processing aquatic mosses used as monitors of heavy metals. Water Res. 17, 985–992. https://doi.org/10.1016/0043-1354(83)90038-6
Wenhua Mao, Yiming Wang, Yueqing Wang, 2013. Real-time Detection of Between-row Weeds Using Machine Vision 0300. https://doi.org/10.13031/2013.15381

Williams, T.G., Flanagan, L.B., 1996. Effect of changes in water content on photosynthesis , transpiration and discrimination against 13CO2 and C18O16O in Pleurozium and Sphagnum. Oecologia 108, 38–46.
Winnicka, K., Melosik, I., 2019. Genetic and expression differences between putative ecotypes of Sphagnum denticulatum Brid. (Sphagnaceae: Bryophyta) subjected to drought stress and rehydration. Perspect. Plant Ecol. Evol. Syst. 37, 39–52. https://doi.org/10.1016/j.ppees.2019.02.004
Woebbecke, D.M., Meyer, G.E., Von Bargen, K., Mortensen, D.A., 1995. Color indices for weed identification under various soil, residue, and lighting conditions. Trans. Am. Soc. Agric. Eng. 38, 259–269. https://doi.org/10.13031/2013.27838
Xiao, L., Yang, G., Zhang, L., Yang, X., Zhao, S., Ji, Z., Zhou, Q., Hu, M., Wang, Y., Chen, M., Xu, Y., Jin, H., Xiao, X., Hu, G., Bao, F., Hu, Y., Wan, P., Li, L., Deng, X., Kuang, T., Xiang, C., Zhu, J.-K., Oliver, M.J., He, Y., 2015. The resurrection genome of *Boea hygrometrica* : A blueprint for survival of dehydration. Proc. Natl. Acad. Sci. 112, 5833–5837. https://doi.org/10.1073/pnas.1505811112
Xu, B., Ohtani, M., Yamaguchi, M., Toyooka, K., Wakazaki, M., Sato, M., Kubo, M., Nakano, Y., Sano, R., Hiwatashi, Y., Murata, T., Kurata, T., Yoneda, A., Kato, K., Hasebe, M., Demura, T., 2014. Contribution of NAC transcription factors to plant adaptation to land. Science (80-.). 343, 1505–1508. https://doi.org/10.1126/science.1248417
Xue, J., Su, B., 2017. Significant remote sensing vegetation indices: A review of developments and applications. J. Sensors 2017. https://doi.org/10.1155/2017/1353691
Yu, Z., Loisel, J., Brosseau, D.P., Beilman, D.W., Hunt, S.J., 2010. Global peatland dynamics since the Last Glacial Maximum. Geophys. Res. Lett. 37, 1–5. https://doi.org/10.1029/2010GL043584

CHAPTER 2 – CONSERVED MOLECULAR RESPONSES TO DESICCATION IN *SPHAGNUM*

Chapter statement:

This chapter is a modified version of previously published research in the peer-reviewed Journal of Experimental Botany as "*Molecular and physiological responses to desiccation indicate the abscisic acid pathway is conserved in the peat moss, Sphagnum*" (DOI: https://doi.org/10.1093/jxb/erac133). To reference any of the results mentioned in this chapter, please refer to the aforementioned publication and cite as:

Candida Nibau, Willem van de Koot, Dominic Spiliotis, Kevin Williams, Tina Kramaric, Manfred Beckmann, Luis Mur, Yuji Hiwatashi, John H Doonan, Molecular and physiological responses to desiccation indicate the abscisic acid pathway is conserved in the peat moss, *Sphagnum*, *Journal of Experimental Botany*, *Volume* 73, Issue 13, 16 July 2022, Pages 4576–4591, https://doi.org/10.1093/jxb/erac133

In this chapter, which is by and large the work of Candida Nibau, I have contributed by assisting with experimental design, methodology and analysis of sections pertaining to chlorophyll fluorescence, RNA extraction and induction. Furthermore, with Candida Nibau and John Doonan, I jointly supervised Dominic Spiliotis during his year in industry research, who carried out preliminary experiments to determine the best droughting conditions and assisted in data acquisition,. The sections involving transformations on *P. patens* and the associated phylogenies were carried out entirely by Candida Nibau and Yuji Hiwatashi. The ABA tissue content analysis was performed by Tina Kramaric, Manfred Beckmann and Luis Mur.

Data availability

All data supporting the findings of this study are available within the paper and within its supplementary materials published online.

Chapter summary

Mosses of the genus *Sphagnum* are the main components of peatlands, a major carbon-storing ecosystem. Changes in precipitation patterns are predicted to affect water relations in this ecosystem, but the effect of desiccation on the physiological and molecular processes in *Sphagnum* is still largely unexplored. Here we show that different *Sphagnum* species have differential physiological and molecular responses to desiccation but, surprisingly, this is not directly correlated with their position in relation to the water table. In addition, the expression of drought responsive genes is increased upon water withdrawal in all species. This increase in gene expression is accompanied by an increase in abscisic acid (ABA), supporting a role for ABA during desiccation responses in *Sphagnum*. Not only do ABA levels increase upon desiccation, but *Sphagnum* plants pre-treated with ABA display increased tolerance to desiccation, suggesting that ABA levels play a functional role in the response. In addition, many of the ABA signalling components are present in *Sphagnum* and we demonstrate, by complementation in *Physcomitrium patens*, that *Sphagnum* ABI3 is functionally conserved. The data presented here, therefore, support a conserved role for ABA in desiccation responses in *Sphagnum*.

2.1 - Introduction

One of the biggest challenges facing primordial plants as they moved to terrestrial environments was how to cope with water stress. Arguably, the most important development of the water-to-land transition was the development of systems that allowed the plant to maintain an internal water potential independently from the water potential of the environment. These include the development of vascular systems, physical barriers to water loss in the form of cuticles and of complex drought-responsive cellular signalling pathways, all features of vascular plants. However, some plants developed strategies to avoid water stress by living in water-saturated terrestrial environments, increasing plant density or reducing plant size to reduce evaporation. Others evolved physiological mechanisms to tolerate short periods of drought and a few can survive nearly full desiccation.

Despite this, a degree of tolerance to water loss is necessary in all the habitats that are not constantly water saturated. Even short periods of mild drought have deleterious effects in terms of plant growth and development, and plants need to develop strategies to mitigate these. Understanding these strategies is even more important given climate change scenarios where temperature and rainfall are predicted to become more stochastic.

Traditionally, plant responses to drought have been defined as escape (accelerating reproduction), avoidance (developing strategies to maintain high internal water content) and tolerance (maintaining growth under low internal water content). Drought tolerance has been extensively studied in vascular plants and involves the activation of mechanisms to prevent water loss and increase water uptake, and pathways leading to the induction of drought responsive genes (Chaves et al., 2003; Yao et al., 2021). Central to these tolerance processes is the stress hormone abscisic acid (ABA). ABA rapidly increases at the onset of drought and triggers a complex and multi-layered signalling cascade leading to the transcription of drought responsive genes that enable the plant to maintain and adapt physiological processes under drought (Ali et al., 2020).

Although most attention has focused on the effect of drought on agricultural systems, drought also poses a significant threat to wetland environments such as peatlands (Stirling et al., 2020). Peatlands are important carbon-storing ecosystems in temperate and boreal regions and they are now seen as crucial to climate change

mitigation strategies (Leifeld and Menichetti, 2018). Reversing human impact on peatland degradation often involves restoring the water table and vegetational cover on bare peat surfaces. However, response of key plants in these peatland ecosystems to drought is poorly understood.

Mosses of the genus *Sphagnum* are major components of acidic peatlands where they regulate water relations and carbon sequestration through peat accumulation. In common with all bryophytes, *Sphagnum* mosses are poikilohydric meaning that they are unable to maintain internal water potential different from their environment (Raven, 1995). Although typical mosses lack many of the adaptations of vascular plants to reduce water loss such as cuticle and stomata, they have developed alternative specialised features to store and regulate water distribution across the plant (Charron and Quatrano, 2009; Proctor et al., 2007). These include morphological adaptations such as long and densely packed branches, growing in tightly packed cushions to prevent evaporation and the development of specialised water storage cells that use water tension to keep the plant hydrated while minimally affecting gas exchange (Dilks and Proctor, 1979; Proctor, 2000; Proctor et al., 2007). While *Sphagnum* does have pseudostomata, these are functionally different from stomata in higher plants. These pseudostomata cannot be closed, and are only found on the base of the sporophyte, where they are thought to facilitate desiccation, consequently causing capsule dehiscence and facilitating spore dispersal (Duckett et al., 2007; Duckett and Pressel, 2018).

Physiological adaptations include the development of desiccation tolerance that enables mosses to recover after completely drying out (Oliver et al., 2005). This is achieved through the presence of constitutive mechanisms of cellular protection and a rehydration-induced repair and recovery process (Proctor et al., 2007). These mechanisms are well studied in the moss *Tortula ruralis*, where the constitutive expression of Late Embryogenic Abundant (LEA) proteins is essential for cellular protection and maintaining membrane integrity during drying (Oliver et al., 2005). The development of desiccation avoidance and tolerance mechanisms may have allowed mosses to colonise a wide range of habitats across all continents, making the group very successful and resilient (Charron and Quatrano, 2009).

Unlike most bryophytes, *Sphagnum* species have been considered to be drought and desiccation-intolerant (Clymo, 1973; Clymo and Hayward, 1982). More recently, this view has been challenged and while some authors report low recovery

even after mild desiccation, other studies suggest that *Sphagnum* shoots can tolerate strong desiccation (reviewed in (Hájek and Vicherová, 2014)). The ability (or otherwise) of *Sphagnum* to survive water-limiting conditions would have implications for the restoration and management of peatland ecosystems. With predicted changes in climatic patterns, peatlands are considered to be key to mitigation strategies. Therefore, understanding how *Sphagnum* mosses respond to drought and desiccation is necessary and timely (Leifeld and Menichetti, 2018).

There may be intrinsic variation in desiccation tolerance within the genus. A typical peatland consists of a variety of microhabitats ranging from permanently flooded pools, wet depressions (hollows), elevated hummocks and everything in between. Access to the water table in these microhabitats is different and it has been proposed that the *Sphagnum* species that inhabit each habitat have evolved different mechanisms to cope with changes in water availability (Johnson et al., 2015). Thus, hummock species that grow further away from the water table are expected to be better at maintaining colony water content and thus avoiding desiccation, while hollow species with constant access to the water table would be less desiccation tolerant. Experimental evidence seems to show that this is not always the case, with some studies finding no differences between position along the water table and desiccation tolerance (Wagner and Titus, 1984) while others find that hollow species actually show better recovery after desiccation (Schipperges and Rydin, 1998).

While some of the physiological mechanisms for *Sphagnum* response to water limiting conditions have been investigated, including the loss and recovery of photosynthetic function, not much is known about the molecular responses to desiccation (Hájek and Vicherová, 2014; Schipperges and Rydin, 1998; Wagner and Titus, 1984; Winnicka and Melosik, 2019). It has previously been shown that drought responsive gene expression is upregulated in *Sphagnum* when subjected to drought and that ABA increases desiccation tolerance in *Sphagnum* (Hájek and Vicherová, 2014; Marschall and Borbély, 2011; Winnicka and Melosik, 2019). Despite this, a systematic and comparative analysis including both physiological and molecular responses of different *Sphagnum* species from different microhabitats to controlled drought and rehydration is lacking.

Here we show that desiccation responses differ in different *Sphagnum* species from the same blanket bog. Photosynthetic function and water loss is different between the species and this translates into differential activation of drought

responsive gene expression. Our data confirm that ABA pre-treatment improves desiccation tolerance in *Sphagnum* and, significantly, that ABA levels increase upon desiccation in *Sphagnum.* Finally, we show that components of the ABA signalling pathway in *Sphagnum* are functional when expressed in *Physcomitrium* (*Physcomitrella*) *patens* (*P. patens*). Our results therefore support a functional role for ABA and ABA responsive genes in desiccation responses in *Sphagnum*.

2.2 - Materials and Methods

2.2.1 - Site collection and plant material

Sphagnum species were collected from a minerotrophic mire in Pen y Garn (SN791758) situated in the Cambrian Mountains, Wales, UK. The mire is located at the base of a mountain and contains dense carpets of *Sphagnum* as well as several pool areas that exhibit mild flow after heavy rain. Four *Sphagnum* species; *Sphagnum fallax* (Cuspidata), *Sphagnum papillosum* (Sphagnum), *Sphagnum capillifolium* (Acutifolia) and *Sphagnum inundatum* (Subsecunda) were selected to cover the four most abundant taxonomic sections within the genus and the different habitats within the mire (Figure 2.1). For each species, four different areas within the bog were selected for collection. In each area, stem density was manually scored and the height of the water table measured. Blocks of moss were lifted, carefully retaining the structural coherence of the canopy, and brought back to the laboratory. Data shown here is from a collection on the 3rd of May 2021 but we collected at different times during the 2020/2021 season with similar results.

2.2.2 - Desiccation experiment

The desiccation experiments were performed in plastic square Petri dishes (cosms, Figure 2.1) where one side of both the lid and the base were removed so that there is a 20 cm^2 opening. The plates were positioned vertically so that the opening is uppermost. The same day they were collected, *Sphagnum* stems from the blocks were separated, cut to a length of 7 cm and placed in each cosm at the same density as determined in the field. Each *S. fallax* cosm had 33 stems, *S. papillosum* 24, *S. capillifolium* 38 and *S. inundatum* 12. We prepared cosms for eight independent time points and four replica cosms per time point in a total of sixty-four cosms per species. Each cosm was weighed to make sure they were all approximately the same weight. The cosms were then placed in a tub filled with water so that about 2/3 of the cosm was submerged and left overnight, allowing for full hydration of the moss. The following morning the excess water was allowed to drain from the plates for 1 h. All the cosms were weighed (starting weight) and chlorophyll fluorescence measured (see below). Four replicas (0 days) were taken and capitula harvested for relative water content measurements (RWC), ABA analysis and RNA extraction. Plates were

again weighed, imaged and 4 replica collected after 2, 4, 7 and 9 days for *S. fallax*, *S. capillifolium* and *S. inundatum*. After 9 days water withdrawal, 4 cosms for these three species were placed in a tub of water and allowed to re-hydrate for 24h and then the excess water allowed to drain for 1 h after which plates were weighed, imaged and harvest as before (re-wet time point). For *S. papillosum* samples were collected at 2, 4, 7, 9 and 13 days after water withdrawal before re-watering.

2.2.3 - Chlorophyll fluorescence

We used the chlorophyll fluorescence parameter Fv/Fm, which provides a measure of the maximum efficiency of Photosystem II, as a proxy for drought stress, Water loss inhibits the metabolic processes that are required for photosynthesis leading to a decrease in the Fv/Fm ratio (Murchie and Lawson, 2013). Each cosm was placed in the centre of a CF Imager (Technologica, Essex, UK) after a minimum of 20 minutes dark-adaption period. Focus and aperture size were adjusted for each sample separately as indicated by the operating software, and de-noised in the 'map' image to remove non-*Sphagnum* pixels as described in the manufacturer's protocol. Minimum fluorescence (Fo) was measured using low intensity lighting. Maximum fluorescence (Fm) was measured using a saturating pulse of 6843 µmol m^{-2} s^{-1} PPFD (Photosynthetic Photon Flux Density) PAR (Photosynthetic Active Radiation), after which Fv/Fm was calculated using the formula (Fm – Fo)/Fm. In order to determine how chlorophyll fluorescence values change in the different parts of the *Sphagnum* stem as it dries, areas containing the different zones (capitula, live stem, senescing stem) were manually selected and Fv/Fm calculated for these areas.

2.2.4 - Relative Water Content

Relative water content (RWC) was calculated for each plate by weighing the fresh 4 capitula and then allowing them to completely dry in an oven at 80°C for at least 24h before weighing them again (dry weight). RWC was calculated as a difference between fresh and dry weight divided by dry weight and expressed as a percentage relative to the non-droughted material.

2.2.5 - RNA extraction and qPCR

Capitula from the different species were harvested at the different time points as described above and ground to a fine powder in liquid nitrogen, 500 mg were used for ABA analysis and the rest for RNA extraction using the Spectrum Total RNA kit (Sigma) with in-column DNase treatment (Qiagen) following the manufacturer's instructions. RNA integrity was determined by gel electrophoresis and 500 ng of total RNA was used to prepare cDNA using the Supercript III First Strand Synthesis System (Invitrogen). Quantitative polymerase chain reactions (qPCRs) were performed using a LightCycler 480 (Roche). Drought responsive genes were selected based on a study (Cuming et al., 2007) in *P. patens* and *Sphagnum* homologues identified using Phytozome (https://phytozome.jgi.doe.gov/). The gene identifiers for both *P. patens* and *Sphagnum* are included in Supplementary Table 2.1. Specific primers able to amplify the genes in the four different species were designed using Primer 3 (Supplementary Table 2.1). Typically, 10 ng of cDNA were used in a 20 µl reaction containing 0.25 µM of each primer and 10 µl LightCycler® 480 SYBR Green I Master (Roche). Three biological samples per species, per time point were used and each reaction was done in triplicate. *Sphagnum* EF1α (Sphfalx03G087000) and GAPDH (Sphfalx16G076000) transcripts were used as references (Winnicka and Melosik, 2019), (see Supplementary Table 2.1 for primer sequences). Data were analysed using the LightCycler® 480 Software (Roche). The data shown are averages ± SD of three biological replicates.

2.2.6 - ABA measurements

Capitula from the different species were harvested at the different time points as described above and ground in liquid nitrogen to a fine powder. For each sample 500-50 mg of tissue was weighed and extraction performed in 70 % (v/v) HPLC grade MeOH (Fisher Scientific) with ultra- pure H_2O (18.2 Ω). The samples were analysed in a flow infusion electro-spray ionisation high resolution mass spectrometry (FI-ESI-MS). The mass spectra were acquired on an Accela (ThermoFinnigan, San Jose CA) ultra-performance liquid chromatography system coupled to an Exactive Orbitrap (ThermoFinnigan, San Jose CA) mass spectrometer.

A

Species	*S. fallax*	*S. papillosum*	*S. capillifolium*	*S. inundatum*
Subgenus	Cuspidata	Sphagnum	Acutifolia	Subsecunda
Habitat	Hollow/Lawn	Hummock	Hummock	Hollow/Pool
Distance to water table	12.3 cm (n=55) (min 2- max 23)	11.3 cm (n=43) (min 1- max 30)	22.4 cm (n=7) (min 12- max 30)	5.6 cm (n=11) (min 0- max 7)

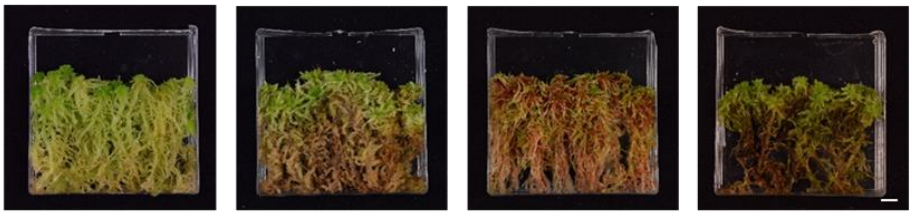

B

C

Figure 2.1. Details of the species used in this study and experimental set up. A. Four *Sphagnum* species, *S. fallax*, *S. papillosum*, *S. capillifolium* and *S. inundatum* belonging to the most abundant subgenera and spanning a range of microhabitats as indicated were used. Mean distances to the water table, as measured over 3 years at the Pen y Garn site are also shown. Top images show the species in the field (scale bar 10 cm) and bottom images after they have been assembled into square petri dishes opened at the top to allow evaporation (cosms) at a density comparable to that observed in the field (scale bar 1 cm). B. Desiccation treatment set up. The cosms were placed upright in a tray and kept in the greenhouse under natural light conditions. C. Morphology of the different *Sphagnum* species as indicated. Top row, whole plants; Bottom row detached capitula detail. Scale bar 1 cm.

An aliquot of 20 µL was delivered to the ESI source in 70 % (v/v) HPLC grade MeOH (Fisher Scientific) with ultra- pure H_2O (18.2 Ω). The flow rate was 200 µL min^{-1} for the first 1.5 min and 600 µL min^{-1} for the remaining 1.5 minutes. Both ionisation modes were acquired. ABA peak intensities (*m/z* 263.129 [M-H]-) where converted to µg/mL concentration based on the derivation of a standard curve based on commercially obtained ABA (Sigma-Aldrich, UK) that was assessed by FI- FI-ESI-MS. Values obtained were them adjusted for the sample RWC. RWC values for time point 0 were considered to be 1 and all the other values calculated in relation to that.

2.2.7 - ABA and desiccation treatments

S. *fallax* plants were placed in cosms as described above at a density of 33 plants per plate, four plates per each of the three ABA treatments and two desiccation regimes, 24 plates in total. The plates were then placed in tubs filled with water, 10 μM ABA or 50 μM ABA solution so that about 2/3 of the cosm was submerged and left for 24 h. After this time, the liquid was drained out and excess allowed to drain from the plates for 1 h. All the cosms were weighed (starting weight) and chlorophyll fluorescence measured (see above) and this corresponded to time point 0. Plates were again weighed, imaged every day until each plate reached a value of Fv/Fm of 0.2. At that point the plate was immediately rehydrated in water overnight (1 day water withdrawal) or left for 4 days before rehydration (4 days water withdrawal) according to what treatment it was part of. Plates were then weighed and chlorophyll fluorescence measured 1 and 2 days after rehydration. Chlorophyll fluorescence recovery was calculated as the ratio of the Fv/Fm measurement at day 2 after re-watering and the Fv/Fm measurement on day 0.

2.2.8 - Phylogenetic analysis of ABA signalling genes in *Sphagnum*

For the construction of the phylogenetic trees, we used a data set of homologs from *Arabidopsis thaliana* (*Arabidopsis thaliana* Araport11, (Cheng et al., 2017)), *Oriza sativa* (*Oryza sativa* v7.0, (Ouyang et al., 2007)), *Selaginella moellendorffii* (*Selaginella moellendorffii* v1.0, (Banks et al., 2011)), *Marchantia polymorpha* (*Marchantia polymorpha* v3.1, (Bowman et al., 2017)), *Physcomitrium patens* (*Physcomitrium patens* v3.3, (Lang et al., 2018)), *Sphagnum fallax* (*Sphagnum fallax* v1.1, DOE-JGI, http://phytozome.jgi.doe.gov/), *Sphagnum magellanicum* (*Sphagnum magellanicum* v1.1, DOE-JGI, http://phytozome.jgi.doe.gov/) and *Ceratopteris richardii* (*Ceratopteris richardii* v2.1, DOE-JGI, http://phytozome.jgi.doe.gov/, for ABI3 only). The homologs were obtained with a BLASTP search against the proteome database from Phytozome 13 (https://phytozome-next.jgi.doe.gov) (Goodstein et al., 2012). Deduced amino acid sequences aligned using MAFFT (Katoh et al., 2019). After elimination of all positions of gaps and short sequences manually, conserved amino acid residue were used to calculate for each gene using

the Maximum Likelihood method and JTT model (Jones et al., 1992) to construct a ML tree in MEGA-X (Kumar et al., 2018). Statistical support for internal branches by bootstrap analyses (Felsenstein, 1985) was calculated using 1000 replications. All sequences were obtained using the Arabidopsis homologues as query. To build the tree for ABI3 proteins, a significant similarity E-value < 1e-10 was used, amino acid sequences lacking conserved B1, B2 and B3 regions (Marella et al., 2006) were deleted from the alignment and 191 amino acid residues were used to calculate evolution distances for 18 genes. For SnRK2 an E-value < 1e-63 was used and 300 amino acid residues were used to calculate evolution distances for 35 genes. For PYR1 the E-value was < 1e-11 and 129 amino acid residues were used to calculate evolution distances for 48 genes. For ABI1 an E-value < 1e-35 was used and 234 amino acid residues were used to calculate evolution distances for 53 genes. For ABI5, an E-value < 1e-8 was used, the amino acid sequences lacking a conserved domain (bZIP_plant_BZIP46: cd14707) were deleted from the alignment and 53 amino acid residues were used to calculate evolution distances for 47 genes.

2.2.9 - *Sphagnum* ABI gene identification and cloning

Sphagnum ABI3 homologues were identified using the *P. patens* ABI3C protein sequence (Pp3c4_7328V3.1) to interrogate the translated *Sphagnum fallax* database in Phytozome (https://phytozome.jgi.doe.gov/) (Goodstein et al., 2012). Specific primers were designed for the selected candidate genes and used to amply the corresponding transcripts from *Sphagnum* cDNA (Supplementary Table 2.1). The transcript from Sphfalx01G102500 (that we called *SphABI3-16*) was the most abundant under our conditions and the full length cDNA cloned into pDONR207 using Gateway technology (Invitrogen). *PpABI3A* coding region was amplified with specific primers (Supplementary Table 2.1) from *P. patens* cDNA and then cloned into pENTR/D-TOPO (Invitrogen) according to manufacturer's instructions. *SphABI3-16*, and *PpABI3A* full length cDNA sequences were transferred to pMN601 expression vector (Yoshida et al., 2019) under the control of the EF1α promoter by LR reaction (Gateway, Invitrogen).

2.2.10 - *P. patens* transformation and ABA sensitivity assays

SphABI3-16 and *PpABI3A* in pMN601 and pMN601 empty vector were used to transform the *P. patens ⊿abi3* strain (Khandelwal et al., 2010) by the polyethylene glycol–mediated method as previously described (Nishiyama et al., 2000). Colonies carrying a successful insert were selected on BCDAT plates containing 75μg/ml nourseothricin (NTC, Sigma). The presence of the insert, the targeting to the *PTA-1* locus and the presence of single and multiple insertions were detected by PCR using specific primers as detailed in Supplementary Figure 2.1 and Supplementary Table 2.1. Lines carrying the transgene were selected and transgene expression confirmed by qPCR using SphABI3-16 specific primers (Supplementary Table 2.1). For the colony growth in ABA medium, 10 single leaves of each of the different genotypes were removed from young gametophytes and transferred to both BCD media and BCD media supplemented with 25 μM ABA and incubated at 25°C for 32 days.

After this time, plates were scanned and colony diameter measured in ImageJ (https://imagej.nih.gov/). Percentage of growth in the ABA media was calculated in relation to colonies grown in BCD media alone. For the ABA protonemal growth assays, an equal amount of material for each genotype was homogenised in sterile water and used to inoculate BCDAT plates overlaid with cellophane disks (3 mL per plate) and allowed to grow for 7 days. After this time, cellophane disks were then transferred to BCD plates and BCD plates supplemented with 25 μM ABA (three replica per genotype, per treatment) and grown for a further 14 days. After this time, plates where imaged in colour using a flatbed scanner at a resolution of 300dpi using a white background. For each image, the red, green and blue channels were separated and binary masks were created in R (version 3.5.2) from the RGB .tif image. The binary masks were reapplied to the original image to create a pair of images with Green-dominant-pixels and Red-dominant pixels respectively. Green pixels were counted using the filters: [green:blue > 1.5] and [green:red > 1.05] and Red pixels were counted using the filters: [green:blue > 1.5] and [red:green > 1.05]. The percentage of green-dominant pixels in the treatment compared to the control was calculated for each line. The presence of red-dominant pixels was used as a proxy for stress in the treatment plates.

2.3 - Results

2.3.1 - Differential responses of *Sphagnum* species to controlled desiccation

To establish if *Sphagnum* species show differential desiccation responses related to their position within habitat, we chose four local species, representing the four major subgenera and with different distributions across the water table. *Sphagnum fallax* (subgenus Cuspidata) is found in lawns and hummocks, *Sphagnum papillosum* (subgenus Sphagnum) and *Sphagnum capillifolium* (subgenus Acutifolia) are predominantly hummock species, while *Sphagnum inundatum* (subgenus Subsecunda) is a typical hollow/pool species (Figure 2.1A). All four species are present in the bog at Pen y Garn (van de Koot et al., 2021) at different distances to the water table. *S. capillifolium* grows further away from the water table while *S. inundatum* is found primarily in ponds. *S. fallax* and *S. papillosum* occur at similar distances from the water table (Figure 2.1A). These four *Sphagnum* species were collected from the site (Figure 2.1A top row images) and subjected to a desiccation treatment in cosms, under greenhouse conditions (Figure 2.1A bottom row, B).

Besides occupying different microhabitats we noted marked morphological differences between the species, including colony density that may affect responses to desiccation treatments (Figure 2.1C). To take this into consideration, the average stem density in the field was determined for each species and used when planting the cosms. Cosms were weighed and imaged regularly over the water withdrawal period. Fresh weight loss and relative water content was calculated for each time point and the stress caused by water withdrawal assessed by measuring the photosynthetic activity recovery of PSII by calculating the Fv/Fm parameter in dark adapted samples (Maxwell and Johnson, 2000). *S. fallax*, *S. capillifolium* and *S. inundatum* showed similar rates of fresh weight loss and, 9 days after water withdrawal, plant weight was down to less than 10% of the original weight (Supplementary Figure 2.2). *S. papillosum* showed much slower fresh weight loss and did not reach the same stage of desiccation until 13 days after water withdrawal (Supplementary Figure 2.2). *Sphagnum*'s ability to store water has been attributed to anatomical features such as the size of capitula and the shape of the branches as well as the shape and number of specialised water-storage hyaline cells (Bengtsson et al., 2020). To take this into account, we calculated the Relative Water Content (RWC) for each sample. As seen with the fresh weight loss, *S. fallax*, and *S. inundatum*

showed a rapid decrease in RWC and by 7 days after water withdrawal the RWC of the capitula was near zero, while *S. capillifolium* showed a slightly slower decrease (Figure 2.2A). *S. papillosum* again showed a slow decrease in RWC across time and only reaching a similar point to the other species at day 13 (Figure 2.2A).

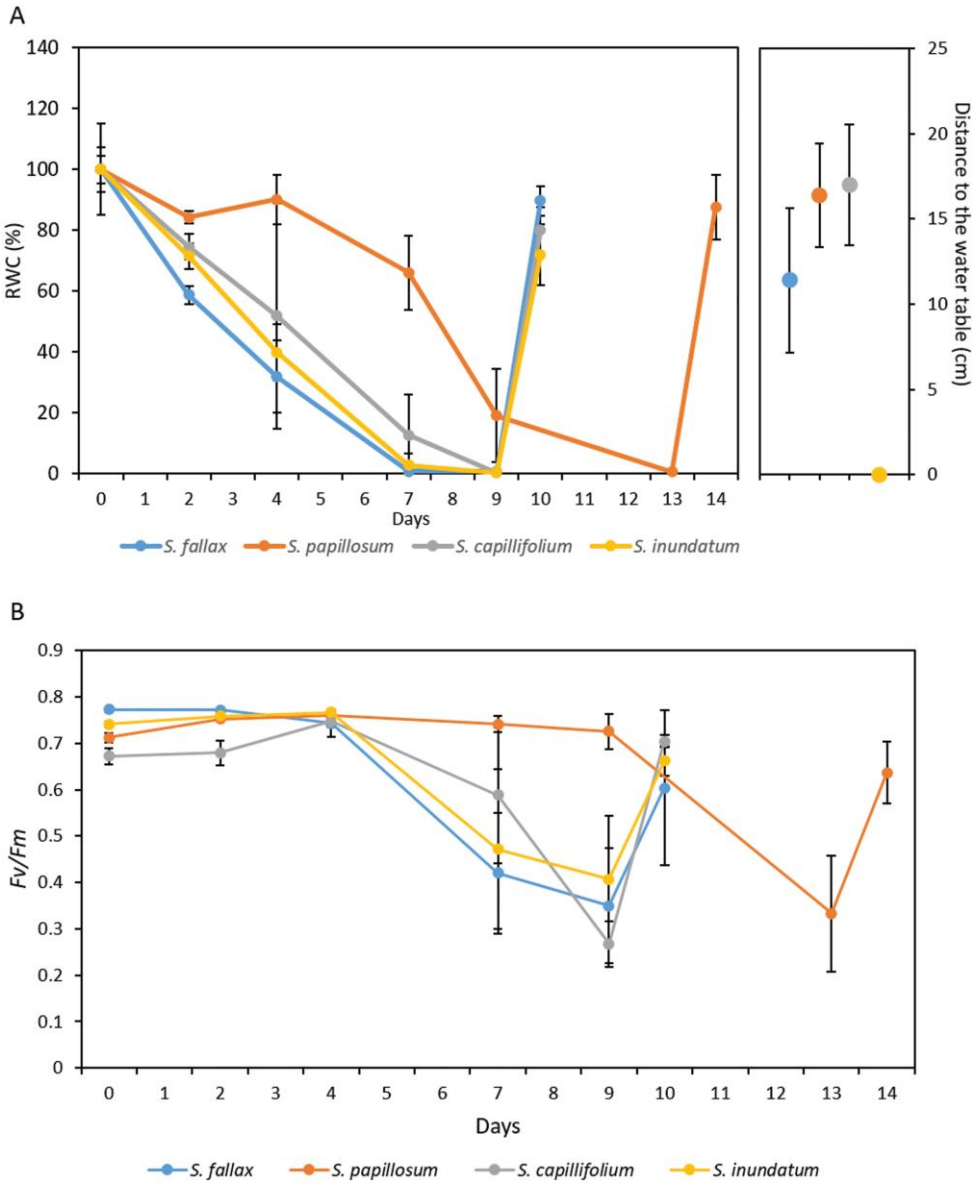

Figure 2.2. The effect of desiccation on relative water content (RWC) and chlorophyll fluorescence in the four different *Sphagnum* species.
Numbers on the *x* axis indicate days after water withdrawal. *S. fallax*, *S. capillifolium* and *S. inundatum* were re-watered on day 9 and *S. papillosum* on day 13.
A. Changes in relative water content (RWC) across the water withdrawal period for the different species. RWC was set to 100% for time zero and the percentage for the other time points calculated in relation to that time point. Data represent averages ± SD of four replica plates. The right-hand side panel show the water table height, average values ± SD for four measurements for the four species at the time of harvest.
B. The effect of desiccation on chlorophyll fluorescence (measured as Fv/Fm, see methods) over time in the four different species as indicated. Data represent average ± SD of four replica plates.

While the slower decrease in *S. papillosum* and to a lesser extent in *S. capillifolium* can be correlated with their position in relation to the water table, the same is not true for *S. fallax* and *S. inundatum* as they show similar rates of fresh weight loss despite being collected at different water table distances (Figure 2.2A). We next looked at the effect of desiccation on the photosynthetic activity of the different species by calculating the Fv/Fm ratio (see methods). Within the first four days after water withdrawal, the Fv/Fm ratio stayed constant or even showed a small increase in some of the species (Figure 2.2B). This increase in photosynthetic activity might be due to the reduction of the excess surface water allowing improved gas exchange. From day four onwards, the Fv/Fm ratio started to decrease, and as observed with the RWC, this decrease was more pronounced in *S. fallax* and *S. inundatum* and slightly slower in *S. capillifolium* (Figure 2.2B). By day nine, these three species showed Fv/Fm values between 0.2 and 0.4. In *S. papillosum*, the ratio Fv/Fm decreased more slowly and only reached a value of 0.3 at day thirteen (Figure 2.2B). At Fv/Fm values between 0.2 and 0.4, full recovery was still possible when plates were re-watered (Figure 2.2B). We also measured Fv/Fm recovery after re-watering when compared to the starting Fv/Fm ratio (Supplementary Figure 2.3). *S. capillifolium*, present at higher water table distances, fully recovered while *S. inundatum* and *S. papillosum* had recovery rates of around 90%. *S. fallax* showed high variation in recovery between replicas with three out of four replicas making full recovery and one not recovering (Supplementary Figure 2.3).

In addition to whole plant responses, we also looked at how different parts of the *Sphagnum* plant responded to desiccation. For this, we divided the chlorophyll fluorescence images in three regions, one encompassing the capitulum (top), the other the middle section of the stem (middle) and the last the basal senescing stem region (base) and calculated the Fv/Fm ratio for these regions across the water withdrawal period. The general changes in Fv/Fm of the three regions for the four species mirrored what was seen for the whole plant but there were differences in the rate of change (Supplementary Figure 2.4). While the three regions show similar starting values for Fv/Fm, as expected the top region showed a faster decrease in Fv/Fm suggesting a faster drying rate (Supplementary Figure 2.3A) while the base, less exposed to air flow, dried more slowly (Supplementary Figure 2.4C).

2.3.2 - Induction of drought-responsive genes in the different *Sphagnum* species

After determining that there were indeed differences in physiological responses to desiccation, we next asked if these changes are accompanied by changes in the expression of drought-responsive genes. For this we selected four genes known to be strongly upregulated upon drought in the moss *P. patens* (Cuming et al., 2007) and identified the *Sphagnum* homologues (Supplementary Table 2.1). AWPM19 is a drought-induced membrane protein that in rice promotes ABA influx into the cell (Yao et al., 2018); late embryogenesis abundant proteins group 3 (LEAs group 3) are also induced in response to desiccation and are important during seed maturation (Battaglia et al., 2008); synaptotagmins maintain membrane integrity under stress conditions (Schapire et al., 2008) and ABI3 is a central component of the ABA-induced desiccation tolerance in the moss *P. patens* (Khandelwal et al., 2010).

We observed increased expression of all genes as desiccation progressed but the magnitude of the change was different for each species (Figure 2.3). *S. fallax* and *S. papillosum* showed larger increases in expression of the genes with expression peaking at day seven, while in *S. capillifolium* and *S. inundatum* the relative increases were more modest (Figure 2.3). Interestingly, these two species show higher basal levels of expression in untreated material (Supplementary Figure 2.5). We observed a marked decrease in drought-responsive gene expression 24h after re-watering except for *S. papillosum* where expression was maintained at high levels (Figure 2.3). It is worth noting the high variability between the three biological samples seen in the large SD observed, especially at later time points, which probably reflect different drying rates for each cosm.

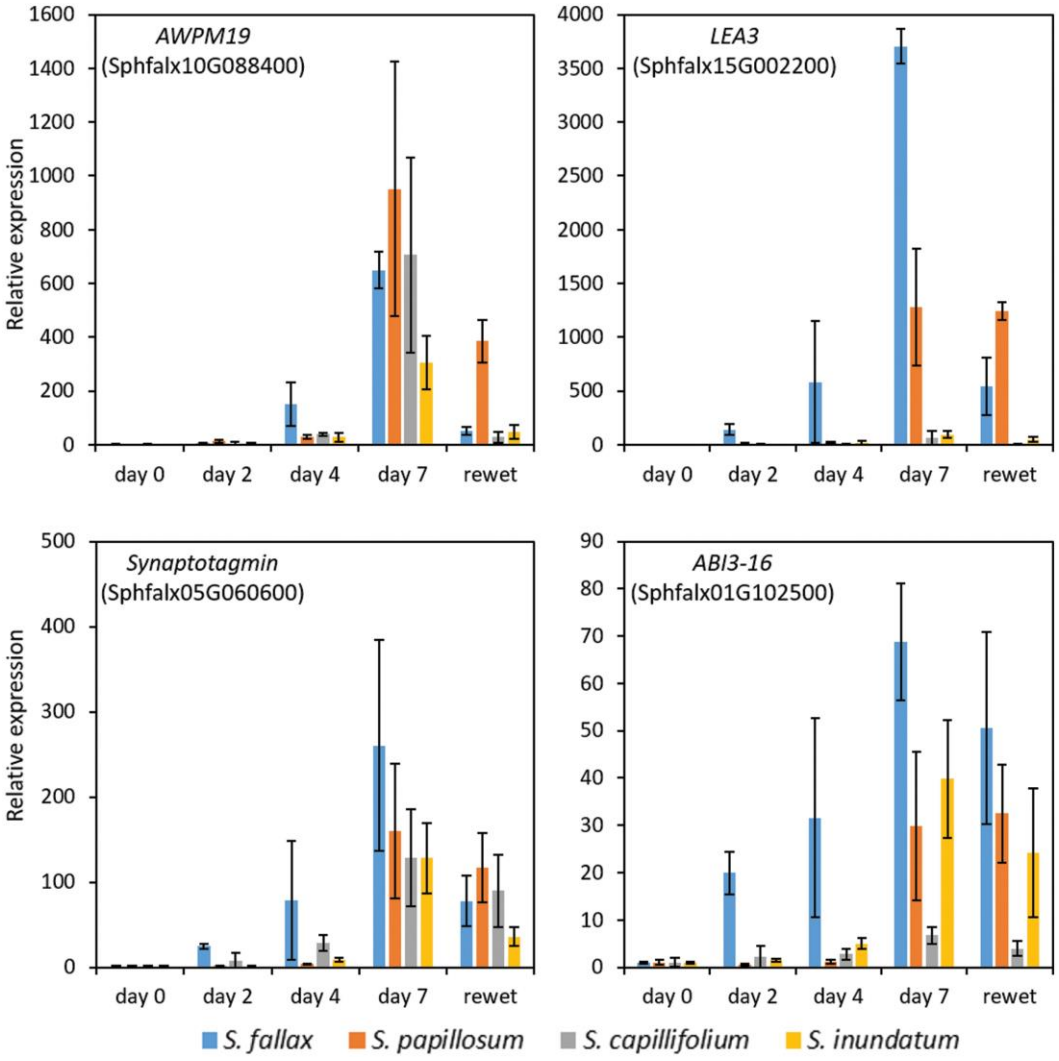

Figure 2.3. Analysis of drought-responsive gene expression in the four different *Sphagnum* species.
Plants in cosms were droughted for 7 d and then re-watered. Samples for RNA extraction were collected at 0, 2, 4, and 7 d and from re-watered material (0, 4, 7, 9 d and re-watered for S. papillosum). Expression of AWPM19 (Sphfalx10G088400), LEA3 (Sphfalx15G002200), Synaptotagmin (Sphfalx05G060600), and ABI3-16 (Sphfalx01G102500) was determined by qPCR using EF1α (Sphfalx03G087000) and GAPDH (Sphfalx16G076000) as reference genes as indicated over each graph. Each sample was done in triplicate and data represent means ±SD of three biological replicates. Expression at day 0 was set to 1 and all the other expression values calculated in relation to day 0.

2.3.3 - ABA mediates desiccation responses in *Sphagnum*

It is well established that ABA is a central regulator of drought responses in plants and that ABA production increases upon drought. Despite this, not much is known about the role of ABA in desiccation tolerance in *Sphagnum*. We measured ABA concentration per gram fresh weight, across the water withdrawal period for all

species. As the amount of water held by the plants varies drastically between samples as they dry, we adjusted the values using the RWC for each sample (see methods). We detected a low concentration of ABA in well-watered material (day 0) for all four species but ABA levels generally increased as drought progressed, peaking around day 4 (Figure 2.4A), preceding the peak of ABA-dependent gene expression at day 7 (Figure 2.3). Similar to what was observed with ABA-induced gene expression, the increase was more pronounced in *S. fallax* (Figure 2.4A). We also observed significant increases in endogenous ABA for *S. capillifolium* at day 7, while ABA levels increased slightly but not significantly in *S. papillosum* and *S. inundatum* (Figure 2.4A). Twenty-four hours after being re-watered, ABA levels had not yet returned to basal levels in the four species (Figure 2.4A).

Increases in ABA and ABA-responsive gene expression underpin drought responses, increasing the ability of the plants to tolerate mild drought (Chaves et al., 2003). To determine if this is also the case in *Sphagnum*, we tested the effect of ABA pre-treatment on the desiccation response of *S. fallax* plants in cosms. We used two ABA concentrations, 10μM and 50μM to pre-treat *S. falla*x plants for 24h before water withdrawal. Desiccation responses were evaluated by measuring photosynthetic performance by calculating the Fv/Fm ratio. *S. fallax* plants were allowed to dry until Fv/Fm reached 0.2 and kept (i) at this value for 24h and then re-watered or (ii) for 4 days and then re-watered. After re-watering, Fv/Fm was again measured and the percentage recovery (Fv/Fm after re-watering/starting Fv/Fm*100) was calculated for all treatments. Pre-treatment with either 10μM or 50μM ABA increased Fv/Fm recovery after 24h at 0.2 Fv/Fm, while at the harsher treatment of four days at Fv/Fm of 0.2, only 50μM ABA significantly improved recovery (Figure 2.4B).

Taken together, these data suggest that ABA is an important component of drought responses in *Sphagnum*.

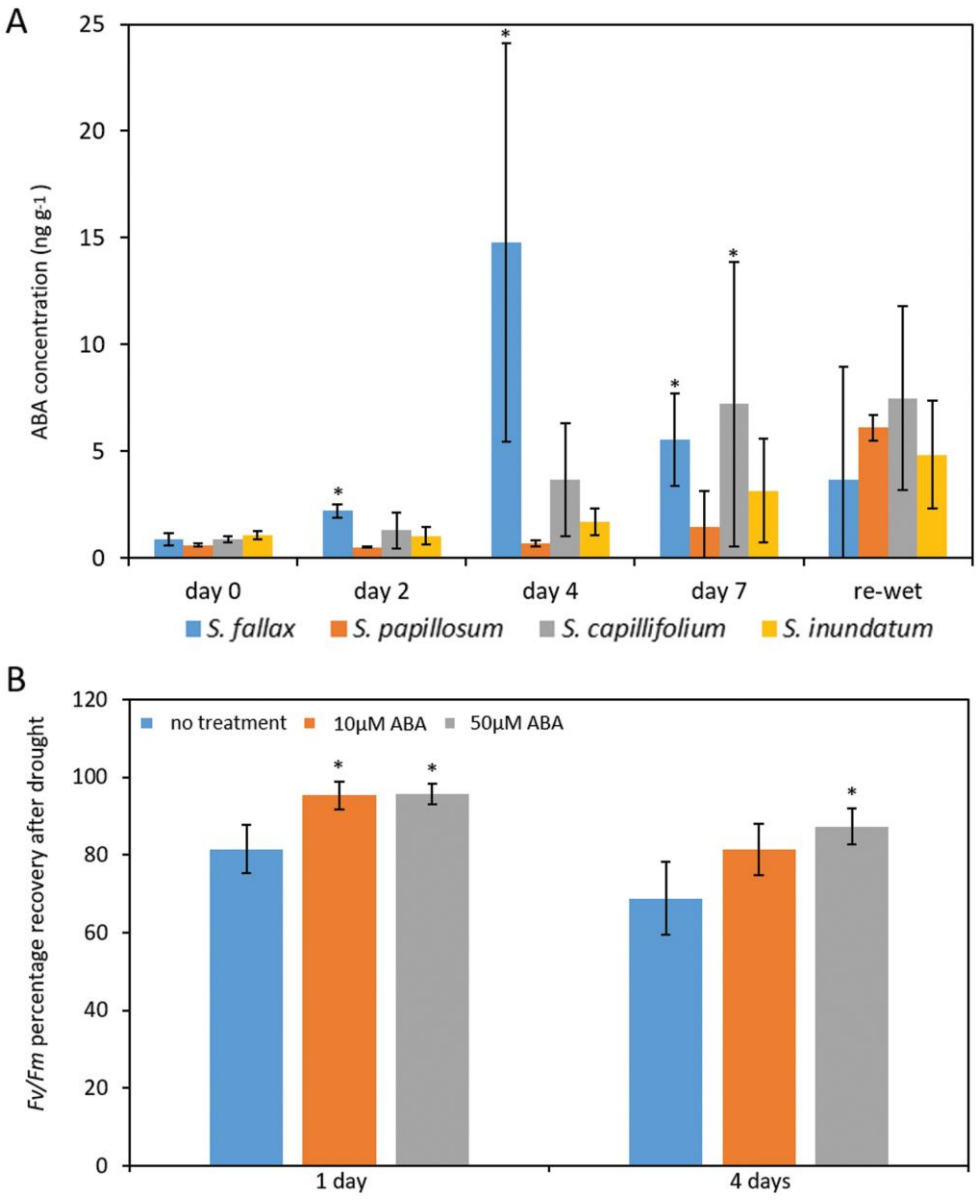

Figure 2.4. ABA signalling pathways are activated upon desiccation in *Sphagnum*. (A) Desiccation increases ABA in *Sphagnum*. Capitula from the different species were harvested at 0, 2, 4, 7 d after drought and from re-watered samples. ABA levels were determined by GC-MS. ABA concentrations were then adjusted in relation to the relative water content of each sample. Data represent means ±SE for three biological replicates. (B) ABA pre-treatment improves desiccation tolerance in *Sphagnum*. *Sphagnum fallax* plants were desiccated until Fv/Fm value reached 0.2 and kept at this stage for 1 or 4 d before re-watering as indicated. The percentage Fv/Fm recovery was calculated at day 2 after re-watering in relation to the initial Fv/Fm values. Data represent means ±SD for four replicate plates. *Significantly different from the untreated plants, $P<0.05$.

2.3.4 - Many genes involved in ABA signalling pathways are conserved in *Sphagnum*

Many of the ABA signalling components from perception to signal transduction have been identified in the model plant *Arabidopsis* and found to be conserved across many other species (Cai et al., 2017; Sun et al., 2020). Querying of the available *Sphagnum* genome sequences (*S. fallax* and *S. magellanicum*) showed that these components are also present in *Sphagnum* (Supplementary Figure 2.6-8). All the core ABA signalling proteins, PYR/RYL (ABA receptors, Supplementary Figure 2.6), SnRK2 (ABA-signalling regulators, Supplementary Figure 2.7), and ABI5s (transcription factors phosphorylated by activated SnRK2, Supplementary Figure 2.7) were found in the *Sphagnum* genome. In particular, the phylogenetic trees of PYR/RYC and SnRK2 indicate that bryophyte species have fewer PYR/RYC and SnRK2 genes than vascular plants (Supplementary Figure 2.7,8). Surprisingly, while homologues of the clade F of protein phosphatases (PP2Cs) are present in *Sphagnum*, we were not able to find any homologues for clade A (Supplementary Figure 2.9). This clade of PP2Cs is found in other bryophytes and includes Arabidopsis ABI1/2, HAB1/2, and AHG1/3 that together with PYR act as co-receptors for ABA (Nishimura et al., 2010).

The plant-specific ABI3 family of transcription factors plays a critical role during seed development desiccation tolerance and is an important regulator of ABA-mediated responses to abiotic stresses (Sakata et al., 2010). In *P. patens* mutants (*Δabi3*) lacking three of the ABI3 genes (*PpABI3A/B/C*) have increased drought and desiccation tolerance and reduced sensitivity to exogenously applied ABA (Khandelwal et al., 2010; Tan et al., 2017; Zhao et al., 2018).
In order to determine if these functions are conserved in ABI3 proteins from *Sphagnum* moss, we cloned one of the five *Sphagnum* ABI3 homologues (Figure 2.5; SphABI3-16 (Sphfalx01G102500)) and asked if it could rescue the *Δabi3* phenotype. When grown on media supplemented with 25µM ABA for 32 days, wild type *P. patens* shows around 20% of the growth in the ABA-free media while the *Δabi3* mutant shows a growth of around 50% (Figure 2.6A,B). This increased growth is maintained when the *Δabi3* mutant is transformed with an empty vector construct however, growth returns to wild type levels when the *Δabi3* mutant is transformed with the endogenous *PpABI3A* gene (Figure 2.6A,B).

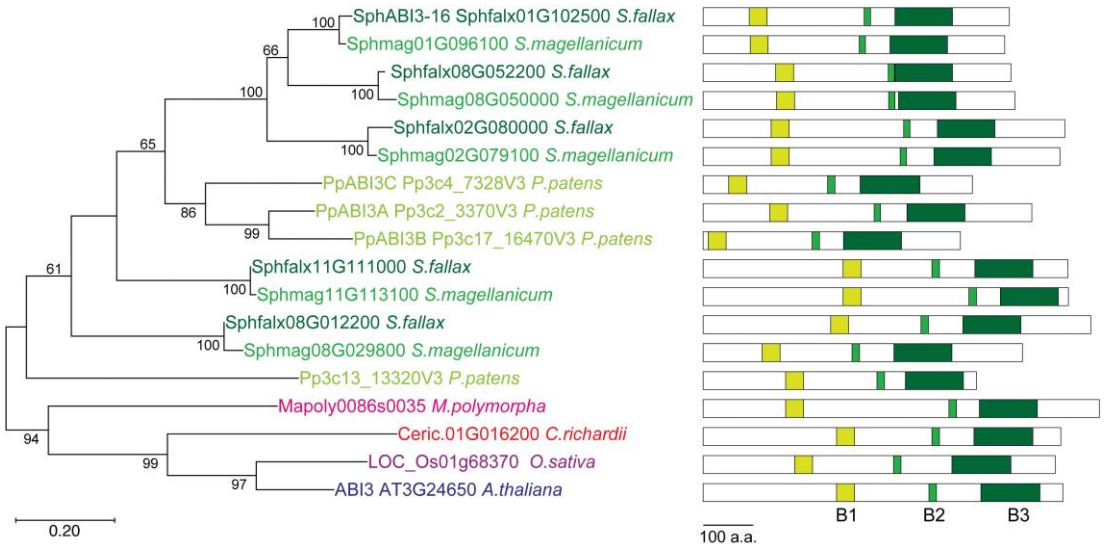

Figure 2.5. A phylogenetic tree of ABI3 proteins.
The tree was constructed with the maximum likelihood method using the JTT-based matrix. The tree with the highest log likelihood is shown. Bootstrap values of >50% are shown on the branches. Horizontal branch length is proportional to the estimated evolutionary distance. Schematic representations of the corresponding protein structure, including the conserved B1–B3 domains indicated by the green boxes, are also shown.

When the *Δabi3* mutant is transformed with *SphABI3-16*, growth in ABA media is also inhibited returning to wild type levels in lines #31 and #37(Figure 2.6A,B). Interestingly, in line #7, growth is indistinguishable from the untransformed *Δabi3* mutant (Figure 2.6A,B) but, despite carrying the *SphABI3-16* construct we could not detect expression in this line(Figure 2.6C). As the transgene in this line is not found at the *PTA-1* locus, the lack of expression might be due to where the transgene was inserted within the genome.

Exogenous ABA application is also known to affect protonemal growth and choronemal cell morphology in *P. patens*. Protonemal growth is inhibited when wild type *P. patens* is grown on media containing 25μM ABA (Figure 2.6D,E). Consistent with having decreased sensitivity to ABA, this growth inhibition is not observed in the *Δabi3* mutant. Expression of *PpABI3A* in the *Δabi3* mutant background recovers the wild type phenotype (Figure 2.6D,E). Expression of *SphABI3-16* in the *Δabi3* mutant background not only restored growth sensitivity to ABA, but also resulted in the protonemal growth becoming oversensitive to exogenous ABA application (Figure 2.6D,E). Interestingly, the *Δabi3* lines expressing either *PpABI3A* or *SphABI3-16* when grown on ABA media, also produced increased amount of red pigments suggesting increased stress levels in

these plants (Supplementary Figure 2.10). Another effect of ABA application is the increased branching of chloronemal cells. As expected from the reduced sensitivity of the *Δabi3* mutant, we observed reduced chloronemal branching when this line was grown on ABA-containing media (Figure 2.6 A, bottom row). Consistent with the results described above, the *Δabi3* mutant transformed with either the endogenous *PpABI3A* or *SphABI3-16* showed wild-type like phenotype of increased branching (Figure 2.6 A, bottom row).

These data indicate that *Sphagnum* contains an ABA signalling system functionally equivalent to that of other mosses and higher plants, further supporting a role for ABA during desiccation responses in *Sphagnum*.

2.4 - Discussion

By using a comprehensive physiological and molecular approach, we show that different *Sphagnum* species do respond differently to a controlled induced desiccation, but, surprisingly, this is not always correlated with their position relative to the water table.

Sphagnum mosses have been considered to be desiccation-avoiding rather than tolerant (Clymo, 1973; Clymo and Hayward, 1982). In this scenario, they have evolved systems to store large amounts of water with 90% of all water stored in extracellular spaces and 10% in hyaline cells (Clymo and Hayward, 1982). Detached *Sphagnum* capitula have been shown to have a water content of 700-1200% relative to plant weight for optimal photosynthesis (Bengtsson et al., 2016), high values as compared to other bryophytes and most other land plants. Of the four species that we used for our studies, *S. inundatum* showed the highest capitula water content (2498%±181), followed by *S. papillosum* (2121%±205) and *S. fallax* and *S. capillifolium* having similar water content values (1458%±107 and 1441%±217).

Unexpectedly these values do not correlate with their position along the water table (Figure 2.2A) but are probably a reflection of plant morphology (Figure 2.1). Both *S. papillosum* and *S. inundatum* have larger capitula than the other two species and have longer more densely packed branches, which are able to store larger amounts of water (Figure 2.1). After water withdrawal, all species except *S. papillosum* lose water very quickly reaching a RWC 10-20% within a week. The slower fresh weight loss in *S. papillosum* is probably due to a combination of larger capitula and longer branches and the densely packed canopy they form. On the other hand, while *S. inundatum* plants also have large capitula, they are found in pools at low plant density and this may explain the fast fresh weight loss.

A recent study by (Bengtsson et al., 2020) showed that there is a correlation between anatomical traits such as leaf width and hyaline cell pore size and water retention. The authors also showed similar relationships between RWC and Fv/Fm for *S. fallax* and *S. papillosum* species in common with our study. Interestingly, their pool species *S. cuspidatum*, also showed high initial RWC as we observed in *S. inundatum* (Bengtsson et al., 2020). Although previous studies (Schipperges and Rydin, 1998) suggest that at RWC levels lower than 10-20% *Sphagnum* plants do not recover, we found that even at RWC values near zero, recovery after re-watering was

nearly 100% (Figure 2.2A). It should be noted that we found that longer periods at RWC<10% do affect survival in all species (data not shown).

Our data show that the initial rapid fresh weight loss rate does not have an immediate impact on the physiological status as determined by the Fv/Fm ratio that measures the quantum efficiency of photosystem II and gives an indirect measure of plant stress (Figure 2.2B). For *S. fallax*, S. *capillifolium* and *S. inundatum*, the Fv/Fm ratio is stable for the first 4-5 days suggesting that the plant is not stressed at RWC of around 50%. The first physiological signs of stress appear between day 5 and day 7 after water withdrawal. During this period, the RWC falls to less than 20% and there is a sharp decrease in the Fv/Fm ratio to values between 0.4-0.6, accompanied by the induction of the expression of drought related genes (Figure 2.3). At day 9, the RWC nears zero and the Fv/Fm ratio decreases to around 0.2. For *S. papillosum* on the other hand, this is not attained until day 13, again underscoring the high water holding capacity of this species. As early as 24h after re-watering, both the RWC and the Fv/Fm ratio recover to levels close to the starting point suggesting that *Sphagnum* is able to tolerate mild desiccation without significant plant damage. While some studies describe similar levels of recovery, others report very poor recovery after desiccation (Gerdol et al., 1996; Hájek and Beckett, 2008; Hájek and Vicherová, 2014; Wagner and Titus, 1984). One possible factor in these differences is the levels of hardening that the plants were subjected to before the experiment. The plants we used had been naturally exposed to varied degrees of desiccation and rehydration in the field and we did not allow for any greenhouse adaptation time. They may have developed a degree of hardening that is impacting on the observed desiccation tolerance.

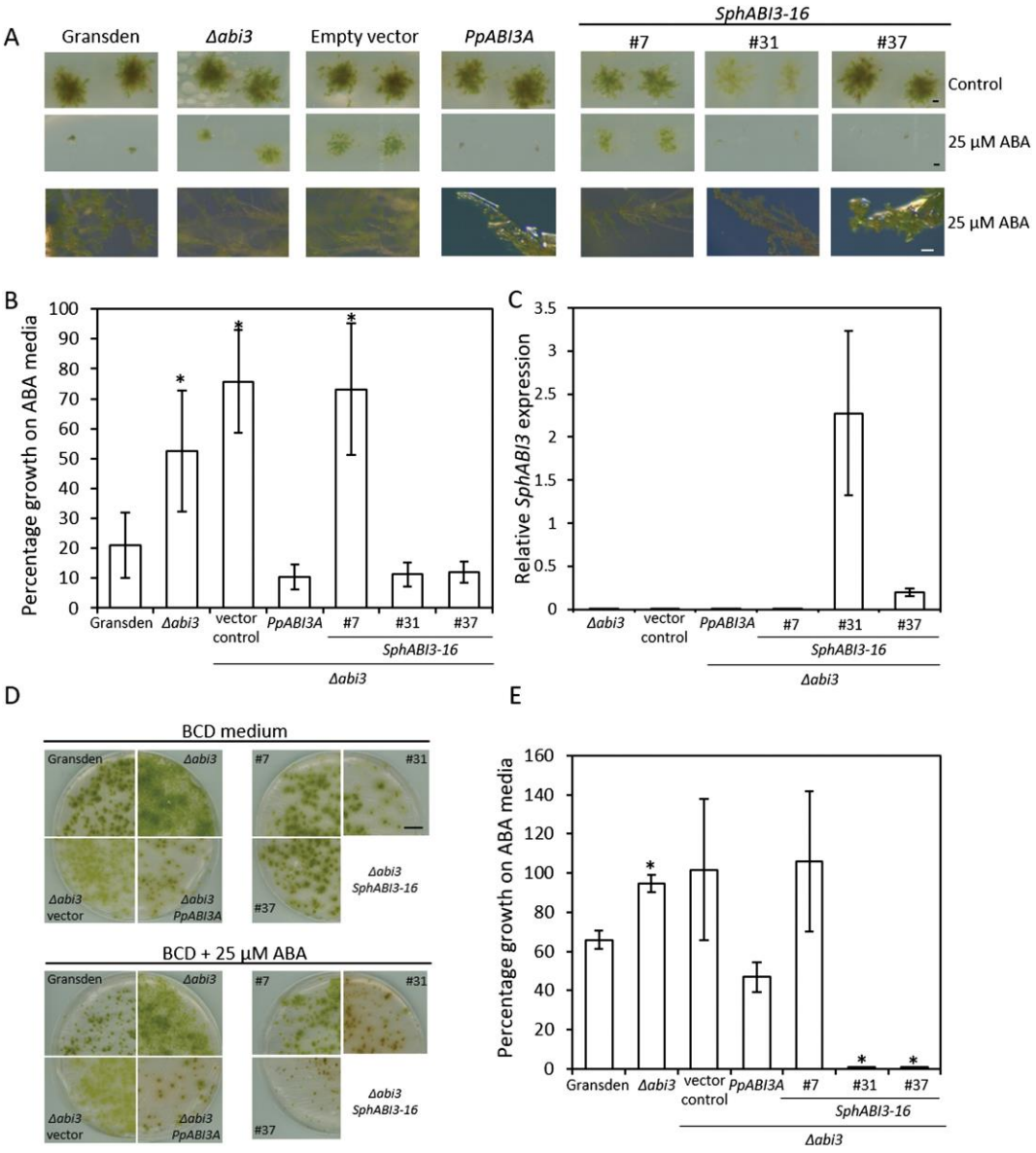

Figure 2.6. *Sphagnum* ABI3 rescues the phenotype of the Δabi3 mutant in *P. patens*.
(A) Colony growth in wild type *P. patens* (Gransden), Δabi3 mutant, and Δabi3 mutant transformed with all the different potential rescue constructs as indicated. Single leaves were grown in BCD medium (top row) or BCD medium supplemented with 25 µM ABA (middle row) for 32 d. Scale bar: 500µm. Bottom row shows detail of the colony structure of the plants grown in the ABA medium (scale bar: 100 µm).
(B) Relative colony growth in ABA medium for wild type (Gransden), Δabi3 mutant, and the rescue transformants as shown above. After 32 d growth, colony diameter was measured and the percentage of growth in the ABA-containing medium was calculated in relation to the media without ABA. Data show means ±SD of 10 colonies. *Significantly different from wild type, P<0.001.
(C) Increased ABI3 expression in the transformed Δabi3 mutant was confirmed by qPCR. Data show means ±SD of three replicates. Expression of P. patens EF1α was used as a reference. (D, E). Protonemal growth of wild type (Gransden), Δabi3 mutant and the rescue transformants in BCD medium or BCD medium supplemented with 25 µM ABA as indicated.
(D) Representative images of each genotype after 14 d growth.
(E) Quantification of protonemal growth. After 14 d growth, plates were scanned and growth (total green pixels in the image) was calculated for each plate. The percentage of growth in

the ABA containing medium was calculated in relation to the medium without ABA. Data show means ±SE of three plates per genotype. *Significantly different from wild type, P<0.001.

In agreement with some recent studies, we did not observe significant differences in desiccation tolerance between hummock and hollow species (Bengtsson et al., 2020; Hájek and Beckett, 2008; Hájek and Vicherová, 2014; Oliver et al., 2005; Proctor et al., 2007; Schipperges and Rydin, 1998; Wagner and Titus, 1984).

The molecular signatures of drought responses seem to be conserved in *Sphagnum* as many of the genes found to be up-regulated by drought in other species are also upregulated in drying *Sphagnum* (Figure 2.3 and data not shown) and together with the observed increases in ABA, suggest the existence of an inducible desiccation response pathway in *Sphagnum*.

2.4.1 - ABA as an important component of desiccation responses in *Sphagnum*

Evolutionary analysis of ABA signalling pathways suggest that ABA has been used ancestrally as a stress hormone in land plants and that it might have evolved to enable drought and desiccation tolerance in the new land environment (Cuming, 2019; Sun et al., 2020; Wang et al., 2015). Many of the ABA synthesis, perception and signalling components have been identified in a range of land plants and their functions seem to be broadly maintained (Guillory and Bonhomme, 2021). In the mosses *P. patens* and *Funaria* drought has been shown to increase endogenous ABA concentrations (Knight et al., 1995; Werner et al., 1991). ABA pre-treatment has been shown to increase drought tolerance in several crop species (An et al., 2014; Brito et al., 2020; Changning et al., 2014; Lu et al., 2009; Skowron and Trojak, 2021; Wei et al., 2015) and also in mosses, including one study in *Sphagnum* (Beckett et al., 2000; Hájek and Beckett, 2008; Khandelwal et al., 2010; Wagner and Titus, 1984). We also observed an increase of endogenous ABA during desiccation in *Sphagnum*. ABA levels were at the highest at day 4 (Figure 2.4), preceding the peak of ABA-induced gene expression observed at day 7 (Figure 2.3). ABA levels did not increase after day 4 in line with what was observed in other species (Scholz et al., 2015). Notably, 24h after the plants were re-watered, we observed decreased gene

expression but levels of ABA were still high suggesting that it takes longer for ABA levels to return to normal in re-watered *Sphagnum* plants. In *S. fallax*, the more desiccation sensitive of the species used, the increases in ABA levels were the highest while more modest increases were seem in *S. capillifolium*. In the most desiccation resistant species, *S. papillosum*, levels of ABA were lowest and possibly sampling at later time points would be necessary to detect larger increases in ABA.

In *S. inundatum*, ABA levels stayed constant at low levels and this was also the case for drought responsive gene expression (Figure 2.3, 2.4). Being a hollow species, one would expect that *S. inundatum* would need to quickly respond to the lack of water, and, as it has been proposed that it does not possess the same desiccation avoidance mechanisms as hummock species (Mazziotta et al., 2019), which may have adapted by evolving the faster ABA-dependent pathways. Our data suggest that this may not be the case and *S. inundatum* relies on other mechanisms for desiccation tolerance such as the proposed resource acquisition (Mazziotta et al., 2019). Alternatively as the basal level of drought-responsive gene expression is high in this species when compared to the others (Supplementary Figure 2.5), it is possible that some aspects of the desiccation response may be constitutively activated in this species.

2.4.2 - ABA-mediated drought signalling is conserved in *Sphagnum*

Sphagnum species also merit attention in the context of the plant's transition from aquatic to terrestrial life. A critical step in the water to land transition was the acquisition of desiccation tolerance and, although Sphagna are thought to be mainly desiccation avoidant, our data suggest that they have a basal level of desiccation tolerance and this involves, at least in part, ABA. We found that the main components of ABA responses are conserved in *Sphagnum* with the notable exception of clade A PPC2As that include the ABA co-receptor ABI1 (Bhaskara et al., 2019; Nishimura et al., 2010). The fact that we were not able to find ABI1 homologues in the *Sphagnum* genome could be due to the homology thresholds we used although this is unlikely as we were able to find homologues in *P. patens* and *M. polymorpha*. Another possibility is that these genes are not correctly annotated in the *Sphagnum* genome versions that we used to build our phylogenies (*S. fallax* v1.1 and *S. magellanicum* v1.1). Otherwise, the prospect that ABI1 homologues not being

present in *Sphagnum* raises the interesting possibility that *Sphagnum* has co-adopted other proteins, maybe PP2Cs from other clades for example clade F that seems to have expanded in *Sphagnum* (Supplementary Figure 2.9), as ABA co-receptors.

Our data also shows that the function of ABA signalling components is conserved in *Sphagnum* as demonstrated by the ABI3 protein. In tracheophytes, ABI3 was first identified as a seed specific transcriptional activator (Finkelstein and Somerville, 1990). While its role during seed development remains best documented, ABI3 has been found to be important in other vegetative tissues where it controls developmental transitions, and stress responses (Bedi et al., 2016; Rohde et al., 2000). Its functions extend outside seeded plants and may have even diversified in mosses where we find an expansion of the number of ABI3 proteins (five in *Sphagnum fallax* and four in *P. patens* compared to one in Arabidopsis and one in rice; Figure 2.5). In *P. patens,* loss of function mutants in three of the *ABI3* genes show decreased ABA sensitivity and are more sensitive to desiccation and other stresses (Khandelwal et al., 2010; Marella et al., 2006; Takenaka et al., 2007; Tan et al., 2017; Zhao et al., 2018). We found that heterologous expression of the *Sphagnum* ABI3 orthologue rescues the phenotype of loss of function *Δabi3* mutant in *P. patens* (Figure 2.6).

This is the first time that an ABA-pathway gene from *Sphagnum* has been functionally characterized and has several implications. The first is that ABA-mediated responses to stress are conserved in *Sphagnum* as was observed for other mosses (Cuming, 2019; Guillory and Bonhomme, 2021). It will be interesting to determine if the role of ABA in other developmental pathways such as gametophyte development and spore germination is also conserved in *Sphagnum*. In addition, there is evidence that, although there is broader conservation of ABA pathways in other mosses, the molecular and physiological responses as well as the interaction with other hormone pathways are different from the ones observed in vascular plants. Further detailed studies in *Sphagnum* will give better insight into the evolution of ABA signalling pathways (Cuming, 2019; Guillory and Bonhomme, 2021).

Secondly, our studies confirm the usefulness of using *P. patens* as a heterologous functional expression system for species without an established transformation protocol (Rensing et al., 2020). The ease of transformation and the existence of well-characterised mutants in many of the developmental and stress signalling pathways in *Physcomitrium* are valuable resources to test the functionality

of other *Sphagnum* genes. Lastly, our data support earlier observations that *Sphagnum* is able to tolerate significant levels of dehydration without losing photosynthetic capacity and this should be taken into consideration when modelling the global responses of peatlands to changes in climate patterns especially precipitation (Cruz de Carvalho et al., 2019; Dise, 2009; Hájek and Vicherová, 2014; Oliver et al., 2005; Proctor, 2000; Proctor et al., 2007; Rastogi et al., 2020; Schipperges and Rydin, 1998; Wagner and Titus, 1984).

2.5 - References

Ali, S., Hayat, K., Iqbal, A., Xie, L., 2020. Implications of abscisic acid in the drought stress tolerance of plants. Agronomy 10, 1–28. https://doi.org/10.3390/agronomy10091323

An, Y., Zhou, P., Liang, J., 2014. Effects of exogenous application of abscisic acid on membrane stability, osmotic adjustment, photosynthesis and hormonal status of two lucerne (Medicago sativa L.) genotypes under high temperature stress and drought stress. Crop Pasture Sci. 65, 274–286. https://doi.org/10.1071/CP13162

Banks, J.A., Nishiyama, T., Hasebe, M., Bowman, J.L., Gribskov, M., DePamphilis, C., Albert, V.A., Aono, N., Aoyama, T., Ambrose, B.A., Ashton, N.W., Axtell, M.J., Barker, E., Barker, M.S., Bennetzen, J.L., Bonawitz, N.D., Chapple, C., Cheng, C., Correa, L.G.G., Dacre, M., DeBarry, J., Dreyer, I., Elias, M., Engstrom, E.M., Estelle, M., Feng, L., Finet, C., Floyd, S.K., Frommer, W.B., Fujita, T., Gramzow, L., Gutensohn, M., Harholt, J., Hattori, M., Heyl, A., Hirai, T., Hiwatashi, Y., Ishikawa, M., Iwata, M., Karol, K.G., Koehler, B., Kolukisaoglu, U., Kubo, M., Kurata, T., Lalonde, S., Li, K., Li, Y., Litt, A., Lyons, E., Manning, G., Maruyama, T., Michael, T.P., Mikami, K., Miyazaki, S., Morinaga, S.-I., Murata, T., Mueller-Roeber, B., Nelson, D.R., Obara, M., Oguri, Y., Olmstead, R.G., Onodera, N., Petersen, B.L., Pils, B., Prigge, M., Rensing, S.A., Riaño-Pachón, D.M., Roberts, A.W., Sato, Y., Scheller, H. V, Schulz, B., Schulz, C., Shakirov, E. V, Shibagaki, N., Shinohara, N., Shippen, D.E., Sørensen, I., Sotooka, R., Sugimoto, N., Sugita, M., Sumikawa, N., Tanurdzic, M., Theißen, G., Ulvskov, P., Wakazuki, S., Weng, J., Willats, W.W.G.T., Wipf, D., Wolf, P.G., Yang, L., Zimmer, A.D., Zhu, Q., Mitros, T., Hellsten, U., Loqué, D., Otillar, R., Salamov, A., Schmutz, J., Shapiro, H., Lindquist, E., Lucas, S., Rokhsar, D., Grigoriev, I. V, 2011. The Selaginella Genome IdentifiesGenetic Changes Associated withthe Evolution of Vascular Plants. Science (80-.). 332, 960–964.

Battaglia, M., Olvera-Carrillo, Y., Garciarrubio, A., Campos, F., Covarrubias, A.A., 2008. The enigmatic LEA proteins and other hydrophilins. Plant Physiol. 148, 6–24. https://doi.org/10.1104/pp.108.120725

Beckett, R.P., Csintalan, Z., Tuba, Z., 2000. ABA treatment increases both the desiccation tolerance of photosynthesis, and nonphotochemical quenching in the moss Atrichum undulatum. Plant Ecol. 151, 65–71. https://doi.org/10.1023/A

Bedi, S., Sengupta, S., Ray, A., Nag Chaudhuri, R., 2016. ABI3 mediates dehydration stress recovery response in Arabidopsis thaliana by regulating expression of downstream genes. Plant Sci. 250, 125–140. https://doi.org/10.1016/j.plantsci.2016.06.006

Bengtsson, F., Granath, G., Cronberg, N., Rydin, H., 2020. Mechanisms behind species-specific water economy responses to water level drawdown in peat mosses. Ann. Bot. 126, 219–230. https://doi.org/10.1093/aob/mcaa033

Bengtsson, F., Granath, G., Rydin, H., 2016. Photosynthesis, growth, and decay traits in Sphagnum - a multispecies comparison. Ecol. Evol. 6, 3325–3341. https://doi.org/10.1002/ece3.2119

Bhaskara, G.B., Wong, M.M., Verslues, P.E., 2019. The flip side of phospho-signalling: Regulation of protein dephosphorylation and the protein phosphatase 2Cs. Plant Cell Environ. 42, 2913–2930. https://doi.org/10.1111/pce.13616

Bowman, J.L., Kohchi, T., Yamato, K.T., Jenkins, J., Shu, S., Ishizaki, K., Yamaoka,

S., Nishihama, R., Nakamura, Y., Berger, F., Adam, C., Aki, S.S., Althoff, F., Araki, T., Arteaga-Vazquez, M.A., Balasubrmanian, S., Barry, K., Bauer, D., Boehm, C.R., Briginshaw, L., Caballero-Perez, J., Catarino, B., Chen, F., Chiyoda, S., Chovatia, M., Davies, K.M., Delmans, M., Demura, T., Dierschke, T., Dolan, L., Dorantes-Acosta, A.E., Eklund, D.M., Florent, S.N., Flores-Sandoval, E., Fujiyama, A., Fukuzawa, H., Galik, B., Grimanelli, D., Grimwood, J., Grossniklaus, U., Hamada, T., Haseloff, J., Hetherington, A.J., Higo, A., Hirakawa, Y., Hundley, H.N., Ikeda, Y., Inoue, K., Inoue, S. ichiro, Ishida, S., Jia, Q., Kakita, M., Kanazawa, T., Kawai, Y., Kawashima, T., Kennedy, M., Kinose, K., Kinoshita, T., Kohara, Y., Koide, E., Komatsu, K., Kopischke, S., Kubo, M., Kyozuka, J., Lagercrantz, U., Lin, S.S., Lindquist, E., Lipzen, A.M., Lu, C.W., De Luna, E., Martienssen, R.A., Minamino, N., Mizutani, Masaharu, Mizutani, Miya, Mochizuki, N., Monte, I., Mosher, R., Nagasaki, H., Nakagami, H., Naramoto, S., Nishitani, K., Ohtani, M., Okamoto, T., Okumura, M., Phillips, J., Pollak, B., Reinders, A., Rövekamp, M., Sano, R., Sawa, S., Schmid, M.W., Shirakawa, M., Solano, R., Spunde, A., Suetsugu, N., Sugano, S., Sugiyama, A., Sun, R., Suzuki, Y., Takenaka, M., Takezawa, D., Tomogane, H., Tsuzuki, M., Ueda, T., Umeda, M., Ward, J.M., Watanabe, Y., Yazaki, K., Yokoyama, R., Yoshitake, Y., Yotsui, I., Zachgo, S., Schmutz, J., 2017. Insights into Land Plant Evolution Garnered from the Marchantia polymorpha Genome. Cell 171, 287-304.e15. https://doi.org/10.1016/j.cell.2017.09.030

Brito, C., Dinis, L.T., Ferreira, H., Moutinho-Pereira, J., Correia, C.M., 2020. Foliar pre-treatment with abscisic acid enhances olive tree drought adaptability. Plants 9. https://doi.org/10.3390/plants9030341

Cai, S., Chen, G., Wang, Yuanyuan, Huang, Y., Marchant, D.B., Wang, Yizhou, Yang, Q., Dai, F., Hills, A., Franks, P.J., Nevo, E., Soltis, D.E., Soltis, P.S., Sessa, E., Wolf, P.G., Xue, D., Zhang, G., Pogson, B.J., Blatt, M.R., Chen, Z.H., 2017. Evolutionary conservation of ABA signaling for stomatal closure. Plant Physiol. 174, 732–747. https://doi.org/10.1104/pp.16.01848

Changning, L., Litao, Y., Srivastava, M., Yangrui, L., 2014. Foliar application of abscisic acid improves drought tolerance of sugarcane plant under severe water stress. Int. J. Agric. Innov. Res. 3, 101–107.

Charron, A.J., Quatrano, R.S., 2009. Between a rock and a dry place: The water-stressed moss. Mol. Plant 2, 478–486. https://doi.org/10.1093/mp/ssp018

Chaves, M.M., Maroco, J.P., Pereira, J.S., 2003. Understanding plant responses to drought - From genes to the whole plant. Funct. Plant Biol. 30, 239–264. https://doi.org/10.1071/FP02076

Cheng, C.Y., Krishnakumar, V., Chan, A.P., Thibaud-Nissen, F., Schobel, S., Town, C.D., 2017. Araport11: a complete reannotation of the Arabidopsis thaliana reference genome. Plant J. 89, 789–804. https://doi.org/10.1111/tpj.13415

Clymo, R.S., 1973. The Growth of Sphagnum: Some Effects of Environment. J. Ecol. 61, 849. https://doi.org/10.2307/2258654

Clymo, R.S., Hayward, P.M., 1982. The Ecology of Sphagnum, in: Bryophyte Ecology. Springer Netherlands, Dordrecht, pp. 229–289. https://doi.org/10.1007/978-94-009-5891-3_8

Cruz de Carvalho, R., Maurício, A., Pereira, M.F., Marques da Silva, J., Branquinho, C., 2019. All for One: The Role of Colony Morphology in Bryophyte Desiccation Tolerance. Front. Plant Sci. 10, 1–12. https://doi.org/10.3389/fpls.2019.01360

Cuming, A.C., 2019. Evolution of ABA signaling pathways, Advances in Botanical Research. Elsevier Ltd. https://doi.org/10.1016/bs.abr.2019.06.003
Cuming, A.C., Cho, S.H., Kamisugi, Y., Graham, H., Quatrano, R.S., 2007. Microarray analysis of transcriptional responses to abscisic acid and osmotic, salt, and drought stress in the moss, Physcomitrella patens. New Phytol. 176, 275–287. https://doi.org/10.1111/j.1469-8137.2007.02187.x
Dilks, T.J.K., Proctor, M.C.F., 1979. Photosynthesis, Respiration and Water Content in Bryophytes. New Phytol. 82, 97–114. https://doi.org/10.1111/j.1469-8137.1979.tb07564.x
Dise, N.B., 2009. Peatland response to global change. Science (80-.). 326, 810–811. https://doi.org/10.1126/science.1174268
Duckett, J. G., Pressel, S., P'Ng, K. M. Y., & Renzaglia, K. S. (2009). Exploding a myth: The capsule dehiscence mechanism and the function of pseudostomata in Sphagnum. New Phytologist, 183(4), 1053–1063. https://doi.org/10.1111/j.1469-8137.2009.02905.x
Duckett, J. G., & Pressel, S. (2018). The evolution of the stomatal apparatus: Intercellular spaces and sporophyte water relations in bryophytes—two ignored dimensions. Philosophical Transactions of the Royal Society B: Biological Sciences, 373(1739). https://doi.org/10.1098/rstb.2016.0498
Felsenstein, J., 1985. Confidence Limits on Phylogenies: An Approach Using the Bootstrap. Evolution (N. Y). 39, 783–791.
Finkelstein, R.R., Somerville, C.R., 1990. Three classes of abscisic acid (ABA)-insensitive mutations of arabidopsis define genes that control overlapping subsets of ABA responses. Plant Physiol. 94, 1172–1179. https://doi.org/10.1104/pp.94.3.1172
Gerdol, R., Bonora, A., Gualandri, R., Pancaldi, S., 1996. CO2 exchange, photosynthetic pigment composition, and cell ultrastructure of Sphagnum mosses during dehydration and subsequent rehydration. Can. J. Bot. 74, 726–734. https://doi.org/10.1139/b96-091
Goodstein, D.M., Shu, S., Howson, R., Neupane, R., Hayes, R.D., Fazo, J., Mitros, T., Dirks, W., Hellsten, U., Putnam, N., Rokhsar, D.S., 2012. Phytozome: A comparative platform for green plant genomics. Nucleic Acids Res. 40, 1178–1186. https://doi.org/10.1093/nar/gkr944
Guillory, A., Bonhomme, S., 2021. Phytohormone biosynthesis and signaling pathways of mosses, Plant Molecular Biology. Springer Netherlands. https://doi.org/10.1007/s11103-021-01172-6
Hájek, T., Beckett, R.P., 2008. Effect of water content components on desiccation and recovery in Sphagnum mosses. Ann. Bot. 101, 165–173. https://doi.org/10.1093/aob/mcm287
Hájek, T., Vicherová, E., 2014. Desiccation tolerance of Sphagnum revisited: a puzzle resolved. Plant Biol. 16, 665–773. https://doi.org/10.1111/plb.12126
Johnson, M.G., Granath, G., Tahvanainen, T., Pouliot, R., Stenøien, H.K., Rochefort, L., Rydin, H., Shaw, A.J., 2015. Evolution of niche preference in Sphagnum peat mosses. Evolution (N. Y). 69, 90–103. https://doi.org/10.1111/evo.12547
Jones, D.T., Taylor, W.R., Thornton, J.M., 1992. The rapid generation of mutation data matrices from protein sequences. Bioinformatics 8, 275–282. https://doi.org/10.1093/bioinformatics/8.3.275
Katoh, K., Rozewicki, J., Yamada, K.D., 2019. MAFFT online service: Multiple sequence alignment, interactive sequence choice and visualization. Brief. Bioinform. 20, 1160–1166. https://doi.org/10.1093/bib/bbx108

Khandelwal, A., Cho, S.H., Marella, H., Sakata, Y., Perroud, P.F., Pan, A., Quatrano, R.S., 2010. Role of ABA and ABI3 in desiccation tolerance. Science (80-.). 327, 546. https://doi.org/10.1126/science.1183672

Knight, C.D., Sehgal, A., Atwal, K., Wallace, J.C., Cove, D.J., Coates, D., Quatrano, R.S., Bahadur, S., Stockley, P.G., Cuming, A.C., 1995. Molecular responses to abscisic acid and stress are conserved between moss and cereals. Plant Cell 7, 499–506. https://doi.org/10.2307/3870110

Kumar, S., Stecher, G., Li, M., Knyaz, C., Tamura, K., 2018. MEGA X: Molecular evolutionary genetics analysis across computing platforms. Mol. Biol. Evol. 35, 1547–1549. https://doi.org/10.1093/molbev/msy096

Lang, D., Ullrich, K.K., Murat, F., Fuchs, J., Jenkins, J., Haas, F.B., Piednoel, M., Gundlach, H., Van Bel, M., Meyberg, R., Vives, C., Morata, J., Symeonidi, A., Hiss, M., Muchero, W., Kamisugi, Y., Saleh, O., Blanc, G., Decker, E.L., van Gessel, N., Grimwood, J., Hayes, R.D., Graham, S.W., Gunter, L.E., McDaniel, S.F., Hoernstein, S.N.W., Larsson, A., Li, F.W., Perroud, P.F., Phillips, J., Ranjan, P., Rokshar, D.S., Rothfels, C.J., Schneider, L., Shu, S., Stevenson, D.W., Thümmler, F., Tillich, M., Villarreal Aguilar, J.C., Widiez, T., Wong, G.K.S., Wymore, A., Zhang, Y., Zimmer, A.D., Quatrano, R.S., Mayer, K.F.X., Goodstein, D., Casacuberta, J.M., Vandepoele, K., Reski, R., Cuming, A.C., Tuskan, G.A., Maumus, F., Salse, J., Schmutz, J., Rensing, S.A., 2018. The Physcomitrella patens chromosome-scale assembly reveals moss genome structure and evolution. Plant J. 93, 515–533. https://doi.org/10.1111/tpj.13801

Leifeld, J., Menichetti, L., 2018. The underappreciated potential of peatlands in global climate change mitigation strategies. Nat. Commun. 9, 1–7. https://doi.org/10.1038/s41467-018-03406-6

Lu, S., Su, W., Li, H., Guo, Z., 2009. Abscisic acid improves drought tolerance of triploid bermudagrass and involves H2O2- and NO-induced antioxidant enzyme activities. Plant Physiol. Biochem. 47, 132–138. https://doi.org/10.1016/j.plaphy.2008.10.006

Marella, H.H., Sakata, Y., Quatrano, R.S., 2006. Characterization and functional analysis of ABSCISIC ACID INSENSITIVE3-like genes from Physcomitrella patens. Plant J. 46, 1032–1044. https://doi.org/10.1111/j.1365-313X.2006.02764.x

Marschall, M., Borbély, P., 2011. Photosynthetic responses of the desiccation intolerant Sphagnum angustifolium in relation to increasing its desiccation tolerance by exogenous ABA. Acta Biol. Szeged. 55, 119–121.

Maxwell, K., Johnson, G.N., 2000. Chlorophyll fluorescence—a practical guide. J. Exp. Bot. 51, 659–668. https://doi.org/10.1093/jxb/51.345.659

Mazziotta, A., Granath, G., Rydin, H., Bengtsson, F., Norberg, J., 2019. Scaling functional traits to ecosystem processes: Towards a mechanistic understanding in peat mosses. J. Ecol. 107, 843–859. https://doi.org/10.1111/1365-2745.13110

Murchie, E.H., Lawson, T., 2013. Chlorophyll fluorescence analysis: A guide to good practice and understanding some new applications. J. Exp. Bot. 64, 3983–3998. https://doi.org/10.1093/jxb/ert208

Nishimura, N., Sarkeshik, A., Nito, K., Park, S.Y., Wang, A., Carvalho, P.C., Lee, S., Caddell, D.F., Cutler, S.R., Chory, J., Yates, J.R., Schroeder, J.I., 2010. PYR/PYL/RCAR family members are major in-vivo ABI1 protein phosphatase 2C-interacting proteins in Arabidopsis. Plant J. 61, 290–299. https://doi.org/10.1111/j.1365-313X.2009.04054.x

Nishiyama, T., Hiwatashi, Y., Sakakibara, K., Kato, M., Hasebe, M., 2000. Tagged

mutagenesis and gene-trap in the moss, Physcomitrella patens by shuttle mutagenesis. DNA Res. 7, 9–17. https://doi.org/10.1093/dnares/7.1.9
Oliver, M.J., Velten, J., Mishler, B.D., 2005. Desiccation tolerance in bryophytes: A reflection of the primitive strategy for plant survival in dehydrating habitats? Integr. Comp. Biol. 45, 788–799. https://doi.org/10.1093/icb/45.5.788
Ouyang, S., Zhu, W., Hamilton, J., Lin, H., Campbell, M., Childs, K., Thibaud-Nissen, F., Malek, R.L., Lee, Y., Zheng, L., Orvis, J., Haas, B., Wortman, J., Buell, R.C., 2007. The TIGR Rice Genome Annotation Resource: Improvements and new features. Nucleic Acids Res. 35, 8–11. https://doi.org/10.1093/nar/gkl976
Proctor, M.C.F., 2000. The Bryophyte Paradox: Tolerance of Desiccation, Evasion of Drought. Plant Ecol. 151, 41–49.
Proctor, M.C.F., Oliver, M.J., Wood, A.J., Alpert, P., Stark, L.R., Cleavitt, N.L., Mishler, B.D., 2007. Desiccation-tolerance in bryophytes: A review. Bryologist 110, 595–621. https://doi.org/10.1639/0007-2745(2007)110[595:DIBAR]2.0.CO;2
Rastogi, A., Antala, M., Gąbka, M., Rosadziński, S., Stróżecki, M., Brestic, M., Juszczak, R., 2020. Impact of warming and reduced precipitation on morphology and chlorophyll concentration in peat mosses (Sphagnum angustifolium and S. fallax). Sci. Rep. 10. https://doi.org/10.1038/s41598-020-65032-x
Raven, J.A., 1995. The early evolution of land plants: Aquatic ancestors and atmospheric interactions. Bot. J. Scotl. 47, 151–175. https://doi.org/10.1080/03746609508684827
Rensing, S.A., Goffinet, B., Meyberg, R., Wu, S.Z., Bezanilla, M., 2020. The moss physcomitrium (Physcomitrella) patens: A model organism for non-seed plants. Plant Cell 32, 1361–1376. https://doi.org/10.1105/tpc.19.00828
Rohde, A., Kurup, S., Holdsworth, M., 2000. ABI3 emerges from the seed. Trends Plant Sci. 5, 418–419. https://doi.org/10.1016/S1360-1385(00)01736-2
Sakata, Y., Nakamura, I., Taji, T., Tanaka, S., Quatrano, R.S., 2010. Regulation of the ABA-responsive Em promoter by ABI3 in the moss Physcomitrella patens: Role of the ABA response element and the RY element. Plant Signal. Behav. 5, 1061–1066. https://doi.org/10.4161/psb.5.9.11774
Schapire, A.L., Voigt, B., Jasik, J., Rosado, A., Lopez-Cobollo, R., Menzel, D., Salinas, J., Mancuso, S., Valpuesta, V., Baluska, F., Botella, M.A., 2008. Arabidopsis synaptotagmin 1 is required for the maintenance of plasma membrane integrity and cell viability. Plant Cell 20, 3374–3388. https://doi.org/10.1105/tpc.108.063859
Schipperges, B., Rydin, H., 1998. Response of photosynthesis of Sphagnum species from contrasting microhabitats to tissue water content and repeated desiccation. New Phytol. 140, 677–684.
Scholz, S.S., Reichelt, M., Vadassery, J., Mithöfer, A., 2015. Calmodulin-like protein CML37 is a positive regulator of ABA during drought stress in Arabidopsis. Plant Signal. Behav. 10. https://doi.org/10.1080/15592324.2015.1011951
Skowron, E., Trojak, M., 2021. Effect of exogenously-applied abscisic acid, putrescine and hydrogen peroxide on drought tolerance of barley. Biologia (Bratisl). 76, 453–468. https://doi.org/10.2478/s11756-020-00644-2
Stirling, E., Fitzpatrick, R.W., Mosley, L.M., 2020. Drought effects on wet soils in inland wetlands and peatlands. Earth-Science Rev. 210, 103387.

https://doi.org/10.1016/j.earscirev.2020.103387
Sun, Y., Pri-Tal, O., Michaeli, D., Mosquna, A., 2020. Evolution of Abscisic Acid Signaling Module and Its Perception. Front. Plant Sci. 11, 1–9. https://doi.org/10.3389/fpls.2020.00934
Takenaka, A., Oka, M., Taji, T., Tanaka, S., Sakata, Y., 2007. Functional analysis of ABI3/VP1 homologous genes from Physcomitrella patens. Plant Cell Physiol. 48, S58–S58.
Tan, T., Sun, Y., Peng, X., Wu, G., Bao, F., He, Y., Zhou, H., Lin, H., 2017. ABSCISIC ACID INSENSITIVE3 is involved in cold response and freezing tolerance regulation in Physcomitrella patens. Front. Plant Sci. 8. https://doi.org/10.3389/fpls.2017.01599
van de Koot, W.Q.M., van Vliet, L.J.J., Chen, W., Doonan, J.H., Nibau, C., 2021. Development of an image analysis pipeline to estimate Sphagnum colony density in the field. Plants 10, 1–17. https://doi.org/10.3390/plants10050840
Wagner, D.J., Titus, J.E., 1984. Comparative desiccation tolerance of two Sphagnum mosses. Oecologia 62, 182–187.
Wang, C., Liu, Y., Li, S.S., Han, G.Z., 2015. Insights into the origin and evolution of the plant hormone signaling machinery. Plant Physiol. 167, 872–886. https://doi.org/10.1104/pp.114.247403
Wei, L., Wang, L., Yang, Y., Wang, P., Guo, T., Kang, G., 2015. Abscisic acid enhances tolerance of wheat seedlings to drought and regulates transcript levels of genes encoding ascorbate-glutathione biosynthesis. Front. Plant Sci. 6, 1–11. https://doi.org/10.3389/fpls.2015.00458
Werner, O., Ros Espín, R.M., Bopp, M., Atzorn, R., 1991. Abscisic-acid-induced drought tolerance in Funaria hygrometrica Hedw. Planta 186, 99–103. https://doi.org/10.1007/BF00201503
Winnicka, K., Melosik, I., 2019. Genetic and expression differences between putative ecotypes of Sphagnum denticulatum Brid. (Sphagnaceae: Bryophyta) subjected to drought stress and rehydration. Perspect. Plant Ecol. Evol. Syst. 37, 39–52. https://doi.org/10.1016/j.ppees.2019.02.004
Yao, L., Cheng, X., Gu, Z., Huang, W., Li, S., Wang, L., Wang, Y.F., Xu, P., Ma, H., Ge, X., 2018. The AWPM-19 family protein OsPM1 mediates abscisic acid influx and drought response in rice. Plant Cell 30, 1258–1276. https://doi.org/10.1105/tpc.17.00770
Yao, T., Zhang, J., Xie, M., Yuan, G., Tschaplinski, T.J., Muchero, W., Chen, J.G., 2021. Transcriptional Regulation of Drought Response in Arabidopsis and Woody Plants. Front. Plant Sci. 11, 1–12. https://doi.org/10.3389/fpls.2020.572137
Yoshida, M.W., Yamada, M., Goshima, G., 2019. Moss kinesin-14 KCBP accelerates chromatid motility in anaphase. Cell Struct. Funct. 44, 95–104. https://doi.org/10.1247/csf.19015
Zhao, M., Li, Q., Chen, Z., Lv, Q., Bao, F., Wang, X., He, Y., 2018. Regulatory mechanism of ABA and ABI3 on vegetative development in the moss Physcomitrella patens. Int. J. Mol. Sci. 19, 1–19. https://doi.org/10.3390/ijms19092728

CHAPTER 3 - STEM DENSITY INFLUENCES *SPHAGNUM* DROUGHT SURVIVAL

Data availability

The data pertaining to this chapter can be accessed at (DOI NOT YET AVAILABLE)

Chapter summary

Peatlands have become a focal point in climate mitigation strategies as these ecosystems have significant carbon sequestration capacities when healthy but release CO_2 and other greenhouse gases when damaged. However, as drought episodes become more frequent and prolonged, organisms key to the functioning of peatlands are increasingly under pressure from desiccation. The *Sphagnum* peat mosses, which keep the ecosystem waterlogged and promote peat formation, are only mildly desiccation tolerant in comparison to other mosses. The role of *Sphagnum* colony structure is poorly understood in the context of desiccation resilience. In this study, the hypothesis that stem density affects water holding capacity and therefore desiccation resilience is addressed. Five *Sphagnum* species, representing the subgenera *Sphagnum*, *Acutifolia, Cuspidata* and *Subsecunda* and various ecological niches, were arranged in defined densities in *in vitro* cosms and subjected to desiccation. Higher densities were capable of holding larger quantities of water per unit of biomass, which increased their resilience. Even short drought was shown to have long term negative effects on photosynthetic function of *Sphagnum* plants. Manipulating relative humidity of isolated plants indicates that even 95% would eventually lead to significant stress. These results highlight the potential importance of colony density and regular water supply for plant survival. Our results may inform peatland restoration strategies in projects aiming to reintroduce *Sphagnum* on damaged peatland surfaces.

3.1 - Introduction

Sphagnum peatmosses have become a focal point for research because of their importance to peatland ecosystems. These bryophytes, through their large water storage capacity and acidifying properties, promote the accumulation of organic matter in these ecosystems, aiding peat formation and ultimately sequestering carbon. Carbon sequestration in peatlands is estimated to account for approximately 25% of all soil-sequestered carbon globally (Loisel et al., 2021; Yu et al., 2010), making peatlands one of the largest terrestrial carbon stores.

One of the main threats to the functioning of these peatlands is drought, as it leads to desiccation and potential death of the *Sphagnum*. The increasing prevalence of drought affecting peatlands can be both directly and indirectly attributed to anthropogenic activity (Warren et al., 2017). Lack of precipitation for prolonged periods is becoming more common globally as a consequence of climate change, and drainage of peatlands for agriculture, horticulture or fuel has damaged the water table regulatory capacity of many of these ecosystems. When peat is desiccated, it stops functioning as a carbon sink and instead becomes a carbon source, as the accumulated dead organic matter is exposed to oxygen and releases greenhouse gases.

3.1.1 – *Sphagnum* as desiccation avoider

The *Sphagnum* mosses are, compared to other bryophytes, not desiccation tolerant. As such, they have strict habitat preference and grow exclusively in very wet or humid habitats. Highly desiccation tolerant mosses such as *Tortula* Hedw. can live on exposed substrates, such as rock surfaces, with very limited or intermittent water availability and have evolved specific mechanisms to deal with these environments. However, the effect of desiccation on *Sphagnum* is of renewed interest in the context of habitat restoration (Bengtsson et al., 2020; Hájek and Beckett, 2008; Hájek and Vicherová, 2014; Mccarter and Price, 2014).

Although *Sphagnum* mosses have retained molecular responses to drought that are found in other bryophytes (Nibau et al., 2022; Winnicka and Melosik, 2019), they are unable to fully revive after severe desiccation suggesting loss of some physiological functions. Instead, they appear to have evolved characteristics to manipulate the peatland environment in order to reduce the likelihood of

desiccation. (Oliver et al., 2009, 2000). Therefore, *Sphagnum* mosses are typically labelled ‘desiccation avoiders’ rather than desiccation tolerant (Hájek and Vicherová, 2014).

3.1.2 – Desiccation avoidance adaptations

Water table regulation in peatlands depends, at least in part, on these bryophytes (Clymo and Hayward, 1982) and the environment they engineer is unfavourable to many other plant species (Marschall and Proctor, 2004). *Sphagnum* plants have several adaptations that are thought to aid them in holding large quantities of water and transportation. Firstly, they have specialised water storage cells, referred to as hyaline cells (Bengtsson et al., 2020; Kremer and Drinnan, 2004). These hyaline cells are elongated hollow cells, in the case of *Sphagnum* often with pores, that make up around 80% of the bulk *Sphagnum* volume (van Breemen, 1995) and enable the storage of large water volumes and are found on all *Sphagnum* leaflets as well as on the outside of the stems. However, the individual water storage capacity of hyaline cells is not the only advantage, as they increase water conductivity along the stem (van Breemen, 1995).

Secondly, *Sphagnum* plants have two types of branches, known as ‘spreading’ and ‘pendent’ branches, that aid uptake and transport of water through *Sphagnum* colonies. These branches offer two directions of water movement, namely lateral and vertical respectively. The spreading branches extend laterally from the main stem, aiding water uptake from precipitation and water exchange between individual plants in a colony (Rice, 2012), whilst the pendent branches are appressed downwards along the stem, wicking water upwards from the water table to the meristematic areas at the top of the stem in the capitulum, the head of the plant (Silvola and Aaltonen, 1984; Stenøien et al., 1997). As a result, has been estimated that up to 90% of all *Sphagnum* water retention is extracellular, stored in the capillary spaces formed between the pendent branches (Clymo and Hayward, 1982; Rydin and Clymo, 1989), allowing individual *Sphagnum* to hold over 2000% their own biomass in water (Bengtsson et al., 2020, 2016; Clymo and Hayward, 1982; Nibau et al., 2022).

3.1.3 – The potential role of colony density

A potential third mechanism for water retention that has been poorly investigated is colony (or plant) density. *Sphagnum* mosses typically grow in dense colonies that can take the shape of, for example, lawns, mats, hummocks and tussocks (Figure 3.1A-D). The numerical density of plants within colonies might be affected by inherent genetic factors specific to each species such as capitulum size and stem branching. However, microclimatic conditions of the growth site might be equally or more important in explaining variation (Elumeeva et al., 2011). Thus, in drier habitats, a denser colony might confer an advantage as this would reduce the area of individual plants exposed to airflow by reducing surface roughness, which reduces evaporation (Rice, 2012); while in wetter habitats colony density may be unimportant such as in pools and pond margins where water loss can easily be replenished. In other bryophytes, colony structure and morphology was found be associated with slower drying (Cruz de Carvalho et al., 2019), and a study including four *Sphagnum* species found that increased plant density was correlated with increased water retention capacity (Elumeeva et al., 2011).

Despite the potential impact of colony density for peatland restoration projects, especially projects in which *Sphagnum* is planted on damaged peat surfaces for the purpose of recolonisation, the importance and consequences of this trait are poorly understood. Little experimental data and field data has been collected, as colony density estimation is a labour intensive task. Recent developments of tools for automated high throughput quantification may enable easier collection of density data (van de Koot et al., 2021).

Using five selected *Sphagnum* species, representing four subgenera, namely *Acutifolia, Cuspidata, Sphagnum* and *Subsecunda*, as well as a range of habitat types including mire lawns, pools and forest floor, the effect of colony density on desiccation was tested. Increased colony density was found to always improve desiccation resilience in the *Sphagnum* species, as higher densities had a larger absolute water holding capacity. While the daily rate of water loss was similar between densities, suggesting density did not reduce the rate of evaporation, having a larger amount of water available increased desiccation resilience. Consequently, colonies at reduced plant density recovered slower than those at higher densities simply because the former had either reached lower water content or spent a longer

time at low water content. Even a relatively short period of desiccation could debilitate the photosynthetic capacity of *Sphagnum* for a longer period. Thus our main finding is that higher densities significantly increased the maximum relative water content of the colony, independent of species and improves *Sphagnum* desiccation tolerance. Plant density should therefore be considered when designing peatland restoration projects, particularly those that aim to re-establish more complex and functional ecosystems.

3.2 – Materials and methods

Five species of *Sphagnum*, representing the subgenera Acutifolia, Cuspidata, Sphagnum and Subsecunda were collected from colonies growing in the Cambrian mountains and coastal regions in West Wales. *S. quinquefarium* was collected from a humid, mixed deciduous-coniferous woodland (Coed y Darren, SN677835) on the northern side of a hill, where it carpets the majority of the forest floor with no direct access to the water table. The four other species, *S. capillifolium, S. fallax, S. inundatum* and *S. papillosum* were collected from a blanket bog at the foot of Pen y Garn (SN791758), which is mostly ombrotrophic but mildly minerotrophic due to its position below the mountain. Sods of approximately 650 cm^2 were cut out whilst retaining the colony structure, and transferred into rectangular blue boxes (Gratnells Ltd, Harlow, UK, inner size 28.5x23.5x14.5 cm) with 9 drainage holes in their bottom. The mosses were kept outside on the south-east facing side of the National Plant Phenomics Centre (NPPC, Plas Gogerddan) glasshouse in shallow trays with approximately 3 cm of standing water, ensuring the *Sphagnum* was saturated. The moss was allowed to acclimatise for at least two weeks prior to the experiments, and were kept for the duration of the experiments, of which repeats were conducted during multiple seasons.

3.2.1 – Manipulated colony density experiments

Individual plants of each species were arranged into microcosms at 10, 20, 30 or 40 plants, cut to a uniform size and placed in a vertical microcosm consisting of a square petri dish, of which one side was removed (top side when the microcosms were placed vertically) to allow for evaporation (Figure 3.1E, previously described in Nibau et al. 2022). The cross sectional area available for the plants and evaporation was 20 cm^2, meaning the density in the cosms was 0.5, 1, 1.5 or 2 plants cm^{-2}. However, in this text the densities will be referred to as 10, 20, 30 and 40, after the respective number of plants in each cosm. In a previous study of *Sphagnum* in the same area the naturally occurring densities of these species were recorded to be approximately 1.9 plants cm^{-2} for *S. capillifolium*, 1.65 plants cm^{-2} for *S. fallax*, 0.6 plants cm^{-2} for *S. inundatum*, 1.2 plants cm^{-2} for *S. papillosum*, and 1.34 plants cm^{-2} for *S. quinquefarium* (Nibau et al., 2022; van de Koot et al., 2021) (Figure 3.1A-D). Six cosms per density per species were prepared, of which two were allocated to the

control group and the remaining four to the experimental group. The microcosms were randomised and kept in a shallow tray containing 1 cm of standing water for two weeks prior to the experiment in a controlled environment with a temperature of approximately 22-24 ^{o}C.

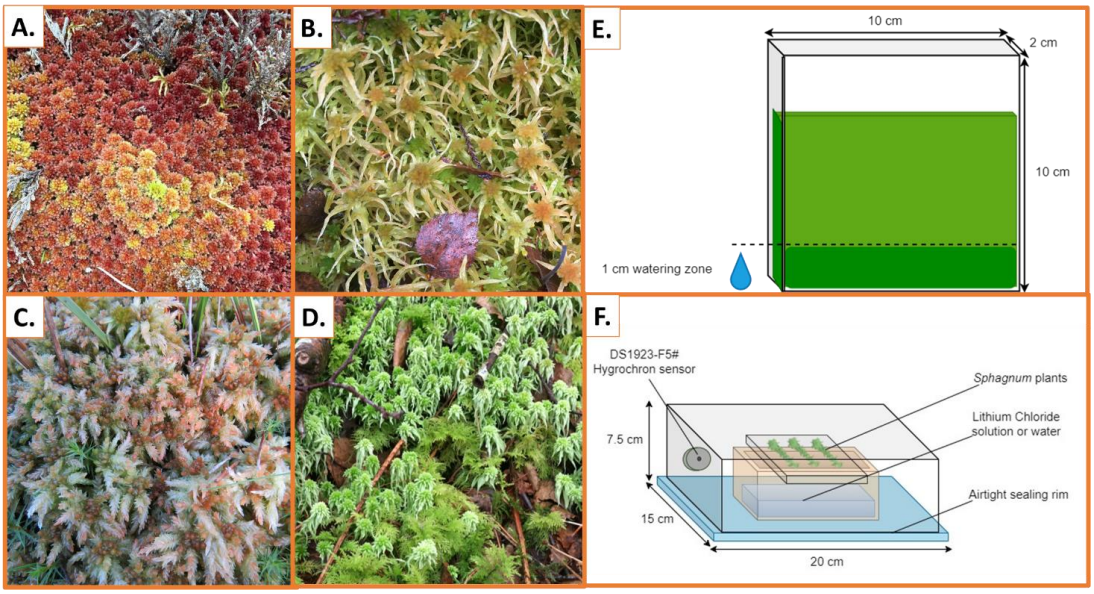

Figure 3.1. Natural (A-D) canopy density indicating variable density in four species of *Sphagnum*, namely A. *S. capillifolium*, B. *S. fallax*, C. *S. papillosum* and D. *S. quinquefarium*. These densities may be partly species specific and correspond to the habitats preference of each species, i.e. hummock (A and C), lawn (C and D) or hollow (B). These four species and S. inundatum were arranged in various densities in horizontal microcosms (E), with permanent access to water. Only the top of the cosm was open, allowing for passive evaporation. F. The LiCl mediated RH cosms were used to assess each species' resilience to lowered RH. A DS1923-F5# Hygrochron measured changes in RH during the experiment.

All cosms in the experimental group were subjected to a three-week drought period by transfer to a dry tray in the same CE compartment, followed by one week of recovery when they were watered as before, whilst the control group was kept well-watered for the duration of the experiment. The efficiency of photosynthesis was assessed three times weekly through measurement of the chlorophyll fluorescence parameter Fv/Fm in a CF Imager (Technologica, Essex, UK) following the manufacturers protocol, which provides an estimate of the efficiency of photosystem II. This variable quantifies the efficiency of photosystem II (PSII) and was used in combination with water content and weight measurements to measure the effect of density on the retention of photosynthetic functioning, and has been previously used to measure the negative impact of low moisture on *Sphagnum*

photosynthesis (Bengtsson et al., 2020; Chiapusio et al., 2022; Hájek and Beckett, 2008)

As water is essential for photosynthesis and metabolic processes related to the maintenance of the photosynthetic apparatus, this measurement was used as a proxy for desiccation stress (Maxwell and Johnson, 2000; Murchie and Lawson, 2013). Prior to measurement of Fv/Fm, the cosms were dark-adapted for at least 20 minutes to ensure non-photochemical quenching (NPQ) and other photo-inhibitory effects did not negatively affect the measurement of maximum fluorescence (Fm). A map image was used to threshold and filter noise from the images prior to measurement. For the measurement of Fm, a saturating pulse of 6843 µmol m^{-2} s^{-1} PPFD (Photosynthetic Photon Flux Density) PAR (Photosynthetic Active Radiation) was used. Subsequently Fv/Fm was calculated using the formula (Fm – Fo)/Fm, where Fo is the minimum fluorescence signal from dark adapted material. In addition, the weight of the cosms was recorded immediately after the chlorophyll fluorescence measurement for each cosm including the control group. At the end of the experiment, the plants were again weighed to measure wet weight, dried to constant weight (for 72 hours) in an oven at 80 ^{o}C, after which the gravimetric water content could be calculated for each timepoint the difference between fresh and dry weight divided by dry weight.

3.2.2 - Drought period resilience experiment

In addition to the three week drought experiment described above, *S. quinquefarium* was also subjected to drought periods of 1, 2 and 4 weeks with subsequent recovery, to evaluate the effect of density on desiccation tolerance against variable drought periods and subsequent recovery. This species was selected as it was the most abundant in our local area, and was also the median species in terms of Fv/Fm and water content response in the pilot experiment (Figure 3.2). Using the methodology described above, photosynthesis and water content were measured over time in response to desiccation and subsequent re-wetting.

3.2.3 –Relative humidity experiments

To investigate the tolerance of the various *Sphagnum* species to variations in relative humidity (RH), individual plants were transferred to an air-tight microcosm containing 100 ml of defined concentration Lithium Chloride (LiCl) solutions (Hay et al., 2008) (Figure 3.1F). These solutions allowed the RH in the cosms to be controlled to specific levels, which were 80, 90 and 95% RH. DS1923-F5# Hygrochron (Maxim Integrated) RH and temperature loggers were used to measure the RH within the cosms to ensure required RH levels were achieved. Control cosms containing only water or silica gel were measured and resulted in RH levels of approximately 100 and 13% humidity.

Plants were extracted from the blue boxes outside the NPPC glasshouse, cut to approximately uniform sizes and weighed prior to being placed in the air-tight RH microcosms. The Fv/Fm of the plants within the cosms was then measured 4 times over the course of 7 days, after which the plants were removed from the cosms and weighed again. The CF Imager protocol for the measurement of Fv/Fm was identical to that of the colony density experiment, with the addition that the plants in the image were identified using the auto-region feature. Finally, the entire plants were oven dried to constant weight (48 hours at 80 ^{o}C) and their dry weight measured. Gravimetric water content was subsequently calculated as the difference between fresh and dry weight divided by dry weight. In between experimental replicates, the Hygrochron loggers were analysed and if the RH of a cosm was substantially different (>2% deviation) from the designated RH treatment, the LiCl solution was replaced.

3.2.4 – Statistical analyses

Statistical analyses were carried out in RStudio version 4.0.3 (RStudio Team, 2020) using the packages car (Fox and Weisberg, 2019) and ggpubr (Kassambara, 2016). Data visualisation and plotting was done in Python, with the packages Seaborn (Waskom et al., 2020) and Matplotlib (Hunter, 2007). Statistics that involve the dry weight measurements were limited to data collected on the final day of the corresponding experiment, as this was the day after which the plants were dried and measured. As all data was normally distributed after the removal of outliers, parametric T-tests were used to calculate significance of difference between normally distributed data comparisons, and Pearson product-moment correlation was used to test for correlation between variables.

3.3 - Results

In order to determine the effect of colony density on water loss and photosynthetic capabilities of different *Sphagnum* species, five species were arranged into various densities and subjected to a three-week drought period followed by one week of rewetting for recovery. Over the course of the experiment, the cosms containing the *Sphagnum* plants were weighed and photosynthetic capability measured, monitoring the relation between loss of water content and photosynthesis.

3.3.1 - The effects of colony density on water loss and photosynthesis

During drought, gravimetric water content was found to reduce relatively steadily over time, whilst Fv/Fm changed quickly and suddenly after a brief period of stability with sometimes even a slight increase in Fv/Fm values (Figure 3.2A-B). Increased plant density significantly increased the time it took for water content to decrease, and for Fv/Fm to be reduced. This was potentially caused by the fact that the higher densities started with higher water contents ($g\ g^{-1}$). Consequently these higher densities were subjected to less time at low water contents, and their Fv/Fm recovered more quickly than that of lower density cosms, presumably because they suffered less desiccation-induced damage to their photosystems.

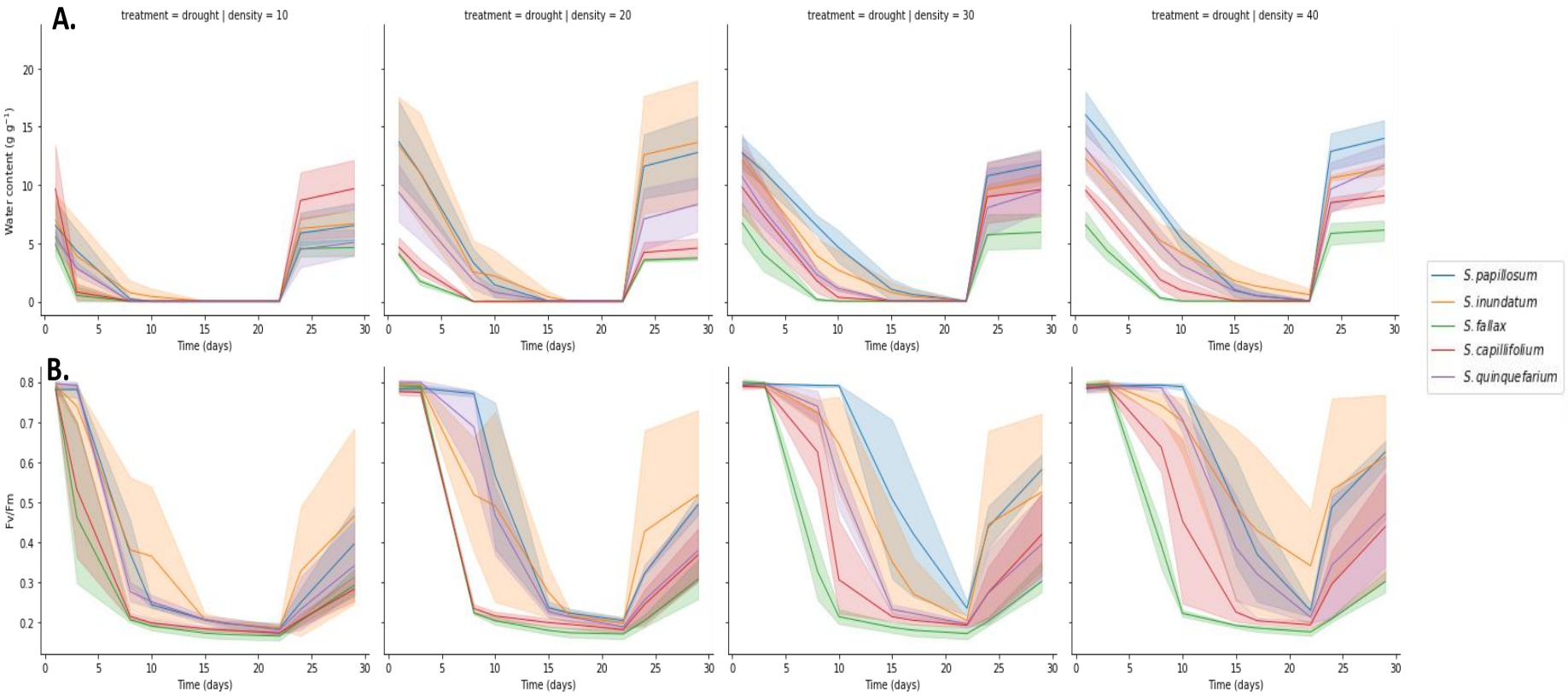
A.
treatment = drought | density = 10
treatment = drought | density = 20
treatment = drought | density = 30
treatment = drought | density = 40
Water content (g g⁻¹)
Time (days)
B.
Fv/Fm
Time (days)
S. papillosum
S. inundatum
S. fallax
S. capillifolium
S. quinquefarium

Figure 3.2. Effect of manipulated canopy density on relative water content and photosynthetic efficiency during an imposed drought scenario.
Water content (A) and Fv/Fm (B) change over time in each species at four densities, subjected to 3 weeks of drought and subsequent rewetting on day 22. *S. papillosum* and *S. inundatum* consistently start with higher water content, allowing them to retain their photosynthetic performance for longer than the other three species. *S. fallax* and *S. capillifolium* in particular quickly deteriorated, although rate of water loss as observed in the slope of the decrease in water content, and is particularly apparent in the 30 and 40 stem density microcosms.

In general, *S. papillosum*, *S. inundatum* and, at the larger densities, *S. quinquefarium*, started with greater water content than *S. fallax* and *S. capillifolium*. However, the rate of water loss in grams per day appears to be similar between the five species during the first three days of drought, when the plants started from a fully saturated state. This indicated that rate of water loss was not significantly affected by density in this experiment, but was possibly limited by the amount of surface exposure.

Only *S. fallax* lost significantly ($p<0.01$**) more weight than *S. papillosum*, which lost the least amount of weight. When the different densities were compared within each species, only *S. papillosum* indicated a significant difference ($p<0.05$*) between density 40 and densities 20 and 30 (Supplementary Figure 3.1B). For all other species, there were no significant differences in daily weight loss during the first 3 days between the density treatments, suggesting density does not affect rate of water loss. In all densities and species, re-watering after the drought period immediately increased cosm water content to pre-experiment amounts (Figure 3.2A).

After 1 week of drought exposure, the 10-plant density cosms containing either *S. fallax* and *S. capillifolium* lost nearly their entire water content and their photosynthetic capabilities (Fv/Fm ~ 0.200) (Figure 3.2B). *S. inundatum* and *S. papillosum* appeared to be more desiccation resistant at this density than the other three species, whilst *S. quinquefarium* was the intermediate of all species. The relative responses to desiccation were similar for each of the different plant densities, with *S. inundatum* and *S. papillosum* consistently being more desiccation resistant, *S. fallax* and *S. capillifolium* being the most susceptible to desiccation and *S. quinquefarium* being intermediate. All species showed some photosynthetic recovery after re-watering, with better recovery at larger densities. However, most cosms

suffered irreversible loss of chlorophyll in apical parts of the plants and in some cases developed fungal infections on the capitula.

The increase in desiccation recovery from higher densities, as seen in the higher recovery of Fv/Fm in Figure 3.2, could be explained in part by the biomass of plants in each cosm, as they would potentially contain larger numbers of water holding hyaline cells. However, there was no significant correlation between dry weight, as a proxy for the potential number of hyaline cells in a cosm, and water content at day 29 (the final day of the experiment, on which the dry weight was measured) for any of the species except *S. capillifolium*, which was only weakly correlated ($p<0.05$*, $r = -0.42$) (Figure 3.3A). Dry weight and weight at the final timepoint (day 29) were significantly correlated for each species ($p<0.01$** or $p<0.001$***), with Pearson product-moment correlation r values between 0.54 (*S. papillosum*) and 0.67 (*S. inundatum*) (Figure 3.3B).

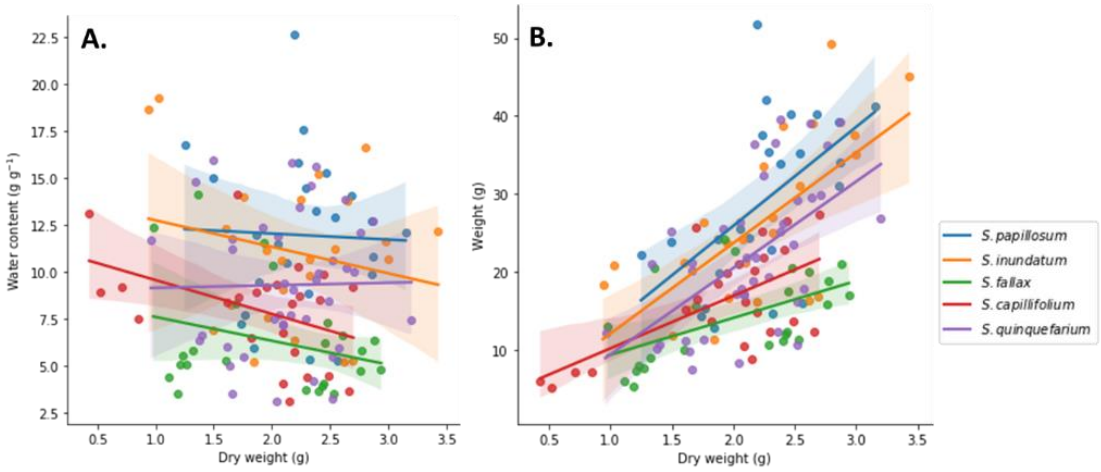

Figure 3.3. Dry weight as an explanatory factor for water content and weight shows that water content is independent of dry mass.
Correlations between A. Dry weight and cosm water content for each species. Interestingly, *S. capillifolium* was the only species to have a significant correlation ($p<0.05$*) between these two variables, suggesting most water is stored outside of the tissues. B. Dry weight did significantly correlate with fresh weight for each species.

In summary, the results suggested that higher colony densities were capable of holding larger water contents, which consequently resulted in slower desiccation and reduced loss of photosynthetic capabilities, and a stronger recovery from desiccation.

3.3.2 - Various drought period durations further highlight density-driven desiccation resistance in *S. quinquefarium*

As *S. quinquefarium* was the most accessible and abundant species available for collection with minimal impact on the local ecosystem, as well as being approximately intermediate in its drought response of the five species used, this species was selected for colony density experiments that tested the resilience of the various densities to three discrete drought periods, namely one, two and three weeks of drought followed by rewetting (Figure 3.4). As observed in the previous experiment (using multiple species), larger densities retained photosynthetic capacity for a longer period than smaller densities for all treatments (Figure 3.4B), and water loss at the beginning of the experiment was not significantly different between the different densities (Supplementary Figure 3.1B), suggesting the rate of water loss is not be affected by the density of the colony. Water content recovered immediately upon re-wetting for all densities, as was the case in the experiment using multiple species.

As the relative water content increased with plant density, canopies with higher densities retained photosynthetic function for longer periods under drought. recovering to larger Fv/Fm values more rapidly than smaller densities (Figure 3.4B). For the lowest densities, namely 10 and 20 plants per cosm, a single week of drought stress was sufficient to debilitate photosynthetic capacity for the remainder of the experimental period, as indicated by Fv/Fm values with a mean of < 0.700. Despite being fully rewetted for three weeks, these two densities never recovered to their starting Fv/Fm values or those of the control cosms, instead only recovering to 0.600-0.700 (~75-87.5% recovery). Longer drought periods of two and three weeks also caused loss of photosynthetic capacity in the larger densities, with the 30 plant density recovering less than 50% of its original photosynthetic capacity. These results suggest that, although larger densities may protect *Sphagnum* colonies from desiccation and consequential loss of photosynthesis, even relatively short drought periods can cause long-term physiological damage.

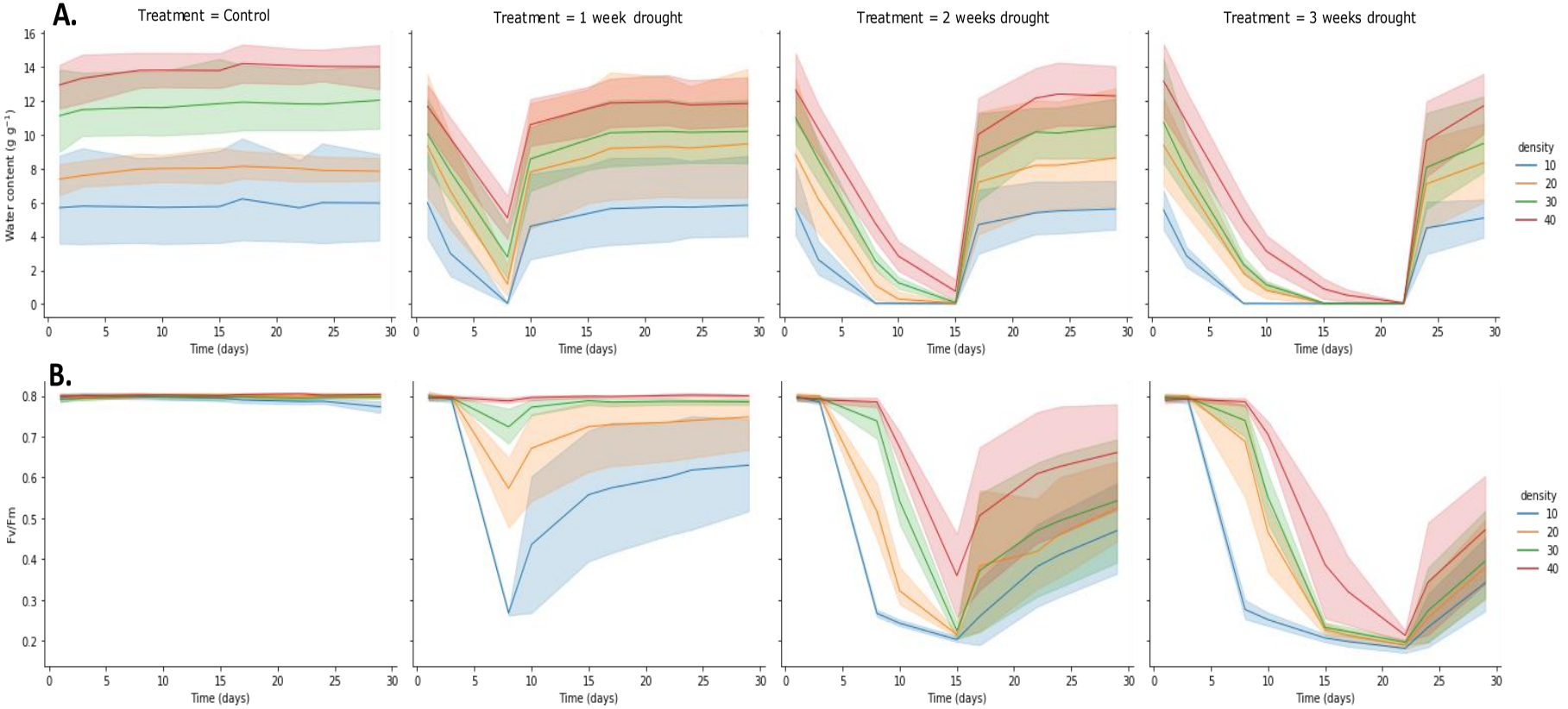
A.
Treatment = Control
Treatment = 1 week drought
Treatment = 2 weeks drought
Treatment = 3 weeks drought
Water content (g g⁻¹)
Time (days)
density
10
20
30
40
B.
Fv/Fm
Time (days)
density
10
20
30
40

Figure 3.4. Increased stem density promotes resilience to drought.
Loss and recovery of water content (A) and photosynthetic functioning (B) in *S. quinquefarium* subjected to three drought periods. Density increased water content capacity and allowed plants to tolerate drought for longer as their water stores were larger. Fv/Fm recovered more strongly after short drought periods and slower after prolonged desiccation.

As observed in the multi-species experiment, gravimetric water content, expressed as grams of water per gram of dry weight, increased with larger densities (Figure 3.5A). The difference in relative water content when all data was combined at timepoint 29 was highly significant ($p<0.001$***) between every density, with the exception of the difference between 30 and 40 plants, which was of lower significance ($p<0.05$*). Timepoint 29 was selected as it was the timepoint at which dry weight was measured, and all samples were in a saturated state with water content recovered to pre-experiment levels. A water content increase, albeit not significant, was also visible over time in the control treatment and all drought period treatments when recovering for *S. quinquefarium* (Figure 3.4A). This effect was also observed in the multiple species experiment (Figure 3.5B), but was more pronounced in the experiment using only *S. quinquefarium*.

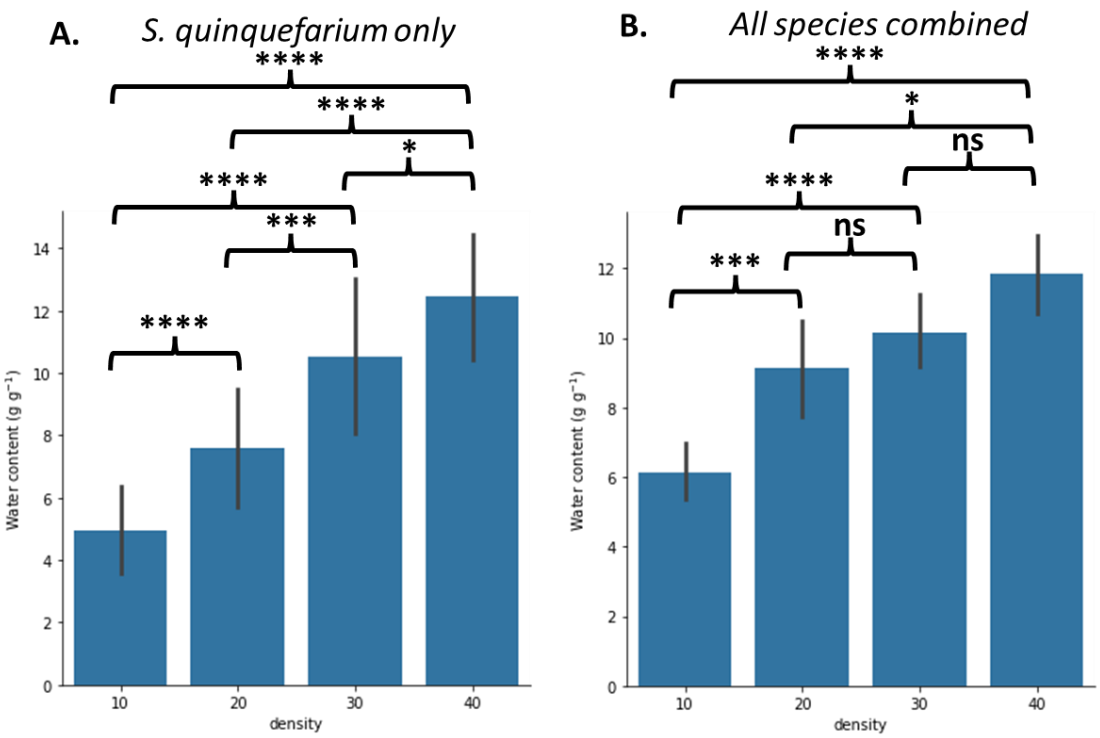

Figure 3.5. Increased plant density increases relative water content (water content per unit biomass).
Water content increases with increases in density for A. *S. quinquefarium* experiment data and B. the multiple species experiment. Although relative water content generally increased incrementally with each increase in density, the difference became less significant towards higher densities, suggesting a maximum saturation can be reached.

Since capillary action is a function of distance, the increase in relative water content is hypothesised to be caused by the potential for additional capillary action between neighbouring plants (Figure 3.6). When plant stems are spaced apart, each stem acts as an independent unit and therefore water holding capacity is determined by the water held within and between the tissues on each stem. When plants are more densely spaced, there would be additional opportunities for water to be held by capillary action between the tissues of neighbouring plants. Larger plant surface availability consequently appeared to enable the larger densities to store a larger volume of water independent of their actual mass.

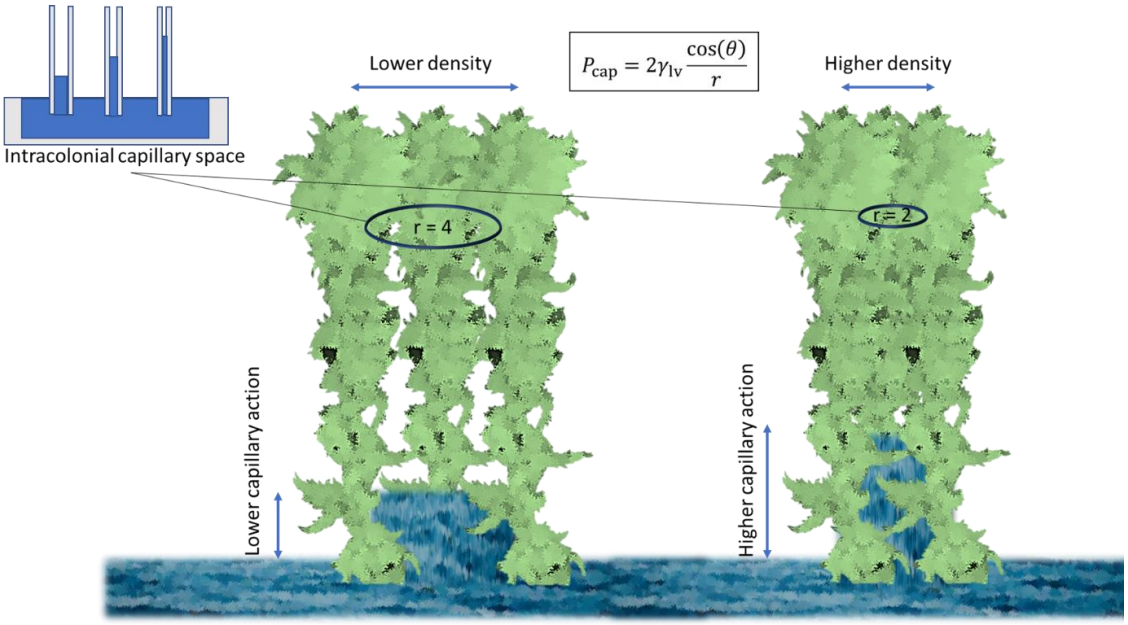

Figure 3.6. Schematic of the proposed *Sphagnum* colony density capillary action mechanism. Similar to the classical example of capillary action using a series of increasingly narrow tubes, where a decrease in tube radius (r) results in stronger capillary pressure (P_{cap}), an increasingly higher density narrows the space between individual plant stems, generating additional capillary action between adjacent branches and stems. Through this mechanism, a denser *Sphagnum* colony is capable of holding a larger gravimetric water content (grams of water per gram dry mass)(Figure 3.5).

3.3.3 - Single plant responses to desiccation

To test whether the resilience of individual plants to various relative humidity regimes differed between species, the five species were placed in air-tight cosms containing Lithium Chloride (Figure 3.1F), which regulated relative humidity within the cosms. Water only cosms were used as control and, when measured, had a relative humidity of near 100%. Silica gel was also used as an extreme treatment and generated a relative humidity of approximately 13%.

All five species were capable of retaining (near) normal photosynthetic functioning throughout the experiment in the cosms that contained only water (Figure 3.7A). However, even a mild regime of 95% relative humidity diminished the Fv/Fm values of all species after five days. *S. capillifolium* and *S. fallax* responded more rapidly to a low relative humidity. As with the colony density experiment, *S. quinquefarium* was the intermediate species of the five, whilst *S. papillosum* and *S. inundatum* exhibited the strongest resilience to reduced relative humidity. Most species are capable of tolerating a lower relative humidity of 95%,

whilst at 90% relative humidity species differences become clear in terms of tolerance. Only *S. papillosum* could tolerate a 90% relative humidity treatment for a week before becoming photosynthetically stressed (Fv/Fm < 0.500), whilst none of the species could maintain photosynthetic function for a week under 80% relative humidity.

As the species weren't acclimatised to the experimental conditions, fluctuations in starting water content and Fv/Fm were expected despite being kept at saturated conditions outside the NPPC glasshouse. However, for all species and treatments, the starting water contents were very consistent (Figure 3.7B). *S. papillosum* did exhibit a very large variation in starting water content, as indicated by the error bars. However, this is likely the result of also having the largest water content in general, as *S. papillosum* plants in some cases had double the water content of the other species. After *S. papillosum*, *S. inundatum* and *S. fallax* had the largest water contents at the start of the experiment, approximately equalling each other. Despite this near equal starting water content however, *S. fallax* responded negatively to the relative humidity treatments of 90% and 95% much quicker than *S. inundatum* (Figure 3.7A), indicating that starting water content was not the only factor affecting desiccation speed.

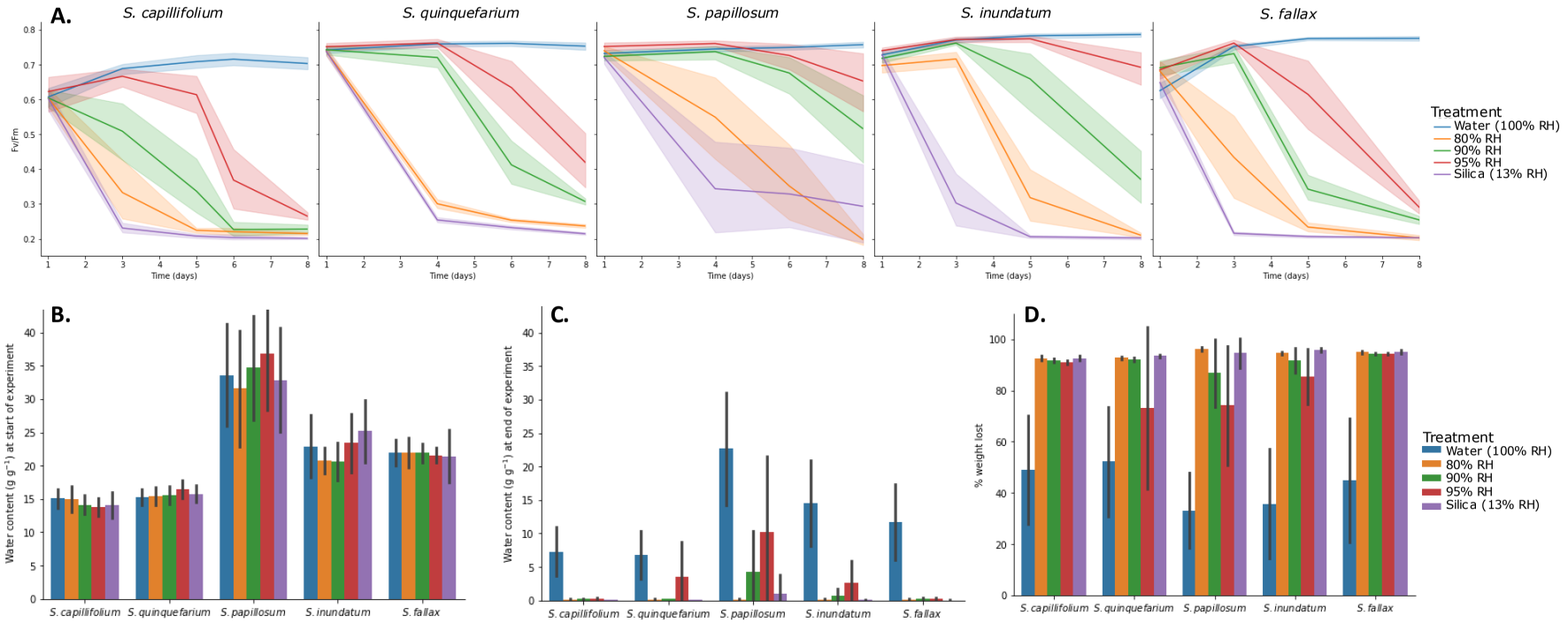
A.
S. capillifolium
S. quinquefarium
S. papillosum
S. inundatum
S. fallax
Fv/Fm
Time (days)
Treatment
Water (100% RH)
80% RH
90% RH
95% RH
Silica (13% RH)
B.
Water content (g g⁻¹) at start of experiment
C.
Water content (g g⁻¹) at end of experiment
D.
% weight lost
S. capillifolium
S. quinquefarium
S. papillosum
S. inundatum
S. fallax

Figure 3.7. Individual plant responses to desiccation in relative humidity cosms.
A. Fv/Fm loss over time in Lithium Chloride mediated relative humidity cosms. All five species photosynthesised normally in cosms with only water despite losing weight, but started suffering when relative humidity was 95% or below. *S. papillosum* and *S. inundatum* retained their photosynthetic capacity longer than the other three species, with *S. capillifolium* and especially *S. fallax* responding negatively very quickly to low RHs.
B. Water content differed between species at the start of the experiment, but was relatively consistent between treatments. *S. papillosum* held almost twice the water content of the other species, whilst *S. fallax* and *S. capillifolium* held the lowest water contents.
C. At the end of the experiment, *S. papillosum* still had the largest water contents of all species, which most likely caused it to retain its photosynthetic functioning the longest (A). In all species, the remaining water contents corresponded to the relative humidity treatments, with the severest treatments resulting in the lowest water contents and the control treatments retaining larger water contents, although all species lost water over the course of the experiment.
D. Fractionally, all species lost >90% of their weight over the course of the experiment in the 80% RH and silica cosms. Cosms containing only water typically allowed the *Sphagnum* species to retain over half of their original weight.

Furthermore, as all species lost weight in the water only cosms at near 100% relative humidity (Figure 3.7B-D), this suggests that high humidity alone can only temporarily compensate for a lack of precipitation. Even at 95% relative humidity most species lost up to 70% of their original water weight (Figure 3.7B-D), and at 80% relative humidity > 90% of water weight was lost. In nature, relative humidity fluctuates mostly between day and night, meaning such extreme durations at low relative humidity are unlikely to occur. However, this experiment indicates that for *Sphagnum*, consistently higher relative humidity is preferred and may be essential when there is a lack of precipitation or water access.

3.4 - Discussion

While colony density has been suggested as an ecological variable influencing *Sphagnum* water retention and desiccation resilience (Bengtsson et al., 2020; Clymo and Hayward, 1982; Elumeeva et al., 2011), the specific effects of plant density remain unclear. Our results indicate that higher plant densities can hold larger amounts of water per unit of biomass (Figure 3.5) although density did not, in general, significantly affect rate of absolute water loss in grams (Supplementary Figure 3.1). These two factors combine to support the hypothesis that higher plant density is a potential desiccation mitigation strategy for *Sphagnum* colonies in drought sensitive habitats (Figure 3.6). Furthermore, even short drought periods have long term negative effects on *Sphagnum* photosynthetic functioning (Figure 3.2B, 3B), and the five species used in the experiments require 100% relative humidity at least occasionally for survival, as even 95% RH was not sufficient to sustain all species for a week (Figure 3.7A).

Sphagnum water dependence has been well documented and reflects their ecosystem preferences. Although efforts are underway to retain and restore of the peat areas in the northern hemisphere (Caporn et al., 2018; Muster et al., 2015; Temmink et al., 2017), many peatlands still suffer from damage inflicted centuries ago when drainage attempts were made or peat was cut for fuel (González et al., 2014). While these projects employ large scale rewetting of previously cut areas, or the planting of so-called '*Sphagnum* plugs' to re-establish *Sphagnum* communities, little data underpins choice as to the composition and quality of the plugs. The results presented in this study could potentially offer the suggestion that at least, more is better when it comes to plant densities and plug sizes. Increasing the density in the cosms from 10 to 20, or from 0.5 to 1 plant cm^{-2}, allowed the photosynthetic capabilities to be retained for longer in most species (Figure 3.2B). For all species, higher densities slowed the desiccation process which consequentially facilitated recovery upon rewetting. The significance of density for desiccation resilience was further highlighted by the drought duration experiment on *S. quinquefarium*, which showed that even short drought periods could reduce the photosynthetic capacities of low density *Sphagnum* and for a longer period (Figure 3.4B).

Plant densities in natural stands were estimated to be approximately 1.9 plants cm^{-2} for *S. capillifolium*, 1.65 plants cm^{-2} for *S. fallax*, 0.6 plants cm^{-2} for *S.*

inundatum, 1.2 plants cm^{-2} for *S. papillosum*, and 1.34 plants cm^{-2} for *S. quinquefarium* in the collection sites (Nibau et al., 2022; van de Koot et al., 2021). In the context of these artificial density experiments, the densities of *S. papillosum* and *S. inundatum*, which were of similar size and weight, may reflect the niches they were found in in the collection site. *S. inundatum* was collected from a shallow pool and its margins, where it has direct access to surface water nearly throughout the year. *S. papillosum* however, occurs higher above the water table and may be more reliant on precipitation. This may explain why *S. papillosum* has a larger density, as this could increase its water holding capacity, whilst *S. inundatum* does not require this additional capacity due to its permanent water access. Such environmentally driven variation in density has been previously documented for a number of bryophytes including *Sphagnum* (Elumeeva et al., 2011), and in some bryophyte species density was shown to improve desiccation resilience (Cruz de Carvalho et al., 2019). *S. capillifolium* had the highest density, and is also the species growing highest above the water table in this experiment, forming dense hummocks. Although this large density can in part be explained by the fact that *S. capillifolium* is a relatively small sized species, its hummocks are known to be very dense which may allow this species to occupy its niche above the water table by increasing its water holding capacity.

Whilst canopy density was often assumed to also increase water retention by reducing evaporation (Rice, 2012) as less area of each individual plant would be exposed to surface air currents and more branches would intercept evaporation from below, the results of the density experiments presented in this study show that for each species, generally, the rate of water loss was not significantly different between the density treatments. In the experiment, there was little airflow in the area in which the *Sphagnum* cosms were kept, and the plants were not subjected to lateral airflow as the cosm enclosed the entire colony structure from the sides (Figure 3.1E). Therefore, evaporation was limited to moisture rising from and escaping through the 20 cm^2 gap at the top of the cosms. Whilst this would still theoretically allow spreading branches to intercept this evaporation, the limited airflow meant that all evaporation was passive and not driven by active air currents. Although the results suggest that density, in a passive setting, does not affect rate of water loss, the effect of canopy density and closedness in an experiment with directional airflow may yield

different results, as this would include effects of changes in boundary layers caused by canopy roughness (Rice et al., 2008, 2005).

The main feature associated with desiccation resilience as a result of density, was the increase of relative water content (g of water g^{-1} dry biomass). Higher densities were able to hold much more water per unit of mass than lower densities. This water is potentially stored in extracellular spaces that are favourable for surface tension between stems and branches (Figure 3.6). It was previously claimed that up to 90% of all *Sphagnum* weight is stored externally although the data supporting this claim was limited (Clymo and Hayward, 1982), and they did not ascertain the location of water storage, the fact that dry weight and water content were not correlated for nearly all species, and only weakly correlated for *S. capillifolium* (Figure 3.3A), supports the idea that the water storage is not entirely within plant tissues.

However, although relative water content was a mitigating factor for most species' desiccation tolerance, there were also species differences that may be attributed to different variables. In the relative humidity experiments for example, *S. fallax* typically started with a larger water content than *S. quinquefarium* and similar to *S. inundatum*, but was lost photosynthetic capacity more rapidly in all RH treatments than either of those species and retained less water in each treatment than those species (Figure 3.7A-D). This supports the idea that species specific traits may affect desiccation resilience to a degree, such as structural anatomy traits related to branch number and thickness (Hájek and Vicherová, 2014; Kangas et al., 2014). This difference might be attributed to the traditional 'hummock' and 'hollow' division (Bengtsson et al., 2018; Johnson et al., 2015; Schipperges and Rydin, 1998), where hummock species are said to grow more densely and hold more water to avoid desiccation, whilst hollow species avoid desiccation by growing in predominantly wet areas (Hájek and Beckett, 2008). In the experiments performed here, *S. papillosum* and *S. capillifolium* represented hummock species, whilst *S. inundatum* and *S. fallax* represented hollow species. Contrary to the traditional view that only hummock species store large quantities of water as drought avoidance strategy, all the species used in the experiments reported herein were capable of storing larger quantities of water when grown as a dense hummock-type colony arrangement.

Our results suggest that plant density should receive more focus when considering *Sphagnum* adaptation and ecosystem restoration. Although artificial

density arrangements may not always reflect species behaviour under stable field conditions, they may provide a framework for our understanding of the importance of colony density, especially during restoration. While species differed in desiccation resilience, higher densities slowed desiccation and allowed the retention of photosynthetic function for longer. Plant density therefore could be critical as even a mild reduction of relative humidity for a short period causes long term debilitation of photosynthesis and physiology.

3.5 - References

Bengtsson, F., Granath, G., Cronberg, N., Rydin, H., 2020. Mechanisms behind species-specific water economy responses to water level drawdown in peat mosses. Ann. Bot. 126, 219–230. https://doi.org/10.1093/aob/mcaa033

Bengtsson, F., Granath, G., Rydin, H., 2016. Photosynthesis, growth, and decay traits in Sphagnum - a multispecies comparison. Ecol. Evol. 6, 3325–3341. https://doi.org/10.1002/ece3.2119

Bengtsson, F., Rydin, H., Hájek, T., 2018. Biochemical determinants of litter quality in 15 species of Sphagnum. Plant Soil 425, 161–176. https://doi.org/10.1007/s11104-018-3579-8

Caporn, S.J.M., Rosenburgh, A.E., Keightley, A.T., Hinde, S.L., Riggs, J.L., And Buckler, M., 2018. Sphagnum restoration on degraded blanket and raised bogs in the UK using micropropagated source material: a review of progress. Mires Peat 20, 1–17. https://doi.org/10.19189/MaP.2017.OMB.306

Chiapusio, G., Binet, P., Bertheau, C., Priault, P., 2022. Sphagnum physiological responses to elevated temperature, nitrogen, CO2 and low moisture in laboratory and in situ microhabitats: a review. Aquat. Ecol. 8. https://doi.org/10.1007/s10452-021-09924-8

Clymo, R.S., Hayward, P.M., 1982. The Ecology of Sphagnum, in: Bryophyte Ecology. Springer Netherlands, Dordrecht, pp. 229–289. https://doi.org/10.1007/978-94-009-5891-3_8

Cruz de Carvalho, R., Maurício, A., Pereira, M.F., Marques da Silva, J., Branquinho, C., 2019. All for One: The Role of Colony Morphology in Bryophyte Desiccation Tolerance. Front. Plant Sci. 10, 1–12. https://doi.org/10.3389/fpls.2019.01360

Elumeeva, T.G., Soudzilovskaia, N.A., During, H.J., Cornelissen, J.H.C., 2011. The importance of colony structure versus shoot morphology for the water balance of 22 subarctic bryophyte species. J. Veg. Sci. 22, 152–164. https://doi.org/10.1111/j.1654-1103.2010.01237.x

Fox, J., Weisberg, S., 2019. An R Companion to Applied Regression, 3rd ed. Sage Publications, Thousand Oaks CA.

González, E., Henstra, S.W., Rochefort, L., Bradfield, G.E., Poulin, M., 2014. Is rewetting enough to recover Sphagnum and associated peat-accumulating species in traditionally exploited bogs? Wetl. Ecol. Manag. 22, 49–62. https://doi.org/10.1007/s11273-013-9322-6

Hájek, T., Beckett, R.P., 2008. Effect of water content components on desiccation and recovery in Sphagnum mosses. Ann. Bot. 101, 165–173. https://doi.org/10.1093/aob/mcm287

Hájek, T., Vicherová, E., 2014. Desiccation tolerance of Sphagnum revisited: a puzzle resolved. Plant Biol. 16, 665–773. https://doi.org/10.1111/plb.12126

Hay, F.R., Adams, J., Manger, K., Probert, R., 2008. The use of non-saturated lithium chloride solutions for experimental control of seed water content. Seed Sci. Technol. 36, 737–746. https://doi.org/10.15258/sst.2008.36.3.23

Hunter, J.D., 2007. Matplotlib: A 2D graphics environment. Comput. Sci. Eng. 9, 90–95. https://doi.org/10.1109/MCSE.2007.55

Johnson, M.G., Granath, G., Tahvanainen, T., Pouliot, R., Stenøien, H.K., Rochefort, L., Rydin, H., Shaw, A.J., 2015. Evolution of niche preference in Sphagnum peat mosses. Evolution (N. Y). 69, 90–103. https://doi.org/10.1111/evo.12547

Kangas, L., Maanavilja, L., Hájek, T., Juurola, E., Chimner, R.A., Mehtätalo, L.,

Tuittila, E.S., 2014. Photosynthetic traits of Sphagnum and feather moss species in undrained, drained and rewetted boreal spruce swamp forests. Ecol. Evol. 4, 381–396. https://doi.org/10.1002/ece3.939
Kassambara, A., 2016. ggpubr package, R documentation [WWW Document]. URL https://www.rdocumentation.org/packages/ggpubr/versions/0.1.1 (accessed 2.8.21).
Kremer, C.L., Drinnan, A.N., 2004. Secondary walls in hyaline cells of Sphagnum. Aust. J. Bot. 52, 243–256. https://doi.org/10.1071/BT03010
Loisel, J., Gallego-Sala, A. V., Amesbury, M.J., Magnan, G., Anshari, G., Beilman, D.W., Benavides, J.C., Blewett, J., Camill, P., Charman, D.J., Chawchai, S., Hedgpeth, A., Kleinen, T., Korhola, A., Large, D., Mansilla, C.A., Müller, J., van Bellen, S., West, J.B., Yu, Z., Bubier, J.L., Garneau, M., Moore, T., Sannel, A.B.K., Page, S., Väliranta, M., Bechtold, M., Brovkin, V., Cole, L.E.S., Chanton, J.P., Christensen, T.R., Davies, M.A., De Vleeschouwer, F., Finkelstein, S.A., Frolking, S., Gałka, M., Gandois, L., Girkin, N., Harris, L.I., Heinemeyer, A., Hoyt, A.M., Jones, M.C., Joos, F., Juutinen, S., Kaiser, K., Lacourse, T., Lamentowicz, M., Larmola, T., Leifeld, J., Lohila, A., Milner, A.M., Minkkinen, K., Moss, P., Naafs, B.D.A., Nichols, J., O'Donnell, J., Payne, R., Philben, M., Piilo, S., Quillet, A., Ratnayake, A.S., Roland, T.P., Sjögersten, S., Sonnentag, O., Swindles, G.T., Swinnen, W., Talbot, J., Treat, C., Valach, A.C., Wu, J., 2021. Expert assessment of future vulnerability of the global peatland carbon sink. Nat. Clim. Chang. 11, 70–77. https://doi.org/10.1038/s41558-020-00944-0
Marschall, M., Proctor, M.C.F., 2004. Are bryophytes shade plants? Photosynthetic light responses and proportions of chlorophyll a, chlorophyll b and total carotenoids. Ann. Bot. 94, 593–603. https://doi.org/10.1093/aob/mch178
Maxwell, K., Johnson, G.N., 2000. Chlorophyll fluorescence—a practical guide. J. Exp. Bot. 51, 659–668. https://doi.org/10.1093/jxb/51.345.659
Mccarter, C.P.R., Price, J.S., 2014. Ecohydrology of Sphagnum moss hummocks: Mechanisms of capitula water supply and simulated effects of evaporation. Ecohydrology 7, 33–44. https://doi.org/10.1002/eco.1313
Murchie, E.H., Lawson, T., 2013. Chlorophyll fluorescence analysis: A guide to good practice and understanding some new applications. J. Exp. Bot. 64, 3983–3998. https://doi.org/10.1093/jxb/ert208
Muster, C., Gaudig, G., Krebs, M., Joosten, H., 2015. Sphagnum farming: the promised land for peat bog species? Biodivers. Conserv. 24, 1989–2009. https://doi.org/10.1007/s10531-015-0922-8
Nibau, C., van de Koot, W., Spiliotis, D., Williams, K., Kramaric, T., Beckmann, M., Mur, L., Hiwatashi, Y., Doonan, J.H., 2022. Molecular and physiological responses to desiccation indicate the abscisic acid pathway is conserved in the peatmoss, Sphagnum. J. Exp. Bot. 1–16. https://doi.org/https://doi.org/10.1093/jxb/erac133
Oliver, M.J., Hudgeons, J., Dowd, S.E., Payton, P.R., 2009. A combined subtractive suppression hybridization and expression profiling strategy to identify novel desiccation response transcripts from Tortula ruralis gametophytes. Physiol. Plant. 136, 437–460. https://doi.org/10.1111/j.1399-3054.2009.01245.x
Oliver, M.J., Velten, J., Wood, A.J., 2000. Bryophytes as experimental models for the study of environmental stress tolerance: Tortula ruralis and desiccation-tolerance in mosses. Plant Ecol. 151, 73–84. https://doi.org/10.1023/A:1026598724487

Rice, S.K., 2012. The cost of capillary integration for bryophyte canopy water and carbon dynamics. Lindbergia 35, 53–62.
Rice, S.K., Aclander, L., Hanson, D.T., 2008. Do bryophyte shoot systems function like vascular plant leaves or canopies? Functional trait relationships in Sphagnum mosses (Sphagnaceae). Am. J. Bot. 95, 1366–1374. https://doi.org/10.3732/ajb.0800019
Rice, S.K., Gutman, C., Krouglicof, N., 2005. Laser Scanning Reveals Bryophyte Canopy Structure. New Phytol. 166, 695–704. https://doi.org/10.1111/j.1469-8137.2005.01327.x
RStudio Team, 2020. RStudio: Integrated Development for R.
Rydin, H., Clymo, R.S., 1989. Transport of carbon and phosphorus compounds about Sphagnum. Proc. R. Soc. London. B. Biol. Sci. 237, 63–84. https://doi.org/10.1098/rspb.1989.0037
Schipperges, B., Rydin, H., 1998. Response of photosynthesis of Sphagnum species from contrasting microhabitats to tissue water content and repeated desiccation. New Phytol. 140, 677–684.
Silvola, J., Aaltonen, H., 1984. Water content and photosynthesis in the peat mosses Sphagnum fuscum and S . angustifolium. Ann. Bot. Fenn. 21, 1–6.
Stenøien, H.K., Bakken, S., Flatberg, K.I., 1997. Phenotypic Variation in the Sphagnum Recurvum Complex: a Cultivation Experiment. J. Bryol. 19, 731–750. https://doi.org/10.1179/jbr.1997.19.4.731
Temmink, R.J.M., Fritz, C., van Dijk, G., Hensgens, G., Lamers, L.P.M., Krebs, M., Gaudig, G., Joosten, H., 2017. Sphagnum farming in a eutrophic world: The importance of optimal nutrient stoichiometry. Ecol. Eng. 98, 196–205. https://doi.org/10.1016/j.ecoleng.2016.10.069
van Breemen, N., 1995. How Sphagnum bogs down other plants. Trends Ecol. Evol. 10, 270–275. https://doi.org/10.1016/0169-5347(95)90007-1
van de Koot, W.Q.M., van Vliet, L.J.J., Chen, W., Doonan, J.H., Nibau, C., 2021. Development of an image analysis pipeline to estimate Sphagnum colony density in the field. Plants 10, 1–17. https://doi.org/10.3390/plants10050840
Warren, M., Frolking, S., Dai, Z., Kurnianto, S., 2017. Impacts of land use, restoration, and climate change on tropical peat carbon stocks in the twenty-first century: implications for climate mitigation. Mitig. Adapt. Strateg. Glob. Chang. 22, 1041–1061. https://doi.org/10.1007/s11027-016-9712-1
Waskom, M., Gelbart, M., Botvinnik, O., Ostblom, J., Hobson, P., Lukauskas, S., Gemperline, D.C., Augspurger, T., Halchenko, Y., Warmenhoven, J., Cole, J.B., Ruiter, J. de, Vanderplas, J., Hoyer, S., Pye, C., Miles, A., Swain, C., Meyer, K., Martin, M., Bachant, P., Quintero, E., Kunter, G., Villalba, S., Brian, Fitzgerald, C., Evans, C., Williams, M.L., O'Kane, D., Yarkoni, T., Brunner, T., 2020. mwaskom/seaborn: v0.11.1 (December 2020). https://doi.org/10.5281/ZENODO.4379347
Winnicka, K., Melosik, I., 2019. Genetic and expression differences between putative ecotypes of Sphagnum denticulatum Brid. (Sphagnaceae: Bryophyta) subjected to drought stress and rehydration. Perspect. Plant Ecol. Evol. Syst. 37, 39–52. https://doi.org/10.1016/j.ppees.2019.02.004
Yu, Z., Loisel, J., Brosseau, D.P., Beilman, D.W., Hunt, S.J., 2010. Global peatland dynamics since the Last Glacial Maximum. Geophys. Res. Lett. 37, 1–5. https://doi.org/10.1029/2010GL043584

CHAPTER 4 - DEVELOPMENT OF AN IMAGE ANALYSIS PIPELINE TO ESTIMATE *SPHAGNUM* COLONY DENSITY IN THE FIELD

Chapter statement:

This chapter is a modified version of research previously published as "*Development of an image analysis pipeline to estimate Sphagnum colony density in the field*" (DOI: https://doi.org/10.3390/plants10050840). To reference any of the results mentioned in this chapter, please refer to the aforementioned publication and cite as:

van de Koot, Willem Q. M., Larissa J. J. van Vliet, Weilun Chen, John H. Doonan, and Candida Nibau. 2021. "Development of an Image Analysis Pipeline to Estimate *Sphagnum* Colony Density in the Field" Plants 10, no. 5: 840. https://doi.org/10.3390/plants10050840

The produced Python script can be found as text attached in Appendix 3, and on Github (https://github.com/NPPC-UK/Capitula--ounter/blob/main/Capitulum_counting_pipeline.py).

In this chapter, I was responsible for the conceptual design of the algorithm, the experimental design and methodology of the verification, and data acquisition. The programming of the algorithm was carried out by Larissa van Vliet, with some minor contributions by Weilun Chen (the GUI). Candida Nibau, Dominic Spiliotis, Larissa van Vliet and Karen Askew helped count the false positives and negatives.

Data availability

The data pertaining to this chapter can be accessed at (https://doi.org/10.20391/9ba4df8f-2d28-4bce-b9b8-ec6368b636e0)

Chapter summary

Sphagnum peatmosses play an important part in water table management of many peatland ecosystems. Keeping the ecosystem saturated, they slow the breakdown of organic matter and release of greenhouse gases, facilitating peatland's function as a carbon sink rather than a carbon source. Although peatland monitoring and restoration programs have increased recently, there are few tools to quantify traits that *Sphagnum* species display in their ecosystems. Colony density is often described as an important determinant in the establishment and performance in *Sphagnum* but detailed evidence for this is limited. Here we describe an image analysis pipeline that accurately annotates *Sphagnum* capitula and estimates plant density using open access computer vision packages. The pipeline was validated using images of different *Sphagnum* species growing in different habitats, taken on different days and with different smartphones. The developed pipeline achieves high accuracy scores and we demonstrate its utility by estimating colony densities in the field and detecting intra and inter-specific colony densities and their relationship with habitat. This tool will enable ecologists and conservationists to rapidly acquire accurate estimates of *Sphagnum* density in the field without the need of specialised equipment.

4.1 - Introduction

In recent years, there has been a renewed interest in the study and restoration of peatlands. Although peatlands only cover 2-3% of the earth's surface (Rydin and Jeglum, 2015) they store around a third of the world's soil carbon. Overextraction of peat and government subsidised bog drainage for agricultural purposes have led to the degradation of many peatland ecosystems. In addition, changes in global climate patterns, especially precipitation, have accelerated peatland degradation in some regions (Gallego-Sala and Colin Prentice, 2013; Heinemeyer and Swindles, 2018). Peatlands are a critical part of the global carbon cycle and their conservation and restoration is key if we are to meet global climate targets (Charman et al., 2013).

Key to conservation efforts is understanding the interactions between the plant communities in the peatland ecosystem and their responses to environmental changes (González et al., 2014; Mazziotta et al., 2019; Rastogi et al., 2020; Wang et al., 2013). A main component in many peatland ecosystems is the peatmoss, *Sphagnum*, which is often given the status of 'ecosystem engineer' (Bengtsson et al., 2020; Hájek and Vicherová, 2014; Johnson et al., 2015; Weston et al., 2018). Many of the species in this genus are bog specialists that waterlog and acidify the environment, excluding many potential competitors and creating optimal peat-forming conditions.

Sphagnum mosses possess specialised morphological and physiological adaptations for water retention, which promote carbon sequestration through peat accumulation. The photosynthetically active tissues of *Sphagnum* mosses are located at or near the surface and each shoot of *Sphagnum* bears a dense array of growing branches at the top called the capitulum. In the capitulum region, branches elongate much more rapidly than shoot internodes, producing the characteristic compact hemispherical shape. Below the capitulum region, the branches tend to stop growing and internode elongation increases. Further down the stem, the lack of light causes the death of the lower branches and, characteristic to *Sphagnum* mosses, the rate of degradation of the dead material may be so low that it allows the formation of peat. The peat layer plays an important role in carbon sequestration, water storage, and prevention of surface desiccation. The acidic waterlogged conditions in the peat can slow or prevent the growth of most other plants and microorganisms (Rydin et al., 2006). Despite its importance in the maintenance of the peat ecosystem, we are only

starting to understand how *Sphagnum* growth and development responds to environmental changes, specifically to drought.

The Sphagna are not desiccation tolerant (DT) and are generally restricted to wet and humid habitats. However, different niche preferences between the species have been linked to the micro-climate and, specifically, to the accessibility of ground water (Johnson et al., 2015). Some species are specialised but others can grow across a range of habitats. The basis of these preferences and adaptations to the different habitats remain poorly understood. Generally, it is accepted that *Sphagnum* avoids desiccation by a combination of having a large water storage capacity, the ability to retain water within organ spaces, and strong capillary forces that replenish the surface evaporated water from the peat layer below (Clymo and Hayward, 1982; Proctor, 2000). *Sphagnum* holds large amounts of water, perhaps more per unit of biomass than any other group of land plants. Some of the water is stored in specialised cells, but the majority is retained within extracellular spaces (Clymo and Hayward, 1982).

The ability to store water in extracellular spaces is due to morphological adaptations of the *Sphagnum* plant, including densely packed leaves and branches, and the production of long pendant branches that act as wicks (Bengtsson et al., 2020; Glime, 2017). In other bryophytes, colony density has been shown to have a significant impact on water retention by reducing the amount of free space between individual shoots and trapping moisture below the canopy (Bengtsson et al., 2020; Cruz de Carvalho et al., 2019; Elumeeva et al., 2011). Although this has also been suggested for *Sphagnum*, there is little experimental data. The density of the canopy can be defined as the number of capitula per unit area but the arrangement of leaves and branches also varies and may contribute to water relations. Species-specific canopy traits could be plastic and change according to the habitat or alternatively, canopy traits could influence the habitats that a given species colonises (Bengtsson et al., 2016; Hayward and Clymo, 1983).

Canopy density is not only important to determine drought tolerance, but is also a critical determinant in the successful establishment of peat plugs in bog restoration projects. Many of the natural peatlands in the UK have been subjected to extensive human intervention and are now considered to be degraded. Despite this, bogs are now recognised as important and diverse habitats and many restoration projects are under way across the country. Although *Sphagnum* re-introduction has

been mostly done using mixed plugs (Caporn et al., 2018), optimal densities and combinations of species are not known. Estimation of *Sphagnum* mosses colony density in the field is a time consuming process and as far as we know, easy-to-use protocols are not yet available.

Methods for estimating canopy density are well established for trees and other large plants, but few have been applied to bryophytes (Abdollahnejad et al., 2017; Harris et al., 2006; Rice et al., 2005). These methods exploit a range of imaging techniques, including aerial photography, satellites, and laser scanning. Data from these methods ranges from simple density measures to the physiological status of the plants using various vegetation indices. In recent years, there has been an upsurge in the development of imaging techniques being applied to plants. Increased image resolution and advances in image analysis have facilitated monitoring growth and development (del Valle et al., 2018; Feng et al., 2019; Hüther et al., 2020; Li et al., 2014) and are easily applied to both small and large scale surveys. However, many imaging techniques require specialised equipment like sophisticated imaging platforms that cannot easily be used in the field, or access to unmanned aerial systems, that often do not provide the necessary detail for many studies. High-resolution cameras have become ubiquitous on smartphones, and these have great potential for the collection of imaging data through citizen science. The development of appropriate analytical tools could increase the monitoring capacity of conservationists. In addition, such tools could enable scientists to rapidly acquire large amounts of data and help standardise data collection and analyses.

Here, we describe the development of a simple, robust and user-friendly image analysis pipeline to determine *Sphagnum* canopy density in the field using images acquired with a standard smartphone. We show the accuracy and applicability of the method for images acquired in different sites and for different *Sphagnum* species. Using the developed pipeline, we show that densities of several *Sphagnum* species are different in the field and quantify how densities differ within the same species growing in different sites.

4.2 - Materials and Methods

4.2.1 - Site selection

Sphagnum species from several different local ecosystems were selected to cover the four most abundant taxonomic sections within the genus, namely *Sphagnum*, *Acutifolia*, *Subsecunda* and *Cuspidata* (Table 4.1) and to provide a reasonably representative mixture of the sizes and shapes that are typically found in the genus. *Sphagnum* colonies were imaged at three field sites, Coed y Darren (SN677835), Pen y Garn (SN791758) and Llyn Pendam (SN709838) (Figure 4.1). The selected sampling sites covered a range of *Sphagnum* niches, such as wet woodland, minerotrophic mire and blanket bog. Within each site, several patches of each moss species were selected. In order to encompass as much morphological, physiological and imaging diversity as possible, images were acquired across these sites in different seasons and under different weather conditions.

Table 4.1**.** Location, *Sphagnum* species, subgenus, and number of images of each species per location.

Location	**Species**	**Subgenus**	**n. of images**
Coed y Darren	*S. quinquefarium* Warnstorf 1886	*Acutifolia*	23
Pen y Garn	*S. fallax* Klinggräff 1881	*Cuspidata*	9
	S. inundatum Russow 1894	*Subsecunda*	4
	S. papillosum Lindberg 1872	*Sphagnum*	12
	S. fallax & S. papillosum (mix)		5
Llyn Pendam	*S. auriculatum* Schimp.	*Subsecunda*	11
	S. fallax	*Cuspidata*	10
	S. papillosum	*Sphagnum*	8
Total			82

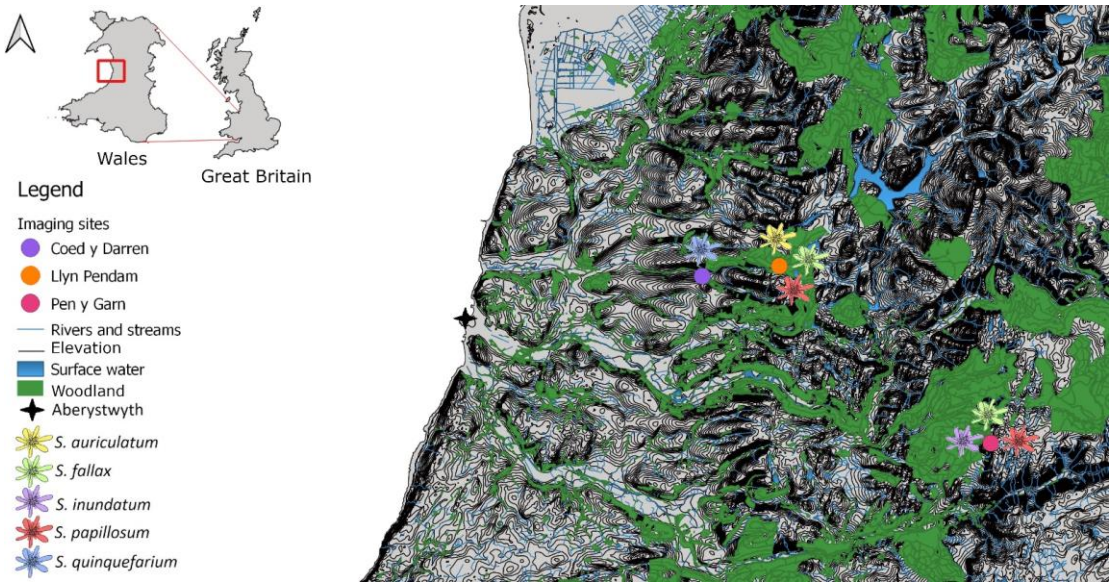

Figure 4.1. A map showing major surface water bodies, elevation lines, major woodlands and the locations of the sampled sites around Aberystwyth, Wales and the species present at each site. Coed y Darren is a humid mixed woodland, with *S. quinquefarium* covering much of the forest floor. Llyn Pendam is connected to several other lakes by small streams, with mostly gravel shores with *S. auriculatum* growing on or near the shoreline, and *S. papillosum* growing near the in- and outflow streams. Pen y Garn is located in the Cambrian mountains with an ombrotrophic blanket bog covering its peak and ombrotrophic to minerotrophic mires at its base, with several pools that exhibit flow after heavy rain. Contains OS data © Crown copyright and database right 2020.

4.2.2 - Field image acquisition

Images were acquired with a simple, purpose-built imaging rig that is easy and inexpensive to build, portable and flexible enough to allow the use of different smartphones or cameras (Figure 4.2). The rig consisted of a rectangular imaging area (31x26cm) delineated by a blue surround that held a colour card (greywhitebalancecolourcard.co.uk) and supported a 35cm high platform on which the smartphone was placed (Figure 4.2A, B). The blue frame facilitates easy removal from the image, as blue is a distinct colour not usually found in nature, and ensures a standard field of view (FOV) for each acquisition. The presence of a commercial colour card was used as a landmark and to aid white balance correction. To ensure general utility, both Apple (iPhone 6s and 7) and Samsung J3 smartphones were utilised. The rig was placed on a selected patch of *Sphagnum*, making sure that the lighting on the region of interest (ROI) was homogenous. The imaging sites were selected based on the presence of appropriate types of moss but also areas with low amounts of vascular plants, as they might obstruct the imaging. Special care was paid

to making sure that the whole frame was seen in the picture, that the view of the colour card was not obstructed, and the image was not overexposed (Figure 4.2C). A black plastic screen was used to block direct sunlight and ensure homogeneous illumination. A total of 82 images were collected across the different sites and from different days, 30 from Pen y Garn, 29 from Llyn Pendam, and 23 from Coed y Darren (Table 4.1). All images used are available at https://doi.org/10.20391/9ba4df8f-2d28-4bce-b9b8-ec6368b636e0.

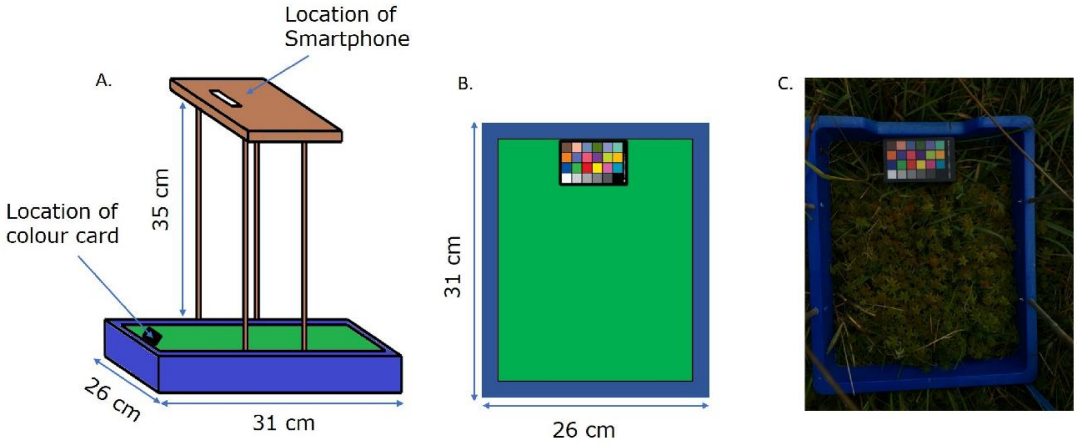

Figure 4.2. Schematic overview of the imaging rig. A. Lateral view. B. Top view. C. Field image taken using the rig. The blue surround of the image facilitates removal in pre-processing, whilst the colour card provides an internal standard.

4.2.3 - Image processing pipeline

A computer vision and image processing pipeline was developed in Python 3 (Van Rossum and Drake, 2009) (http://www.python.org) and is available, together with instructions for use at http://www.github.com/NPPC-UK/Capitula-Counter as Python file. Image blurring, colour conversion and cropping were carried using the OpenCV package (Bradski, 2000) and exposure compensation was done using the PlantCV package (Fahlgren et al., 2015). The interactive GUI for thresholding in the HSV (Hue, Saturation & Value) S colour channel (used for masking non-*Sphagnum* objects in the image) was developed using the PySimpleGUI package (The PySimpleGUI Organization, 2020). Capitula detection was performed in the YCrCb Cb colour channel, where Y is luma and Cb and Cr are Chroma blue and Chroma red respectively, using the Difference of Gaussian Blob detection function from the

scikit-image package (Van Der Walt et al., 2014). This function blurs an image multiple times with increasing standard deviations and stacks the resulting blurred images into a cube. In this cube, local maxima of pixel values are detected as concentrations of high values which detects them as 'blobs' in the image. In our case, the contrast between the background material and the capitula enables the function to find the capitula as local maxima that are then annotated as blobs. The annotations were saved as .jpg image files and listed in a .csv-file with their positional coordinates and dimensions. The number of annotations per image was written to a separate .csv file containing a list of all the images. All the image annotation raw data is available at https://doi.org/10.20391/9ba4df8f-2d28-4bce-b9b8-ec6368b636e0.

4.2.4 - Thresholding channel selection

To determine the optimal colour channels for thresholding and annotation, a subset of 19 images was thresholded and annotated in a variety of colour-space combinations. Images were manually thresholded in 5 different commonly used colour space channels, namely HSV H, HSV S, LAB (where L is lightness, A is the green/red chromatic axis and B the blue/yellow axis) A, YCrCb Y, YCrCb Cr, as well as 3 mathematically constructed image representations: Chromatic difference, HSV difference and Green difference (Supplementary Figure 4.1). Chromatic difference has been previously described (del Valle et al., 2018; Hüther et al., 2020).

Two new colour spaces, HSV difference and Green difference were designed to increase the contrast between the capitula and the background, by amplifying the channels (HSV H and RGB green respectively). The equations used to calculate HSV difference and Green difference can be found in Supplementary Table 4.1. All the resulting 152 images (19 images thresholded in the 8 different colour spaces) were manually checked for the quality of the masks. The images with poor segmentation, where the distinction between *Sphagnum* and non-*Sphagnum* material was not clear, or where too much *Sphagnum* was also masked were discarded. 48 images from the different channels (HSV H (n=6), HSV S (n=15), LAB A (n=2), YCrCb Y (n=1), YCrCb Cr (n=3), Chromatic difference (n=4), HSV difference (n=13) and Green difference (n=4)) were taken forward and annotated in 3 different colour channels: LAB B, YCrCb Cb inverted and HSV S (Supplementary Figure 4.1), resulting in 144

annotated images. Each image was divided into 16 grid cells of equal size. For each image, 4 randomly selected grid cells were scored for true positives (correctly identified capitula), false positives (incorrectly identified as capitula) and false negatives (capitula not identified by the annotation) using the FIJI software (https://fiji.sc/). The obtained scores were used to calculate precision, recall and F-measure (Tharwat, 2018) using the following formulas:

$$\text{Precision} = \left(\frac{\text{Count} - \text{False positives}}{\text{Count}}\right)$$

$$\text{Recall} = \left(\frac{\text{Count} - \text{False positives}}{(\text{Count} - \text{False positives}) + \text{False negatives}}\right)$$

$$\text{F-measure} = \left(2 * \frac{\text{Precision} * \text{Recall}}{\text{Precision} + \text{Recall}}\right)$$

The higher the F-measure, the more accurate the identification of the *Sphagnum* capitula is. Images that had an F-measure lower than 0.60 or higher than 0.85 were reviewed by a second counter to confirm the counts.

4.2.5 - Pipeline validation

To verify the accuracy of the automated counts, a subset of 24 images from the field was manually counted independently by 4 individuals using the cell counter function in Fiji (Schindelin et al., 2012) and F-measures were calculated as described above.

4.2.6 - Statistical analysis

All statistical analyses were carried out in RStudio version 4.0.3 (RStudio Team, 2020) using the packages car (Fox and Weisberg, 2019) and ggpubr (Kassambara, 2016). Data and file manipulation was done in Python 3 (Van Rossum and Drake, 2009) using the glob (Van Rossum and Drake, 2009), numpy (Harris et al., 2020), and pandas (McKinney, 2010; Reback et al., 2020) packages in Python. Figures were generated using Matplotlib (Hunter, 2007) and seaborn (Waskom et al., 2020) in Python. Comparisons between colour channels, species and counts were done through multivariate type III ANOVAs with Wilcoxon rank sum tests as pairwise comparison, as the data was unbalanced. Site comparisons were tested using Tukey's honest significant difference test. Information on the statistical tests used for each analysis is included in the figure legends.

4.3 - Results

4.3.1 - Development of an image processing and analysis pipeline

In order to accurately measure colony density from the images acquired in the field, we developed a capitula detection and counting pipeline using Python. This pipeline and instructions for use are freely available at the NPPC GitHub (http://www.github.com/NPPC-UK/Capitula-Counter) as a Python file. A schematic representation of the pipeline used for image processing and analysis is depicted in Figure 4.3.

The pipeline consists of two sections: Pre-processing and Annotation. The main steps in the pre-processing section are ROI detection, rotation, perspective correction and size standardisation, white balance correction, and finally cropping to the centroid. The cropped centroid then enters the annotation section where the image is first transformed to the HSV S colour channel, and thresholded to generate a mask. The masked image is then transformed to the YCrCb Cb colour channel, in which it is then annotated. Each step of the pipeline is described in detail in the following sections.

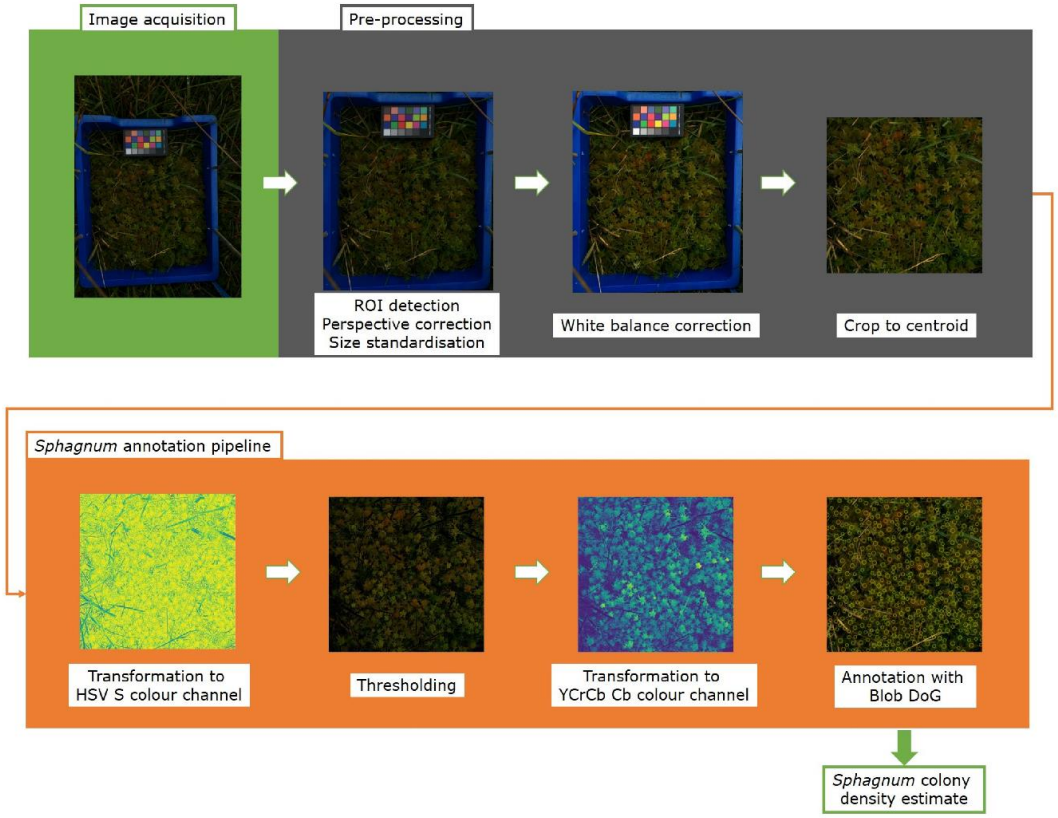

Figure 4.3. The capitulum counting image processing pipeline. After image acquisition, the images are pre-processed in Python using the OpenCV package, which involves detecting the blue frame, rotating it and correcting the perspective. Then, using the PlantCV package, the colour card is used to correct the white balance of the image. The final step of the pre-processing crops the image to the 800x800 pixels centroid, removing the blue frame and colour card. After pre-processing, the image enters the annotation pipeline. First, the image is transformed to the HSV colour space channel S, in which it is subsequently thresholded to mask non-*Sphagnum* material. After thresholding, the image is converted to the YCrCb colour space channel Cb and the capitula are annotated using the Blob DoG function from the scikit-image package. From this colony density is estimated and data saved in a .csv file.

4.3.1.1 - Pre-processing pipeline

The first step in the segmentation pipeline used the blue frame to detect and select the image area that it is to be analysed (ROI) (Figure 4.3). Initially, the image is blurred using the blur function from the OpenCV package and a 50 x 50 kernel. This step is necessary to reduce noise caused by grass located outside the blue box or covering the edges of the blue box. Subsequently, the original image is converted to the HSV-colour space using the colour conversion function from OpenCV, which is the function used for all colour conversions in this pipeline. The blur and the HSV-colour space facilitate thresholding of the blue frame to produce the image mask,

which is then eroded to reduce noise caused by stray pixels. The mask is filtered and the four corners of the square located. To increase the robustness of this method the position of the lower right corner was calculated using the other three corners and knowledge of the frame shape. This takes into account unexpected blue pixels outside the frame or inadvertent differences in the camera orientation. The position of all four corners of the frame was then fed into the 'getPerspectiveTransform' function from OpenCV that calculates the transformation matrix to correct the perspective. The 'warpPerspective' function was used in turn to crop the image, correct the perspective and transform the dimensions to a standard size. The resulting output, where the inside edges of the frame define the portion of the image, was used for downstream analysis.

Although exposure correction was not essential for estimating canopy density, it might be useful if the images are to be subsequently used to measure other parameters, such as pixel colour or saturation. Over-exposed images cannot be corrected easily due to information loss, We also included a white balance correction step using the colour card and the PlantCV package (Fahlgren et al., 2015) (Figure 4.3). As the colour card is always in the same position in our images, the positional coordinates (in our case 390x, 250y) were used and fed into the white balance function of the PlantCV package. This significantly reduced computational time, was less error-prone and less noise sensitive. The Auto-Detect Colour Card function can be used to find the white colour chip in the card if coordinates are not available.

After white balance correction, the images were further cropped to remove the blue frame and the colour card (Figure 4.3). Since all the images had the same shape and size, the x and y-coordinates from which the image was cropped were always the same (121x, 351y), and produce a cropped centroid with a width and height of 800 pixels, which corresponded to a size of 347 cm^2. These dimensions can be easily adjusted for different imaging area sizes.

4.3.1.2 - Thresholding optimisation

The first step in the annotation pipeline is image thresholding, where the non-*Sphagnum* material is removed from the image. This is done by identifying the pixel value range containing the *Sphagnum* material and using the pixels outside this range to create a mask. The mask is then used to remove all the non-*Sphagnum* pixels from

the image. As this step is critical for the success of the annotation, we developed an interactive GUI using the PySimpleGUI package (The PySimpleGUI Organization, 2020). The GUI allows intuitive manipulation of the desired value ranges. After the image is cropped, the user is prompted to adjust the threshold in the interactive GUI window. The upper and lower thresholds can be adjusted for each image in order to obtain an image with the highest possible contrast between the capitula and the other plant material. A threshold was considered good when it sufficiently removed large amounts of non-*Sphagnum* material, whilst only minimally affecting the centre of the *Sphagnum* capitula.

However, for sets of images of similar lighting or if high throughput is required, the user has the option to select general thresholding values for all the images. For this, we created a pop-up window at the start of the pipeline, which asks whether the user wants the version with the GUI and manually threshold each image or enter specific thresholding values that will automatically be applied for all images. For the majority of our images, we found that the upper threshold was usually constant at 256 while the lower value varied with the colour of the material as indicated in Supplementary Table 4.2. To avoid manual thresholding, the values in this table can be entered at the start. In the case of sets of images with variable colour and exposure, a general lower threshold of 125 can also be used as we show that it yielded similar results to manual thresholding (Supplementary Figure 4.2).

4.3.1.3 - Thresholding and annotation channel selection

The performance of the pipeline relies on two key factors. The first one is achieving a good contrast between the *Sphagnum* and background material, such as grasses, so a mask can be created and the background material removed. This is done by using an appropriate thresholding colour channel to create a mask. The second is to achieve a good enough contrast between the individual capitula so they can be detected by the Blob DoG function as local maxima and annotated as *Sphagnum* capitula. This can be achieved by selecting an appropriate annotation colour channel. In order identify the more suitable thresholding and annotation channels, 19 images were thresholded in 5 different colour spaces (HSV H, HSV S, LAB A, YCrCb Y, YCrCb Cr, Chromatic difference, HSV difference and Green difference). The images with better thresholding were annotated in three colour spaces (LAB B, YCrCb Cb

inverted and HSV S) (Supplementary Figure 4.1) as detailed in the methods. F-measures, that reflect how accurate a classifier is, were used to assess the performance of the various channel combinations.

Our analysis of the performance of different combinations of thresholding and annotation channels found that the combination of thresholding channel HSV S and annotation channel YCrCb Cb resulted in a high mean F-measure (0.77) (Supplementary Figure 4.3). Although the F-measure for thresholding channel HSV S was not significantly different from other thresholding channels within annotation channel YCrCb Cb, it had the largest sample size (n=15) and was therefore considered most reliable. The high performance of the YCrCb Cb as an annotation channel was maintained when the different species were considered separately (Supplementary Figure 4.4). The full comparison of the different thresholding and annotation channels can be found in supplemental Supplementary Figure 4.3.

4.3.1.4 - Blob detection and capitula counting

The last step in the pipeline was identification of *Sphagnum* capitula. For this, images segmented in the HSV S channel and transformed into the YCrCb Cb channel were fed into the Blob DoG (Difference of Gaussian) detection of the scikit-image package, which is a popular, open access package under constant development. Blob DoG creates blurred copies of the original image and calculates the difference for each pixel between the blurred copies, allowing edge detection based on when the value of a pixel changes from positive to negative or from negative to positive. The identified blobs were then overlaid on the original cropped image as annotations (Figure 4.3). Finally, the annotations are saved as a list containing their coordinates and dimensions, with the number of rows equalling the total number of annotations in the image. The length of this list for each separate image was written to a separate spreadsheet as the number of plants counted by the pipeline. All these are provided as .csv files.

4.3.2 - Estimation of pipeline accuracy

Having established that the HSV S and YCrCb Cb channels were optimal for thresholding and annotation, a new set of 34 previously unused images was run

through the pipeline using these channels as the default. Together with the images that had been run through these channels in the pipeline development stage, the resulting in a total of 68 images (Supplementary Table 4.3), were scored for true positives, false positives and false negatives to calculate the evaluative scores.

The pipeline achieves a mean F-measure of 0.77 which indicates that it correctly identifies the capitula correctly 77% of the time when all species are combined. When we looked at each species separately (Figure 4), the highest F-measures were achieved by images of *S. quinquefarium* (0.93), *S. fallax* (0.90) and *S. inundatum* (0.91) while *S. papillosum* had the lowest F-measure (0.50) suggesting that the method does not perform as well for this species (Figure 4.4). We should note that a low number of images were used for *S. inundatum* (n=4) and the mixed colonies of *S. fallax* and *S. papillosum* (n=4) (Supplementary Table 4.3), and this could affect their mean F-measures.

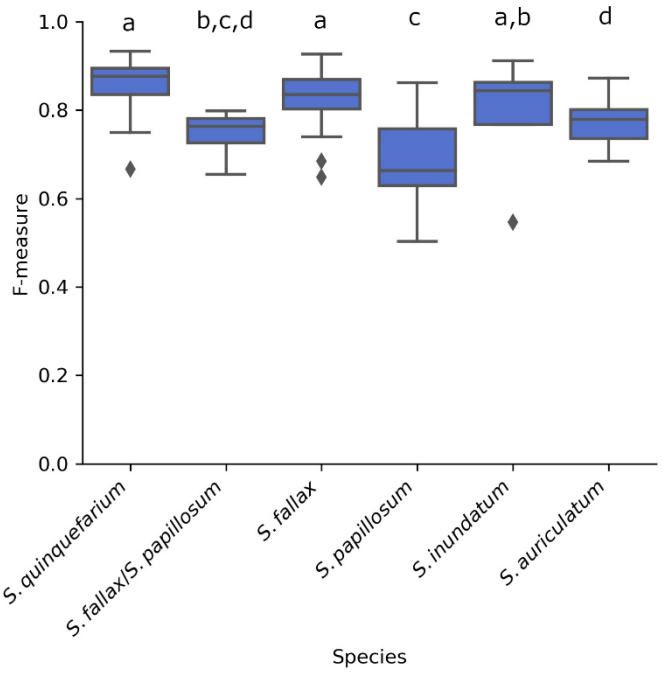

Figure 4.4. F-measures of the 68 images thresholded in HSV S and annotated in YCrCb Cb for each of the 5 species as well as mixed colonies of *S. fallax* and *S. papillosum* as indicated. Letters above the boxplots indicate significance groups for $p<0.01$ as determined by Wilcoxon rank rum test.

Automated and manual counts were compared to determine the accuracy of the software in the identification of *Sphagnum* capitula. For this, a subset of 24 images, consisting of 5 images of each species except for *S. inundatum*, of which only 4 images were available, were run through the software and also counted manually using Fiji by 4 counters.

As can been seen in Figure 4.5, there were significant differences between the number of capitula counted by each of the counters, underlining the difficulties in this process. All of the manual counts were significantly lower than the automated counts ($p<0.0001$****) (Figure 4.5) indicating that, although the pipeline was able to achieve high F-measures, it typically overestimates the number of plants in an image.

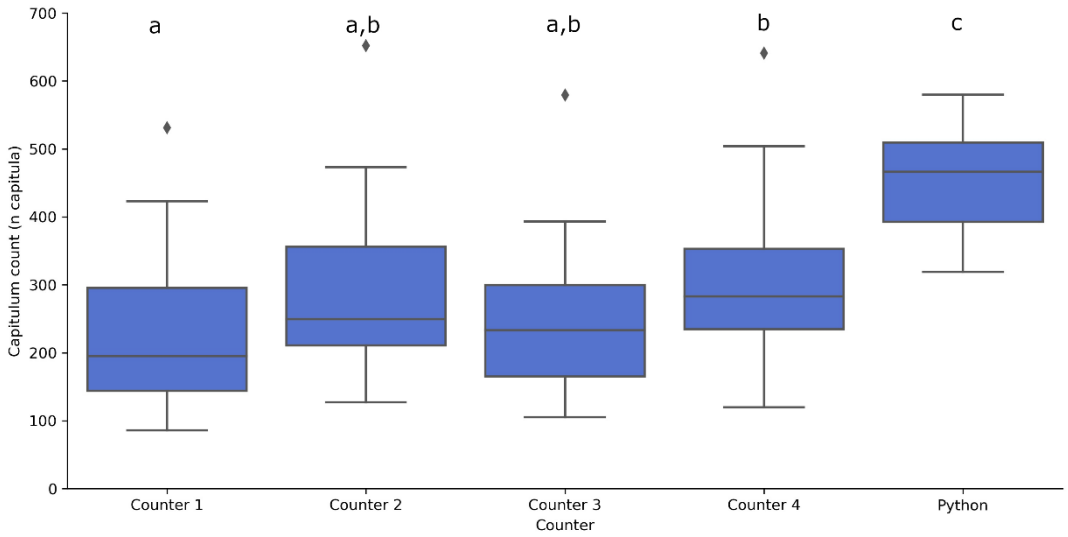

Figure 4.5. Number of capitula counted by the four human counters and the automated counting function in 24 images. The automated function was significantly different from the counters, and Counter 1 and Counter 4 differed significantly from each other. Letters above boxplots indicate significance groups for $p<0.05$ between a and b and $p<0.0001$ for c as determined by multivariate type III ANOVA with Wilcoxon rank sum tests.

In order to determine if there was a correlation between the manual and automated counts, a model was created which contained the manual count, automated count and species. For the model we used the 64 images described above to calculate the F-measures. The manual count for these images was calculated by adding the true positives and the false negatives scored by the counters. Both linear and log models were fitted to the data, and these performed similarly based on the Akaike Index Criterion (AIC) and residual standard error (Figure 4.6, Supplementary

Table 4.4 & 4.5). As the linear and log models were not significantly different form each other (p=0.173), we decided to use the linear regression model as it was the least complex interpretation of the data. The linear model was highly significant ($p<0.001$***, $R^2=0.63$) and had a slope of 0.483 (Figure 4.6, Supplementary Table 4.4), indicating that there is a linear relationship between the automated counts and the manual counts. Furthermore, the model indicated that this linear relationship was maintained across species (Supplementary Table 4.4), and a Kruskal-Wallis test indicated that there was no significant difference between the manual counters (p>0.32).

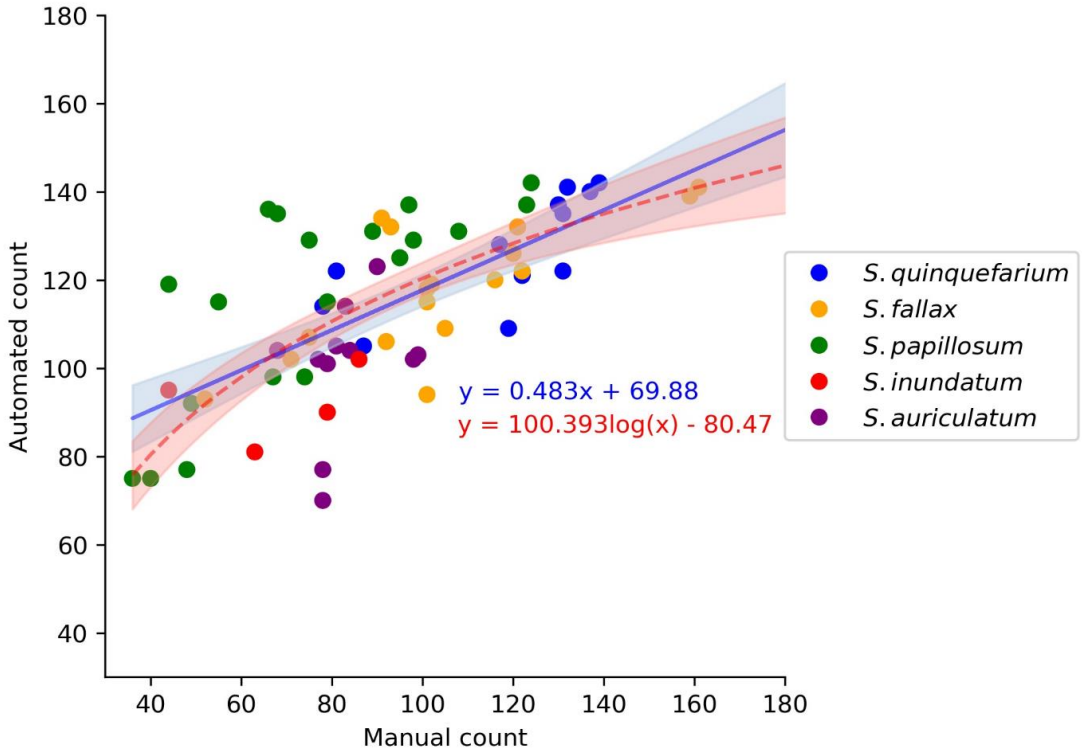

Figure 4.6. Comparison of the linear (blue line) and log (red dashed line) models for the manual count and automated count (n=64). These models do not differ significantly (t-test, p=0.173) and although the log model had a slightly lower AIC and residual standard error (Supplementary Table 4.4 and S5), we chose the linear model as it was the least complex way to explain the data.

As there was a linear relationship between the manual and automated counts, the data obtained from the model was used to calculate a correction factor for the automated counts. This correction factor was calculated as the mean of the manual count divided by the mean automated count, resulting in a correction factor of 0.81.

When this blanket correction factor was applied to the automated counts, they were no longer significantly different from the manual counts for *S. fallax*, *S. inundatum* and *S. auriculatum* (Figure 4.7A). However, as *S. papillosum* and *S. quinquefarium*'s corrected counts were still significantly different from the manual counts, species-specific correction factors were also calculated (Supplementary Table 4.6). Using these species-specific correction factors, the adjusted automated counts were no longer significantly different from the manual counts for any of the species (Figure 4.7B).

Given these data, an extra step was added to the pipeline before the colony density estimation. This step included the blanket correction as default but this can be changed to use the species-specific correction factor described here or independently calculated.

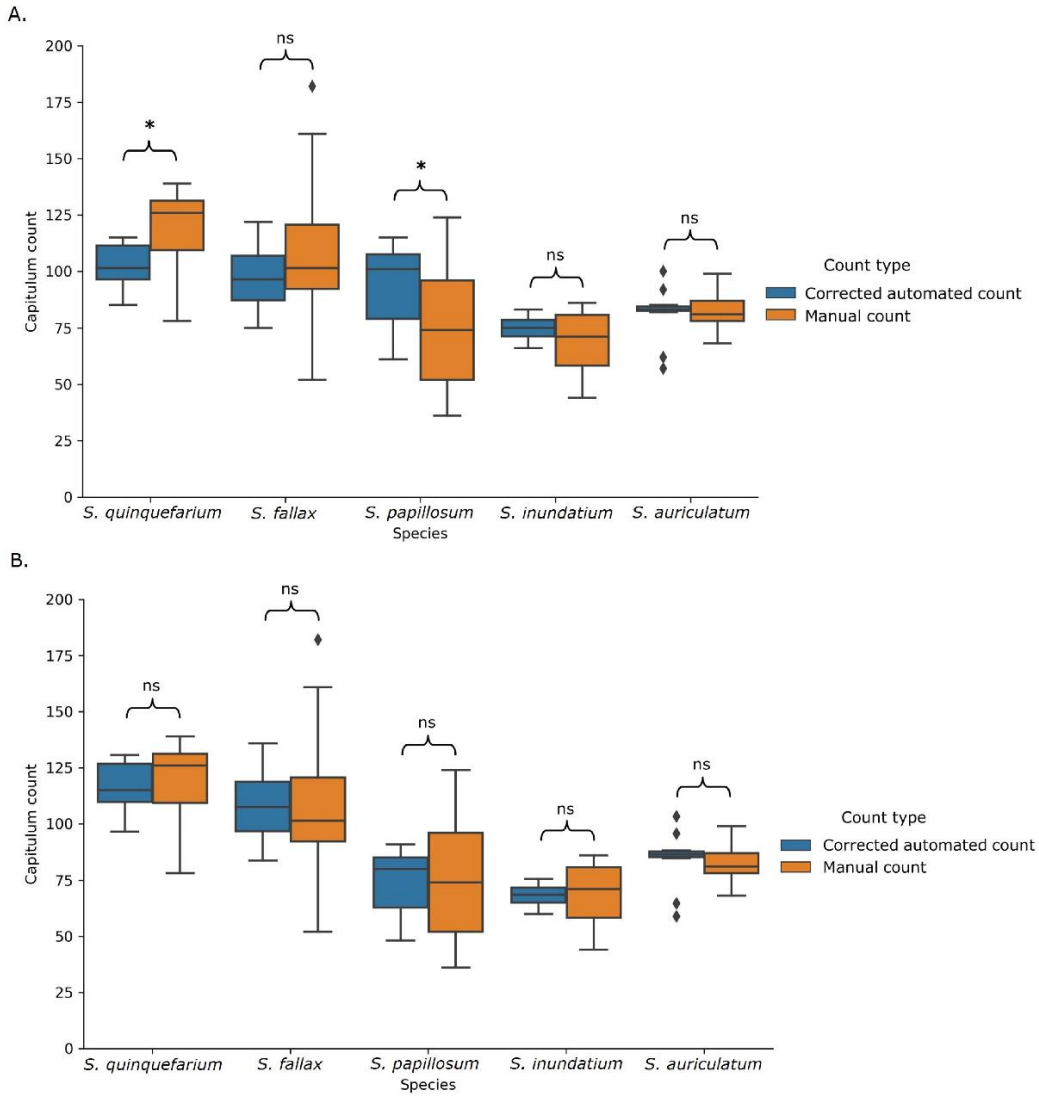

Figure 4.7. Blanket (A) and species-specific (B) corrected automated counts and the corresponding manual counts. Using the blanket correction (A), the corrected automated count still differed significantly for two of the five species. Using the species-specific correction (B) (Supplementary Table 4.6), there were no longer significant differences. ns indicates valued not significantly different for each other and * indicates significance at $p<0.05$ as calculated using a multivariate type III ANOVAs with Wilcoxon rank sum test. Sample size per species can be found in Supplementary Table 4.3.

4.3.3 - Estimation of capitula density in field images

In order to determine if there were density differences between species and if different habitats influence species density, we analysed images containing different *Sphagnum* species from different sites. The species-specific correction factor was used for each species. Indeed, we observed differences in plant density (number of plants per cm^2) for the different species and for the different habitats (Figure 4.8).

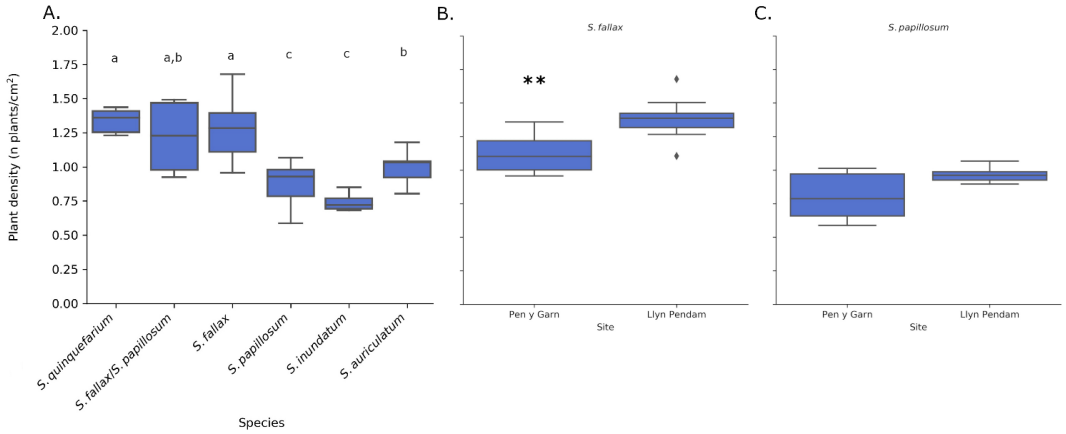

Figure 4.8. Plant density per cm^2 for 5 species of *Sphagnum* (A) for all sample sites combined, using the corrected counts. There were significant differences ($p<0.05$, Wilcoxon rank sum test) between the species and for *S. fallax* also between sample sites Pen y Garn and Llyn Pendam ($p<0.01$, Tukey HSD test) (B). For *S. papillosum* the density was slightly higher at Llyn Pendam (C) but not significantly. Sample size per species and area can be found in Supplementary Table 4.3.

S. quinquefarium had the highest mean density (1.34 plants/cm^2), closely followed by *S. fallax* (1.67 plants/cm^2) (Figure 4.8A). *S. inundatum* had the lowest mean density (0.74 plants/cm^2). These densities are similar to the ones obtained by manual counts in the field (*S. fallax* (1.47 plants/cm^2), *S. papillosum* (1.24 plants/cm^2) and *S. inundatum* (0.65 plants/cm^2)). There was no significant difference in density for *S. quinquefarium* with *S. fallax* and mixed stands of *S. fallax* and *S. papillosum.* Interestingly, mixed stands of *S. fallax* and *S. papillosum* seemed to have a density overlapping with both species separately. *S. inundatum* and *S. auriculatum*, two closely related species but imaged in two different habitats, were also significantly different.

We then looked at the effect of habitat on colony density for a given species. Both *S. fallax and S. papillosum* were found in Pen y Garn, a minerotrophic mire and Llyn Pendam, a lakeshore habitat. We observed significant differences in the density of *S. fallax* between the two sites, with higher density observed in the drier lakeshore habitat (Figure 4.8B). As for *S. papillosum* we observed a slight but not significant difference between both sites ($p = 0.07$) with the higher density observed at the Llyn Pendam as seen for *S. fallax* (Figure 4.8C).

Finally, to demonstrate the scalability of the method, a further 160 independent images of both *S. fallax* and *S. papillosum* were acquired from a

previously unrecorded section of Pen y Garn at the far end of the bog. The images were acquired in one morning over a period of 4 hours and were then fed to the pipeline. Even with manual thresholding for each image, the total analysis took less than 30 min, showing that the method has the capacity to acquire and analyse hundreds of images in a day. When default threshold values were used (125-256) instead of manually thresholding, the run-time of the 160 images through the pipeline on a regular consumer laptop was less than 5 minutes. The average densities observed for *S. fallax* (1.27 plants/cm^2) and S. papillosum (0.90 plants/cm^2) (Figure 4.9) were similar to those obtained previously for Pen y Garn (1.11 and 0.82 plants/cm^2 for *S. fallax* and *S. papillosum* respectively) (Figure 4.8). These data show that our method can easily be scaled up and it is time- and cost-effective in relation to manual methods.

Taken together our data show that the developed pipeline can be used to accurately assess *Sphagnum* colony density in the field and could detect significant species and habitat differences that may be relevant to ecological and conservation studies.

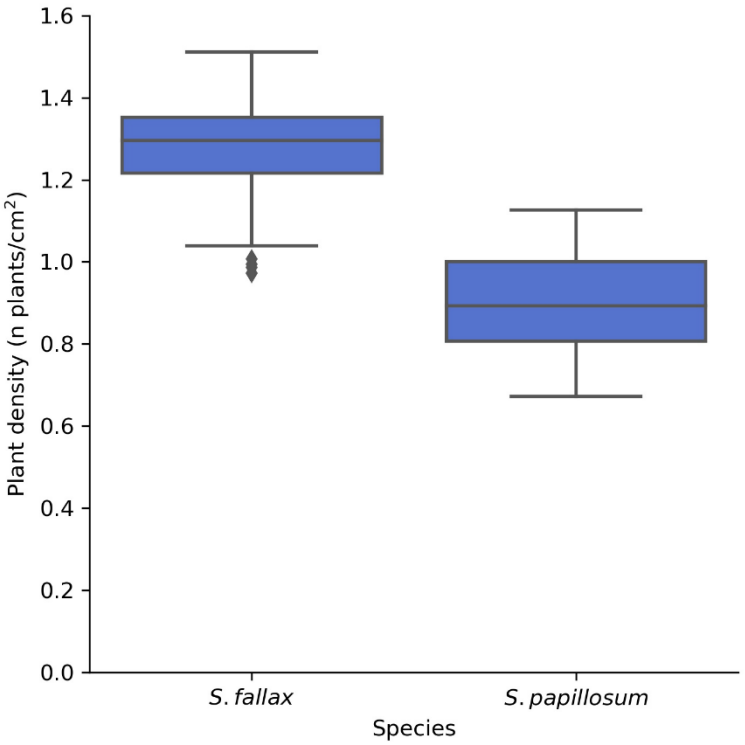

Figure 4.9. Plant density of *S. fallax* (n=83) and *S. papillosum* (n=77) from a previously unrecorded section of Pen y Garn. The images were taken over a period of 4 hours and the analysis, when carried out manually, took less than 30 minutes. When fully automated, the analysis of these 160 images took less than 5 minutes, highlighting the potential for high throughput of this method.

4.4 - Discussion

Plant density varies between *Sphagnum* cushions and is thought to affect evaporation rates (Bengtsson et al., 2020; Elumeeva et al., 2011; Schipperges and Rydin, 1998). However, tools for the quantification of density have not been developed and therefore this still requires either destructive sampling or visual counting, both of which are time consuming. The image analysis pipeline presented in this study provides a tool for *Sphagnum* researchers that can quickly, and with similar accuracy as a human, provide an estimate of plant density. The pipeline uses images captured in the field with minimal disturbance and allows for intra and inter-specific comparisons. Being image-based, the procedure could be scaled and easily adapted for citizen-science projects.

Our pipeline can analyse any reasonably exposed image acquired with a standard smartphone, although having a frame of defined size and colour and acquiring the image using lower exposure settings on the phone worked best. The frame design not only ensured that the phone was kept at a constant distance from the imaging area but the presence of the blue frame facilitated positional information and the selection of the region of interest (ROI) for each image. The pipeline is also very user-friendly requiring only minimal input in the form of file paths for source and destination directories, after which a pop-up window allows for the selection of the intuitive GUI window for thresholding, or the input of custom threshold values to run a uniform large image set.

Finally, the pipeline is robust. The images were collected periodically from marked patches across the 2020 season and so covered a range of drought states and colours that are typical for *Sphagnum* in the field. In addition, in some sites, the *Sphagnum* patches were variable in size or had a variable number of higher plants growing through them. Although one might expect that the presence excessive non-*Sphagnum* material might have been a problem, our results suggest that this did not have a significant influence on the final counts. During the precision analysis, we used a randomised grid selection for each image and while some grid cells had mostly *Sphagnum* material, others had large amounts of non-*Sphagnum* plants. Despite this, statistical analysis showed that there was a highly significant relationship between the number of annotations in the image and the number of annotations in the selected grid cells, indicating that these grid cells were

representative for the entire image (data not shown). In both of these cases, the inclusion of an interactive easy to use manual thresholding step in the pipeline was a critical factor for performance.

Our analysis also showed that transforming images into HSV colour space for thresholding gave the best results as the F-measures were consistently high for both annotation spaces LAB and YCrCb. The inclusion of a two-step colour transformation process in the annotation pipeline proved to be the most effective as the different properties of HSV and YCrCB made HSV more suitable for thresholding whilst YCrCb and LAB significantly outperformed HSV in annotation. Presumably, this is a result of HSV providing a better contrast between the *Sphagnum* and non-moss material, whilst YCrCb and LAB provide a better contrast between individual capitula. Similar to our results, HSV and YCrCb have been suggested to be among the best colour spaces for image classification in deep learning models (Feng et al., 2019; Gowda and Yuan, 2019), although the research into image processing methods such as these is still very limited for applied plant science.

A few recent studies have looked at *Sphagnum* density in the field and, using manual counts, found that increased shoot density positively affected photosynthetic capacity (Bengtsson et al., 2016). However, as our data shows, individual researchers can return significantly different counts of plants per area. Our image analysis pipeline eliminates this person-dependent variation and was able to detect distinct density differences between species, within species between habitats and between species that are closely related (*S. inundatum* and *S. auriculatum)*.

The highest densities were found for *S. fallax* and *S. quinquefarium*. In peatland restoration projects, species like *S. fallax* are often favoured (Hinde et al., 2010), usually unintentionally, due to their more competitive, pioneer nature compared to many other species. They are often attributed to a wider range of habitats and are more drought tolerant compared to typical bog species such as *S. papillosum* (Johnson et al., 2015; Mazziotta et al., 2019). *S. quinquefarium* in this study came from the most ‘atypical’ *Sphagnum* habitat, as Coed y Darren is a humid woodland on a predominantly north-facing slope with no accessible water table. In this habitat, *S. quinquefarium* is entirely dependent on combination of precipitation events and ambient humidity. In this context, it is plausible that a higher plant

density is favoured for this species as a denser canopy could help retain water vapour on the forest floor.

The same consideration could be applied to *S. fallax*, although Pen y Garn and Llyn Pendam are more typical wet *Sphagnum* habitats. At these sites *S. fallax* grows in patches: in Pen y Garn, at the edges of hummocks of *S. papillosum* and at Llyn Pendam in a flush at the north side of the lake.

The low density found for *S. inundatum* at Pen y Garn may be related to its habitat. *S. inundatum* was found in pools which remain saturated throughout the year and as such, density would be irrelevant for humidity retention. Its closely related species, *S. auriculatum*, had a slightly higher density, despite being somewhat larger in size than *S. inundatum*. At Llyn Pendam, this species grows on the shore of the lake and is subjected to fluctuations in the water level, and even occasionally drying out in prolonged drought periods. Therefore, higher plant densities at intermittently dry sites such as Llyn Pendam, could be an advantage. However, *S. inundatum* was locally less common than the other species and we had the lowest number of images so further sampling would be needed to support these findings.

The plant density of *S. papillosum* was surprisingly low, given that this species forms dense hummocks and mats. This could be explained by the difference in capitulum size between *S. papillosum* and the other species in this study. Typically, *S. papillosum* is fairly robust and their capitulum diameter can be much larger than that of the other species (Clymo and Hayward, 1982).

The density differences observed for the same species across two different sites could also be explained based on the water availability in each site. Higher capitulum densities were observed for for *S. fallax* and *S. papillosum* at Llyn Pendam when compared to Pen y Garn. While Pen y Garn is a permanently wet blanket bog, with little variation in water table, access to the water table at Llyn Pendam is more intermittent and partly dependent on runoff precipitation from the adjacent hills. Thus higher plant densities could be favoured in the latter site. As these differences in density are possibly a result of the microclimatological variation between sites, this neglected variable may also be useful for peatland restoration projects. The density values for these species could help determine an optimal amount of plants to use in so-called '*Sphagnum* plugs', which are planted on bare peat to restore the habitat (Caporn et al., 2018).

We have shown that the *Sphagnum* annotation pipeline has the ability to capture density differences between species with a wide range of morphological variation and across habitats, making it a useful and easy to apply to for field ecological studies. In addition, the magnitude and variation in the automated count is similar to those found manually by different people, indicating that this tool is equally reliable.

Besides its direct use in capturing, quantifying and immortalising data on ecologically relevant sites, we envisage that the *Sphagnum* annotation pipeline will have other uses. As part of the counting process, our pipeline places annotations on the images that could be further utilised to rapidly delimit ROI's for co-registration with other modalities. For example, ROIs of capitula could be overlaid on images of the same subject site taken with multispectral, hyperspectral or chlorophyll fluorescence imagers. The pipeline could be used to generating large, reliable datasets to train machine-learning algorithms to quantify biological and physiological traits in *Sphagnum* to set up a high throughput image monitoring framework.

4.5 - References

Abdollahnejad, A., Panagiotidis, D., Surový, P., 2017. Forest canopy density assessment using different approaches - Review. J. For. Sci. 63, 107–116. https://doi.org/10.17221/110/2016-JFS

Bengtsson, F., Granath, G., Cronberg, N., Rydin, H., 2020. Mechanisms behind species-specific water economy responses to water level drawdown in peat mosses. Ann. Bot. 126, 219–230. https://doi.org/10.1093/aob/mcaa033

Bengtsson, F., Granath, G., Rydin, H., 2016. Photosynthesis, growth, and decay traits in Sphagnum - a multispecies comparison. Ecol. Evol. 6, 3325–3341. https://doi.org/10.1002/ece3.2119

Bradski, G., 2000. The OpenCV Library. Dr. Dobb's J. Softw. Tools.

Caporn, S.J.M., Rosenburgh, A.E., Keightley, A.T., Hinde, S.L., Riggs, J.L., And Buckler, M., 2018. Sphagnum restoration on degraded blanket and raised bogs in the UK using micropropagated source material: a review of progress. Mires Peat 20, 1–17. https://doi.org/10.19189/MaP.2017.OMB.306

Charman, D.J., Beilman, D.W., Blaauw, M., Booth, R.K., Brewer, S., Chambers, F.M., Christen, J.A., Gallego-Sala, A., Harrison, S.P., Hughes, P.D.M., Jackson, S.T., Korhola, A., Mauquoy, D., Mitchell, F.J.G., Prentice, I.C., Van Der Linden, M., De Vleeschouwer, F., Yu, Z.C., Alm, J., Bauer, I.E., Corish, Y.M.C., Garneau, M., Hohl, V., Huang, Y., Karofeld, E., Le Roux, G., Loisel, J., Moschen, R., Nichols, J.E., Nieminen, T.M., MacDonald, G.M., Phadtare, N.R., Rausch, N., Sillasoo, U., Swindles, G.T., Tuittila, E.S., Ukonmaanaho, L., Väliranta, M., Van Bellen, S., Van Geel, B., Vitt, D.H., Zhao, Y., 2013. Climate-related changes in peatland carbon accumulation during the last millennium. Biogeosciences 10, 929–944. https://doi.org/10.5194/bg-10-929-2013

Clymo, R.S., Hayward, P.M., 1982. The Ecology of Sphagnum, in: Bryophyte Ecology. Springer Netherlands, Dordrecht, pp. 229–289. https://doi.org/10.1007/978-94-009-5891-3_8

Cruz de Carvalho, R., Maurício, A., Pereira, M.F., Marques da Silva, J., Branquinho, C., 2019. All for One: The Role of Colony Morphology in Bryophyte Desiccation Tolerance. Front. Plant Sci. 10, 1–12. https://doi.org/10.3389/fpls.2019.01360

del Valle, J.C., Gallardo-López, A., Buide, M.L., Whittall, J.B., Narbona, E., 2018. Digital photography provides a fast, reliable, and noninvasive method to estimate anthocyanin pigment concentration in reproductive and vegetative plant tissues. Ecol. Evol. 8, 3064–3076. https://doi.org/10.1002/ece3.3804

Elumeeva, T.G., Soudzilovskaia, N.A., During, H.J., Cornelissen, J.H.C., 2011. The importance of colony structure versus shoot morphology for the water balance of 22 subarctic bryophyte species. J. Veg. Sci. 22, 152–164. https://doi.org/10.1111/j.1654-1103.2010.01237.x

Fahlgren, N., Feldman, M., Gehan, M.A., Wilson, M.S., Shyu, C., Bryant, D.W., Hill, S.T., McEntee, C.J., Warnasooriya, S.N., Kumar, I., Ficor, T., Turnipseed, S., Gilbert, K.B., Brutnell, T.P., Carrington, J.C., Mockler, T.C., Baxter, I., 2015. A versatile phenotyping system and analytics platform reveals diverse temporal responses to water availability in Setaria. Mol. Plant 8, 1520–1535. https://doi.org/10.1016/j.molp.2015.06.005

Feng, X., Zhan, Y., Wang, Q., Yang, X., Yu, C., Wang, H., Tang, Z.Y., Jiang, D., Peng, C., He, Y., 2019. Hyperspectral imaging combined with machine learning

as a tool to obtain high-throughput plant salt-stress phenotyping. Plant J. 1448–1461. https://doi.org/10.1111/tpj.14597
Fox, J., Weisberg, S., 2019. An R Companion to Applied Regression, 3rd ed. Sage Publications, Thousand Oaks CA.
Gallego-Sala, A. V., Colin Prentice, I., 2013. Blanket peat biome endangered by climate change. Nat. Clim. Chang. 3, 152–155. https://doi.org/10.1038/nclimate1672
Glime, J.M., 2017. Water Relations: Conducting Structures, in: Bryophyte Ecology. pp. 1–25.
González, E., Henstra, S.W., Rochefort, L., Bradfield, G.E., Poulin, M., 2014. Is rewetting enough to recover Sphagnum and associated peat-accumulating species in traditionally exploited bogs? Wetl. Ecol. Manag. 22, 49–62. https://doi.org/10.1007/s11273-013-9322-6
Gowda, S.N., Yuan, C., 2019. ColorNet: Investigating the Importance of Color Spaces for Image Classification. Lect. Notes Comput. Sci. 11364 LNCS, 581–596. https://doi.org/10.1007/978-3-030-20870-7_36
Hájek, T., Vicherová, E., 2014. Desiccation tolerance of Sphagnum revisited: a puzzle resolved. Plant Biol. 16, 665–773. https://doi.org/10.1111/plb.12126
Harris, A., Bryant, R.G., Baird, A.J., 2006. Remote sensing of Sphagnum stress: A proxy for near-surface wetness conditions in northern peatlands? Eur. Sp. Agency, (Special Publ. ESA SP.
Harris, C.R., Millman, K.J., van der Walt, S.J., Gommers, R., Virtanen, P., Cournapeau, D., Wieser, E., Taylor, J., Berg, S., Smith, N.J., Kern, R., Picus, M., Hoyer, S., van Kerkwijk, M.H., Brett, M., Haldane, A., del Río, J.F., Wiebe, M., Peterson, P., Gérard-Marchant, P., Sheppard, K., Reddy, T., Weckesser, W., Abbasi, H., Gohlke, C., Oliphant, T.E., 2020. Array programming with NumPy. Nature 585, 357–362. https://doi.org/10.1038/s41586-020-2649-2
Hayward, P.M., Clymo, R.S., 1983. The Growth of Sphagnum: Experiments on, and Simulation of, Some Effects of Light Flux and Water-Table Depth. J. Ecol. 71, 845–863. https://doi.org/10.2307/2259597
Heinemeyer, A., Swindles, G.T., 2018. Unraveling past impacts of climate change and land management on historic peatland development using proxy-based reconstruction, monitoring data and process modeling. Glob. Chang. Biol. 24, 4131–4142. https://doi.org/10.1111/gcb.14298
Hinde, S., Rosenburgh, A., Wright, N., Buckler, M., Caporn, S., 2010. Sphagnum re-introduction project : A report on research into the re-introduction of Sphagnum mosses to degraded moorland. Moors Futur. Rep. 31.
Hunter, J.D., 2007. Matplotlib: A 2D graphics environment. Comput. Sci. Eng. 9, 90–95. https://doi.org/10.1109/MCSE.2007.55
Hüther, P., Schandry, N., Jandrasits, K., Bezrukov, I., Becker, C., 2020. ARADEEPOPSIS, an automated workflow for top-view plant phenomics using semantic segmentation of leaf States. Plant Cell 32, 3674–3688. https://doi.org/10.1105/tpc.20.00318
Johnson, M.G., Granath, G., Tahvanainen, T., Pouliot, R., Stenøien, H.K., Rochefort, L., Rydin, H., Shaw, A.J., 2015. Evolution of niche preference in Sphagnum peat mosses. Evolution (N. Y). 69, 90–103. https://doi.org/10.1111/evo.12547
Kassambara, A., 2016. ggpubr package, R documentation [WWW Document]. URL https://www.rdocumentation.org/packages/ggpubr/versions/0.1.1 (accessed 2.8.21).
Li, L., Zhang, Q., Huang, D., 2014. A review of imaging techniques for plant

phenotyping. Sensors 14, 20078–20111. https://doi.org/10.3390/s141120078
Mazziotta, A., Granath, G., Rydin, H., Bengtsson, F., Norberg, J., 2019. Scaling functional traits to ecosystem processes: Towards a mechanistic understanding in peat mosses. J. Ecol. 107, 843–859. https://doi.org/10.1111/1365-2745.13110
McKinney, W., 2010. Data Structures for Statistical Computing in Python. Proc. 9th Python Sci. Conf. 1, 56–61. https://doi.org/10.25080/majora-92bf1922-00a
Proctor, M.C.F., 2000. The Bryophyte Paradox: Tolerance of Desiccation, Evasion of Drought. Plant Ecol. 151, 41–49.
Rastogi, A., Antala, M., Gąbka, M., Rosadziński, S., Stróżecki, M., Brestic, M., Juszczak, R., 2020. Impact of warming and reduced precipitation on morphology and chlorophyll concentration in peat mosses (Sphagnum angustifolium and S. fallax). Sci. Rep. 10. https://doi.org/10.1038/s41598-020-65032-x
Reback, J., McKinney, W., jbrockmendel, Bossche, J. Van den, Augspurger, T., Cloud, P., gfyoung, Sinhrks, Klein, A., Roeschke, M., Hawkins, S., Tratner, J., She, C., Ayd, W., Petersen, T., Garcia, M., Schendel, J., Hayden, A., MomIsBestFriend, Jancauskas, V., Battiston, P., Seabold, S., chris-b1, h-vetinari, Hoyer, S., Overmeire, W., alimcmaster1, Dong, K., Whelan, C., Mehyar, M., 2020. pandas-dev/pandas: Pandas 1.0.3. https://doi.org/10.5281/ZENODO.3715232
Rice, S.K., Gutman, C., Krouglicof, N., 2005. Laser Scanning Reveals Bryophyte Canopy Structure. New Phytol. 166, 695–704. https://doi.org/10.1111/j.1469-8137.2005.01327.x
RStudio Team, 2020. RStudio: Integrated Development for R.
Rydin, H., Gunnarsson, U., Sundberg, S., 2006. The Role of Sphagnum in Peatland Development and Persistence, in: Boreal Peatland Ecosystems. Springer Berlin Heidelberg, pp. 47–65. https://doi.org/10.1007/978-3-540-31913-9_4
Rydin, H., Jeglum, J.K., 2015. The Biology of Peatlands, The Biology of Peatlands. https://doi.org/10.1093/acprof:osobl/9780199602995.001.0001
Schindelin, J., Arganda-Carreras, I., Frise, E., Kaynig, V., Longair, M., Pietzsch, T., Preibisch, S., Rueden, C., Saalfeld, S., Schmid, B., Tinevez, J.Y., White, D.J., Hartenstein, V., Eliceiri, K., Tomancak, P., Cardona, A., 2012. Fiji: An open-source platform for biological-image analysis. Nat. Methods. https://doi.org/10.1038/nmeth.2019
Schipperges, B., Rydin, H., 1998. Response of photosynthesis of Sphagnum species from contrasting microhabitats to tissue water content and repeated desiccation. New Phytol. 140, 677–684.
Tharwat, A., 2018. Classification assessment methods. Appl. Comput. Informatics. https://doi.org/10.1016/j.aci.2018.08.003
The PySimpleGUI Organization, 2020. PySimpleGUI.org [WWW Document]. PySimpleGUI.org.
Van Der Walt, S., Schönberger, J.L., Nunez-Iglesias, J., Boulogne, F., Warner, J.D., Yager, N., Gouillart, E., Yu, T., 2014. Scikit-image: Image processing in python. PeerJ 2014, 1–18. https://doi.org/10.7717/peerj.453
Van Rossum, G., Drake, F.L., 2009. Python 3 Reference Manual. CreateSpace, Scotts Valley, CA. https://doi.org/10.555/1593511
Wang, X., Song, C., Wang, J., Miao, Y., Mao, R., Song, Y., 2013. Carbon release from Sphagnum peat during thawing in a montane area in China. Atmos. Environ. 75, 77–82. https://doi.org/10.1016/j.atmosenv.2013.04.056
Waskom, M., Gelbart, M., Botvinnik, O., Ostblom, J., Hobson, P., Lukauskas, S.,

Gemperline, D.C., Augspurger, T., Halchenko, Y., Warmenhoven, J., Cole, J.B., Ruiter, J. de, Vanderplas, J., Hoyer, S., Pye, C., Miles, A., Swain, C., Meyer, K., Martin, M., Bachant, P., Quintero, E., Kunter, G., Villalba, S., Brian, Fitzgerald, C., Evans, C., Williams, M.L., O'Kane, D., Yarkoni, T., Brunner, T., 2020. mwaskom/seaborn: v0.11.1 (December 2020). https://doi.org/10.5281/ZENODO.4379347

Weston, D.J., Turetsky, M.R., Johnson, M.G., Granath, G., Lindo, Z., Belyea, L.R., Rice, S.K., Hanson, D.T., Engelhardt, K.A.M., Schmutz, J., Dorrepaal, E., Euskirchen, E.S., Stenøien, H.K., Szövényi, P., Jackson, M., Piatkowski, B.T., Muchero, W., Norby, R.J., Kostka, J.E., Glass, J.B., Rydin, H., Limpens, J., Tuittila, E.S., Ullrich, K.K., Carrell, A., Benscoter, B.W., Chen, J.G., Oke, T.A., Nilsson, M.B., Ranjan, P., Jacobson, D., Lilleskov, E.A., Clymo, R.S., Shaw, A.J., 2018. The Sphagnome Project: enabling ecological and evolutionary insights through a genus-level sequencing project. New Phytol. 217, 16–25. https://doi.org/10.1111/nph.14860

CHAPTER 5 - PREDICTING PEATMOSS HEALTH USING QUANTITATIVE IMAGING

Data availability

The data pertaining to this chapter can be accessed at (DOI NOT YET AVAILABLE)

Chapter summary

Peatlands are increasingly recognised as important ecosystems in carbon mitigation strategies due to their carbon source and sink dynamic. This dynamic is influenced by the fluctuating water table in this environment, where a completely waterlogged situation prevents the breakdown of organic matter whilst a reduced water table facilitates it. *Sphagnum* peatmosses play an important role in these ecosystems, as their unique structure enables them to hold onto large quantities of water. Just as most bryophytes, these plants lack roots, vascular tissue and water retention mechanisms that higher plants have, making them entirely dependent on directly available water from the surface or precipitation. This trait however, makes them suitable as early reporters of drought in peatland ecosystems. When *Sphagnum* dries out, it becomes a much lighter shade of green which opens up the potential for a remote sensing or imaging quantification of drought status. This paper explores the possibility of the use of simple RGB images of *Sphagnum* as a drought assessment tool. By comparing several established vegetational indices and RGB images with physiological data from a glasshouse experiment, and the comparison of RGB images with environmental data from the field, an image analysis pipeline was developed for the extraction of image based data that can be used to interpret the water content of *Sphagnum* plants, and by extension the hydrological status of the ecosystem.

5.1 - Introduction

Globally, peat is estimated to store approximately 25% of all carbon sequestered in soils (Loisel et al., 2021; Yu et al., 2010), making peatlands one of the most important ecosystems in the fight against climate change. Long term carbon storage capacity depends on maintaining a high water table (Clymo and Hayward, 1982; Page and Baird, 2016) which is, in large part, established and maintained by peatmosses from the genus *Sphagnum* L.. In combination with the acidification of the water, these mosses retain water and thus create an anaerobic environment in which dead plant matter cannot be broken down faster than new growth is generated by living plants on the bog surface. These anaerobic conditions reduce the release of greenhouse gasses normally associated with decaying organic matter. Healthy water-saturated peatlands, therefore, function as a carbon sink (Clymo and Hayward, 1982; Gorham, 1957).

Consequently, drying peatlands expose the stored peat to oxygen allowing decomposition of the organic matter, releasing greenhouse gases. Global peatland emissions on average release approximately 412 tonnes CO_2-eq per hectare (Leifeld and Menichetti, 2018). Drying can be caused by anthropogenic activity, either indirectly through global climate warming affecting precipitation patterns, or directly through drainage for land use and the cutting of peat for fuel or horticulture.

Extended periods of drought are thus a considerable threat to the functioning of peatland ecosystems as carbon sinks. Furthermore, the eroded peat soils lose much of their capacity as water stores, leaving adjacent areas susceptible to flooding in the event of heavy precipitation. Finally, important biodiversity is lost, as peatbogs are key habitats for many birds, insects and plants.

5.1.1 - The role of *Sphagnum* in peatlands and its potential for biomonitoring

Because the genus *Sphagnum* is the main component of many northern peatland ecosystems and their water content reflects that of their immediate environment, these plants may serve as an early reporter for fluctuations in peatland hydrology. When *Sphagnum* dries out, it whitens and becomes a much lighter shade of green. This colour change seems due to the large number of hyaline cells which when empty are no longer translucent and reflect light. This phenomenon has been recorded in other bryophytes where the whitening is hypothesised to increase the

reflectance, or albedo (Bowker et al., 2010; Giordano et al., 2009). Increased albedo may protect the plants from high light intensities. Changes in albedo are easily recorded and quantified suggesting that non-destructive image-based biomonitoring could be used for estimation of *Sphagnum* water content.

Bryophytes have long been used to quantify environmental variables (Burton and Peterson, 1979). Bryophytes in general, and *Sphagnum* in particular, occur in many environments and their bioaccumulating properties extend even to microplastics (Ares et al., 2015, 2012; Beike et al., 2015; Capozzi et al., 2018, 2017; Cesa et al., 2015; Fernández et al., 2006; Wehr et al., 1983). Previous image-based research on bryophytes has revolved around estimating ground cover (Benavides and Jesús, 2009), vegetation change (Robinson et al., 2018), photosynthetic functioning and plant health (Lovelock and Robinson, 2002; Malenovský et al., 2017). These works highlighted the capability of image-based research for moss health and species turnover. However, compared to the body of research on higher plants, these methodologies are still rarely used in bryophyte research. When applied to an ecosystem defining genus such as *Sphagnum*, image-based monitoring could yield powerful cost effective tools for the monitoring of ecosystem health.

5.1.2 - Remote sensing and image-based plant phenotyping techniques

Remote sensing quantification methods for higher plants have seen widespread application in agricultural research (Xue and Su, 2017). Using selected wavebands, several vegetational indices have been developed to estimate various biological parameters, such as chlorophyll content (Gitelson and Merzlyak, 1994, 1997; Gitelson et al., 2006), carotenoid content (Gitelson et al., 2006, 2002; Sims and Gamon, 2002),anthocyanin content (Gitelson et al., 2006, 2001; Sims and Gamon, 2002), and also photosynthetic light use efficiency (Gamon et al., 1992, 1990). One key advantage of these methods is their capacity for non-invasive measurements that are less susceptible to researcher bias than many manual measurements. Another is that they are easily scalable, allowing surveillance of large areas and across time: repeated imaging records dynamic changes in plants across seasons and between years.

However, as spectral wavebands are technologically restricting, requiring the use of specialised imaging equipment and waveband filters, the use of indices based

on regular RGB colour images have also become popular (del Valle et al., 2018; Elshikha et al., 2016; Sánchez-Sastre et al., 2020; Woebbecke et al., 1995). RGB images consist of three colour channels, namely R (red), G (green) and B (blue), and each channel is projected on a range of 0-255, where 0 is black and 255 is white, and combinations of these three channels can be used to create every visible colour. RGB-based vegetational indices provide accessible biological variables that can be measured with domestic grade imaging equipment, which makes large scale data acquisition possible with the advent of high resolution smartphone cameras.

To capitalise on the ubiquity of smartphone cameras, the aim of the present work was to identify accessible, non-destructive capitulum water content quantification methods for *Sphagnum* through image analysis. A number of spectral reflectance indices and RGB indices were tested in a glasshouse setting, after which the RGB indices were also tested on outdoor measurements (in natural peatland settings) in combination with biological and ecological variables. We found that greenhouse RGB-based indices and even single RGB colour channels could perform similarly or better than traditional multispectral indices for the correlation with capitulum water content in close-up images of *Sphagnum* capitula. When translated to natural settings, RGB indices and colour channels correlated moderately (rho = -0.49) with capitulum water content. This indicates that, with refinement, traditional RGB images can serve as a desiccation quantification tool for *Sphagnum* capitula and, by extension, peatland health.

5.2 - Methods

5.2.1 - Plant material collection and maintenance

Three species of *Sphagnum* were collected from two sites in Wales. Patches of plants were harvested with minimal disturbance, into rectangular blue boxes (inner size 28.5x23.5x14.5 cm, 0.66 kg). Twenty boxes of *Sphagnum quinquefarium* Warnstorf 1886 were collected from humid, mixed woodland Coed y Darren (SN677835) while 15 boxes of *S. papillosum* Lindberg 1872 and 15 boxes of *S. inundatum* Russow 1894 were collected from a blanket bog at the foot of Pen y Garn mountain (SN791758). These species were selected because they represent three different niche types: the woodland where *S. quinquefarium* grows has no water table and is entirely dependent on precipitation and high humidity. The other two species come from different areas of a blanket bog: *S. inundatum* grows in and at the margins of a pool with mild flow after precipitation caused by runoff from the mountain, while *S. papillosum* grows in lawns and hummocks above the water table. Furthermore, these three species have different colony canopy structures. *S. papillosum* is typically very densely packed, while *S. inundatum* has a very loose structure. *S. quinquefarium* is in between these two extremes, growing in extensive lawns.

Care was taken to retain as much of the original colony structure as possible, while non-*Sphagnum* material was removed and discarded. The weights of filled boxes were approximately equalised for each species. The boxes all had 9 drainage holes in the bottom and were left in shallow trays with approximately 3 cm of standing water to acclimatise and recover from the disturbance at the National Plant Phenomics Centre (NPPC) in Plas Gogerddan, in a south-east facing area outside with only direct sunlight in the morning.

After a recovery period, the boxes were moved onto the NPPC's Gravimetrics phenotyping platform. This glasshouse platform consists of a computer controlled weighing and watering system, which records weights every 10 minutes and automatically waters the plants daily up to a target weight. The experiment was conducted from October until December, to reduce the likelihood of high temperature anomalies. Furthermore, supplementary heating, lighting and air ventilation systems were turned off for the duration of the experiment to minimise the effect of abiotic variables on the drought process. The boxes containing *Sphagnum* were placed into a second blue box of which the drainage holes were

sealed and left to acclimatise to the glasshouse conditions for 2 weeks prior to the experiment, and they were kept up to their saturated weight during the acclimatisation period.

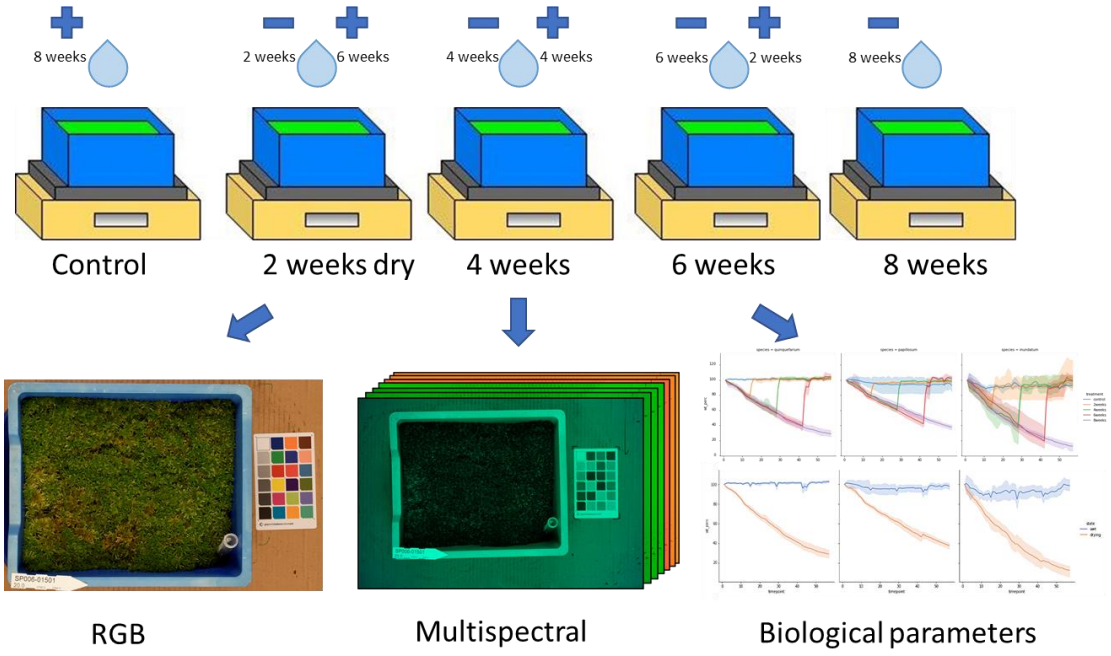

Figure 5.1. Experimental setup of the drought treatments on the NPPC's Gravimetrics platform.
From the five different treatments, RGB and multispectral images were collected in parallel with high resolution weight data, as well as capitulum samples which were later measured for their water content and chlorophyll and carotenoid concentrations.

5.2.2.1 - Drought treatment

To evaluate the potential of the RGB and multispectral indices, the collected *Sphagnum* species were subjected to discrete drought periods, and regularly imaged over the course of the duration. The greenhouse acclimatised boxes were divided into 5 treatments: i. control, ii. 2 weeks of drought and followed by 6 weeks of recovery, iii. 4 weeks of drought and 4 weeks recovery, iv. 6 weeks of drought and 2 weeks of recovery and v. 8 weeks of drought (Figure 5.1), referred to as 2, 4, 6 and 8 week drought treatment respectively. In the recovery stage, the plants were re-watered up to their original target weight. Each treatment contained 4 boxes of *S. quinquefarium* and 3 boxes of *S. papillosum* and *S. inundatum* each.

5.2.2.2 - RGB Imaging

The plants were imaged twice weekly over the course of the drought treatments, for a total 17 times using a custom made imaging rig with lighting provided by two tungsten-halogen photography lamps. The rig was situated in a darkened, dedicated imaging room to prevent extraneous lighting conditions from affecting the imaging area. Images were acquired using a remotely operated Nikon D3300 camera (Nikon, Tokyo, Japan) with a Nikkor 60 mm macro f/2.8 lens (Nikon, Tokyo, Japan). Exposure of 1/10", a f/8 focal ration and ISO 100 were used, ensuring that the focus was maintained for each image. Images were saved as 6000 × 4000, bit depth: 24, RGB with auto white balance in .jpg format. File names were automatically changed to a combination of sample name and imaging date, using the NPPC in-house KatieCam image collection software with sample names supplied in .csv format.

5.2.2.3 - Multispectral Imaging

During each imaging session and directly after the RGB imaging was complete, the imaging rig was converted to facilitate multispectral imaging using a Nikon D3300 with a Nikkor 60 mm macro f/2.8 lens modified to wide-spectrum by having the infrared cut filter removed. The 7 selected wavelength bandpass filters were 510, 532, 550, 568, 700, 750, 780 nm Edmund Optics hard coated OD4 10 nm bandpass filters. Exposure was 1/5", focal ration f/4 and ISO 100. Focus was calibrated through the 700 nm bandpass filter. Images were saved as 6000px × 4000px, bit depth: 24, RGB with auto white balance in .jpg format.

5.2.2.4 - Image quantification

RGB images were analysed using a modified version of the Capitula Counter pipeline (van de Koot et al., 2021). The pipeline processed images as before but also extracted the values of the three RGB colour channels for the entire image, the annotated capitula, and several of the chips on the colour card for quality control purposes. Along with the raw values of the R (red) and G (green) colour channels, several RGB vegetational indices were calculated (as described in Table 5.1), namely AC_{CR}, AC_{CB}, BGR, ExG, GLI, mSoG and mSoR. The values of the B (blue) colour channel were not extracted, as this channel's mode and mean values were found to

change exponentially in response to late stage drought in a pilot experiment (data not shown), making this channel less reliable for tracking drought progression compared to the R and G channels.

Using the multispectral images, several additional vegetational indices were calculated (Table 5.1) which aim to quantify specific plant traits, also known as multispectral indices (MSIs). As the images were collected as RGB images in .jpg format, and the exposure was set to be optimal for the green colour channel of the images, this channel was used for the calculation of the indices. The calculated indices were mNDVI, NDVIgreen (hereafter NDVIg), Ratio, CRI, CRI550, CRI550-780, CRI700, ARI, mARI and PRI. To improve the interpretability of the multispectral data, the indices data was transformed to fit a 0-1 range. The transformations' formulae can be found in Supplementary Table 5.1.

5.2.2.5 - Water content, chlorophyll and carotenoid extraction

At the end of each imaging session, capitula were harvested into cryotubes for chlorophyll and pigment extractions, and into regular microtubes for water content measurement. For *S. quinquefarium*, a cryotube with 2 capitula for chlorophyll and carotenoids and 2 for water content were harvested. For *S. papillosum* and *S. inundatum,* these numbers were 1 and 1 respectively. Care was taken not to disturb the colony morphology during the harvesting of the capitula. The samples were weighed for fresh weight prior to being frozen in liquid nitrogen or dried in an oven for 48 hours. The frozen samples were stored at -80 ^{o}C until extraction. Gravimetric water content was calculated as the difference between fresh weight and dry weight, divided by dry weight.

Table 5.1. RGB and multispectral indices used and their associated formulae.
Most of the indices were originally designed to quantify a variety of plant traits, including the contents of pigments associated with photosynthesis, as well as moisture content and photosynthetic capacity. Some of the indices were developed for plant cover and object detection, which typically increase the contrast of plants with the background material.

Index	Full name	Formula	Target biological trait	Reference
RGB				
AC_{CB}	Anthocyanin content-chroma basic	$\frac{Blue + Red}{Green}$	Anthocyanin content estimation	(del Valle et al., 2018)
AC_{CR}	Anthocyanin content-chroma ratio	$\frac{Green}{\left(\frac{(Blue + Red)}{2}\right)}$	Anthocyanin content estimation	(del Valle et al., 2018)
BGR	Blue to Green	$\frac{Blue}{Green}$	Moisture content estimation	(Elshikha et al., 2016)
ExG	Excessive Green	$(2 * Green) - Red - Blue$	Plant detection (plant-background contrast)	(Sánchez-Sastre et al., 2020; Wenhua Mao et al., 2013; Woebbecke et al., 1995)
GLI	Green Leaf Index	$\frac{(2 * Green) - Red - Blue}{(2 * Green) + Red + Blue}$	Plant cover (plant-background contrast)	(Louhaichi et al., 2001; Sánchez-Sastre et al., 2020)
mSoG	modified Strength of Green	$\frac{Green - Blue}{Red + Green + Blue}$	Chlorophyll content estimation	(Kawashima and Nakatani, 1998; Sánchez-Sastre et al., 2020)
mSoR	modified Strength of Red	$\frac{Red - Blue}{Red + Green + Blue}$	Chlorophyll content estimation	(Kawashima and Nakatani, 1998; Sánchez-Sastre et al., 2020)
Multispectral				
ARI	Anthocyanin Reflectance Index	$\left(\frac{1}{R550}\right) - \left(\frac{1}{R700}\right)$	Anthocyanin content estimation	(Rahimzadeh-Bajgiran et al., 2012)
mARI	modified Anthocyanin Reflectance Index	$\left(\left(\frac{1}{R550}\right) - \left(\frac{1}{R700}\right)\right) * R780$	Anthocyanin content estimation	(Rahimzadeh-Bajgiran et al., 2012)
CRI550	Carotenoid Reflectance Index (550nm)	$\left(\frac{1}{R510}\right) - \left(\frac{1}{R550}\right)$	Carotenoid content estimation	(Rahimzadeh-Bajgiran et al., 2012)
CRI550-780	Carotenoid Reflectance Index (550nm-780nm)	$\left(\frac{1}{R510}\right) - \left(\frac{1}{R780}\right) - \left(0.75 * \left(\frac{1}{R550}\right) - \left(\frac{1}{R780}\right)\right)$	Carotenoid content estimation	(Rahimzadeh-Bajgiran et al., 2012)
CRI700	Carotenoid Reflectance Index (700nm)	$\left(\frac{1}{R510}\right) - \left(\frac{1}{R700}\right)$	Carotenoid content estimation	(Rahimzadeh-Bajgiran et al., 2012)
mCRI	modified Carotenoid Reflectance Index	$\left(\left(\frac{1}{R510}\right) - \left(\frac{1}{R550}\right)\right) * R780$	Carotenoid content estimation	(Rahimzadeh-Bajgiran et al., 2012)
mNDVI	red edge Normalised Difference Vegetation Index	$\frac{R750 - R705}{R750 + R705}$	Chlorophyll content estimation	(Rahimzadeh-Bajgiran et al., 2012)
NDVIg	green Normalised Difference vegetation Index	$\frac{R750 - R550}{R750 + R550}$	Chlorophyll content estimation	(Rahimzadeh-Bajgiran et al., 2012)
PRI	Photochemical Reflectance Index	$\frac{R531 - R570}{R531 + R570}$	Photosynthesis performance estimation	(Gamon et al., 1992; Rahimzadeh-Bajgiran et al., 2012; Sims and Gamon, 2002)
Ratio	Ratio	$\frac{R750}{R700}$	Chlorophyll content estimation	(Rahimzadeh-Bajgiran et al., 2012)

To extract chlorophylls and carotenoids, the frozen samples were transferred to a pre-chilled mortar containing liquid nitrogen. Capitula were ground to a fine powder using 80% Acetone as solvent. The solution was subsequently filtered through Fisherbrand QL100 filter paper into 15 mL tubes, which were kept on ice and away from light. The ground tissue was rinsed in the filter with small amounts of Acetone until the residue was no longer appreciably green, after which the filtrate was made up to a known volume. The absorbance of the filtrate was measured in a BioSpectrometer® basic (Eppendorf, Hamburg, Germany) at 470, 646, 663 and 700 nm, after which chlorophyll and carotenoid content was calculated using the coefficients and equations described in Porra (2006). As water content differed between samples, the measured water contents were used to correct the weights used in the calculations.

5.2.3 - Outdoor imaging

To relate glasshouse results to those from natural settings field, a series of measurements and images were taken from natural stands of moss. The imaging protocol is given in van de Koot et al. (2021). In parallel, 9 capitula were harvested into 3 microtubes for the dominant *Sphagnum* species in the image area and used for the measurement of water content. Furthermore, the distance between the capitula and the water table was measured. Lastly, because *Sphagnum* has very limited control over its evaporation rate, the relative humidity (RH) at the capitula level was measured as this may be a reflection of plant moisture content. To measure RH, a measuring device was developed for the profiling of these microclimatological traits, using miniature DS1923-F5# Hygrochron RH and temperature loggers (Maxim Integrated, San Jose, California, USA). The 4 Hygrochron loggers were located vertically and spaced 1cm below the capitula layer, directly on the capitula layer, and 1 and 2 cm above the capitula layer. These loggers were programmed to record RH and temperature at one minute intervals. The device was placed in a sampling site for a minimum of 5 minutes after which a mean RH and temperature can be calculated for this time period.

Data pertaining to the capitula in each image was extracted from within the annotated regions as defined by the capitulum counting algorithm (van de Koot et al., 2021), but with the slight modification of increasing the annotation radius by a factor

of 2. This largely excluded signal noise from non-*Sphagnum* vegetation in the image (Supplementary Figure 5.1), improving the quality of the data. The increase of the radius of the annotations by was necessary capture the spreading branches at the edge of the capitulum, as the annotations generated by the capitulum counting algorithm are typically positioned around the centre of a capitulum. Vegetational indices and RGB channel parameters (Table 5.1) were calculated from the annotated regions.

5.2.4 - Vegetational indices model selection

To determine which of the vegetational indices best explained the water content of the capitula samples, feature selection methods typically used in machine learning analyses were used. The analyses focussed on water content of the capitulum layer as it represents the imaged portion of the plant. Two linear model analyses were performed for each species separately, of which one contained the RGB based indices, and the other the multispectral indices. A minimal model was also created for each of these, containing the single most highly correlating index variable. The full models, containing all the indices, were subsequently deconstructed stepwise by removing the indices with the highest Variance Inflation Factor (VIF) values one at a time, until the highest VIF value remaining was <5. This final model was then tested against the minimal model (provided it was not identical to the minimal model), after which one of these two models was selected based on their Residual Sum of Squares (RSS) value. If, upon data visualisation, a relationship appeared not to be linear but instead exponential or sigmoidal, a model with a polynomial fit was also tested against the regular linear model.

5.2.5 - Statistics

Pairwise comparisons between timepoints for measured variables were carried out using t-tests when the data conformed to a normal distribution, whilst Wilcoxon rank sum tests were used if this was not the case. Linear models were used to evaluate the relationship between different variables and Pearson's correlation coefficient (using R^2) or Spearman's rank correlation coefficient (using rho) were used for parametric and non-parametric data respectively.

5.3 - Results

To evaluate the potential of RGB-based imaging approaches for the quantification of desiccation status in *Sphagnum*, three species were subjected to variable drought periods in a controlled glasshouse setting. These species were selected for their abundance in the collection site and the fact that they represented three different ecological niches in *Sphagnum*, namely hummocks (*S. papillosum*), hollows (*S. inundatum*) and woodland lawns (*S. quinquefarium*). The experiment provided high resolution weight loss data for all 3 *Sphagnum* species (Figure 2) and their associated capitulum water content dynamics (Supplementary Figure 2). Over the course of the experiment the experimental boxes were frequently imaged and capitula were harvested, and the cosm weight was recorded continuously by the Gravimetrics platform at the NPPC.

5.3.1 - Water loss dynamics

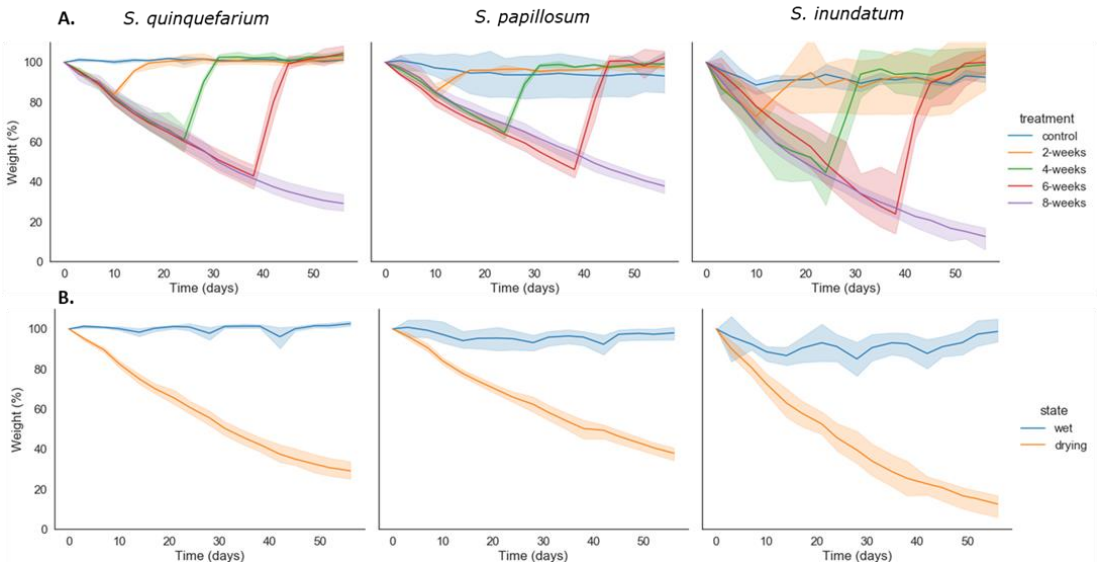

Figure 5.2. Relative mean cosm weight loss over time in 3 different Sphagnum species. A. Weight decayed similarly across treatments, but *S. papillosum* retained the largest proportion of its starting weight in the most severe treatment, whilst *S. inundatum* lost the largest proportion.
B. Weight decay as cumulative of the drought and wet states of all treatments.

Under drought, *S. papillosum* retained the largest fraction of its starting weight, whilst *S. inundatum* had the largest loss (Figure 5.2). Between treatments within

species, rates of weight loss were similar as expected. The water content from the harvested capitula and the weight of the boxes were significantly correlated for each species when only samples undergoing drought were considered ($p < 0.0001$****). Wet samples, classified as the control treatment and previously droughted treatments undergoing rewetting, were excluded as they considerably skewed the data as water content recovered immediately after rewetting, whilst the other variables did not recover as quickly. *S. quinquefarium* had the highest correlation with a Spearman rho value 0.92. The rho of *S. papillosum* and *S. inundatum* were 0.72 and 0.80 respectively (Supplementary Figure 5.2), indicating a possible difference in water retention and within-colony distribution dynamics.

When differences for treatments between timepoints were examined, there was a significant lag between the recovery of box weight and the recovery of the water content in the capitula at the end of the drought period. Weight increases immediately as the Gravimetrics platform waters the box back to its original weight, but capitulum water content was not immediately replenished within the period between automated watering early in the morning and when the capitula were harvested during the day, as evidenced by the lag between box weight and capitulum water content recovery (Supplementary Figure 5.3).

For *S. quinquefarium*, capitulum water content started differing from the initial water content after 14 days of drought, except for the 8 week drought treatment, which already differed significantly from day 10, possibly due to glasshouse position. For *S. inundatum*, this is less consistent but for the majority of treatments appears to be around day 17. In *S. papillosum*, there were no significant differences in water content over time for any of the treatments except the 8 week drought treatment, in which there were significant differences ($p<0.05$*) from the initial water content after day 38. Water content first went below 1 g g^{-1} for *S. quinquefarium* on day 31 in the 8 week drought treatment, and day 17 for *S. inundatum*. For *S. papillosum*, the lowest water content measured was 1.76 g g^{-1}, which may be due to the higher water holding capacity of *S. papillosum*.
Over the course of the drought period, the three species showed similar rates of water loss ($p > 0.05$), namely 39.27, 36.65 and 37.04 g day^{-1} for *S. quinquefarium*, *S. papillosum* and *S. inundatum* respectively (Supplementary Figure 5.4), although when taken as percentage of initial weight, *S. inundatum* lost significantly more ($p<0.001$****) than both other species. *S. papillosum* lost the smallest fraction of

weight of the three, significantly less than *S. quinquefarium* ($p<0.01$**). Fresh weight and dry weight showed that whilst fresh weight in the drought treatment groups declined, dry weight across the treatments remained similar within species, as expected (Supplementary Figure 5.5).

5.3.2 - Chlorophyll and carotenoid contents

Chlorophyll *a* content decreased in drying plants over time for all the species (Supplementary Figure 5.6). For *S. quinquefarium*, the chlorophyll *a* concentration in drying plants differed significantly from wet plants after 14 days of drought ($p<0.05$**). The largest difference was between wet and drying plants at the end of the experiment duration on day 56 ($p<0.001$****). Recovering plants that had been rewet differed significantly from both dry ($p<0.05$*) and wet plants ($p<0.01$**) on day 42, but no longer differed from wet plants on day 56, suggesting the 6-week drought treatment had recovered entirely at that stage. *S. inundatum* had significantly different chlorophyll *a* concentrations on day 42 between wet and drying plants ($p<0.05$*) and between drying and recovering plants ($p<0.001$***). As the relationship between chlorophyll *a*, *b* and carotenoids was highly correlated, this pattern of decrease and recovery was similar for chlorophyll *b* and carotenoids for both *S. quinquefarium* and *S. inundatum*. For *S. papillosum*, which never reached quite as low water contents as the other two species, the chlorophyll *a*, *b* and carotenoid contents in drying plants never significantly differed from wet or recovering plants on any timepoint.

With the aim of estimating the potential of image-based capitulum water content quantification, the images collected during the drought treatments were analysed and vegetational indices, both RGB and multispectral, were generated using the calculations in Table 5.1. These indices have been used to quantify a number of traits, but as the colour change in *Sphagnum* is so significant between the saturated and desiccated state, they could be developed into a quantification tool for capitulum water content.

5.3.3.1 - Correlative strength of the indices with water content and pigments

We evaluated Spearman's rank correlations between indices, capitulum water content and pigment concentrations. Of the 7 RGB indices and the R and G colour channels used to evaluate capitulum water content, Excessive Green (ExG) was best for *S. quinquefarium* (rho = -0.65) and worked well on *S. inundatum* (rho = -0.63) as selected by the feature selection method, although this index performed poorly for *S. papillosum* (rho = -0.25) (Supplementary Table 5.2). *S. papillosum* was consistently the weakest correlating species for every index, possibly due to never reaching as low capitulum water content values as the other two species. However, BGR was the best performing index for water content across the three species, producing rho values of -0.60, -0.55 and -0.67 for *S. quinquefarium*, *S. papillosum* and *S. inundatum* respectively (p<0.0001****, Figure 5.3).

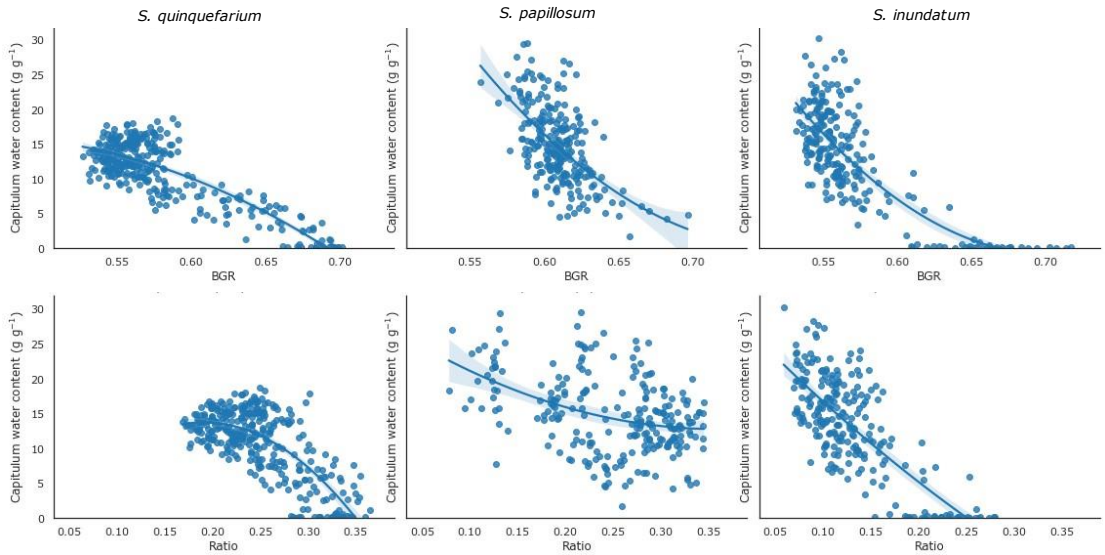

Figure 5.3. Correlations of the strongest RGB index (BGR) and multispectral index (Ratio) with capitulum water content for each of the three species. All correlations with the exception of Ratio for *S. inundatum* were non-linear. The non-linearity could in part be explained by skew caused by the wet control and recovering samples.

Of the 10 MSIs, Ratio was consistently the best correlating variable with capitulum water content for all three species. All correlations were highly significant (p<0.0001****), with the highest rho for *S. inundatum* (-0.67). *S. quinquefarium* and *S. papillosum* had rho's of -0.56 and -0.37 respectively. Although for *S. inundatum* a regular linear model was sufficient, *S. quinquefarium* and *S. papillosum* required an

exponential model which was significantly better ($p<0.001$***). Thus, we concluded that Ratio was the best multispectral index for all three species.

The RGB models for capitulum water content had higher rho for *S. quinquefarium* and *S. papillosum*. For *S. inundatum*, the strength of the correlation between the RGB model and MSI model were identical. When all species data was combined, the Spearman rho correlation between BGR and capitulum water content was still highly significant ($p<0.0001$****) and exponential, but the rho was lower (-0.45) than when the species were analysed separately. The correlation between Ratio and water content was equally significant although the rho was slightly lower (-0.42), although this relationship was linear.

However, when the 'wet' state data was excluded and only the 'drying' data was analysed (n=410), which comprised all treatment groups from onset of drought until rewetting, the relationship between BGR and capitulum water content changed from exponential to linear with a rho of -0.74, and was still highly significant ($p<0.0001$****) (Figure 5.4). Arguably this data subset was a more balanced presentation of the capitulum water content spectrum between saturated and dry, as it removed skew towards high water contents caused by the rewetting periods. Conversely for Ratio, the relationship changed from linear to exponential with a rho of -0.41. This may indicate that BGR is more sensitive to skew from high water content samples, performing more accurately on a more balanced dataset whilst Ratio performs similarly regardless of the skew in the data.

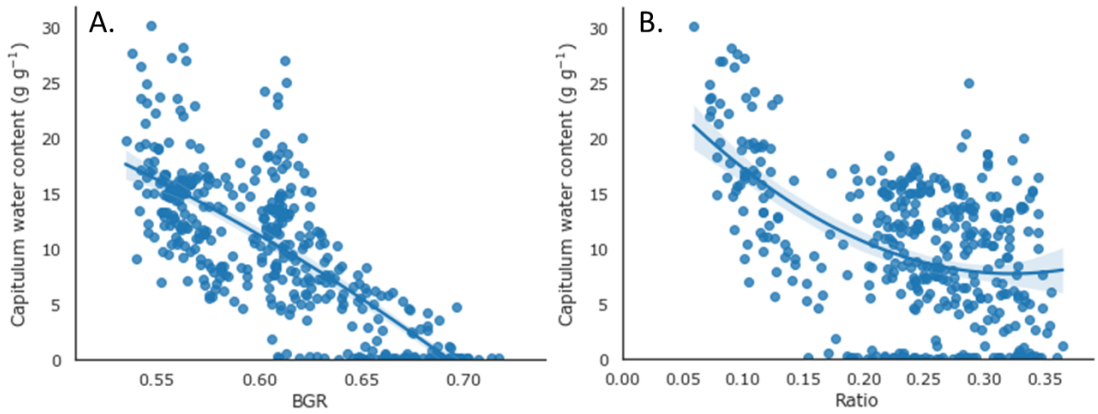

Figure 5.4. Correlations of the best performing indices with capitulum water content, all species drying data combined.
A. BGR correlated strongly linearly with capitulum water content (rho = -0.74, whilst Ratio (B) correlated poorly and non-linear (rho = -0.41). This indicates that BGR was a better explanatory variable for *Sphagnum* capitulum water content than the multispectral index Ratio. As RGB image collection is less constrained by set-up requirements, the advantage of not requiring multispectral imaging for biological variables has the potential to facilitate data collection.

When the relationship of the MSI and RGB indices with the chlorophyll *a*, *b* and carotenoids was evaluated, none of the three pigments correlated as well with the indices as capitulum water content did. For RGB, the R colour channel was consistently the best for each species for all three pigments, producing high correlations ($p<0.001$***) (Supplementary Figure 5.7). However, the rho values for the relationship between these pigments and indices were lower than those from the capitulum water content analyses and, surprisingly, none of the RGB indices outperformed the R colour channel.

The MSI's performed more similarly to the RGB indices in their correlation with the pigments. For *S. quinquefarium* and *S. papillosum*, Ratio produced the strongest correlation, with rho values similar to those of the RGB analysis. For *S. inundatum*, CRI550-780 was the preferred index for chlorophyll *a, b* and carotenoids (rho = 0.63, 0.59 and 0.58 respectively).

5.3.3.2 - Index sensitivity to change over time

To evaluate the sensitivity of the indices to changes in capitulum colour as a result of drought (Figure 5.5A), t-tests and Wilcoxon rank-sum tests were carried out to compare differences between the peak drought timepoint (day 10, 24, 38 and 56 respectively for each of the drought treatments) and other timepoints for BGR and Ratio. For *S. quinquefarium*, treated with a two week drought, no significant differences were detected by neither BGR nor Ratio from timepoint 10. In the four week drought treatment, timepoint 24 differed significantly ($p<0.05$*) for both BGR and Ratio from 7 of the 16 other timepoints, namely timepoint 35 up to and including 56. For BGR, the six week drought treatment found 11 significant differences from timepoint 38, ranging in significance from $p<0.05$* to $p<0.001$*** (Figure 5B).

The higher significance values were found at timepoints further removed from timepoint 38 at the beginning and ending of the experiment. Ratio found only two significant differences ($p<0.05$*) from timepoint 38, which were timepoint 0 and 3. This may in part be due to the distribution of the data, as a Wilcoxon rank-sum test had to be used for Ratio whilst BGR could use a more sensitive t-test. Lastly, the 8 week drought treatment found significant differences between timepoint 56 and all other timepoints until timepoint 42 for BGR, indicating that at timepoint 42 a plateau was reached (Figure 5.5B). This was also the point at which water content reached its lower values. For Ratio, this plateau was reached at timepoint 21, although water content was still around 5 g g^{-1} at that timepoint. For *S. quinquefarium*, these results show that BGR may be more sensitive at detecting differences in water content than Ratio.

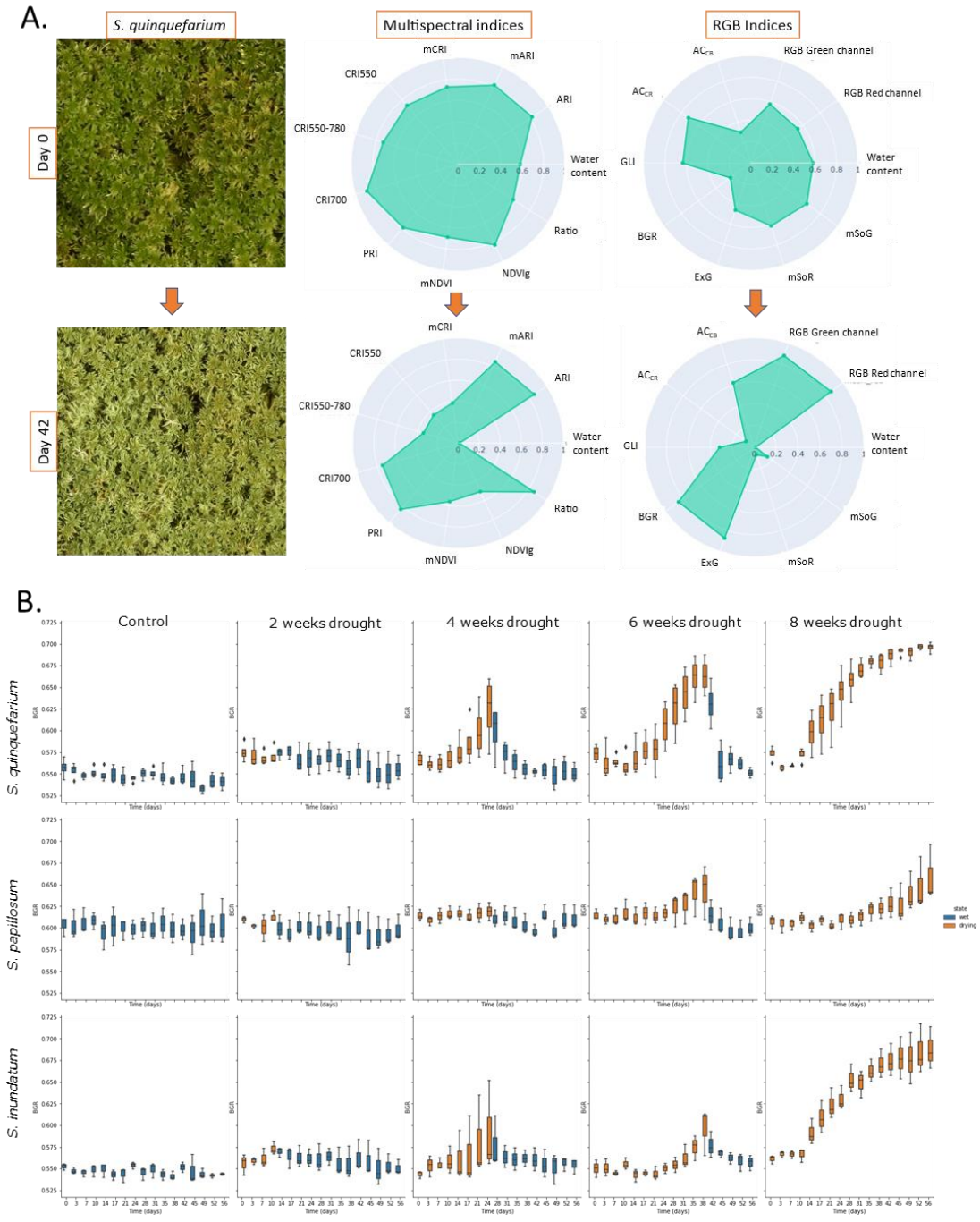

Figure 5.5. Responses of the RGB and multispectral indices to drought over time.
A. Comparison of how capitulum water content and the various multispectral and RGB indices respond to drought in *S. quinquefarium* after 42 days. All variables have been scaled to fit a range of 0-1. Large changes can be observed in nearly all multispectral indices except for ARI, mARI, CRI700 and mNDVI. Of the RGB indices, BGR shows the largest change along with AC_{CR} and ExG.
B. Progression of the BGR index over time (days). The columns indicate from left to right the treatments, namely control, 2 weeks, 4 weeks, 6 weeks and 8 weeks drought. The rows indicate the different species, in the order *S. quinquefarium, S. papillosum, S. inundatum*. Where the boxes are orange the treatment was undergoing drought, whilst blue indicates watering. All species show a distinct increase in BGR values after 6 weeks of drought, although *S. quinquefarium* and *S. inundatum* already show this increase at 4 weeks. In the 8 weeks drought treatment, the response for *S. quinquefarium* and *S. inundatum* is already

flattening as the capitula reached below 1 g g^{-1} water content. In *S. papillosum*, this water content is never reached and the drought response in BGR is still increasing towards the end of the 8 week drought period.

In *S. papillosum*, no significant differences were found between any timepoints for any of the treatments in neither BGR nor Ratio (Figure 5.5B and Supplementary Figures 8-25). This is consistent with the results for water content as indicated (see above), with the exception of the eight week drought treatment, in which capitulum water content started differing significantly from initial values at timepoint 38. The data for BGR and Ratio did trend upwards for the six and eight weeks drought treatments, but not sufficiently for it to be significant.

S. inundatum did not have any significant differences in the two week drought treatment either for both BGR and Ratio, and in the four week drought treatment no timepoint differed significantly from timepoint 24, although timepoint 21 differed from timepoint 0 ($p<0.05$*) for BGR (Figure 5.5B and Supplementary Figures 5.8-5.25). In the six week drought treatment, BGR timepoint 38 differed significantly from every other timepoint except timepoint 42, with p-values ranging from <0.05* to <0.001***. Ratio found differences in the six week treatment between timepoint 38 and every other timepoint except 7, 35, 42 and 45.

The observation that timepoint 42 was not different indicates that the recovery lag in capitulum water content can also be detected by BGR and Ratio. Timepoint 56 was different for BGR from every timepoint up until timepoint 28, after which the values plateau. At timepoint 24 in this treatment, capitulum water content had reached its lowest values. Ratio found no significant difference at between timepoint 24 and the end of the experiment, although it did find small differences at timepoints 31 and 35, presumably due to imaging artefacts. These results show that both BGR and Ratio can be very sensitive enough to measure differences in capitulum water content in different *Sphagnum* species, with BGR performing similarly or even better than Ratio, highlighting the potential for standard RGB imaging technologies to be used instead of multispectral imaging.

5.3.4 - Field imaging experiment validation

To further examine the potential of RGB image based quantification of capitulum water content in *Sphagnum*, a further 175 images comprising 7 different species were taken in natural settings . These species covered a wide range of niches along the hydrological gradient (Johnson et al., 2015), as well as a wider range of the colours typical of the *Sphagnum* genus. Capitulum water content was measured from 9 harvested capitula per image, as well as the relative humidity at canopy level and the distance between the capitulum layer and the water table. RGB indices from the images listed in Table 5.1 were calculated on the regions that were annotated by the capitulum counter algorithm pipeline.

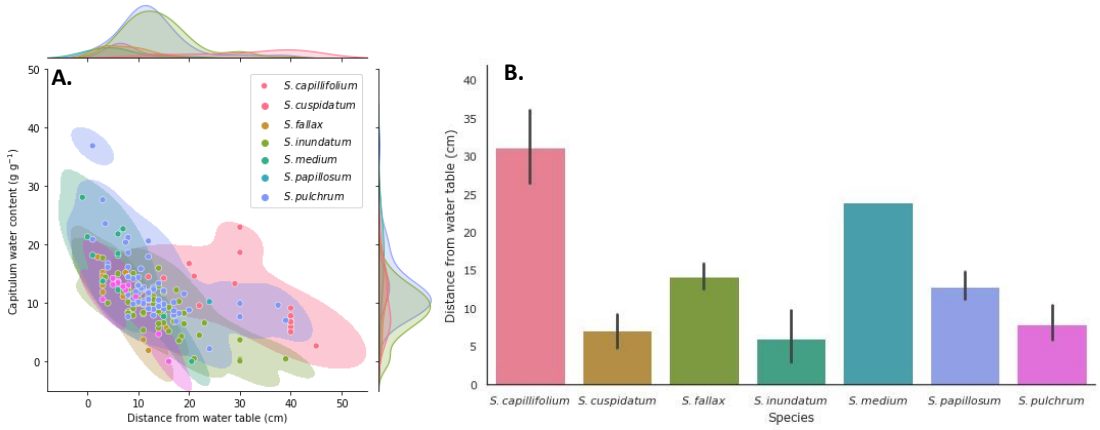

Figure 5.6. Capitulum water content corresponds to distance from water table. All *Sphagnum* species sampled had an inverse relationship between capitulum water content and the distance (cm) between the water table and capitulum canopy (A). The height at which a species is found above the water table is typically related to its respective niche preference (B). The species sampled in the field covered a large range of the possible niches above the water table, but also a wide range of the possible colours found in *Sphagnum*.

Our aim was to evaluate whether it was possible to develop a universal approach for most or all *Sphagnum* species, covering much of the broad range of the natural variation in water table position, colours and water content. An all species analysis indicated a negative relationship between capitulum water content and the distance between the water table and the capitulum (Figure 5.6A), and with all species combined the correlation between capitulum water content and the distance from the water table was highly significant ($p<0.0001$****) with a Spearman rho of -0.67, suggesting that capitulum water content may provide a proxy for the water table in the ecosystem. However, of the four relative humidity sensor positions, the

sensor positioned 2cm above the *Sphagnum* canopy had the strongest correlation with water content (rho 0.32, p<0.001***), indicating that the sensors were only slightly representative of capitulum water content.

Variance Inflation Factor (VIF) values were used to determine which if any RGB indices could explain water content. After stepwise removal of the RGB indices from the full model until the remaining VIF values were <5, the remaining model consisted of RGB R, mSoR and AC_{CB}. This model was not significantly better (p>0.05) than the minimal model using only RGB R, and produced a highly significant (p<0.0001****) Spearman Rank correlation with a rho of -0.47 between capitulum water content and the three RGB indices. The R channel minimum model produced a similar rho of -0.48, and was therefore considered superior as it was also less complex (Figure 5.7). BGR, the strongest correlating RGB index in the glasshouse experiment, only had a correlation value of -0.25, although this was also highly significant (p<0.0001****).

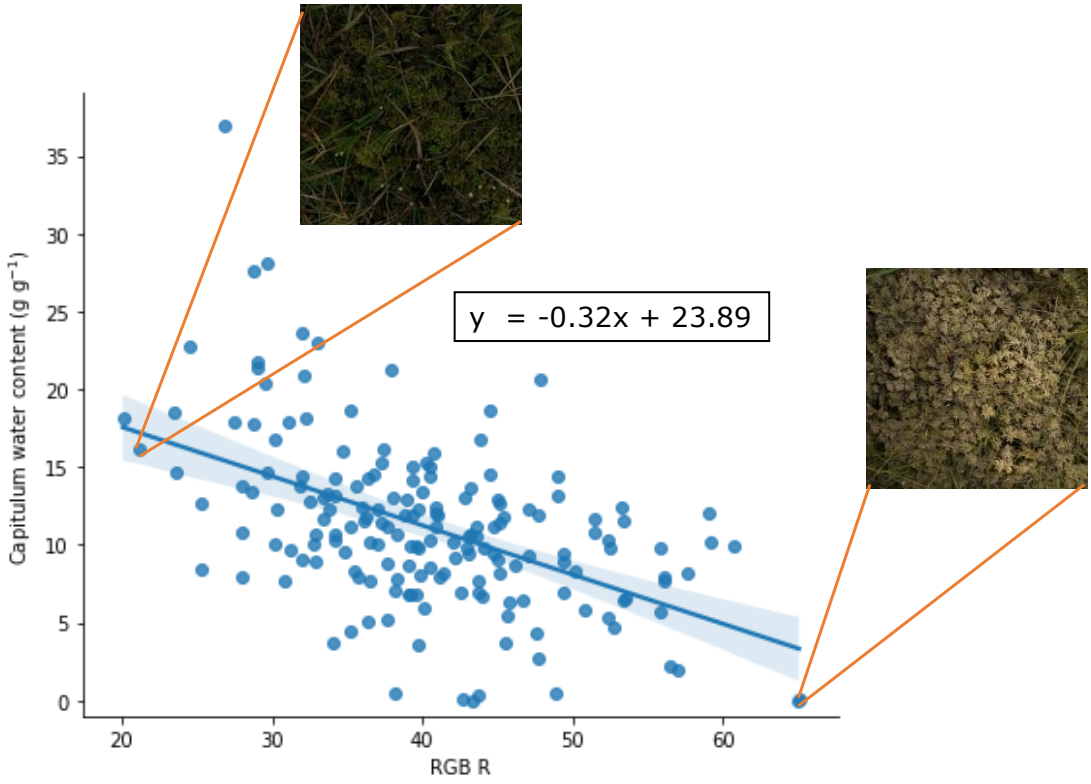

Figure 5.7. The red RGB colour channel correlates strongly with capitulum water content. Data from 175 *Sphagnum* colonies were grouped and show a strong relation between the red colour channel and capitulum water content. An example of a wet *S. papillosum* colony on the left side and a dry *S. fallax* colony on the right side have been included for illustrative purposes. This shows that the use of common RGB images, collected using smartphones, may provide a non-destructive estimate of capitulum water content for Sphagnum biomonitoring.

Considering these results, RGB R might be sufficient to infer capitulum water content from images when combined with ecological variables such as the distance from the water table, enabling non-destructive active biomonitoring of *Sphagnum* plant health by proxy.

5.4 - Discussion

The perceived importance of peatland restoration and function in the northern hemisphere has increased in the context of global climate change (Loisel et al., 2021). *Sphagnum* peatmosses have arguably become the most well-known bryophyte outside the scientific community, and a growing interest from the public in peatlands means there is great potential for citizen science data acquisition. However, very little research has focussed on the development of accessible methodologies for data acquisition in *Sphagnum*. This paper evaluates the potential of image-based water content estimation and provides a comparison between two popular techniques, namely RGB and multispectral imaging. Both methodologies have been widely applied in agricultural research (Li et al., 2014; Malenovský et al., 2017; Robb et al., 2020; Xue and Su, 2017) but, for bryophytes, vegetational indices have been relatively underused. Research on peatlands using vegetational indices has typically employed remote sensing or aerial imaging techniques to analyse the vegetational community in its entirety (Harris et al., 2006). As high quality cameras and GPS have become ubiquitous on smartphones and consumer-grade drones, appropriate software tools to extract useful knowledge would enhance the potential for citizen science projects.

5.4.1 - *Sphagnum*'s desiccation colour change

When *Sphagnum* dries out, it undergoes a distinct change in its hue (Figure 5.3A). This is likely due to the hyaline cells, which make up a large proportion of the plant. As these cells are hollow, they give the plant a whitish shade when dry as the cell walls reflect light (Bowker et al., 2010; Hanson and Rice, 2014). Similar visual responses can be seen in cosmopolitan bryophytes such as *Bryum argenteum*, which was named after the 'silver' colouring it has when dry. In contrast to *Sphagnum*, *Bryum* is a genus with many desiccation tolerant species, being able to fully recover after extended periods of drought and extremely low water content. *Sphagnum* has some rudimentary desiccation tolerant responses (Hájek and Vicherová, 2014; Nibau et al., 2022), and full recovery is possible after some drought. Our results show that after extended drought, damage to photosystems is present as the concentration of chlorophyll *a*, *b* and carotenoids decreased (Supplementary Figure 5.6). However,

upon rewetting, the concentrations of these pigments rapidly recovered to pre-desiccation levels.

5.4.2 - Water retention differences between species

Of the three species used in the glasshouse experiment, *S. papillosum* showed the strongest water retention capacity. It had the lowest weight loss per day and retained the largest relative water content towards the end of the 8 weeks drought treatment. There may be several possible adaptations that enable *S. papillosum* to hold on to such large amounts of water. Compared to *S. quinquefarium* and *S. inundatum*, *S. papillosum* plants are much larger, with an average dry weight of 11.80 mg, compared to 7.79 mg and 7.48 mg for *S. quinquefarium* and *S. inundatum* respectively (Supplementary Figure 5.5). Furthermore, canopies of *S. papillosum* are typically very dense, to the extent where it is very difficult to distinguish individual capitula from an image (van de Koot et al., 2021). This limits the amount of exposed surface and may reduce water loss through evaporation, which is supported by *S. papillosum* losing the smallest fraction of its weight over time compared to the other two species.

On the contrary, *S. inundatum* was the species that dried the quickest and reached the lowest fraction of its starting weight (Figure 5.2, Supplementary Figure 5.4). In terms of colony structure, the plants of this species grow much looser and have much less dense canopies, exposing the capitula from most sides as well as the lower sections of the stems, potentially increasing evaporation rates. In the area from which it was collected, *S. inundatum* grows exclusively in and at the margins of shallow pools at the Pen y Garn site, a situation in which it typically does not have to rely on colony structure as a water retention method.

S. quinquefarium was collected from Coed y Darren, a temperate rainforest-type woodland with high precipitation rates and humidity on a north facing hillside. Compared to the other two species, which came from a blanket bog, this woodland is arguably one of the more extreme environments as the water table fluctuates massively and for most of the year the moss is dependent on rain. Its colony structure is much more like a canopy than that of *S. inundatum*, but not as dense as that of *S. papillosum*. It's weight loss and water content responses are also in between these two species.

5.4.3 - Comparative performance of image-based indices

Of the 7 RGB indices and RGB R and G, all indicated some response to drought during the glasshouse experiment despite not being designed to measure water content. However, as the visual change in *Sphagnum* undergoing desiccation is so apparent, it is to be expected that any kind of RGB measurement will show some response. This is also indicated by how well individual colour channels were capable of measuring the response, with RGB R and G responding more sensitively than some of the calculated indices. The strongest responding index in the glasshouse experiment, BGR, was originally designed to measure moisture content in higher plants (Elshikha et al., 2016). The sensitivity of this index can be explained by the nature of the B colour channel's changes. In a pilot experiment (data not shown), we found that the B channel increased exponentially in the later stages of drought, but did not increase during the early drought period, while the other two channels increased more gradually as drought progressed. As a result, the B channel in isolation was too sensitive to changes in lighting conditions and therefore was not considered robust enough to be useful. In combination with the G channel, however, the BGR index provided a reasonable estimate of desiccation during the experiment.

Amongst the multispectral indices, Ratio was the most sensitive to drought. This index was designed to estimate chlorophyll content and is routinely used in satellite and drone image based vegetation analysis. This index combines the near infrared (NIR) and visible red sections of the light spectrum. However, other multispectral indices also designed to estimate chlorophyll content were far less sensitive, and all multispectral indices were outperformed by the RGB indices for the quantification of water content. For the quantification of the photochemistry pigments, the R colour channel was also the strongest correlating variable. However, in general, the variables that correlated well with water content also correlated well with the pigments, suggesting that this may simply be collinearity caused by the decrease in water content also decreasing the pigment content.

The RGB indices did not perform as well in natural settings as they did in the glasshouse setting. This was expected due to increased number of potentially confounding factors in the natural environment. These factors include less consistent lighting, occlusion from non-*Sphagnum* plants and spatial variation in water content within patches of *Sphagnum* (as compared to the relatively homogeneous material

used in the glasshouse). For example, BGR had a correlation of -0.74 in the glasshouse, it only had a correlation of -0.25 with capitulum water content on the field based images. Instead, the R channel was the strongest correlating variable, with a Spearman rho value of -0.48, although the G channel performed very similarly. The reason why BGR performed poorly on the field data might be due to the shape of the correlations between the three RGB colour channels (Supplementary Figure 5.26). While the R and G channels correlated linearly with each other, the correlation of these two with the B channel was non-linear. As previously mentioned, the B channel was found to be very sensitive to lighting changes, and the uncontrolled lighting conditions of the field data likely affected this channel more than in the controlled lighting of the glasshouse experiment despite the white balance correction step using the colour card (van de Koot et al., 2021).

Overall, our data show that RGB based imaging can be used to estimate capitulum water content in *Sphagnum*. While the correlative strength of the relationship was lower in the field than in the glasshouse, it also shows that experimental set-ups where transects of plants are regularly measured over time, as is common in many conservation sites, can be used to parametrise vegetation plots in a given site by measuring their RGB values during various drought conditions. This would eliminate the need to measure the water content of the plants destructively, and eliminate factors such as researcher bias from plant health assessments

5.5 - References

Ares, A., Aboal, J.R., Carballeira, A., Fernández, J.A., 2015. Do moss bags containing devitalized Sphagnum denticulatum reflect heavy metal concentrations in bulk deposition? Ecol. Indic. 50, 90–98. https://doi.org/10.1016/j.ecolind.2014.10.030

Ares, A., Aboal, J.R., Carballeira, A., Giordano, S., Adamo, P., Fernández, J.A., 2012. Moss bag biomonitoring: A methodological review. Sci. Total Environ. 432, 143–158. https://doi.org/10.1016/j.scitotenv.2012.05.087

Beike, A.K., Spagnuolo, V., Lüth, V., Steinhart, F., Ramos-Gómez, J., Krebs, M., Adamo, P., Rey-Asensio, A.I., Fernández, J.A., Giordano, S., Decker, E.L., Reski, R., 2015. Clonal in vitro propagation of peat mosses (Sphagnum L.) as novel green resources for basic and applied research. Plant Cell. Tissue Organ Cult. 120, 1037–1049. https://doi.org/10.1007/s11240-014-0658-2

Benavides, J.C., Jesús, I.S., 2009. Digitized Images Provide More Accuracy and Efficiency to Estimate Bryophyte Cover. Bryologist 112, 12–18.

Bowker, M.A., Maestre, F.T., Escolar, C., 2010. Biological crusts as a model system for examining the biodiversity-ecosystem function relationship in soils. Soil Biol. Biochem. 42, 405–417. https://doi.org/10.1016/j.soilbio.2009.10.025

Burton, M.A.S., Peterson, P.J., 1979. Metal accumulation by aquatic bryophytes from polluted mine streams. Environ. Pollut. 19, 39–46. https://doi.org/10.1016/0013-9327(79)90111-3

Capozzi, F., Adamo, P., Di Palma, A., Aboal, J.R., Bargagli, R., Fernández, J.A., Lopez Mahia, P., Reski, R., Tretiach, M., Spagnuolo, V., Giordano, S., 2017. Sphagnum palustre clone vs native Pseudoscleropodium purum: A first trial in the field to validate the future of the moss bag technique. Environ. Pollut. 225, 323–328. https://doi.org/10.1016/j.envpol.2017.02.057

Capozzi, F., Carotenuto, R., Giordano, S., Spagnuolo, V., 2018. Evidence on the effectiveness of mosses for biomonitoring of microplastics in fresh water environment. Chemosphere 205, 1–7. https://doi.org/10.1016/j.chemosphere.2018.04.074

Cesa, M., Bertossi, A., Cherubini, G., Gava, E., Mazzilis, D., Piccoli, E., Verardo, P., Nimis, P.L., 2015. Development of a standard protocol for monitoring trace elements in continental waters with moss bags: inter- and intraspecific differences. Environ. Sci. Pollut. Res. 22, 5030–5040. https://doi.org/10.1007/s11356-015-4129-z

Clymo, R.S., Hayward, P.M., 1982. The Ecology of Sphagnum, in: Bryophyte Ecology. Springer Netherlands, Dordrecht, pp. 229–289. https://doi.org/10.1007/978-94-009-5891-3_8

del Valle, J.C., Gallardo-López, A., Buide, M.L., Whittall, J.B., Narbona, E., 2018. Digital photography provides a fast, reliable, and noninvasive method to estimate anthocyanin pigment concentration in reproductive and vegetative plant tissues. Ecol. Evol. 8, 3064–3076. https://doi.org/10.1002/ece3.3804

Elshikha, D.M., Hunsaker, D.J., Bronson, K.F., Sanchez, P.L., 2016. Using RGB-based vegetation indices for monitoring guayule biomass, moisture content and rubber. 2016 Am. Soc. Agric. Biol. Eng. Annu. Int. Meet. ASABE 2016. https://doi.org/10.13031/aim.20162380922

Fernández, J.A., Vázquez, M.D., López, J., Carballeira, A., 2006. Modelling the extra and intracellular uptake and discharge of heavy metals in Fontinalis antipyretica transplanted along a heavy metal and pH contamination gradient.

Environ. Pollut. 139, 21–31. https://doi.org/10.1016/j.envpol.2005.04.036
Gamon, J.A., Field, C.B., Bilger, W., Björkman, O., Fredeen, A.L., Peñuelas, J., 1990. Remote sensing of the xanthophyll cycle and chlorophyll fluorescence in sunflower leaves and canopies. Oecologia 85, 1–7. https://doi.org/10.1007/BF00317336
Gamon, J.A., Peñuelas, J., Field, C.B., 1992. A Narrow-Waveband Spectral Index That Tracks Diurnal Changes in Photosynthetic Efficiency. Remote Sens. Environ. 41, 35–44. https://doi.org/10.1016/0034-4257(92)90059-S
Giordano, S., Colacino, C., Basile, A., Esposito, A., Castaldo-cobianchi, R., 2009. Morphological adaptation to water uptake and transport in the poikilohydric moss Tortula ruralis. G. Bot. Ital. 127, 1123–1132.
Gitelson, A., Merzlyak, M.N., 1994. Spectral Reflectance Changes Associated with Autumn Senescence of Aesculus hippocastanum L. and Acer platanoides L. Leaves. Spectral Features and Relation to Chlorophyll Estimation. J. Plant Physiol. 143, 286–292. https://doi.org/10.1016/S0176-1617(11)81633-0
Gitelson, A.A., Keydan, G.P., Merzlyak, M.N., 2006. Three-band model for noninvasive estimation of chlorophyll, carotenoids, and anthocyanin contents in higher plant leaves. Geophys. Res. Lett. 33. https://doi.org/10.1029/2006GL026457
Gitelson, A.A., Merzlyak, M.N., 1997. Remote estimation of chlorophyll content in higher plant leaves. Int. J. Remote Sens. 18, 2691–2697. https://doi.org/10.1080/014311697217558
Gitelson, A.A., Merzlyak, M.N., Chivkunova, O.B., 2001. Optical Properties and Nondestructive Estimation of Anthocyanin Content in Plant Leaves. Photochem. Photobiol. 74, 38. https://doi.org/10.1562/0031-8655(2001)074<0038:opaneo>2.0.co;2
Gitelson, A.A., Zur, Y., Chivkunova, O.B., Merzlyak, M.N., 2002. Assessing Carotenoid Content in Plant Leaves with Reflectance Spectroscopy. Photochem. Photobiol. 75, 272. https://doi.org/10.1562/0031-8655(2002)075<0272:accipl>2.0.co;2
Gorham, E., 1957. The Development of Peat Lands. Q. Rev. Biol. 32, 145–166. https://doi.org/10.1007/s13398-014-0173-7.2
Hájek, T., Vicherová, E., 2014. Desiccation tolerance of Sphagnum revisited: a puzzle resolved. Plant Biol. 16, 665–773. https://doi.org/10.1111/plb.12126
Hanson, D.T., Rice, S.K., 2014. Photosynthesis in Bryophytes and Early Land Plants, in: Advances in Photosynthesis and Respiration. Springer Science, Dordrecht, pp. 291–308. https://doi.org/10.1007/978-94-007-6988-5
Harris, A., Bryant, R.G., Baird, A.J., 2006. Remote sensing of Sphagnum stress: A proxy for near-surface wetness conditions in northern peatlands? Eur. Sp. Agency, (Special Publ. ESA SP.
Johnson, M.G., Granath, G., Tahvanainen, T., Pouliot, R., Stenøien, H.K., Rochefort, L., Rydin, H., Shaw, A.J., 2015. Evolution of niche preference in Sphagnum peat mosses. Evolution (N. Y). 69, 90–103. https://doi.org/10.1111/evo.12547
Kawashima, S., Nakatani, M., 1998. An algorithm for estimating chlorophyll content in leaves using a video camera. Ann. Bot. 81, 49–54. https://doi.org/10.1006/anbo.1997.0544
Leifeld, J., Menichetti, L., 2018. The underappreciated potential of peatlands in global climate change mitigation strategies. Nat. Commun. 9, 1–7. https://doi.org/10.1038/s41467-018-03406-6
Li, L., Zhang, Q., Huang, D., 2014. A review of imaging techniques for plant

phenotyping. Sensors 14, 20078–20111. https://doi.org/10.3390/s141120078
Loisel, J., Gallego-Sala, A. V., Amesbury, M.J., Magnan, G., Anshari, G., Beilman, D.W., Benavides, J.C., Blewett, J., Camill, P., Charman, D.J., Chawchai, S., Hedgpeth, A., Kleinen, T., Korhola, A., Large, D., Mansilla, C.A., Müller, J., van Bellen, S., West, J.B., Yu, Z., Bubier, J.L., Garneau, M., Moore, T., Sannel, A.B.K., Page, S., Väliranta, M., Bechtold, M., Brovkin, V., Cole, L.E.S., Chanton, J.P., Christensen, T.R., Davies, M.A., De Vleeschouwer, F., Finkelstein, S.A., Frolking, S., Gałka, M., Gandois, L., Girkin, N., Harris, L.I., Heinemeyer, A., Hoyt, A.M., Jones, M.C., Joos, F., Juutinen, S., Kaiser, K., Lacourse, T., Lamentowicz, M., Larmola, T., Leifeld, J., Lohila, A., Milner, A.M., Minkkinen, K., Moss, P., Naafs, B.D.A., Nichols, J., O'Donnell, J., Payne, R., Philben, M., Piilo, S., Quillet, A., Ratnayake, A.S., Roland, T.P., Sjögersten, S., Sonnentag, O., Swindles, G.T., Swinnen, W., Talbot, J., Treat, C., Valach, A.C., Wu, J., 2021. Expert assessment of future vulnerability of the global peatland carbon sink. Nat. Clim. Chang. 11, 70–77. https://doi.org/10.1038/s41558-020-00944-0
Louhaichi, M., Borman, M.M., Johnson, D.E., 2001. Spatially located platform and aerial photography for documentation of grazing impacts on wheat. Geocarto Int. 16, 65–70. https://doi.org/10.1080/10106040108542184
Lovelock, C.E., Robinson, S.A., 2002. Surface reflectance properties of antarctic moss and their relationship to plant species, pigment composition and photosynthetic function. Plant, Cell Environ. 25, 1239–1250. https://doi.org/10.1046/j.1365-3040.2002.00916.x
Malenovský, Z., Lucieer, A., King, D.H., Turnbull, J.D., Robinson, S.A., 2017. Unmanned aircraft system advances health mapping of fragile polar vegetation. Methods Ecol. Evol. 8, 1842–1857. https://doi.org/10.1111/2041-210X.12833
Nibau, C., van de Koot, W., Spiliotis, D., Williams, K., Kramaric, T., Beckmann, M., Mur, L., Hiwatashi, Y., Doonan, J.H., 2022. Molecular and physiological responses to desiccation indicate the abscisic acid pathway is conserved in the peatmoss, Sphagnum. J. Exp. Bot. 1–16. https://doi.org/https://doi.org/10.1093/jxb/erac133
Page, S.E., Baird, A.J., 2016. Peatlands and Global Change: Response and Resilience. Annu. Rev. Environ. Resour. 41, 35–57. https://doi.org/10.1146/annurev-environ-110615-085520
Porra, R.J., 2006. Spectrometric Assays for Plant, Algal and Bacterial Chlorophylls, in: Grimm, B., Porra, R.J., Rüdiger, W., Scheer, H. (Eds.), Chlorophylls and Bacteriochlorophylls. Advances in Photosynthesis and Respiration. Springer Netherlands, Dordrecht, pp. 95–107. https://doi.org/10.1007/1-4020-4516-6_7
Rahimzadeh-Bajgiran, P., Munehiro, M., Omasa, K., 2012. Relationships between the photochemical reflectance index (PRI) and chlorophyll fluorescence parameters and plant pigment indices at different leaf growth stages. Photosynth. Res. 113, 261–271. https://doi.org/10.1007/s11120-012-9747-4
Robb, C., Hardy, A., Doonan, J.H., Brook, J., 2020. Semi-Automated Field Plot Segmentation From UAS Imagery for Experimental Agriculture. Front. Plant Sci. 11, 1–13. https://doi.org/10.3389/fpls.2020.591886
Robinson, S.A., King, D.H., Bramley-Alves, J., Waterman, M.J., Ashcroft, M.B., Wasley, J., Turnbull, J.D., Miller, R.E., Ryan-Colton, E., Benny, T., Mullany, K., Clarke, L.J., Barry, L.A., Hua, Q., 2018. Rapid change in East Antarctic terrestrial vegetation in response to regional drying. Nat. Clim. Chang. 8, 879–884. https://doi.org/10.1038/s41558-018-0280-0

Sánchez-Sastre, L.F., Alte da Veiga, N.M.S., Ruiz-Potosme, N.M., Carrión-Prieto, P., Marcos-Robles, J.L., Navas-Gracia, L.M., Martín-Ramos, P., 2020. Assessment of RGB Vegetation Indices to Estimate Chlorophyll Content in Sugar Beet Leaves in the Final Cultivation Stage. AgriEngineering 2, 128–149. https://doi.org/10.3390/agriengineering2010009

Sims, D.A., Gamon, J.A., 2002. Relationships between leaf pigment content and spectral reflectance across a wide range of species, leaf structures and developmental stages. Remote Sens. Environ. 81, 337–354. https://doi.org/10.1016/S0034-4257(02)00010-X

van de Koot, W.Q.M., van Vliet, L.J.J., Chen, W., Doonan, J.H., Nibau, C., 2021. Development of an image analysis pipeline to estimate Sphagnum colony density in the field. Plants 10, 1–17. https://doi.org/10.3390/plants10050840

Wehr, J.D., Empain, A., Mouvet, C., Say, P.J., Whitton, B.A., 1983. Methods for processing aquatic mosses used as monitors of heavy metals. Water Res. 17, 985–992. https://doi.org/10.1016/0043-1354(83)90038-6

Wenhua Mao, Yiming Wang, Yueqing Wang, 2013. Real-time Detection of Between-row Weeds Using Machine Vision 0300. https://doi.org/10.13031/2013.15381

Woebbecke, D.M., Meyer, G.E., Von Bargen, K., Mortensen, D.A., 1995. Color indices for weed identification under various soil, residue, and lighting conditions. Trans. Am. Soc. Agric. Eng. 38, 259–269. https://doi.org/10.13031/2013.27838

Xue, J., Su, B., 2017. Significant remote sensing vegetation indices: A review of developments and applications. J. Sensors 2017. https://doi.org/10.1155/2017/1353691

Yu, Z., Loisel, J., Brosseau, D.P., Beilman, D.W., Hunt, S.J., 2010. Global peatland dynamics since the Last Glacial Maximum. Geophys. Res. Lett. 37, 1–5. https://doi.org/10.1029/2010GL043584

CHAPTER 6 - DEEPBOG: A DEEP LEARNING SPHAGNUM CAPITULUM DETECTION ALGORITHM

Chapter statement

The methodology described in this chapter, which builds upon the method described in Chapter 4, was developed jointly with Jinle Lin. While I gathered and annotated the images, and counted the false positives and negatives on all the Ireland images with some help from Candida Nibau, they were responsible for the coding and training of the model.

Additionally, this chapter received extra funding from the Welsh Government as part of the Super-Sprint Projects organised by the Wales Data Nation Accelerator, as well as the International Peatland Conservation Council who funded the fieldwork in Northern Ireland.

Data availability

The data pertaining to this chapter can be accessed at (DOI NOT YET AVAILABLE)

Chapter summary

In recent years, peatland ecosystems have received increasing recognition for their importance in global carbon storage. These ecosystems are facing increasing pressure from global climate warning and anthropogenic activities, potentially damaging their functioning as their water table is disrupted. *Sphagnum* peatmosses are an important component of northern hemisphere peatlands, as these plants use their water storage capacity to help keep the ecosystem wet and functioning as carbon sink. While these plants have been the focus of many peatland restoration programmes, there are almost no tools (besides visual inspection by experts) to monitor *Sphagnum* status. Colony density, colour and species diversity are important determinants of plant health. Recent advancements in agriculture and phenotyping research have led to the development of high throughput image-based workflows that enable the non-destructive measurement of such plant traits. To be able to translate these techniques onto *Sphagnum* images, and to measure and monitor the health of these plants and by extension peatlands in general, this project aimed to develop an image-based tool for the detection and quantification of *Sphagnum* peatmosses in standard smartphone photographs. Images were collected from local peatlands in Wales that featured *Sphagnum* plants from various distances, angles and in varying environmental settings. Furthermore, the online repository iNaturalist was used to supplement the dataset with more species and images as they would be taken by non-scientists. Using the convolutional neural network YOLO ('You Only Look Once'), commonly used for object detection, a model was developed that achieved an average precision of over 90%, regularly reaching 100%, and an overall performance of >80% on *Sphagnum* species of all colours and sizes. Ultimately, this tool can be used to quantify colony density in high-throughput, providing a new tool for peatland conservationists to measure an otherwise labour intensive variable.

6.1 - Introduction

Restoration and protection of peatlands is becoming increasingly important as their role in global carbon storage becomes more clear. While peatlands globally occupy only 3% of all land area, they account for 25% of all sequestered soil carbon (Loisel et al., 2021). This carbon is stored in the form of peat, which consists of compressed organic matter. In a functioning peatland, the peat is rarely exposed to oxygen as the ecosystem has a persistent high water table, meaning that the prevailing anaerobic conditions prevent the breakdown of the accumulated organic matter. However, the functioning of peatlands is increasingly under anthropogenic pressure (Page and Baird, 2016; Rastogi et al., 2020). Aside from direct damage to peatlands, where the peat has been cut for fuel, mined for horticulture or the water table has been drained in an attempt to convert it to arable land, changing precipitation patterns and climate warming reduce the amount of annual precipitation on which the majority of peatlands rely.

6.1.1 - *Sphagnum* peat mosses

One of the most important components of healthy temperate peatlands is the bryophyte genus *Sphagnum*, colloquially known as the peatmosses. These mosses have the ability to store very large amounts of water, regularly exceeding 2000% relative water content, or 20 grams of water per gram of biomass (Clymo, 1973; Silvola and Aaltonen, 1984). Important adaptations that enable this large water storage include their specialised hyaline cells, which are dead empty cells lining their branches, stem and leaflets, and their colonial growth form. *Sphagnum* mosses' water holding capacity raises the water table in peatlands, ensuring their functioning as a carbon sink (Clymo and Hayward, 1982). Furthermore, they acidify the water through cation exchange, further reducing decomposition and enabling peat formation. This makes these bryophytes a key factor in peatland restoration projects and conservation (Caporn et al., 2018; Gauthier et al., 2022; Hinde et al., 2010; Leifeld and Menichetti, 2018).

Unlike most bryophytes, *Sphagnum* mosses are not drought tolerant. While they are capable of recovery after brief desiccation, they sustain physiological damage, typically exhibiting signs of senescence (Hájek and Vicherová, 2014; Vitt et al., 2014). As the global climate changes, this may have an impact on the success of

Sphagnum peatland restoration projects. However, most traditional peatland ecology measurements rely on researchers or volunteers conducting manual, labour intensive work and involve specialist equipment. To increase the potential success of peatland restoration projects, it is important that cheap, accessible tools to quantify *Sphagnum* growth and health in the field are developed.

6.1.2 - Recent advances in image-based plant phenotyping

In recent years, the accessibility of artificial intelligence and increasingly affordable computer hardware have sparked a rapid increase of the application of computational automation in plant science. New farming techniques using UAV-collected images (Robb et al., 2020; Sánchez-Sastre et al., 2020; Xiong et al., 2022), as well as high throughput phenotyping platforms (Fahlgren et al., 2015; Li et al., 2014), are providing plant scientists and breeders with new techniques to monitor their plants. Traits such as number of plants and fruits are commonly extracted, but are also employed in novel applications such as discrimination between crop plants and weeds (Hüther et al., 2020; Katoh and Gougeon, 2012; Wenhua Mao et al., 2013).

Despite the rapid advancements of these technologies, fuelled by investment in agricultural research and food security, little of this has been translated to peatland research. The success of UAV-based and other image based methods for crop monitoring motivated us to development automated image-based quantification tools for peatland science. A simple Computer Vision (CV) approach yielded the Capitulum Counter (van de Koot et al., 2021) but this is limited to a defined imaging rig to obtain replicable results.

In recent years, object-detection deep learning models have been applied to the detection of green citrus fruits (Lyu et al., 2022), mapping fruit trees from UAV imagery (Xiong et al., 2022) and the counting of oil palm trees (Chowdhury et al., 2022). The models typically employ the YOLOv5 architecture. YOLO was first published by Redmon et al., 2016, and has quickly been adapted for a variety of object detection tasks. The algorithm divides an image into grid cells and then performs object detection on each grid, which gives this model high processing speed without significant loss of accuracy and making YOLO models fast to train.
The flexibility and accuracy of this method when applied to fruit trees (Chowdhury et al., 2022; Xiong et al., 2022) made us think of its applicability to Sphagnum

capitulum counting since images taken from directly above *Sphagnum* colonies show a resemblance to canopy view images of woodlands and orchards.. In the present paper, we have adapted the annotations obtained by the Capitulum Counter and trained a YOLOv5 deep learning model to automatically detect *Sphagnum* plants in images. Furthermore, the data used to train the model included images taken from a variety of angles and distances, removing some constraints of the previous method.

6.2 - Materials and Methods

6.2.1 - Image acquisition

Sphagnum images of 14 species were collected from multiple sites in mid Wales and Northern Ireland. Initially, an imaging rig (van de Koot et al. 2021) was used to provide consistent image quality, scale and colour standards, but subsequent data were captured in a purposefully less constrained manner from a variety of distances and angles. By diversifying the datasets, any resulting algorithm should be more independent of context and therefore able to extract information from a range of scientific images as well less formal images (i.e. citizen science). A variety of cameras was used, including several generations of iPhones, Samsungs, a Nikon D3300 with 60mm Nikkor macro lens (Nikon, Japan) and a Canon EOS 1200D. This provided a wide variety of resolutions and DPI settings with an aim to achieve broad applicability.

To further supplement the dataset with images taken by non-scientists, images were downloaded from the online repository, iNaturalist. The download was limited to *Sphagnum* images from the United Kingdom to keep the number of entries manageable, and to images that were labelled by iNaturalist as 'Research' quality and on which the identification confidence was high (assigned as 'most agree' by the users of the platform). As the number of *Sphagnum* plants in an image was more valuable than a large number of images, a selection of 20 images from these images was used, which included approximately 9 species (790 total annotated plants), further supplementing the colour and shape diversity of the dataset, and they were taken from various distances and angles.

Lastly, images of non-*Sphagnum* objects were also obtained. These were largely peatland plants such as heather, *Molinia* grasses and a variety of bryophytes including common moss genera such as *Hypnum* and *Polytrichum*.

Table 6.1. Image collection data and numbers of annotations and species.
The images were collected at Cors Fochno, a raised bog in Mid Wales, Coed y Darren, a mixed woodland, Pen y Garn and Mid Wales, and from the online repository iNaturalist. Coed y Darren was the least diverse site, as it is dominated by a carpet of *S. quinquefarium*. This made the number of annotations per image for this site very high compared to the other sites. Although Pen y Garn and Mid Wales provided only 5 images, they made up the second largest amount of annotations. This was because these images were taken using the imaging frame, capturing a relatively large area. iNaturalist provided the most diversity, as species that were not locally available could be included. When combined, a total of 14 species was included in the dataset.

Image source	**Number of Images**	**Number of annotations**	**Number of species per area**
Pen y Garn and Mid Wales	5	1777	3
Cors Fochno	19	847	6
Coed y Darren	21	3725	1
iNaturalist	20	790	9
Total	65	7139	14

6.2.2 - Image annotation

To generate a training dataset, the *Sphagnum* capitula in 65 images were annotated using the VGG Image Annotator (VIA) software (Dutta and Zisserman, 2019). A portion of these, namely the images taken using the imaging rig, were automatically annotated by the Capitulum Counting pipeline (van de Koot et al., 2021). This provided a high-throughput base level of annotations of reasonable accuracy, and only required limited manual correction in VIA to reduce the numbers of false positives and negatives.

Annotation was limited to capitula that were clearly in focus, as the annotation of out of focus capitula would likely introduce too much noise at this early stage of development. Capitula that were occluded by leaf litter, grasses or other material were only annotated if the centre of the capitula was clearly visible and entire, as occlusion is known to confuse deep learning models (Pegoraro and Pflugfelder, 2020; Pflugfelder and Auer, 2021). Each annotation was centred on a capitulum and large enough to include the spreading branches. When all capitula were annotated in a given image, the coordinates and radiuses of the annotations were saved in a .csv format file with the same filename as the image.

6.2.3 - Model training and parameters, software etc.

YOLO v5 (You Only Look Once) (Jocher et al., 2022; Redmon et al., 2016) version YOLOv5l was used as the deep learning architecture to train the model. This architecture was developed by Redmon et al. for the purpose of object detection, and has been previously used in plant detection workflows (Chowdhury et al., 2022; Lyu et al., 2022; Xiong et al., 2022). YOLOv5l is one of 10 pretrained YOLOv5 models of varying computational complexity available from (https://github.com/ultralytics/yolov5), and is a relatively complex model, whilst maintaining fast detection speed.

The final data set for model training consisted of 65 images, of which 41 were in the training data set (4826 annotations). The remaining 24 images were divided into a validation set (16 images, 2088 annotations) and a testing set (8 images, 1034 annotations). The validation set is used by the model to evaluate its performance during training, whilst the testing set is used to evaluate the final model on unseen data. Data augmentation was applied using the Roboflow online platform (Alexandrova et al., 2015) to increase the number of images to 147. The augmentations used were flip and rotation, which were selected and applied randomly by the Roboflow platform.

Table 6.2. Number of images and annotations per annotation class.
The largest annotation class was MossT. As previously mentioned, these included most of the images from Pen y Garn and were taken from a relatively large distance, capturing a large number of plants per image. While the MossN, MossG and MossW classes were more equal in size, MossR was by far the smallest class, and included only a single image.

Class distribution	**Present in n images**	**Number of annotations (after augmentation)**	**Number of species per class**
MossN (iNaturalist)	35	1394	11
MossG (submerged green)	10	1429	4
MossW (bleaching and dry)	18	1016	1
MossT (Thumbnail and rig format)	11	3187	5
MossR (red)	1	113	1
Total	65	7139	14

While initially, all annotations were treated as a single category, the model performed better when the annotations were divided into 5 categories, which were labelled MossT, MossG, MossN, MossW and MossR (Figure 6.1, Table 6.2). This was because these represented discrete categories of images, and reduced the confusion for the model. MossT represented the images originally collected for the Capitulum Counter algorithm (van de Koot et al. 2021), which included the imaging rig and surrounding vegetation. MossG, MossW and MossR represented images of *Sphagnum* that were particularly green (G), white (W, as a result of bleaching or dryness) and red (R). MossN were the images downloaded from online repository iNaturalist, which were varied in their object distances, angles and backgrounds. A number of images from Cors Fochno were also included in the MossN category, as these were purposefully taken in a style similar to that of the iNaturalist photographs, which are more representative for how non-scientists would photograph *Sphagnum*.

Figure 6.1. Example images depicting the annotation classes used in model training. A. MossN images were largely obtained from online repository iNaturalist, and are generally taken from up-close and from a variety of angles. B. MossW images are wet, green plants that are not as defined in shape due to their proximity to the water table, which distorts typical capitulum morphology. C. MossT images were collected as part of the Capitulum Counter algorithm (van de Koot et al. 2021) which used the blue frame as size standard and to crop the image. These images are typically taken from a larger distance, which consequentially increases the number of plants in these images. D. MossW images are dry plants that have become a whiter shade due to their low water content. E. MossR was the smallest class, and contained small red plants such as S. capillifolium.

The model was trained for 269 training on the Google Colaboratory platform (https://colab.research.google.com/), utilising various types of cloud GPU's (Tesla T4, Tesla P100\V100, with 16GB VRAM). Data was resized into 1280*1280px

resolution, and a batch size of 16 was used. The trained model used the validation set during training to evaluate its performance, and finally evaluated its final version using the testing dataset. However, the MossR category was not represented in the testing set, as the quality of the images and annotations for this class in the training set were not sufficient.

6.2.4 - Model validation dataset

The accuracy of the model was tested using a dataset of 413 images and 9 videos, independently collected in Northern Ireland. These contained a wide range of colours, object distances and resolutions, ensuring the model was tested on a dataset that resembles the range of images that might collected by untrained personnel. These images included images of only *Sphagnum*; images of *S* variable amounts of other bryophytes, and images lacking *Sphagnum* or any bryophyte but containing shrubs, bare soil, other bryophyte species, landscapes or animals. These images were ordered into 3 distinct categories, namely images containing *Sphagnum* (242 images, 13 species), images containing 'other bryophytes' (59 images) and images containing 'non-moss' objects and organisms (112 images).

The resulting outputs (annotated images from the model) were evaluated manually for false positives, and false negatives using FIJI (https://fiji.sc/) with the cell counter plugin (Schindelin et al., 2012). While the 'other bryophytes' and 'non-moss' categories were evaluated in their entirety, the *Sphagnum* images were randomly sampled five times for five-fold validation. Of the total 242 *Sphagnum* images, 10% of the images were randomly selected five times, resulting in a final validation set of 94 images after duplicates were removed. These 94 images still included all 13 species, meaning the full range of *Sphagnum* colour and morphological variation was covered.

The false negative category was divided into two subcategories, namely 'true false negatives' and 'false negatives out of focus'. The latter category was added to account for the fact that within the images the model was trained on, only the *Sphagnum* capitula that were in focus were annotated, as out of focus or otherwise occluded capitula may confuse the model. Because the model used the 5 distinct label categories, and subsequently assigned one such category to each annotation, this could result in a single capitulum or non-moss object being annotated twice

albeit in different categories. When this was the case, these were regarded as the model being correct twice. However, it was also possible for the model to annotate a single non-*sphagnum* object twice using the same category, and these were therefore considered as the model being wrong twice.

$$\text{Precision} = \left(\frac{\text{Count} - \text{False positives}}{\text{Count}}\right)$$

$$\text{Recall} = \left(\frac{\text{Count} - \text{False positives}}{(\text{Count} - \text{False positives}) + \text{False negatives}}\right)$$

$$\text{F-measure} = \left(2 * \frac{\text{Precision} * \text{Recall}}{\text{Precision} + \text{Recall}}\right)$$

The model's capitula count and the manually scored false positives and false negatives were subsequently used to calculate precision, recall and F-measure (Tharwat, 2018; van de Koot et al., 2021). Recall and F-measure were calculated twice, once using only the in-focus false negatives and again using the in and out of focus false negatives combined. Additionally, as the model assigned one of the 5 moss categories to each annotation, these were extracted as well so the categories could be assessed for their impact on the quality scores of the model.
The 9 videos of *Sphagnum* colonies, which amounted to 3546 image frames, were also run through the model, but were not evaluated for quality.

6.3 - Results

6.3.1 - Model training

Using the images of annotated *Sphagnum* capitula, the model was trained to annotate capitula in images automatically. After 269 epochs of training, the resulting model had a precision of 0.72 and recall of 0.47, corresponding to an F-measure of 0.57 based on its evaluation using the validation set of 16 images (Supplementary Figure 6.1). On 8 images in the testing set, the mean precision, recall and F-measure were 0.61, 0.59 and 0.60 respectively when a threshold minimum of 0.3 confidence was used (Table 6.3). When the confidence threshold was increased to 0.5, the precision increased to 0.67 whilst the recall lowered to 0.44, resulting in an F-measure of 0.53. The mean average precision (mAP), which provides another weighted score combining precision and recall, as opposed to the unweighted F-measure, had values of 0.587 and 0.553 for the 0.3 and 0.5 confidence thresholds respectively.

Table 6.3. Performance values for the model on its testing set for confidence thresholds of 0.3 and 0.5.
Increasing the confidence threshold from 0.3 to 0.5 did not greatly reduce the F-measure and mAP. MossG performed most similarly to when all classes were combined, whilst MossN performed the worst. MossT was consistent independent of the confidence threshold, possibly because of the annotation size of this class.

Confidence 0.3					
Class	**N annotations**	**Precision**	**Recall**	**F-measure**	**mAP**
All	1034	0.607	0.594	0.600	0.587
MossG	212	0.512	0.623	0.562	0.535
MossN	277	0.399	0.426	0.412	0.381
MossT	393	0.793	0.606	0.687	0.700
MossW	152	0.724	0.724	0.724	0.733

Confidence 0.5					
Class	**N annotations**	**Precision**	**Recall**	**F-measure**	**mAP**
All	1034	0.674	0.440	0.532	0.553
MossG	212	0.632	0.316	0.421	0.481
MossN	277	0.453	0.397	0.423	0.390
MossT	393	0.793	0.606	0.687	0.700
MossW	152	0.817	0.441	0.573	0.643

The best performing classes were MossT and MossW, whilst the worst performing class was MossN. Although MossT was the largest class in the training set (Table 6.2), MossN and MossW were of similar, smaller size. However, as MossN represented all images from iNaturalist, it's possible that it contained too much variety in image characteristics, making it difficult for the model to find defining features.

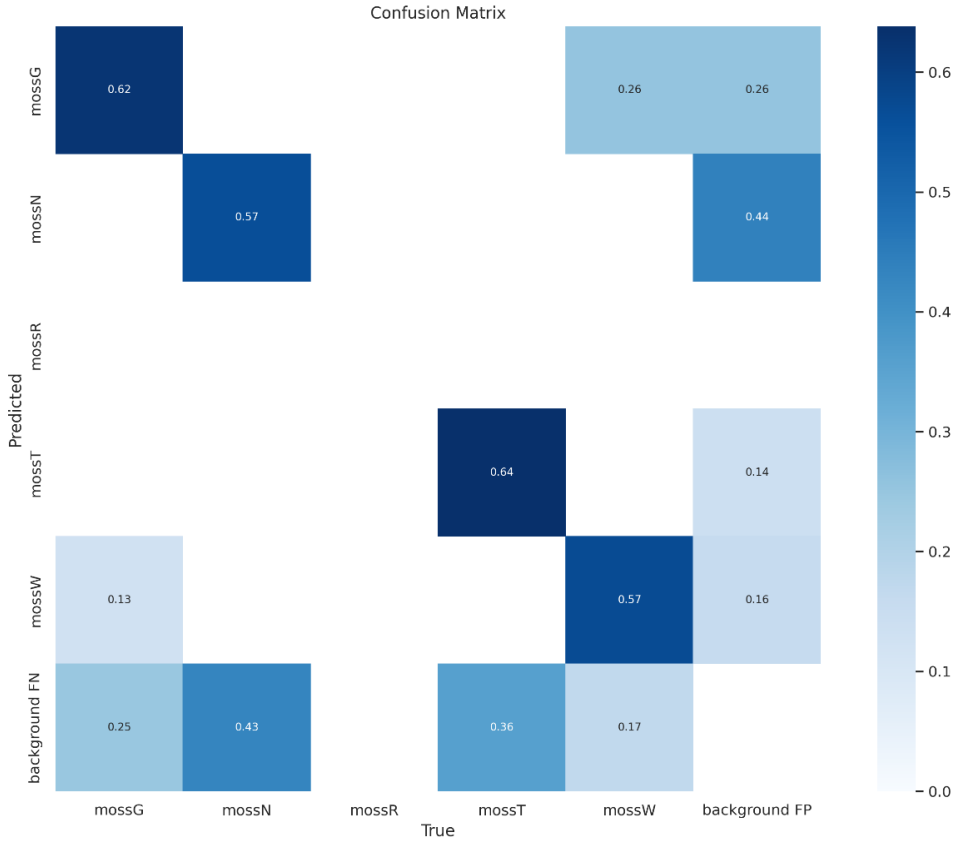

Figure 6.2. Confusion matrix indicating which classes were confused with each other by the model.
All classes performed well across the diagonal, meaning many predictions were accurate. However, the MossN and MossG classes were strongly confused by the background noise, resulting in false positives and false negatives.

This is further visible in the normalised confusion matrix (Figure 6.2), which compares the true annotations with the predicted annotations for each class. Higher values in the confusion matrix mean the model is likely to confuse the two classes, while lower values mean the model doesn't confuse the classes. In this matrix, MossN has the highest confusion with both the background false positives (FP) and false negatives (FN) classes. After MossN, MossT has the highest confusion with

background FN, indicating this class also misses a number of capitula. However, this class has the lowest confusion with background FP, meaning it rarely detects false positives, which was also apparent from its high precision (Table 6.3). Between capitulum classes, only MossG and MossW got confused occasionally by the model, which may be solved by increasing the amount of training data for these classes.

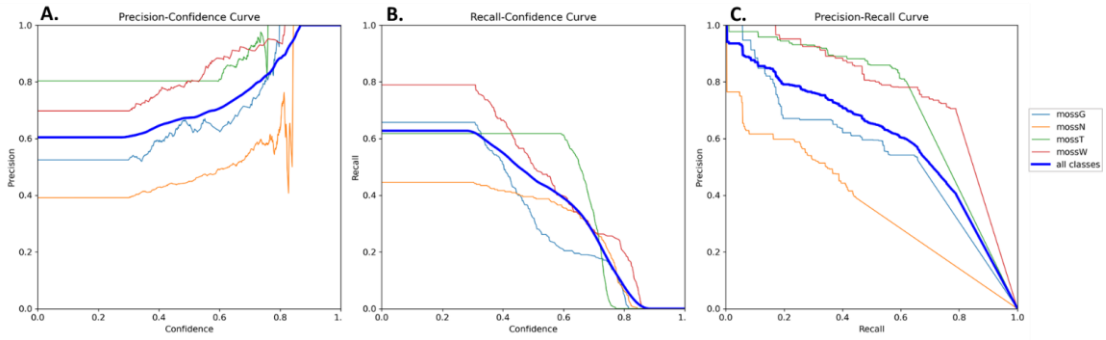

Figure 6.3. Change of the performance indicators precision and recall over increasing confidence thresholds.
A. Precision increased for each class rapidly with increasing confidence, as the number of false positives was reduced. However, recall (B) decreased below 0.5 at a confidence threshold of 0.5. C. In the precision-recall curve considering the trade-off between precision and recall for increasing confidence, MossN was the worst class whilst MossW and MossT had the largest area under the curve, indicating these classes were capable of retaining high recall with increasing precision confidence.

To evaluate the confidence of the model in its predictions, the precision and recall were plotted for each class with increasing confidence (Figure 6.3). As the confidence threshold increases, precision should increase as the model is more certain its predictions are true positives, whilst recall should decrease as there are more false negatives that the model isn't confident enough to annotate. The highest precision for all classes combined was reached at a confidence of 0.869, whilst recall started decreasing after a confidence threshold of 0.3. These two metrics were combined into a precision-recall curve, which shows the trade-off between precision and recall for different thresholds. As a larger area under the curve is desirable, which means precision and recall are both high, MossW and MossT were consistently the best performing classes. Again, MossN was shown to be the worst performing class.

The MossN class contained images collected from iNaturalist and images from Cors Fochno that were purposely taken to mimic iNaturalist photgraphs, which

comprise a larger variety of colours, distances to object, angles and other factors. However, as this class is most representative for how *Sphagnum* photos are typically taken, it was not excluded from the model. Instead, in future iterations, it could be more productive to either subdivide the class into different new categories or to merge the images into the existing categories.

6.3.2 - Model verification

To further evaluate the model, a larger dataset of images not before seen by the model was used. A total of 413 images of *Sphagnum*, other bryophytes and non-moss objects, collected in Northern Ireland, were analysed. The average processing speed of these images by the model was 0.05s per image. Of the 242 *Sphagnum* images, 94 were subsequently checked manually for false positives and negatives. The same was done for the 170 images of other bryophytes and non-moss objects. These images were purposefully taken from a wide range of distances and angles, to provide as much variation as possible.

The Irish *Sphagnum* images had very few false positives, resulting in a mean precision of 0.975 (Figure 6.4A). When out of focus capitula were not considered, recall was 0.732 (Figure 6.4B). When they were considered, recall was lowered to 0.583 (Supplementary Figure 6.2A). For F-measure, these values were 0.831 (Figure 6.4C) and 0.712 (Supplementary Figure 6.2B) for without and with out of focus capitula respectively. The lowest precision for these images, which was 0.713, was reached on an image of a very dense canopy consisting of *S. medium*, *S. capillifolium* and *S. papillosum*, which were also very difficult to discern manually. Recall however, was typically lower on images in which the object distance was relatively high, causing the plants to be smaller and to have less resolution than if they would have been imaged from up close. The image with the lowest recall (0.278), was an image of a dense patch of *S. papillosum* with a *Polytrichum* species growing in between. The capitula of *S. papillosum* were poorly defined in the image due to the high density, again making it difficult to discern by eye. The precision of this image was high however (0.8), and none of the false positives were *Polytrichum* species, meaning the model was capable of distinguishing this common bryophyte genus from *Sphagnum*.

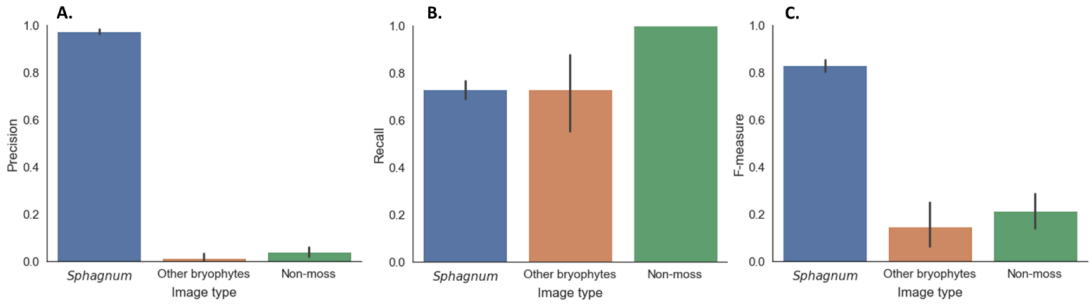

Figure 6.4. Precision, recall and F-measure for each of the image types in the Ireland dataset. A. Precision was very high for the *Sphagnum* images, indicating that there were very few false positives. For the other two image types however, precision was very low, usually 0 as there were no *Sphagnum* in the images. There were however a number of images in these classes that had a few stray *Sphagnum* plants, making the calculation of this variable possible.
B. Recall was a bit lower, suggesting the model was a bit too strict and missing some capitula as a result. As expected, this variable was 1 for the non-moss capitula, as there were no possible false negatives in those images.
C. The F-measure, which is the harmonic mean combining precision and recall, was 0.831 for the *Sphagnum* images. Considering the scores on the Ireland dataset, the model is exceeding the performance it indicated on the testing set (Table 6.2).

While the number of false positives on the *Sphagnum* images was very low, there were a lot of false positives in the images containing no *Sphagnum* (Supplementary Figure 6.3). These images had no false negatives with the exception of some of the images of other bryophytes where a low number of isolated *Sphagnum* plants were present. Images of other bryophytes had more false positives than images of non-moss material, with the highest number of false positives (423) on an image of an *Aulacomnium* sp. colony, which superficially resembled *Sphagnum* spreading branches (Supplementary Figure 6.4A). However, the third highest number of false positives was found on an image of a *Betula* sapling's leaves (Supplementary Figure 6.4B), which are only similar to *Sphagnum* in the sense that they are dispersed green circular areas. Whilst the *Aulacomnium* image was not selected for quality control, the *Betula* image was. This image had a recall of 1, as there were no possible false negatives given the lack of *Sphagnum* in the image. Precision and F-measure were very low (both <0.05), as all found positives were false positives.

Of the five classes, MossN was the biggest annotation class within the images, whilst MossG was the cause of most false positives on the other two types of images (Figure 6.5), accounting for over 80% of false positive annotations. This class

was designed for wet green plants close to the water table, which may lack much of the typical Sphagnum morphological characteristics. While MossR was still used in the model, no annotations were detected of this class. However, red-pigmented *Sphagnum* plants for which MossR was intended were still found. This suggests that MossR is unnecessary as separate class, as its target plant type is covered by the other classes. Ultimately, the model was capable of detecting *Sphagnum* plants of any colour and at varying distances. Performance was best when the plants in an image were captured in sufficient resolution and provided the model with enough detail to be able to discern them as individuals.

This was further indicated when the number of annotations per image was compared with the mean annotation size per image. Using the number of plants per image as proxy for object distance (as more plants fit in an image taken from a greater distance), as well as the mean annotation size within the image as a proxy for plant size in the image, it was clear that images with many annotations and a smaller mean annotation size generally had more false negatives (Supplementary Figure 6.5).

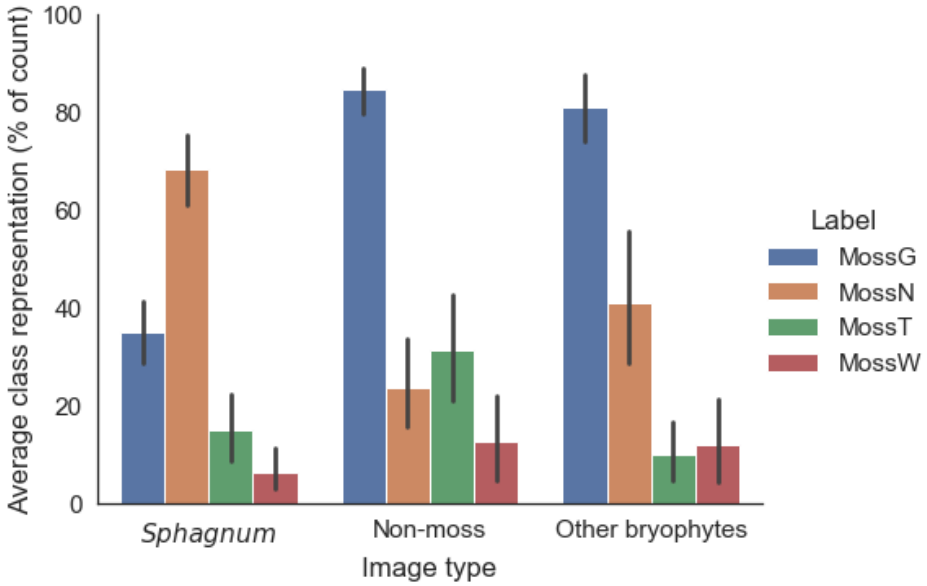

Figure 6.5. Percentual class representation within the Ireland dataset image types. MossN was by far the most common annotation class for *Sphagnum* images, despite this being the worst class in the original testing set. This class was intended to capture images taken at a wide range of distances and angles, which perhaps made it more capable of generalising. MossG was responsible for over 80% of false positives on non-moss and other bryophyte images, suggesting this class is very susceptible to noise.

6.4 - Discussion

In this paper we provide the basis for a deep learning *Sphagnum* detection model. This model built upon the concept and foundation provided by the Capitulum Counter algorithm (van de Koot et al., 2021), which relied upon traditional computer vision but was prone to false positives and negatives. The newly developed model achieves consistently high precision scores whilst maintaining good recall irrespective of image type or *Sphagnum* species. Also, it is no longer dependent on the imaging frame used previously, although a frame or other reference object could be added if required. This makes the model free to fit a wider range of experimental designs, and as it is a deep learning model it can be further trained with new kinds of images when required.

6.4.1 - Model training results versus independent verification

The model achieved a relatively low precision, recall and F-measure on its initial testing dataset (Table 6.3) when compared with the results ultimately achieved on the larger, independent Ireland verification dataset (Figure 6.4). On the original testing dataset, an F-measure of 0.6 was the highest attained when all classes were combined, whilst the Ireland dataset reached an F-measure of 0.831. This could be explained by the types of images used in the training and model's own testing set. Although the training dataset had a very large number of annotations (7139), the number of images in the testing dataset was limited, reducing the variability (8 images, 1034 annotations).

Especially the MossR class, which had the smallest amount of training data, was not detected in any of the Ireland images. This class was conceived to classify the dense canopies of red pigmented *Sphagnum* species such as *S. capillifolium* and *S. medium*, but capitula of these species were instead detected by the other classes. While this could be explained by a data deficiency for this class, as it was the smallest class in the training dataset, the fact that the plants for which the class was intended were still detected suggests that this class may simply be removed from future iterations, as the capitula it was intended to detect were detected by the other classes anyway.

The MossN class was the worst performing class during model training (Figure 6.3). This class contained all the images collected from iNaturalist,

irrespective of their visual content. While the other classes were more defined, the iNaturalist images were very variable in species, plant number, colour, distance and angle. Conversely, this made the MossN class more suitable for the images collected in the Ireland dataset, where it was the most prevalent class (Figure 6.5), suggesting it's a very generalised class. Given the high precision, recall and F-measure of this dataset, the model's own evaluation of MossN appears to underestimate the detection quality of this class, where it had the lowest precision and recall of all classes (Figure 6.3). However, this shows the value of using an independent dataset, not used in creating the model, to separately evaluate model performance.

6.4.2 - False positives and negatives

Although deep learning models are 'black boxes', in which the exact operations are unclear, some insight into their decision making can be deduced from the false positives and negatives. When an image included *Sphagnum*, there were typically very few false positives (Figure 6.6A). However, when there was no *Sphagnum* in the image, there could be a large number of false positives and especially so when the objects in the image looked vaguely like *Sphagnum* capitula (Figure 6.6B). This gives an insight into the characteristics used by the model for detection. As previously mentioned, the largest number of false positives were found on an 'other bryophyte' image of *Aulacomnium palustre* and a 'non-moss' image of *Betula* sp. (Supplementary Figure 6.4).

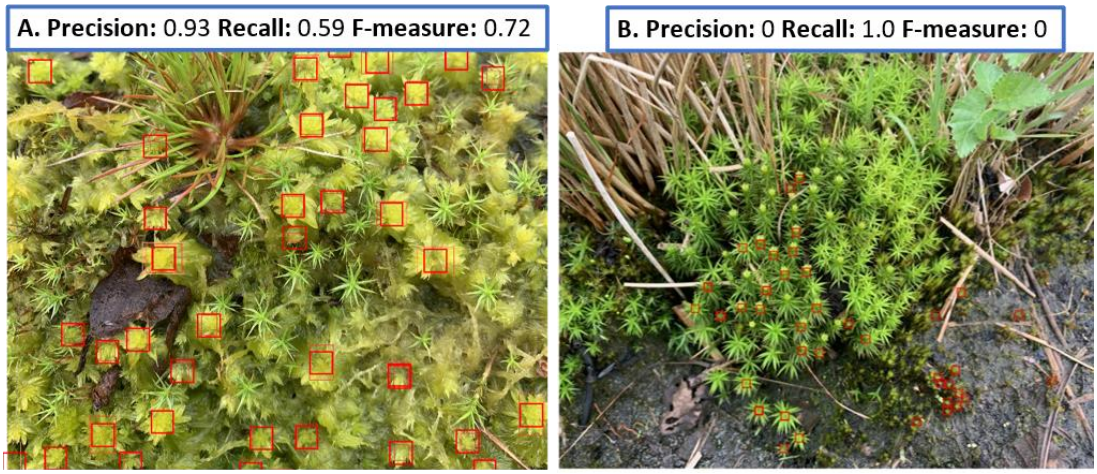

Figure 6.6. Detections by the model on *Sphagnum* and *Polytrichum*
A. When there was *Sphagnum* in an image, the model would only rarely mistake other bryophytes for *Sphagnum* as a false positive.
B. However, when there was no *Sphagnum* in an image, the model would falsely annotate other bryophytes such as *Polytrichum commune* more frequently.

Aulacomnium palustre plants may resemble *Sphagnum* spreading branches superficially, as they consist anatomically of a single stem with concave leaflets and may grow in dense colonies and may be why they are identified by the model as Sphagnum (Supplementary Figure 6.4). Other mosses in the dataset included *Polytrichum* species. Interestingly, when *Polytrichum commune* was in an image without *Sphagnum*, it was often detected as a false positive (Figure 6.6B), whilst *Polytrichum* growing in between a *Sphagnum* colony would not be detected (Figure 6.6A). This suggests that a large number of the false positives may simply be signals that would otherwise be considered noise, but are then strong enough to be detected as there is no *Sphagnum* signal. As most false positives were detected by the MossG class, colour may be the main deciding factor. The images in this class that were used in the training set were wet, green plants that typically did not have the defined *Sphagnum* shape. This could lead the model to focus on colour for this class rather than other structural or morphological characteristics, making it more susceptible to false positives on green non-*Sphagnum* objects. However, this may be avoided by increasing the variety of images in this category.

The *Betula* image, however, does not resemble *Sphagnum* anatomically at all. One interpretation for the relatively large number of false positives on this image is that there are dispersed green patches on a brownish background, which may resemble *Sphagnum* plants against a leaf litter background. This suggests colour is an

important decision component for the model, although when plants of similar colour to *Sphagnum* are included in an image with *Sphagnum*, other decision components are capable of distinguishing *Sphagnum* from other plants such as *Polytrichum*.

6.4.3 - Deep learning model versus Capitulum Counter algorithm

Compared with the Capitulum Counter algorithm, the deep learning model achieved a higher F-measure (0.83) on a larger variability of images. The capitulum counter also produced a high mean F-measure (0.77) but was limited to images taken using the frame. The model is no longer constrained by the requirement for an imaging frame and the white balance step that was included to provide an internal standard between images taken in different lighting conditions is no longer included.

The main increase in F-measure from the capitulum counter algorithm to the deep learning model is driven by the increase in precision. As the capitulum counter used the Blob DoG function of the scikit-image package (Van Der Walt et al., 2014) to find capitula based on contrast, this results in relatively large numbers of false positives. This method relied on adequate masking of non-*Sphagnum* objects in an image to prevent the model from falsely detecting those. This made detection of darker, non-green *Sphagnum* species more difficult, as these occupied a similar colour range to the background noise. However, this also increases the recall as there were fewer false negatives. While the deep learning model had more false negatives as its more discriminatory than the Blob DoG function, it had a consistently high precision and was much more capable of finding non-green *Sphagnum* species, as the model was not limited to using only edge detection. Furthermore, the problem of the model having more false negatives can simply be overcome by adding more data covering the capitula that were currently not annotated to train the model to recognise these in the future. The best way to do this would be to manually annotate the images with low recall from the testing or validation sets and to include those in the training set, a process known as ‘active learning’, covering the data deficiency (Chandra et al., 2020; Kumar et al., 2019; Rawat et al., 2022).

As the new model is more generalised and adaptable, it could potentially function on most experimental setups with minimal effort, whilst modification of the Capitulum Counter was more image format specific. This also applies to the measurement of colony density, which the Capitulum Counter was designed for and

was initially the reason for the defined image area. As the output of the deep learning model is also the number of plants and the spatial coordinates of the plants in the image, the functional data extraction remains the same and can be used provided a size measurement corresponding to the image is taken. Furthermore, an additional step can be added that plots the annotations as a heatmap on the image. This intuitively shows the densest areas of a *Sphagnum* colony in the image (Figure 6.7).

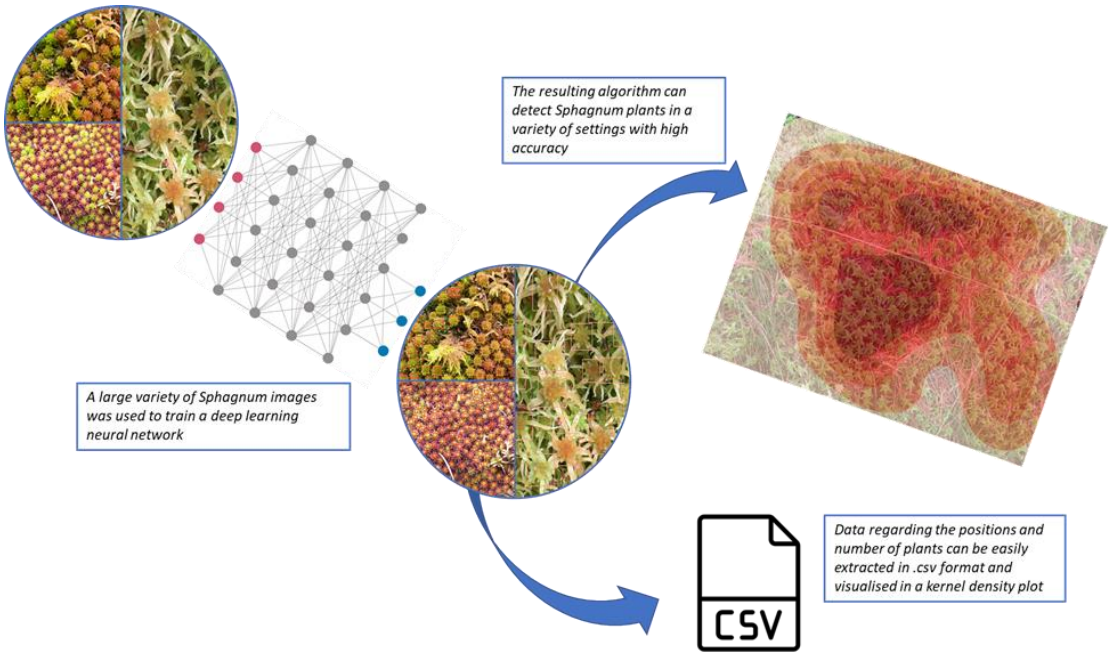

Figure 6.7. Graphic representation of the deep learning model and its potential outputs. The model is compatible with a wide range of *Sphagnum* images, performing well on a variety of colours, shapes, object distances and angles. The data output is presented in a .csv file format containing the number, positions and sizes of the annotations placed on the capitula. Additionally, a heatmap can be generated that intuitively shows the densest areas in a *Sphagnum* colony.

6.4.4 - Potential improvements and further exploitation

One of the main drawbacks of the new model is the lack of a white balance correction step, which would make colour data between images more comparable. This problem may be overcome by the inclusion of a colour card, which can then be annotated and integrated in the model training. When the model is capable of correcting subtle colour differences caused by lighting, colour data may be used for the quantification of biological variables such as water content.

As the model currently has high precision and rarely detects false positives, it can distinguish *Sphagnum* from other vegetation with a high degree of success. However, the inclusion of other vegetation in the data may provide the model with more distinguishing characteristics that could further improve performance as what was otherwise noise becomes more defined. Furthermore, this could provide interesting new insights into plant communities growing amongst *Sphagnum*, as high throughput data collection is facilitated.

In the research presented here we provide a model capable of high throughput *Sphagnum* capitula detection. This is a highly accurate model that can be further developed to overcome its current limitations and may serve as a tool for peatland scientists and conservationists to optimise current workflows that would otherwise require manual measurement by trained professionals. Its general applicability and functionality with video files means that it may be adapted to fit a range of experimental designs, such as low-altitude drones or citizen science moss photo collection, allowing for the advent of high throughput *Sphagnum* image data collection.

6.5 - References

Alexandrova, S., Tatlock, Z., Cakmak, M., 2015. RoboFlow: A flow-based visual programming language for mobile manipulation tasks. Proc. - IEEE Int. Conf. Robot. Autom. 2015-June, 5537–5544. https://doi.org/10.1109/ICRA.2015.7139973

Caporn, S.J.M., Rosenburgh, A.E., Keightley, A.T., Hinde, S.L., Riggs, J.L., And Buckler, M., 2018. Sphagnum restoration on degraded blanket and raised bogs in the UK using micropropagated source material: a review of progress. Mires Peat 20, 1–17. https://doi.org/10.19189/MaP.2017.OMB.306

Chandra, A.L., Desai, S.V., Balasubramanian, V.N., Ninomiya, S., Guo, W., 2020. Active learning with point supervision for cost-effective panicle detection in cereal crops. Plant Methods 16, 1–16. https://doi.org/10.1186/s13007-020-00575-8

Chowdhury, P.N., Shivakumara, P., Nandanwar, L., Samiron, F., Pal, U., Lu, T., 2022. Oil palm tree counting in drone images. Pattern Recognit. Lett. 153, 1–9. https://doi.org/10.1016/j.patrec.2021.11.016

Clymo, R.S., 1973. The Growth of Sphagnum: Some Effects of Environment. J. Ecol. 61, 849. https://doi.org/10.2307/2258654

Clymo, R.S., Hayward, P.M., 1982. The Ecology of Sphagnum, in: Bryophyte Ecology. Springer Netherlands, Dordrecht, pp. 229–289. https://doi.org/10.1007/978-94-009-5891-3_8

Dutta, A., Zisserman, A., 2019. The VIA Annotation Software for Images, Audio and Video. MM 2019 - Proc. 27th ACM Int. Conf. Multimed. 2276–2279. https://doi.org/10.1145/3343031.3350535

Fahlgren, N., Feldman, M., Gehan, M.A., Wilson, M.S., Shyu, C., Bryant, D.W., Hill, S.T., McEntee, C.J., Warnasooriya, S.N., Kumar, I., Ficor, T., Turnipseed, S., Gilbert, K.B., Brutnell, T.P., Carrington, J.C., Mockler, T.C., Baxter, I., 2015. A versatile phenotyping system and analytics platform reveals diverse temporal responses to water availability in Setaria. Mol. Plant 8, 1520–1535. https://doi.org/10.1016/j.molp.2015.06.005

Gauthier, T.J., Elliott, J.B., Mccarter, C.P.R., Price, J.S., 2022. Field-scale compression of Sphagnum moss to improve water retention in a restored bog. J. Hydrol. 612, 128160. https://doi.org/10.1016/j.jhydrol.2022.128160

Hájek, T., Vicherová, E., 2014. Desiccation tolerance of Sphagnum revisited: a puzzle resolved. Plant Biol. 16, 665–773. https://doi.org/10.1111/plb.12126

Hinde, S., Rosenburgh, A., Wright, N., Buckler, M., Caporn, S., 2010. Sphagnum re-introduction project : A report on research into the re-introduction of Sphagnum mosses to degraded moorland. Moors Futur. Rep. 31.

Hüther, P., Schandry, N., Jandrasits, K., Bezrukov, I., Becker, C., 2020. ARADEEPOPSIS, an automated workflow for top-view plant phenomics using semantic segmentation of leaf States. Plant Cell 32, 3674–3688. https://doi.org/10.1105/tpc.20.00318

Jocher, G., Chaurasia, A., Stoken, A., Borovec, J., NanoCode012, Kwon, Y., TaoXie, Michael, K., Fang, J., Imyhxy, Lorna, Wong, C., Yifu, Z., V, A., Montes, D., Wang, Z., Fati, C., Nadar, J., Laughing, UnglvKitDe, Tkianai, YxNONG, Skalski, P., Hogan, A., Strobel, M., Jain, M., Mammana, L., Xylieong, 2022. ultralytics/yolov5: v6.2 - YOLOv5 Classification Models, Apple M1, Reproducibility, ClearML and Deci.ai integrations. https://doi.org/10.5281/zenodo.7002879

Katoh, M., Gougeon, F.A., 2012. Improving the precision of tree counting by combining tree detection with crown delineation and classification on homogeneity guided smoothed high resolution (50 cm) multispectral airborne digital data. Remote Sens. 4, 1411–1424. https://doi.org/10.3390/rs4051411

Kumar, S., Luo, W., Kantor, G., Sycara, K., 2019. Active learning with Gaussian processes for High Throughput Phenotyping. Proc. Int. Jt. Conf. Auton. Agents Multiagent Syst. AAMAS 4, 2078–2080.

Leifeld, J., Menichetti, L., 2018. The underappreciated potential of peatlands in global climate change mitigation strategies. Nat. Commun. 9, 1–7. https://doi.org/10.1038/s41467-018-03406-6

Li, L., Zhang, Q., Huang, D., 2014. A review of imaging techniques for plant phenotyping. Sensors 14, 20078–20111. https://doi.org/10.3390/s141120078

Loisel, J., Gallego-Sala, A. V., Amesbury, M.J., Magnan, G., Anshari, G., Beilman, D.W., Benavides, J.C., Blewett, J., Camill, P., Charman, D.J., Chawchai, S., Hedgpeth, A., Kleinen, T., Korhola, A., Large, D., Mansilla, C.A., Müller, J., van Bellen, S., West, J.B., Yu, Z., Bubier, J.L., Garneau, M., Moore, T., Sannel, A.B.K., Page, S., Väliranta, M., Bechtold, M., Brovkin, V., Cole, L.E.S., Chanton, J.P., Christensen, T.R., Davies, M.A., De Vleeschouwer, F., Finkelstein, S.A., Frolking, S., Gałka, M., Gandois, L., Girkin, N., Harris, L.I., Heinemeyer, A., Hoyt, A.M., Jones, M.C., Joos, F., Juutinen, S., Kaiser, K., Lacourse, T., Lamentowicz, M., Larmola, T., Leifeld, J., Lohila, A., Milner, A.M., Minkkinen, K., Moss, P., Naafs, B.D.A., Nichols, J., O'Donnell, J., Payne, R., Philben, M., Piilo, S., Quillet, A., Ratnayake, A.S., Roland, T.P., Sjögersten, S., Sonnentag, O., Swindles, G.T., Swinnen, W., Talbot, J., Treat, C., Valach, A.C., Wu, J., 2021. Expert assessment of future vulnerability of the global peatland carbon sink. Nat. Clim. Chang. 11, 70–77. https://doi.org/10.1038/s41558-020-00944-0

Lyu, S., Li, R., Zhao, Y., Li, Z., Fan, R., Liu, S., 2022. Green Citrus Detection and Counting in Orchards Based on YOLOv5-CS and AI Edge System. Sensors 22, 1–20. https://doi.org/10.3390/s22020576

Page, S.E., Baird, A.J., 2016. Peatlands and Global Change: Response and Resilience. Annu. Rev. Environ. Resour. 41, 35–57. https://doi.org/10.1146/annurev-environ-110615-085520

Pegoraro, J., Pflugfelder, R., 2020. The Problem of Fragmented Occlusion in Object Detection. arXiv:2004.13076 2004.13076, 2–5.

Pflugfelder, R., Auer, J., 2021. Person Localisation under Fragmented Occlusion*. AVSS 2021 - 17th IEEE Int. Conf. Adv. Video Signal-Based Surveill. 1–8. https://doi.org/10.1109/AVSS52988.2021.9663791

Rastogi, A., Antala, M., Gąbka, M., Rosadziński, S., Stróżecki, M., Brestic, M., Juszczak, R., 2020. Impact of warming and reduced precipitation on morphology and chlorophyll concentration in peat mosses (Sphagnum angustifolium and S. fallax). Sci. Rep. 10. https://doi.org/10.1038/s41598-020-65032-x

Rawat, S., Chandra, A.L., Desai, S.V., Balasubramanian, V.N., Ninomiya, S., Guo, W., 2022. How Useful Is Image-Based Active Learning for Plant Organ Segmentation? Plant Phenomics 2022. https://doi.org/10.34133/2022/9795275

Redmon, J., Divvala, S., Girshick, R., Farhadi, A., 2016. You only look once: Unified, real-time object detection. Proc. IEEE Comput. Soc. Conf. Comput. Vis. Pattern Recognit. 2016-Decem, 779–788. https://doi.org/10.1109/CVPR.2016.91

Robb, C., Hardy, A., Doonan, J.H., Brook, J., 2020. Semi-Automated Field Plot Segmentation From UAS Imagery for Experimental Agriculture. Front. Plant Sci. 11, 1–13. https://doi.org/10.3389/fpls.2020.591886

Sánchez-Sastre, L.F., Alte da Veiga, N.M.S., Ruiz-Potosme, N.M., Carrión-Prieto, P., Marcos-Robles, J.L., Navas-Gracia, L.M., Martín-Ramos, P., 2020. Assessment of RGB Vegetation Indices to Estimate Chlorophyll Content in Sugar Beet Leaves in the Final Cultivation Stage. AgriEngineering 2, 128–149. https://doi.org/10.3390/agriengineering2010009

Schindelin, J., Arganda-Carreras, I., Frise, E., Kaynig, V., Longair, M., Pietzsch, T., Preibisch, S., Rueden, C., Saalfeld, S., Schmid, B., Tinevez, J.Y., White, D.J., Hartenstein, V., Eliceiri, K., Tomancak, P., Cardona, A., 2012. Fiji: An open-source platform for biological-image analysis. Nat. Methods. https://doi.org/10.1038/nmeth.2019

Silvola, J., Aaltonen, H., 1984. Water content and photosynthesis in the peat mosses Sphagnum fuscum and S . angustifolium. Ann. Bot. Fenn. 21, 1–6.

Tharwat, A., 2018. Classification assessment methods. Appl. Comput. Informatics. https://doi.org/10.1016/j.aci.2018.08.003

van de Koot, W.Q.M., van Vliet, L.J.J., Chen, W., Doonan, J.H., Nibau, C., 2021. Development of an image analysis pipeline to estimate Sphagnum colony density in the field. Plants 10, 1–17. https://doi.org/10.3390/plants10050840

Van Der Walt, S., Schönberger, J.L., Nunez-Iglesias, J., Boulogne, F., Warner, J.D., Yager, N., Gouillart, E., Yu, T., 2014. Scikit-image: Image processing in python. PeerJ 2014, 1–18. https://doi.org/10.7717/peerj.453

Vitt, D.H., Crandall-Stotler, B., Wood, A., 2014. Bryophytes: Survival in a dry world through tolerance and avoidance. Plant Ecol. Evol. Harsh Environ. 267–295.

Wenhua Mao, Yiming Wang, Yueqing Wang, 2013. Real-time Detection of Between-row Weeds Using Machine Vision 0300. https://doi.org/10.13031/2013.15381

Xiong, Y., Zeng, X., Chen, Y., Liao, J., Lai, W., Zhu, M., 2022. An Approach to Detecting and Mapping Individual Fruit Trees Integrated YOLOv5 with UAV Remote Sensing. https://doi.org/10.20944/preprints202204.0007.v2

CHAPTER 7 – GENERAL DISCUSSION

7.1 – Background, aims and research objectives

Sphagnum peatmosses are increasingly been recognised for their important role in the peatland ecosystems where they are present. Through their effect on water table fluctuations and acidifying properties, they slow the decay of dead organic matter and promote carbon sequestration through peat formation (Kooijman and Bakker, 1994; van Breemen, 1995).

The extraction of peat, considered a valuable natural resource, has damaged many northern peatlands which has affected the carbon sequestration capacity of these ecosystems. As such, there is a growing interest in peatland restoration projects (Caporn et al., 2018; Gewin, 2020; González et al., 2014; Hinde et al., 2010; Shuttleworth et al., 2019). Such projects generally aim to restore the hydrological function of the peatland, either through manually transplanting *Sphagnum* plants onto damaged areas or by rewetting the environment, and to ultimately restore the ecosystem's functioning as a carbon sink.

Restored peatlands provide more tangible benefits in the fight against global climate change, other than carbon sequestration, for their surrounding areas. This ecosystem has a unique biodiversity for many plant, mocrobial and animal species (Muster et al., 2015), while also mitigating flooding after heavy rain (Gauthier et al., 2022; Shuttleworth et al., 2019).

However, due to changing precipitation patterns, peatlands face increasing pressure from drought periods. This also goes for the *Sphagnum* plants, which are less desiccation tolerant than most bryophytes. Instead, *Sphagnum* relies on desiccation avoidance mechanisms to reduce its vulnerability to drought periods. Such mechanisms include structural adaptations for water retention (Clymo and Hayward, 1982; Kremer and Drinnan, 2004; Ligrone and Duckett, 1998), colony growth (Elumeeva et al., 2011) to limit area exposed to airflow, as well as molecular pathways for desiccation tolerance (Nibau et al., 2022; Winnicka and Melosik, 2019).

With the vulnerability of *Sphagnum* plants and peatlands to desiccation in mind, the aim of this thesis was to provide novel insights into *Sphagnum*'s desiccation responsive mechanisms, and to develop novel monitoring methodologies.

With these aims in mind, the following research objectives were achieved:

- To elucidate the molecular response of *Sphagnum* to desiccation events.
- To understand how colony density affects water content dynamics.
- To assess how the relative humidity-induced desiccation affects individual plants.
- To develop image-based tools for the measurement of *Sphagnum* colony variables in the field.
- To establish the relationship between image-based measurement techniques and measured plant traits.

Combined, these research objectives provide an understanding of *Sphagnum*'s conserved molecular responses, their sensitivity to changes in humidity and the role of colony traits for water retention. Furthermore, new measurement techniques were developed that capitalised on the ubiquity of (smartphone) cameras and the recent increase in accessibility of cutting-edge deep learning architectures.

7.2 – Conserved molecular responses to desiccation

The evolution of mechanisms to maintain internal water potential were essential to enable transition from aquatic environments to the land. Eventually, this struggle for water utilisation and retention would give rise to innovations such as vascular bundles, cuticles and roots, traits that most vascular plants share today. However, it is believed that early land plants probably evolved complex signalling pathways that provided a molecular response to desiccation before the evolution of such structures (Cuming, 2019). Many bryophytes, lacking mechanical water retention and internal water transportation, rely on molecular mechanisms to provide cellular protection against desiccation (Charron and Quatrano, 2009; Proctor et al., 2007).

Sphagnum, traditionally considered to be a desiccation intolerant moss, has recently become a focal point in research for its importance in peatland ecosystems. Although this genus has developed specialised water uptake mechanisms in the form of hyaline cells, their photosynthetic capacity and physiology is negatively affected by prolonged water deficiency (Hájek and Vicherová, 2014; Kangas et al., 2014).

However, the data presented in this thesis show that, despite *Sphagnum*'s desiccation intolerance, the genus has conserved molecular responses homologous to those of many other plants, namely the abscisic acid (ABA) pathway (Nibau et al., 2022). ABA is hypothesised to have originated as a stress hormone to enable the signalling and activation of drought and desiccation stress mechanisms and has also been found in the desiccation tolerant mosses *Funaria* and *P. patens* (Guillory and Bonhomme, 2021; Knight et al., 1995; Sun et al., 2020; Werner et al., 1991). Endogenous ABA concentrations within *Sphagnum* tissues were found to increase when subjected to desiccation. These concentrations remained elevated for some time after re-watering, possibly keeping the desiccation response mechanism primed in anticipation of a second desiccation event, although gene expression decreased. Furthermore, desiccation tolerance was inducible by pre-treating the plants with ABA, improving the recovery of photosynthetic capacity after desiccation.

The ABI3 gene in *Sphagnum* was found to be homologous to those of *Physcomitrium patens*, and could functionally replace *P. patens*' own ABI3 gene in mutants lacking the original. Furthermore, the ABI3gene family was much more diversified than that of *A. thaliana*, with 5 variants found in *S. fallax* compared to only one in *Arabidopsis*. This further suggests that while bryophytes are lacking in

structural adaptations to cope with water loss, they may have more diverse molecular responses than some higher plants.

Understanding the molecular mechanisms underpinning *Sphagnum*'s desiccation responses is essential for the modelling of peatland responses to changing climate patterns, especially precipitation, as well as provide a new insights into the evolution of land plants and gene function adaptation.

7.3 – The importance of colony structure

The importance of colony density has been only passingly mentioned in *Sphagnum* research. Many words have been used to describe types of *Sphagnum* colony growth which imply a structure or density, such as lawn, mat, hummock or tussock. Typically a distinction is made between hummock and hollow species, of which the traditional view is that hummock associated species store large quantities of water as drought avoidance strategy. However, in this thesis, colony density was found to differ within species between habitats. Furthermore, all the species used in the experiments were capable of storing larger quantities of water when forced into a dense hummock-type colony arrangement, suggesting the traditional hummock – hollow distinction does not reflect species specific water retention capacities. Microclimatic conditions of the growth site might be equally or more important in explaining variation in colony density than artificial ecotype groupings (Elumeeva et al., 2011). In drier habitats, for example, a denser colony might be advantageous as this would reduce the area of individual plants exposed to airflow by reducing surface roughness (Rice, 2012), while in wetter habitats colony density may be unimportant such as in pools and pond margins where water loss can easily be replenished.

The results presented here support this hypothesis, and show that higher plant densities are capable of holding larger quantities of water per gram tissue. This is an advantage for plants in desiccation prone areas, as it slows the effect of desiccation and allows the plants to recover quicker afterwards. This extra water content is likely stored in the capillary spaces between branches, leaflets and stems between adjacent plants, as it has been shown previously that up to 90% of all *Sphagnum* water weight is stored externally (Clymo and Hayward, 1982).

In the context of restoration projects, this shows that "more is better" when it comes to transplanting *Sphagnum* plugs or colonies onto new environments. Even a mild regime of 95% relative humidity diminished the Fv/Fm values of individual plants when outside the protection of a colony after just five days, and recovery after even a short period of desiccation limited the photosynthetic capacity of a low density colony.

Thus I provide the first evidence of the functional importance of colony structure in *Sphagnum* and, when combined with the newly developed image

analysis workflows described in the following sections, could allow conservationists and peatland scientists to further incorporate this variable into their studies.

7.4 – Development of desiccation quantification measurements

Although *Sphagnum* mosses have retained molecular responses to drought that are found in other bryophytes (Nibau et al., 2022; Winnicka and Melosik, 2019), they are unable to fully revive after severe desiccation suggesting loss of some physiological functions. As described above, these mosses are instead desiccation avoidant. Their large water holding capacity, which can exceed 20 times their dry biomass and in part enabled by their hyaline cells , allows them to endure for prolonged periods without precipitation. The challenge is quantifying this desiccation and its effect on *Sphagnum*.

Despite the increase in popularity of peatland research, field based measurements on peatlands and *Sphagnum* involve mostly manual measurements, taken by experts and volunteers. While some areas of plant science focussed on crops and model organisms are becoming increasingly automated, little has been done to translate these approaches to peatland science. Remote sensing and high throughput phenotyping are increasingly able to replace the majority of otherwise invasive or destructive measurements, whilst also providing high data throughput and a reduction of manual labour (Gitelson et al., 2006; Hüther et al., 2020; Xue and Su, 2017).

7.4.1 – Automated measurement of colony density

One of the main challenges of translating the colour-based measurements to the field was the noise caused by the other plants growing amongst *Sphagnum*. The Capitulum Counter algorithm, as described in chapter 4, was initially conceived as a way to extract the image data from just the capitula, excluding most noise (van de Koot et al., 2021). While this method improved the data extraction from images, it also allowed for the measurement of colony density.

Colony density as variable is labour intensive to measure. Few studies have used it previously (Bengtsson et al., 2016), despite being referenced regularly and used indirectly in the form of the hummock-hollow gradient (Borkenhagen and Cooper, 2018; Hájek and Vicherová, 2014; Johnson and Shaw, 2015; Schipperges and Rydin, 1998). This distinction typically refers to hummocks as dense, elevated colonies above the water table, and hollows as species occupying pools or other areas closer to the water table without much colony structure. By developing a high-

throughput tool to measure colony density, the importance and plasticity of this variable could be elucidated.

Functionally similar methodologies had been developed for trees, whose canopy structure is analogous to that of *Sphagnum* (Abdollahnejad et al., 2017). The first iteration of the algorithm used a computer vision approach for edge detection, using the contrast between capitulum and background to detect the plants. Using this method, the density of several *Sphagnum* species was measured in the field and was found to differ between species, but also within species between habitats.
However, the computer vision-based approach had several weaknesses. Firstly, to use without modification, a blue frame and colour card is essential. While the blue frame provided a direct size measurement, ensuring comparability between images, it limited the user friendliness of the method. Secondly, the edge detection algorithm followed purely mathematical logic to find capitula, which made it relatively prone to false positives.

To improve and build upon the capitulum counter, a more accurate deep learning model was developed that was free of the constraints of the blue frame, and can be further trained and adapted to any desired experimental setup, and can even be used for detection on video files.

7.4.2 – Colour based measurement of capitulum water content

The development of new, image-based quantification techniques has been facilitated by smartphones. As their cameras now provide excellent image quality, these provide the opportunity for new avenues of peatland data extraction. Image based techniques these techniques have been developed and used on plant phenotyping platforms and satellite imagery (Robb et al., 2020; Sánchez-Sastre et al., 2020; Xue and Su, 2017), but their use on bryophytes has been limited (Harris et al., 2006; Malenovsky et al., 2013; Robinson et al., 2018). Bryophytes have a long history of usage to quantify environmental variables, a practice known as biomonitoring, and *Sphagnum* provides an opportunity to monitor water availability. The colour change that plants undergo when water content is reduced was shown to be measurable using both RGB and multispectral imaging techniques. Surprisingly, the RGB camera images generally performed as well or better than the (more specialised) multispectral images.

Although the strength of the relationship between RGB image values and capitulum water content in the field was not as strong as in a glasshouse setting, further parametrisation on, for example, single plots over time, could provide a new robust measuring tool for peatland scientists that can be easily collected with a smartphone, providing a non-destructive measurement of the water content of *Sphagnum* and by extension the immediate ecosystem.

Given the importance of colony density, and the capacity of RGB images for the measurement of plant health parameters, these detection and quantification algorithms have a strong potential for the advancement of high-throughput *Sphagnum* data collection.

7.5 – Concluding remarks

By combining physiological and molecular biology tools with computer science innovations, the work described here provides new and exciting insights into *Sphagnum* research, and paints a picture of a genus adapted to dealing with large fluctuations in water content.

The automated image-analysis workflows developed in this thesis that enable non-destructive quantification of plant traits The tools developed in this thesis further will allow peatland researchers to more easily measure both water content and colony density. In addition, there is the potential to extract further information from the obtained images. Peatland restoration projects could benefit from further development of automated image-analysis workflows that enable non-destructive quantification of traits that would otherwise be labour intensive to collect. With the growing accessibility of previously expensive equipment such as low-flying drones, the potential to generate high-throughput, high resolution data consistently and more regularly over time as the labour intensiveness is decreased and the analytical capacity increased.

Ultimately, the genus *Sphagnum* will continue to be a feature of many peatlands, and understanding their desiccation tolerance mechanisms will enable conservationists to tailor peatland restoration projects centred around *Sphagnum* to optimise the success of their endeavour.

7.6 - References

Abdollahnejad, A., Panagiotidis, D., Surový, P., 2017. Forest canopy density assessment using different approaches - Review. J. For. Sci. 63, 107–116. https://doi.org/10.17221/110/2016-JFS

Bengtsson, F., Granath, G., Rydin, H., 2016. Photosynthesis, growth, and decay traits in Sphagnum - a multispecies comparison. Ecol. Evol. 6, 3325–3341. https://doi.org/10.1002/ece3.2119

Borkenhagen, A., Cooper, D.J., 2018. Tolerance of fen mosses to submergence, and the influence on moss community composition and ecosystem resilience. J. Veg. Sci. 29, 127–135. https://doi.org/10.1111/jvs.12610

Caporn, S.J.M., Rosenburgh, A.E., Keightley, A.T., Hinde, S.L., Riggs, J.L., And Buckler, M., 2018. Sphagnum restoration on degraded blanket and raised bogs in the UK using micropropagated source material: a review of progress. Mires Peat 20, 1–17. https://doi.org/10.19189/MaP.2017.OMB.306

Charron, A.J., Quatrano, R.S., 2009. Between a rock and a dry place: The water-stressed moss. Mol. Plant 2, 478–486. https://doi.org/10.1093/mp/ssp018

Clymo, R.S., Hayward, P.M., 1982. The Ecology of Sphagnum, in: Bryophyte Ecology. Springer Netherlands, Dordrecht, pp. 229–289. https://doi.org/10.1007/978-94-009-5891-3_8

Cuming, A.C., 2019. Evolution of ABA signaling pathways, Advances in Botanical Research. Elsevier Ltd. https://doi.org/10.1016/bs.abr.2019.06.003

Elumeeva, T.G., Soudzilovskaia, N.A., During, H.J., Cornelissen, J.H.C., 2011. The importance of colony structure versus shoot morphology for the water balance of 22 subarctic bryophyte species. J. Veg. Sci. 22, 152–164. https://doi.org/10.1111/j.1654-1103.2010.01237.x

Gauthier, T.J., Elliott, J.B., Mccarter, C.P.R., Price, J.S., 2022. Field-scale compression of Sphagnum moss to improve water retention in a restored bog. J. Hydrol. 612, 128160. https://doi.org/10.1016/j.jhydrol.2022.128160

Gewin, V., 2020. Bringing back the bogs. Nature 578, 204–208.

Gitelson, A.A., Keydan, G.P., Merzlyak, M.N., 2006. Three-band model for noninvasive estimation of chlorophyll, carotenoids, and anthocyanin contents in higher plant leaves. Geophys. Res. Lett. 33. https://doi.org/10.1029/2006GL026457

González, E., Henstra, S.W., Rochefort, L., Bradfield, G.E., Poulin, M., 2014. Is rewetting enough to recover Sphagnum and associated peat-accumulating species in traditionally exploited bogs? Wetl. Ecol. Manag. 22, 49–62. https://doi.org/10.1007/s11273-013-9322-6

Guillory, A., Bonhomme, S., 2021. Phytohormone biosynthesis and signaling pathways of mosses, Plant Molecular Biology. Springer Netherlands. https://doi.org/10.1007/s11103-021-01172-6

Hájek, T., Vicherová, E., 2014. Desiccation tolerance of Sphagnum revisited: a puzzle resolved. Plant Biol. 16, 665–773. https://doi.org/10.1111/plb.12126

Harris, A., Bryant, R.G., Baird, A.J., 2006. Remote sensing of Sphagnum stress: A proxy for near-surface wetness conditions in northern peatlands? Eur. Sp. Agency, (Special Publ. ESA SP.

Hinde, S., Rosenburgh, A., Wright, N., Buckler, M., Caporn, S., 2010. Sphagnum re-introduction project : A report on research into the re-introduction of Sphagnum mosses to degraded moorland. Moors Futur. Rep. 31.

Hüther, P., Schandry, N., Jandrasits, K., Bezrukov, I., Becker, C., 2020.

ARADEEPOPSIS, an automated workflow for top-view plant phenomics using semantic segmentation of leaf States. Plant Cell 32, 3674–3688. https://doi.org/10.1105/tpc.20.00318
Johnson, M.G., Shaw, A.J., 2015. Genetic diversity, sexual condition, and microhabitat preference determine mating patterns in Sphagnum (Sphagnaceae) peat-mosses. Biol. J. Linn. Soc. 115, 96–113. https://doi.org/10.1111/bij.12497
Kangas, L., Maanavilja, L., Hájek, T., Juurola, E., Chimner, R.A., Mehtätalo, L., Tuittila, E.S., 2014. Photosynthetic traits of Sphagnum and feather moss species in undrained, drained and rewetted boreal spruce swamp forests. Ecol. Evol. 4, 381–396. https://doi.org/10.1002/ece3.939
Knight, C.D., Sehgal, A., Atwal, K., Wallace, J.C., Cove, D.J., Coates, D., Quatrano, R.S., Bahadur, S., Stockley, P.G., Cuming, A.C., 1995. Molecular responses to abscisic acid and stress are conserved between moss and cereals. Plant Cell 7, 499–506. https://doi.org/10.2307/3870110
Kooijman, A.M., Bakker, C., 1994. The acidification capacity of wetland bryophytes as influenced by simulated clean and polluted rain. Aquat. Bot. 48, 133–144. https://doi.org/10.1016/0304-3770(94)90080-9
Kremer, C.L., Drinnan, A.N., 2004. Secondary walls in hyaline cells of Sphagnum. Aust. J. Bot. 52, 243–256. https://doi.org/10.1071/BT03010
Ligrone, R., Duckett, J.G., 1998. Development of the leafy shoot in Sphagnum (Bryophyta) involves the activity of both apical and subapical meristems. New Phytol. 140, 581–595.
Malenovsky, Z., Lucieer, A., Robinson, S., Harwin, S., Turner, D., Veness, T., 2013. Monitoring of Antarctic moss ecosystems using a high spatial resolution imaging spectroscopy. EGU Gen. Assem. Conf. Abstr. 15, 7360.
Muster, C., Gaudig, G., Krebs, M., Joosten, H., 2015. Sphagnum farming: the promised land for peat bog species? Biodivers. Conserv. 24, 1989–2009. https://doi.org/10.1007/s10531-015-0922-8
Nibau, C., van de Koot, W., Spiliotis, D., Williams, K., Kramaric, T., Beckmann, M., Mur, L., Hiwatashi, Y., Doonan, J.H., 2022. Molecular and physiological responses to desiccation indicate the abscisic acid pathway is conserved in the peatmoss, Sphagnum. J. Exp. Bot. 1–16. https://doi.org/https://doi.org/10.1093/jxb/erac133
Proctor, M.C.F., Oliver, M.J., Wood, A.J., Alpert, P., Stark, L.R., Cleavitt, N.L., Mishler, B.D., 2007. Desiccation-tolerance in bryophytes: A review. Bryologist 110, 595–621. https://doi.org/10.1639/0007-2745(2007)110[595:DIBAR]2.0.CO;2
Rice, S.K., 2012. The cost of capillary integration for bryophyte canopy water and carbon dynamics. Lindbergia 35, 53–62.
Robb, C., Hardy, A., Doonan, J.H., Brook, J., 2020. Semi-Automated Field Plot Segmentation From UAS Imagery for Experimental Agriculture. Front. Plant Sci. 11, 1–13. https://doi.org/10.3389/fpls.2020.591886
Robinson, S.A., King, D.H., Bramley-Alves, J., Waterman, M.J., Ashcroft, M.B., Wasley, J., Turnbull, J.D., Miller, R.E., Ryan-Colton, E., Benny, T., Mullany, K., Clarke, L.J., Barry, L.A., Hua, Q., 2018. Rapid change in East Antarctic terrestrial vegetation in response to regional drying. Nat. Clim. Chang. 8, 879–884. https://doi.org/10.1038/s41558-018-0280-0
Sánchez-Sastre, L.F., Alte da Veiga, N.M.S., Ruiz-Potosme, N.M., Carrión-Prieto, P., Marcos-Robles, J.L., Navas-Gracia, L.M., Martín-Ramos, P., 2020. Assessment of RGB Vegetation Indices to Estimate Chlorophyll Content in

Sugar Beet Leaves in the Final Cultivation Stage. AgriEngineering 2, 128–149. https://doi.org/10.3390/agriengineering2010009
Schipperges, B., Rydin, H., 1998. Response of photosynthesis of Sphagnum species from contrasting microhabitats to tissue water content and repeated desiccation. New Phytol. 140, 677–684.
Shuttleworth, E.L., Evans, M.G., Pilkington, M., Spencer, T., Walker, J., Milledge, D., Allott, T.E.H., 2019. Restoration of blanket peat moorland delays stormflow from hillslopes and reduces peak discharge. J. Hydrol. X 2, 1–14. https://doi.org/10.1016/j.hydroa.2018.100006
Sun, Y., Pri-Tal, O., Michaeli, D., Mosquna, A., 2020. Evolution of Abscisic Acid Signaling Module and Its Perception. Front. Plant Sci. 11, 1–9. https://doi.org/10.3389/fpls.2020.00934
van Breemen, N., 1995. How Sphagnum bogs down other plants. Trends Ecol. Evol. 10, 270–275. https://doi.org/10.1016/0169-5347(95)90007-1
van de Koot, W.Q.M., van Vliet, L.J.J., Chen, W., Doonan, J.H., Nibau, C., 2021. Development of an image analysis pipeline to estimate Sphagnum colony density in the field. Plants 10, 1–17. https://doi.org/10.3390/plants10050840
Werner, O., Ros Espín, R.M., Bopp, M., Atzorn, R., 1991. Abscisic-acid-induced drought tolerance in Funaria hygrometrica Hedw. Planta 186, 99–103. https://doi.org/10.1007/BF00201503
Winnicka, K., Melosik, I., 2019. Genetic and expression differences between putative ecotypes of Sphagnum denticulatum Brid. (Sphagnaceae: Bryophyta) subjected to drought stress and rehydration. Perspect. Plant Ecol. Evol. Syst. 37, 39–52. https://doi.org/10.1016/j.ppees.2019.02.004
Xue, J., Su, B., 2017. Significant remote sensing vegetation indices: A review of developments and applications. J. Sensors 2017. https://doi.org/10.1155/2017/1353691

Appendices

Appendix 1 - Supplementary Figures

Chapter 2 Supplementary Figures

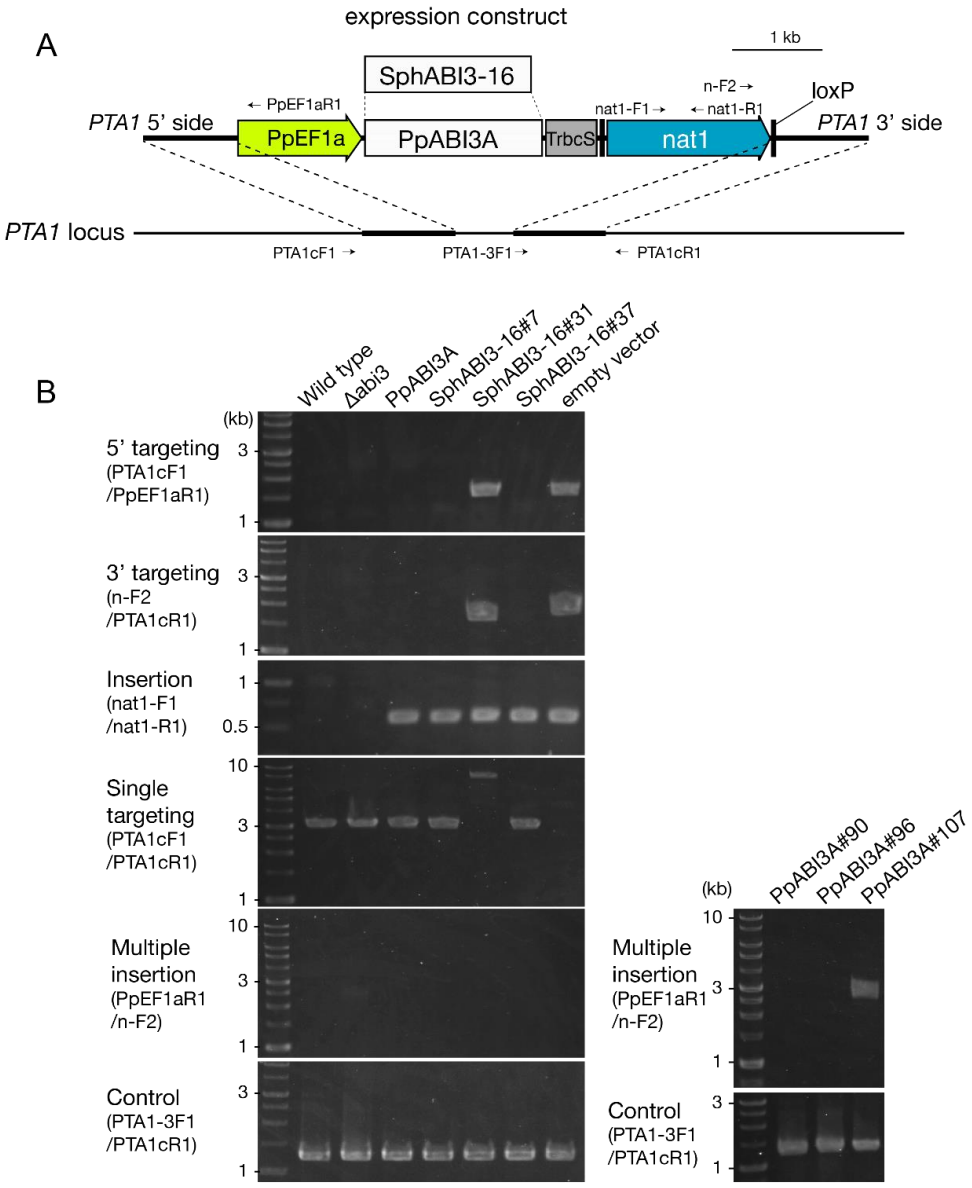

Supplementary Figure 2.1 Targeting of the PpABI3A and SphABI3-16 expression constructs.
(A) Schematics of the targeting of the expression construct into the PTA1-targeting locus. Light green and blue arrows denote a Physcomitrium patens EF1a promotor (PpEF1a) and the nourseothricin resistance cassette (nat1), respectively. White, gray, and black boxes show the DNA fragment encoding PpABI3A or SphABI3-16, the pea rbcS3A terminator (TrbcS), and loxP, respectively. Thick bars indicate targeting region of the PTA1 locus. Small arrows represent the primers (PTA1cF1, PpEF1aR1, PTA1-3F1, nat1-F1, nat1-R1, n-F2, PTA1cR1) for the PCR-based targeting check. (B) PCR to checking the targeting of the inserts. The panels show the PCR-amplified DNA fragments for 5' targeting and 3'targeting to the PTA1

locus, the presence of the insertion, the detection of the insertion being single or multiple, and the PCR control as indicated. The side panel includes PCR controls for the multiple insertion PCR using a line that shows multiple insertions. PpABI3A#90 is the PpABI3A line used in the main panel.

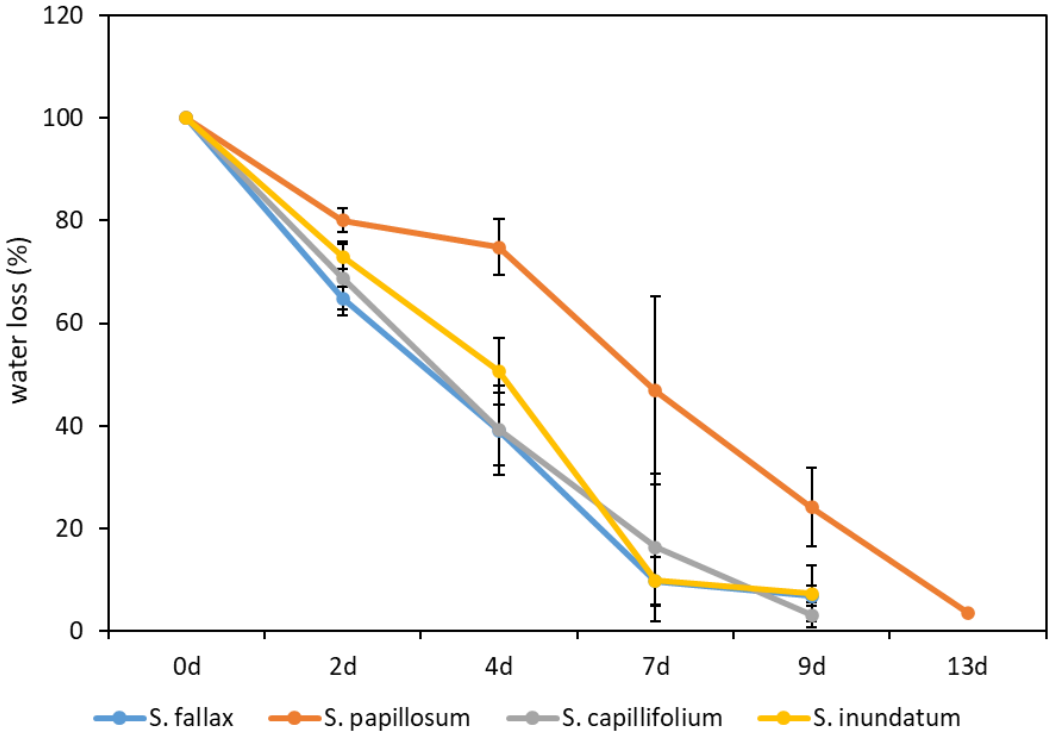

Supplementary Figure 2.2. Percentage fresh weight during the desiccation experiment for the four different *Sphagnum* species as indicated in the graph legend.
The cosms were weighed on the days indicated in the horizontal axis. Percentage water loss was calculated by dividing the final plant weight by the original plant weight for each time point and multiplying by 100. Data represent averages ± SD of four replica plates.

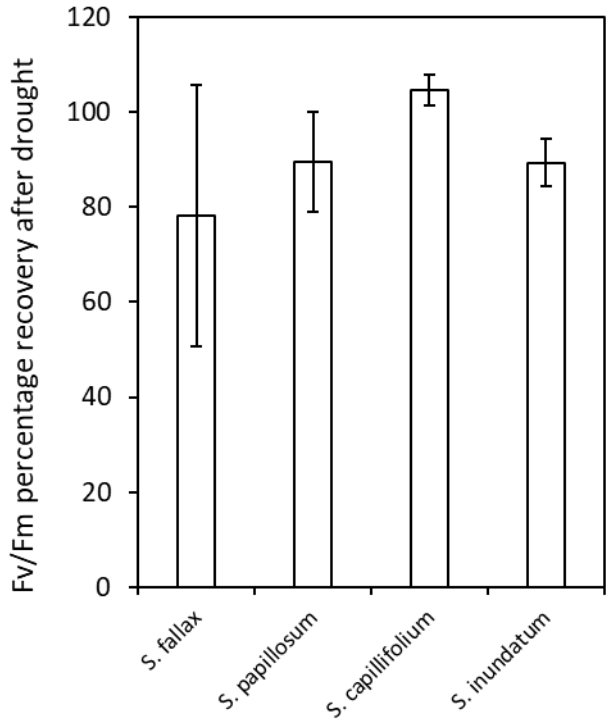

Supplementary Figure 2.3. Chlorophyll fluorescence recovery after desiccation as measured by Fv/Fm.
Recovery was calculated by dividing the Fv/Fm value after re-watering with the Fv/Fm measured at the start of the drought and expressed as a percentage.

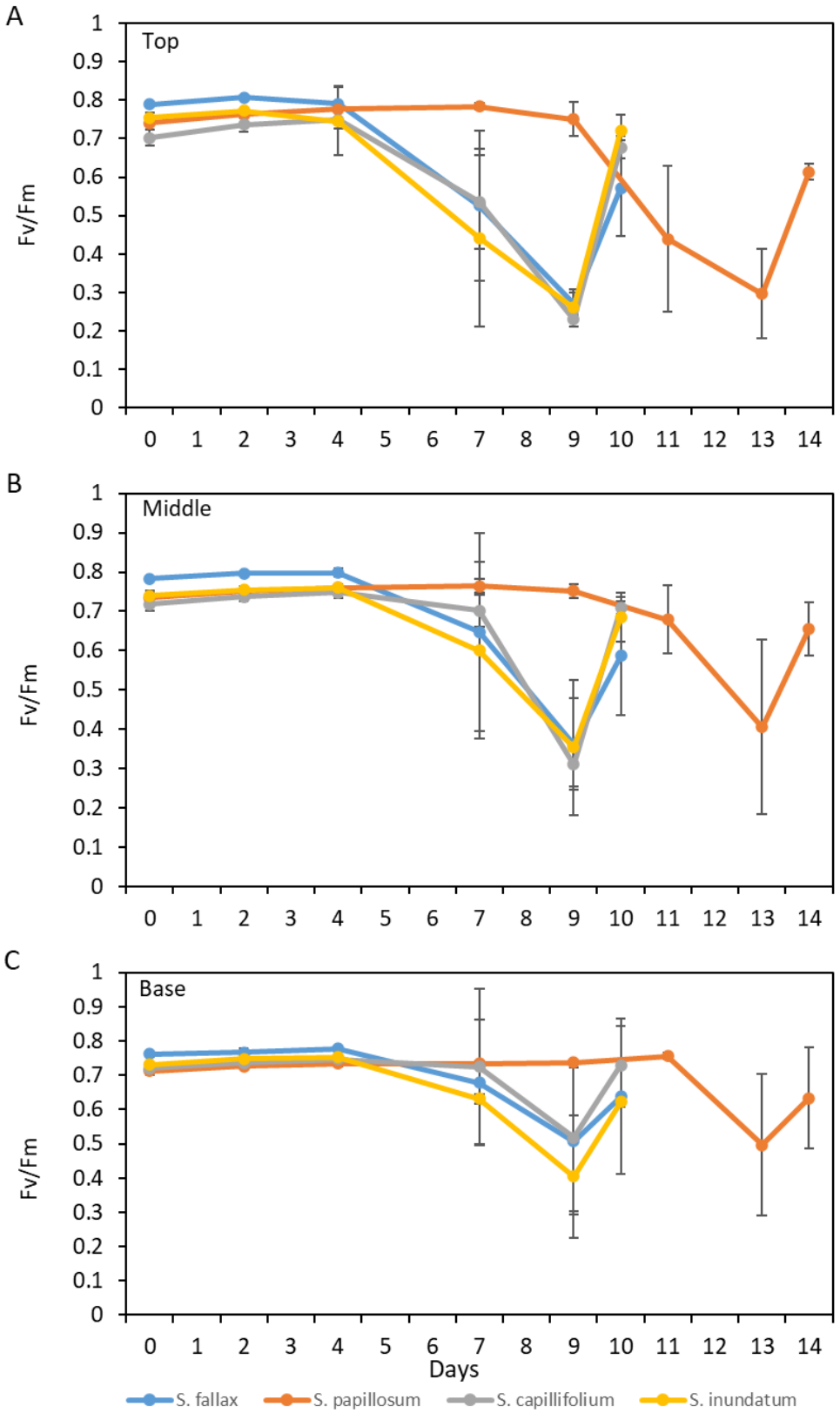

Supplementary Figure 2.4. Changes of chlorophyll fluorescence upon desiccation in different regions of the *Sphagnum* plants for the four different species.
After imaging, plates were divided into; A top region (containing mostly capitula), B middle region (green, active region) and C bottom (senescing area) and the Fv/Fm value for each region determined. Data represent averages ± SD of four replica plates.

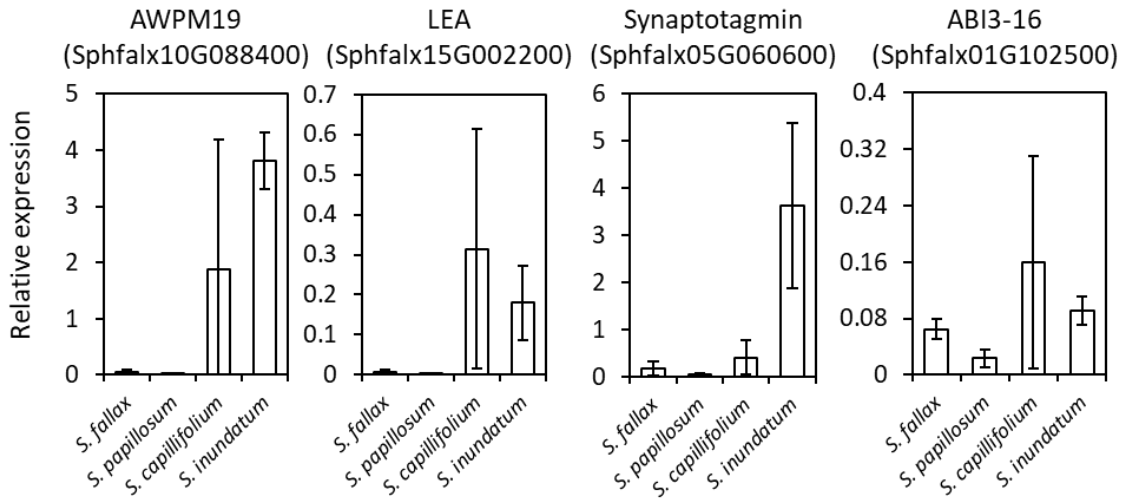

Supplementary Figure 2.5. Basal expression of drought responsive genes is higher in *S. inundatum*.
Expression of AWPM19 (Sphfalx10G088400), LEA (Sphfalx15G002200), Synaptotagmin (Sphfalx05G060600) and ABI3-16 (Sphfalx01G102500) was determined in non-droughted material by qPCR using EF1α (Sphfalx03G087000) GAPDH (Sphfalx16G076000) as references. Each sample was done in triplicate and data represent average ± SE of three biological replicates.

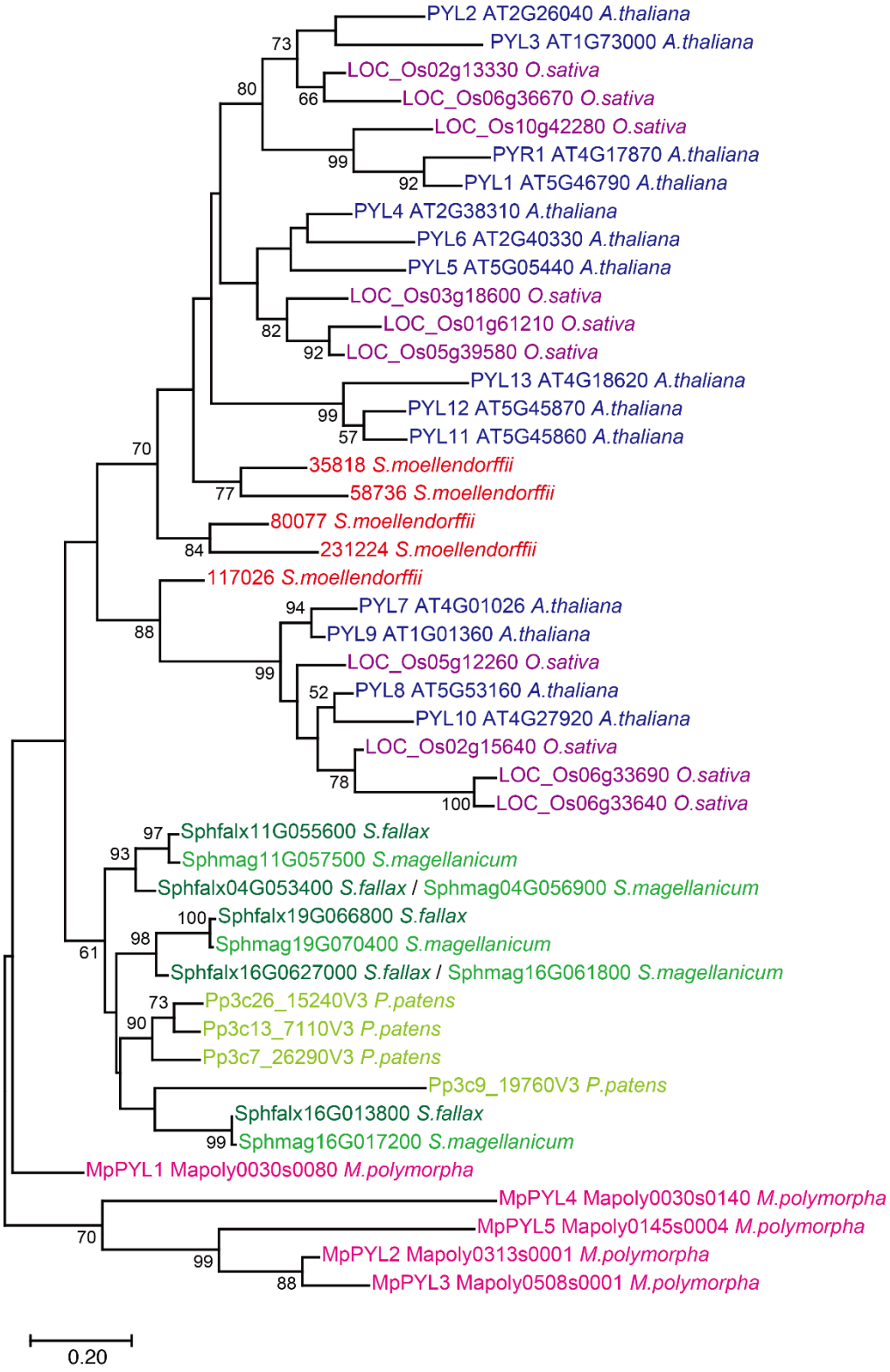

Supplementary Figure 2.6. . ABA signalling components are present and evolutionarily conserved in *Sphagnum* including the ABA-receptor family PYR1/PYL.
The phylogenetic tree of the PYR1/PYL family was constructed using the Maximum Likelihood method using the JTT matrix. This is an unrooted tree and the tree with the highest log likelihood is shown. Bootstrap values of >50% are shown on the branches. Horizontal branch length is proportional to the estimate evolutionary distance. Genes with identical amino acid sequence within the region used for the phylogenetic analysis are described in parallel.

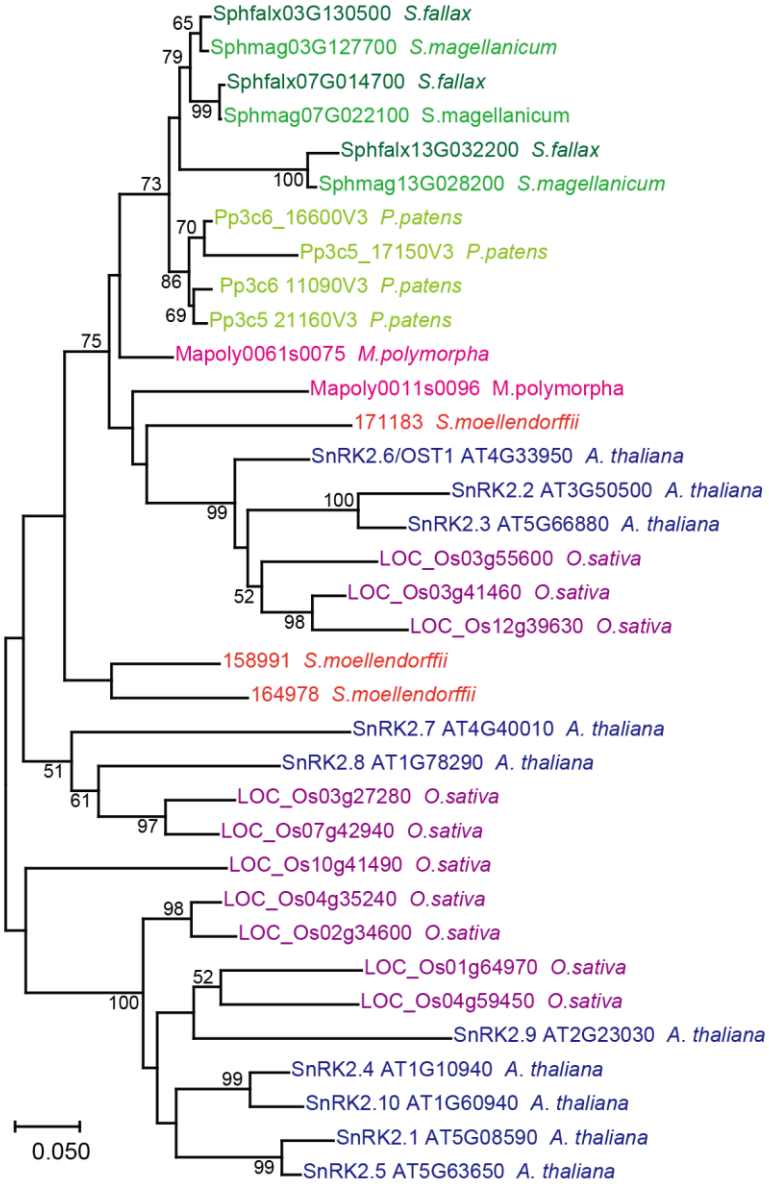

Supplementary Figure 2.7. ABA signalling components are present and evolutionarily conserved in *Sphagnum* including SnRK2.
The phylogenetic tree of the SnRK2 family was constructed using the Maximum Likelihood method using the JTT matrix. This is an unrooted tree and the tree with the highest log likelihood is shown. Bootstrap values of >50% are shown on the branches. Horizontal branch length is proportional to the estimate evolutionary distance.

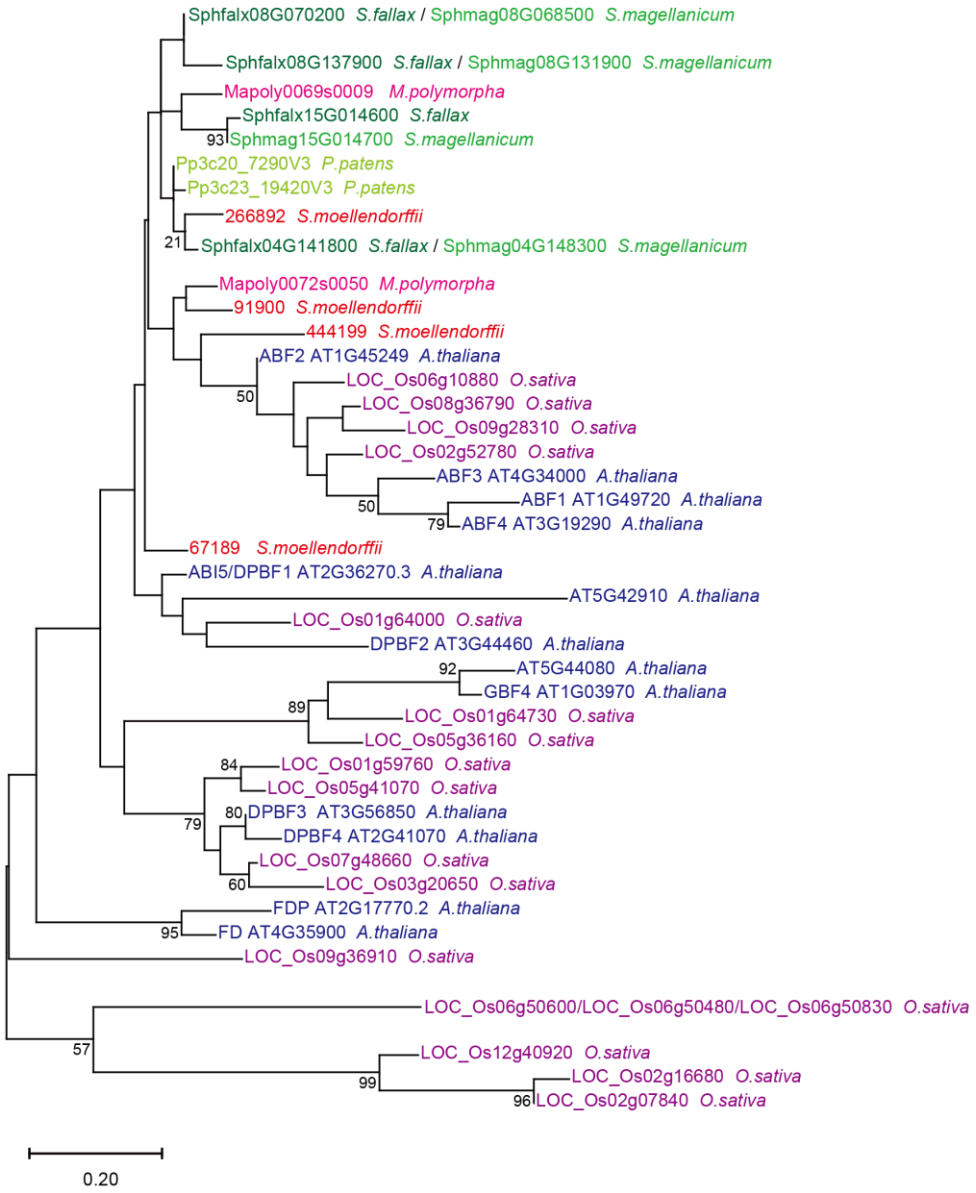

Supplementary Figure 2.8. ABA signalling components are present and evolutionarily conserved in *Sphagnum* including ABI5 and ABI5-related proteins.
The phylogenetic tree of the ABI5 family was constructed using the Maximum Likelihood method using the JTT matrix. This is an unrooted tree of group A bZIPs. The tree with the highest log likelihood is shown. Bootstrap values of >50% are shown on the branches. Horizontal branch length is proportional to the estimate evolutionary distance.

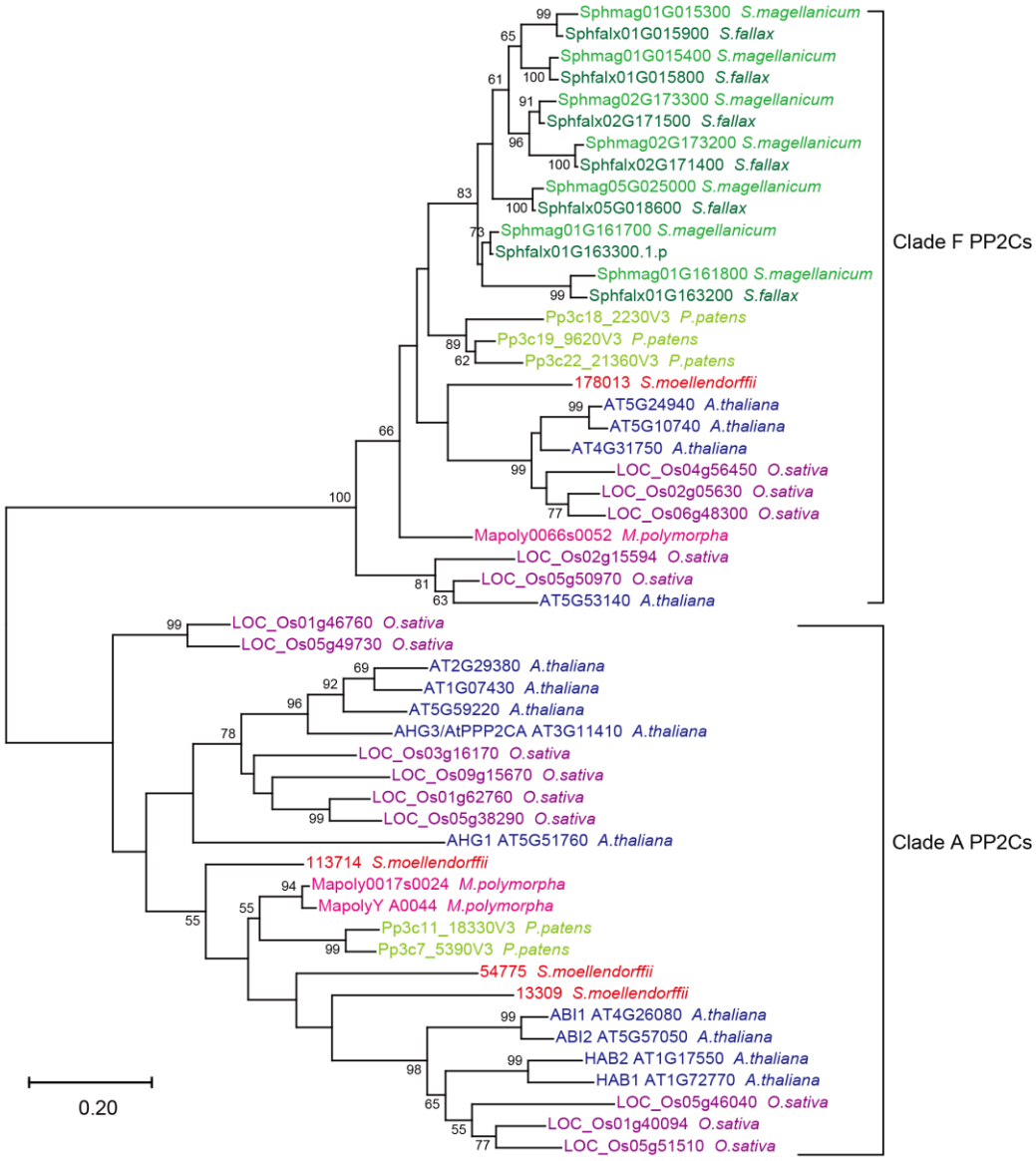

Supplementary Figure 2.9. Clade A PPC2A homologues are absent in *Sphagnum*.
The phylogenetic tree was constructed using the Maximum Likelihood method using the JTT matrix. This is an unrooted tree and the tree with the highest log likelihood is shown. Bootstrap values of >50% are shown on the branches. The clade names follow Bhaskara et al., 2019. Horizontal branch length is proportional to the estimate evolutionary distance. Clade F orthologues were detected for all the species tested. Note that clade F of PP2C does not contain full gene members due to the E-value threshold used. We were unable to identify Clade A homologues in *Sphagnum*.

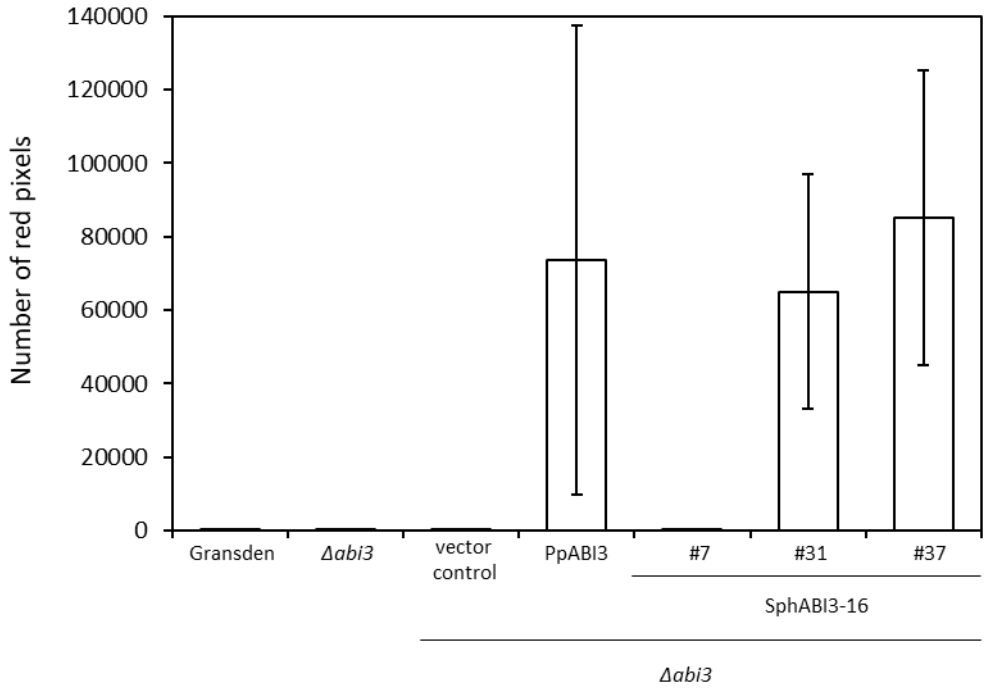

Supplementary Figure 2.10. *P. patens* plants with increased expression of *ABI3* show signs of stress as measured by the presence of red pixels.
Protonema was grown in cellophane disks overlaid on BCD plates. After seven days, it was transferred to BCD media supplemented with 25µM ABA and imaged after 14 days. The number of red pixels in the image was calculated per plate. Data represent averages ± SE of three replica plates.

Chapter 3 Supplementary Figures

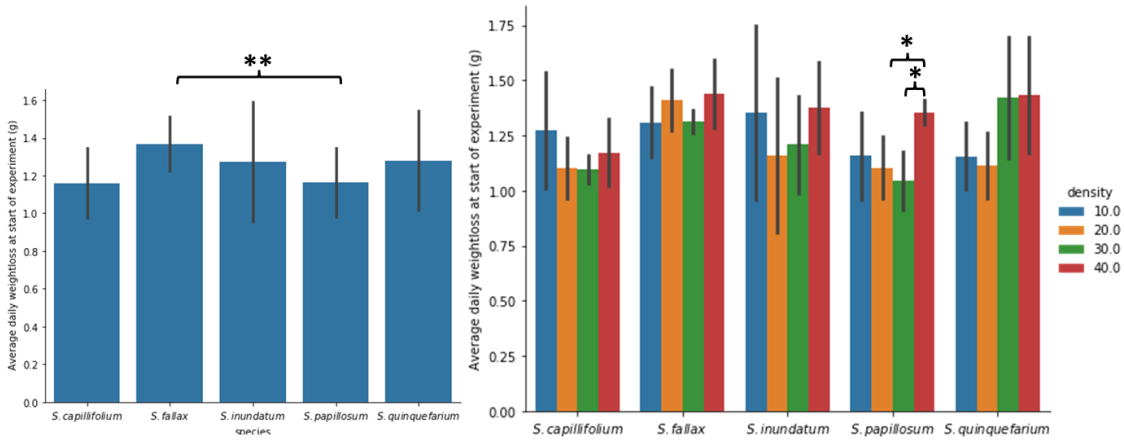

Supplementary Figure 3.1. Average weight loss per day for the first three days for each species and for each density within the species. *S. fallax* and *S. papillosum* were the only two species to differ significantly from each other, with S. fallax losing the largest amount of water daily and *S. papillosum* the least. Within the species, only the 20 and 30 densities differed from the 40 density in *S. papillosum*. These results suggest that species and colony density were of limited effect on water loss in the experiment.

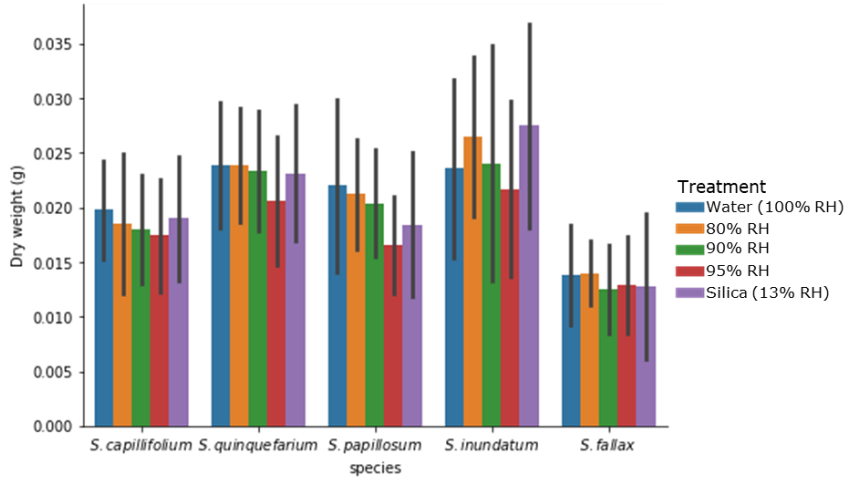

Supplementary Figure 3.2. Mean plant dry weight in the relative humidity experiment cosms. *S. inundatum* was on average the heaviest species, followed by *S. quinquefarium* and *S. papillosum. S. fallax* was the lightest species, despite typically being a larger species *than S. capillifolium* and of similar size to *S. quinquefarium*.

Chapter 4 Supplementary Figures

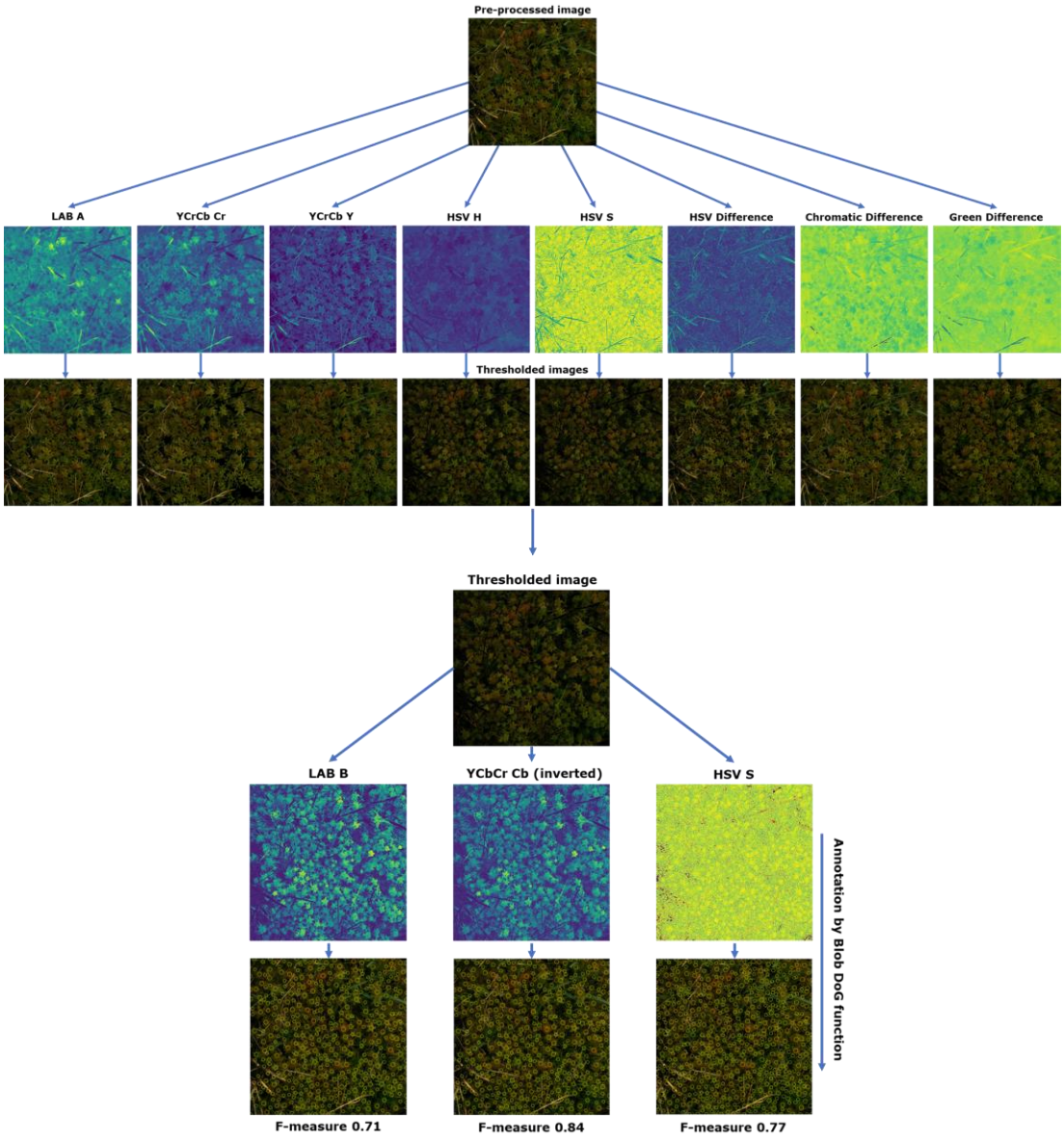

Supplementary Figure 4.1. Process workflow visualisation of our method to find the optimal colour channels for thresholding and annotation.
An image that has gone through the pre-processing step of the pipeline (Figure 4.3) was transformed and thresholded in 8 different colour spaces. Subsequently, the 8 thresholded images were transformed again to a different colour space for annotation, using the Blob DoG function from the plantCV package.

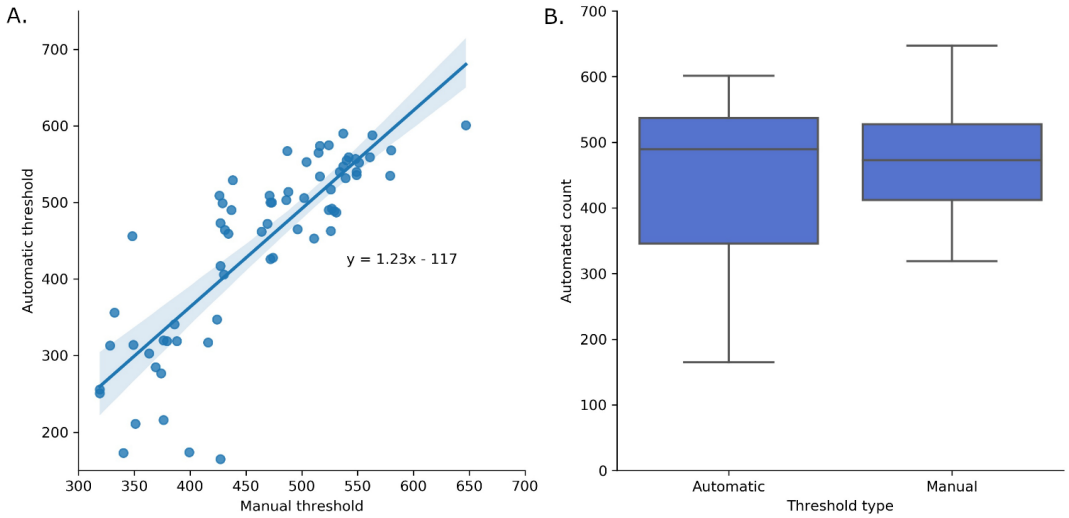

Supplementary Figure 4.2. Linear regression (A) of the 68 images (Supplementary Table 4.3) and the number of capitula counted after manually thresholding and thresholded using the mean lower threshold value 125 (Supplementary Table 4.1).
This relationship was highly significant ($p<0.001$***). An ANOVA of the two counts also detected no significant difference (B).

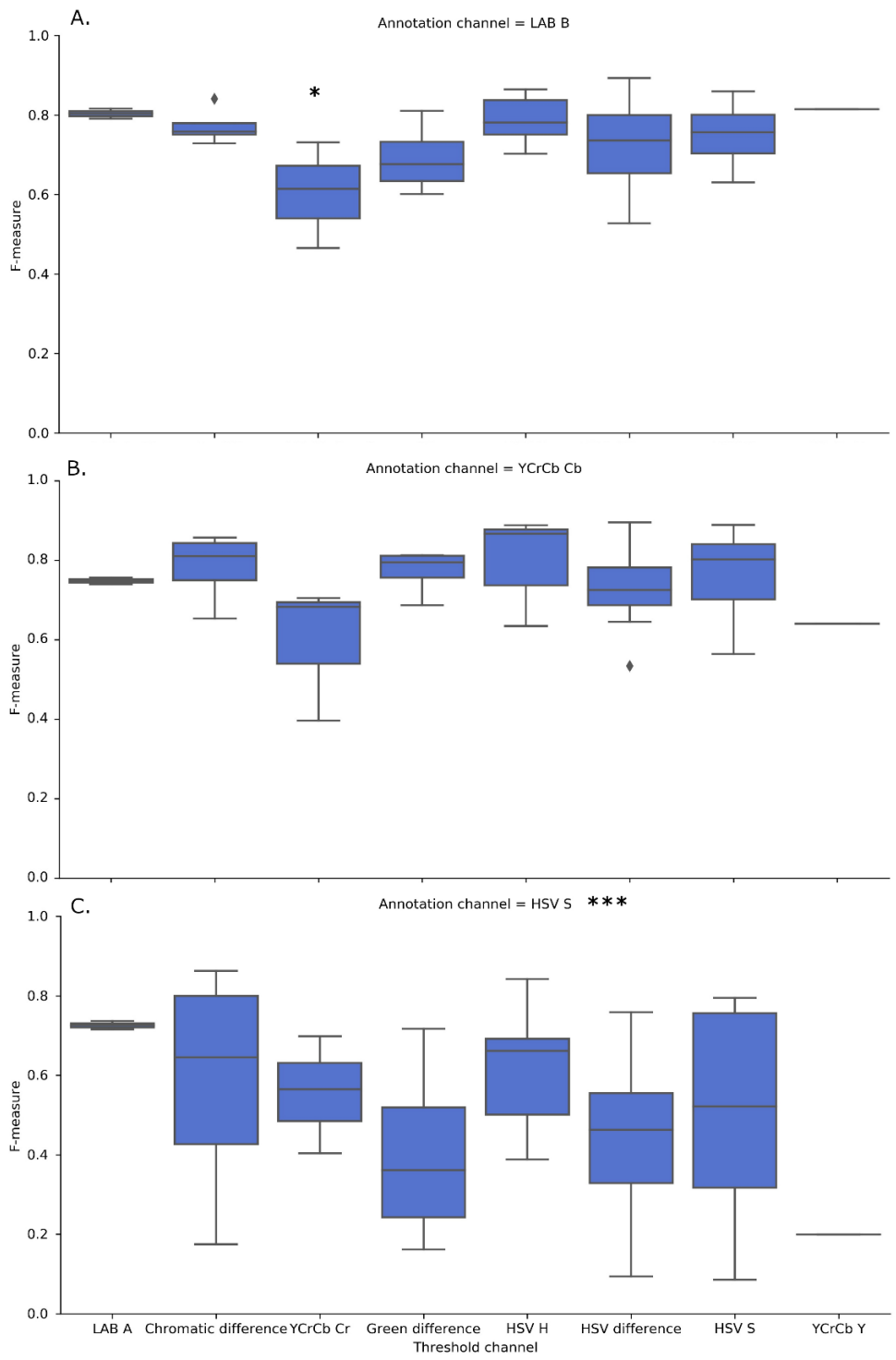

Supplementary Figure 4.3. F-measure distributions of the 144 images, annotated the in LAB B (A), YCrCb Cb (B) and HSV S (C) colour spaces.
(n=48 for each annotation channel, the distribution of the resulting images per thresholding channels were as follows: HSV H (n=6), HSV S (n=15), LAB A (n=2), YCrCb Y (n=1), YCrCb Cr (n=3), Chromatic difference (n=4), HSV difference (n=13) and Green difference (n=4). Asterisks indicate significance calculated using a type III ANOVA ($p<0.05$*, $p<0.001$***). Only the thresholding channel YCrCb Cr differed significantly from other channels in performance as quantified by F-measure for annotation channel LAB B. Annotation channel HSV S differed significantly in performance from LAB B and YCrCb Cb.

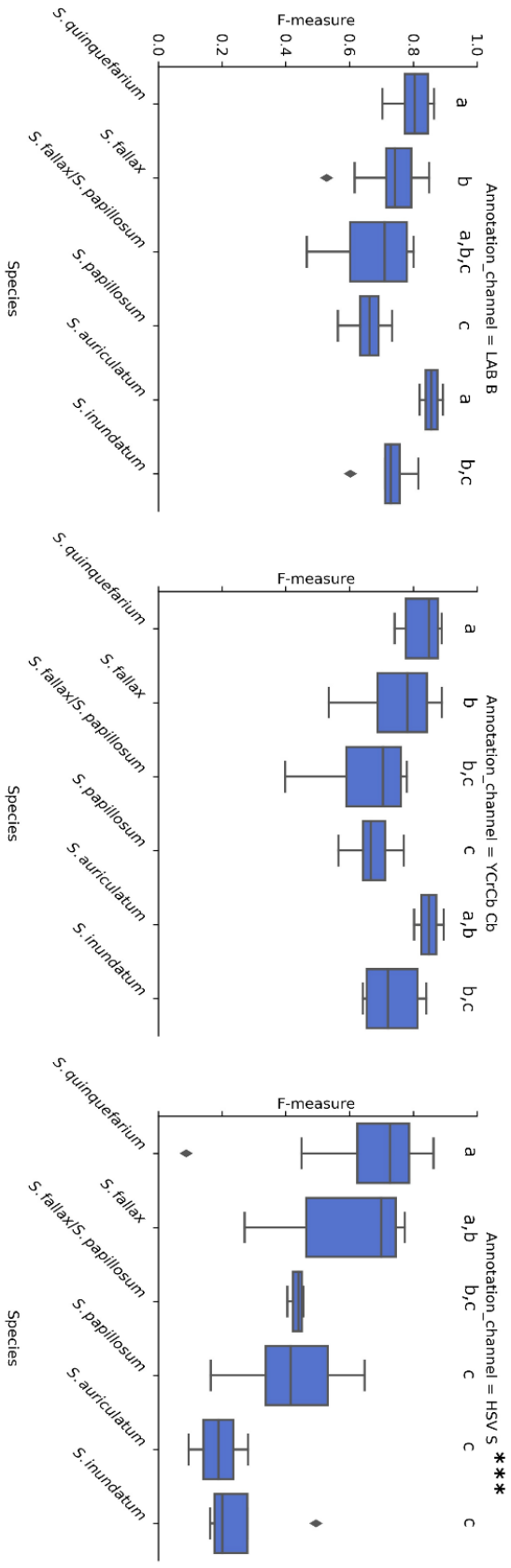

Supplementary Figure 4.4. F-measure distributions of the different species for the three annotation channels.
Only annotation channel HSV S differed significantly ($p<0.001$), and within the annotation channels the different groups indicate significance ($p<0.05$).

Chapter 5 Supplementary Figures

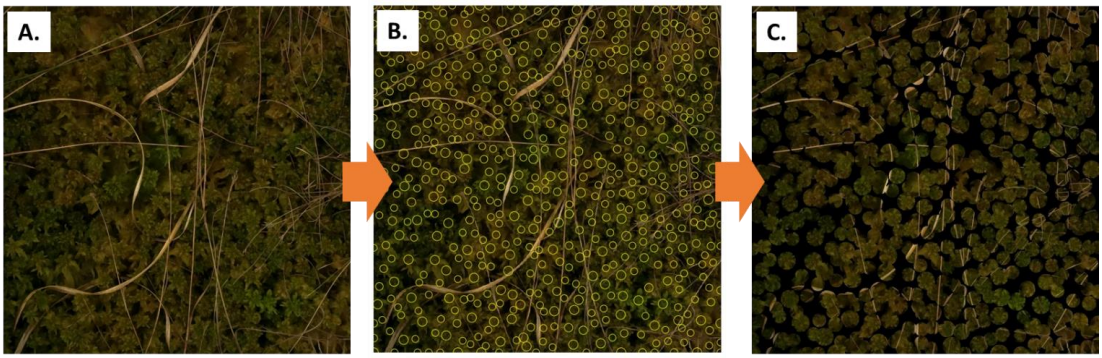

Supplementary Figure 5.1. Use of the capitulum counter annotations for precision data extraction.
The original image (A) was run through the capitulum counter algorithm (B) (van de Koot et al. 2021). These annotations were subsequently enlarged and everything outside of the annotations was removed from the image (C). This reduced non-moss noise when pixel data was subsequently extracted.

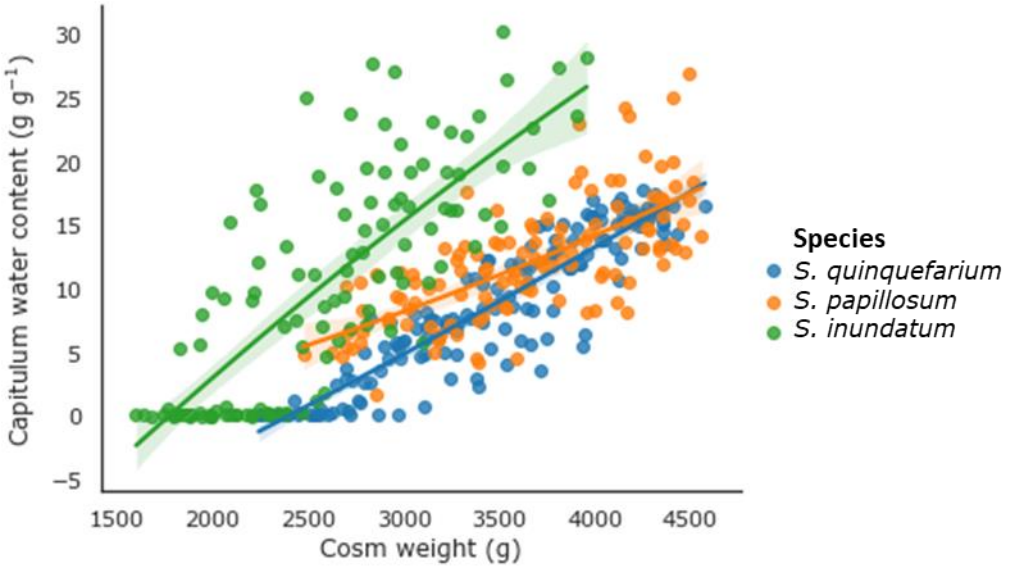

Supplementary Figure 5.2. Correlations of cosm weight and capitulum water content (g g^{-1}). The relationship between these two variables was highly correlated, although there were slight differences in the slopes of the species. This may indicate that *S. papillosum*, which has a less steep slope, distributes or retains water content differently.

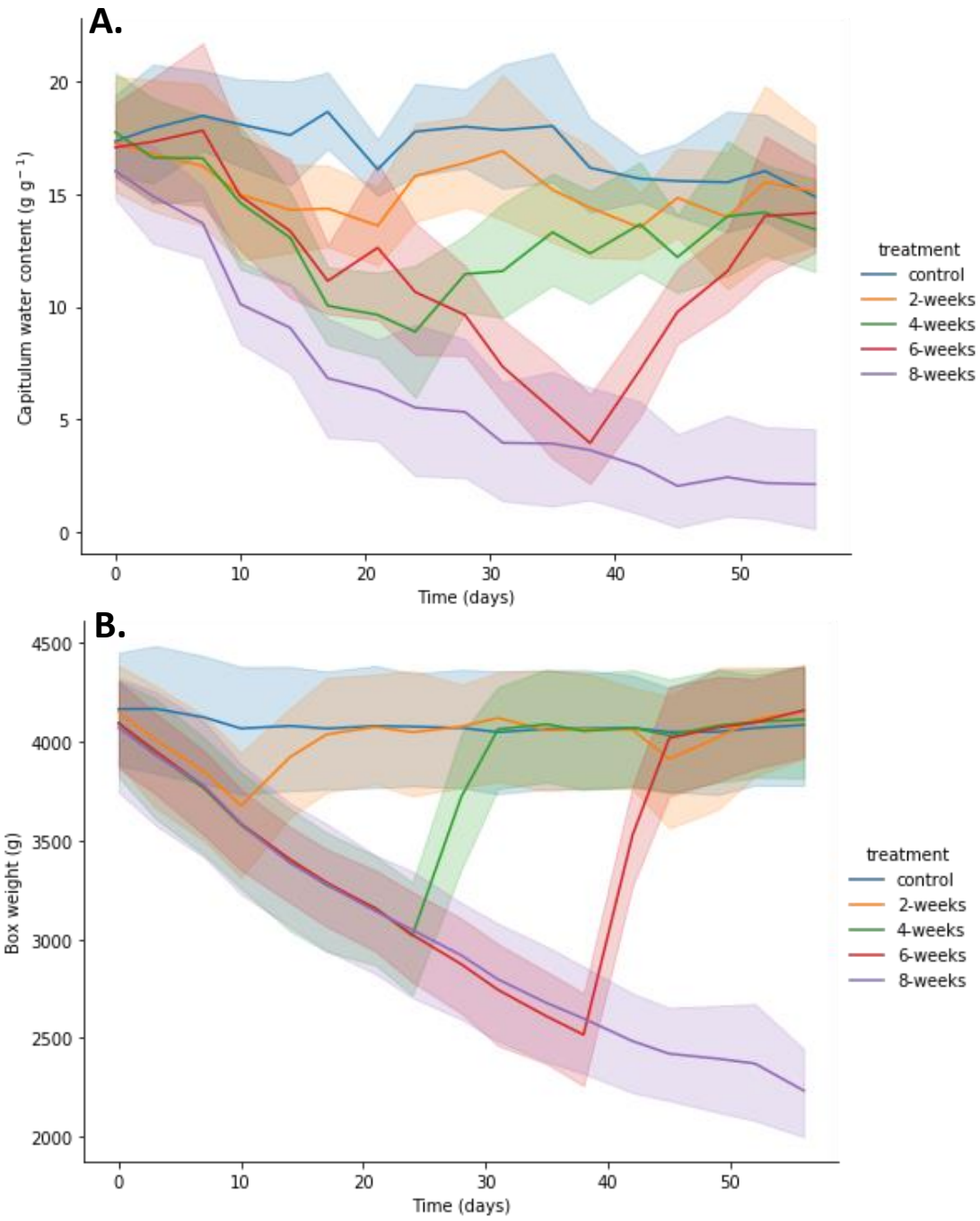

Supplementary Figure 5.3. Lag between capitulum water content recovery and box weight recovery.
While the Gravimetric system rewatered the boxes to their target weight after drought, recovering weight instantly, capitulum water content lagged behind in recovery speed. This is particularly clear in the 6-weeks treatment, where weight is replenished on day 42 while capitulum water content does not reach pre-desiccation levels until day 50.

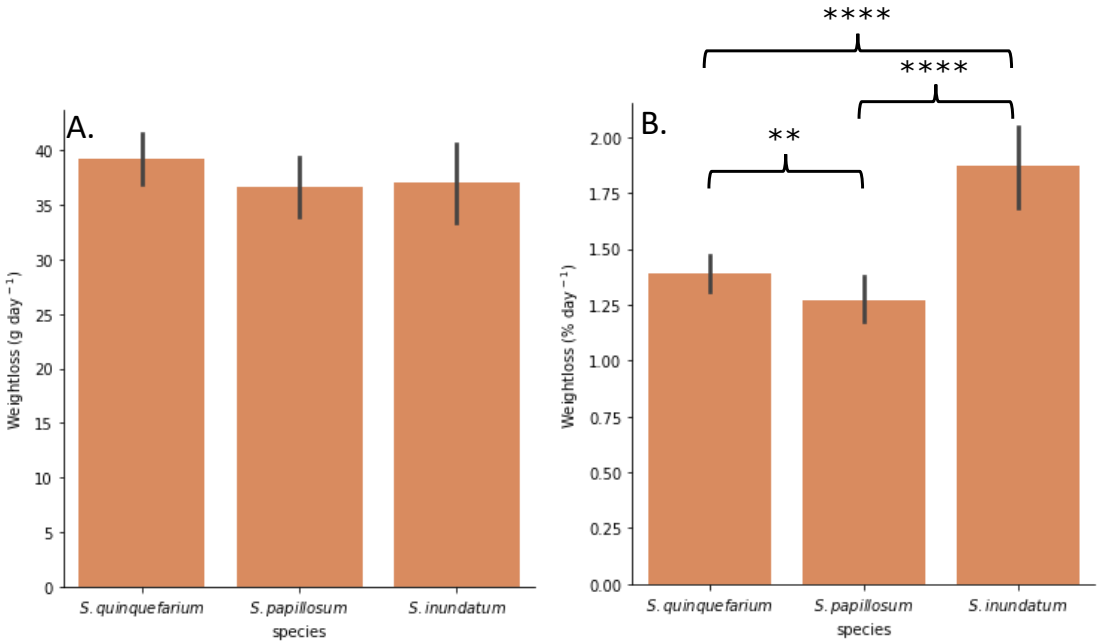

Supplementary Figure 5.4. Interspecific differences in daily weight loss.
While each species lost comparatively similar quantities of water daily in grams, *S. inundatum* lost fractionally a larger portion of its water content daily. *S. papillosum* lost the smallest fraction of its weight daily, suggesting this species had superior water retention capacity.

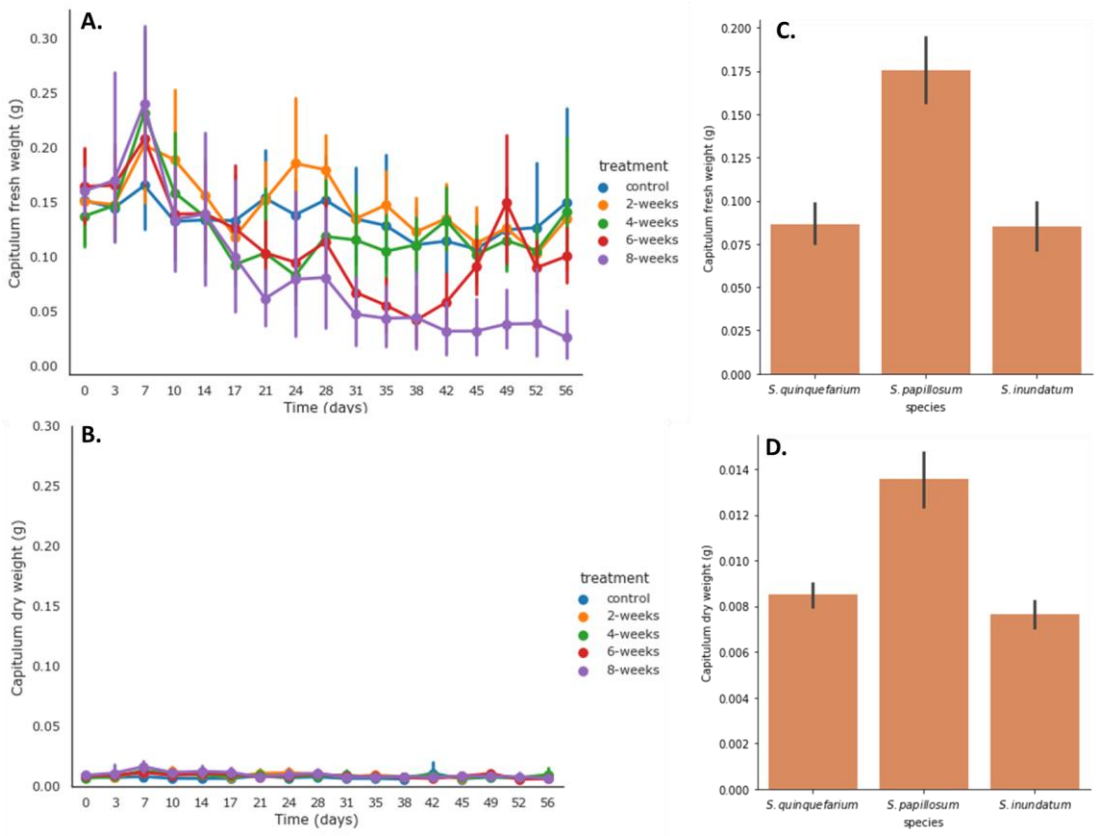

Supplementary Figure 5.5. Capitulum fresh weight and dry weight over the course of the glasshouse experiment.
While fresh weight clearly exhibitited the patterns of weight loss associated with water loss (A), dry weight was relatively stable over the course of the experiment (B). *S. papillosum* capitula were nearly twice as heavy as the other two species, both when wet (C) and dry (D).

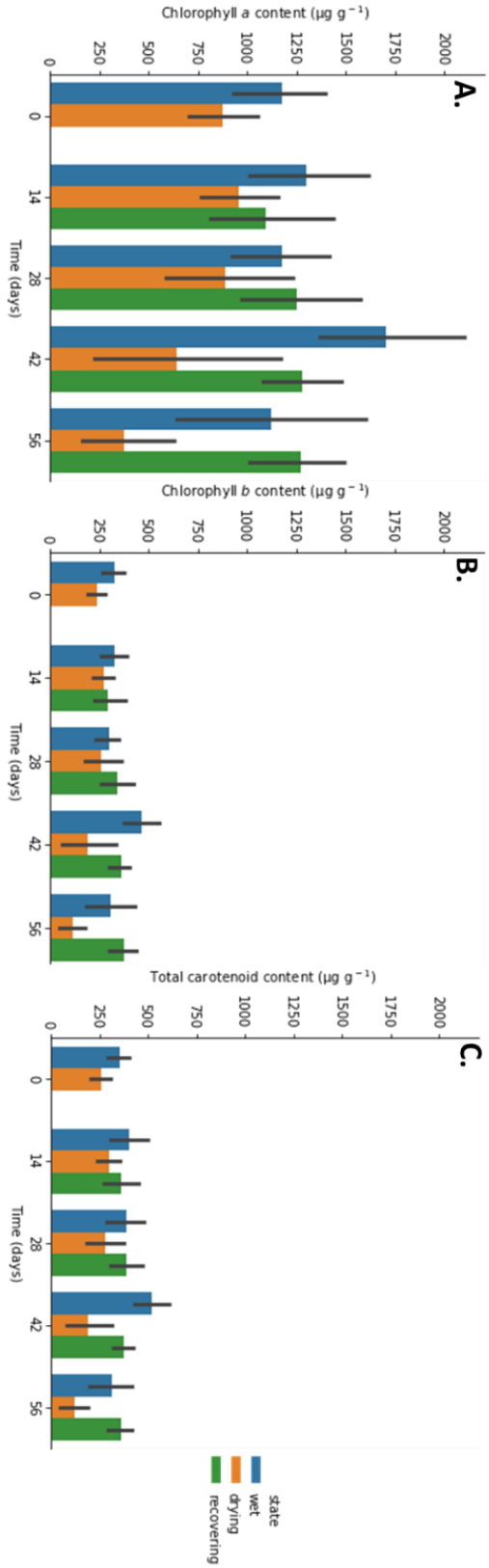

Supplementary Figure 5.6. Chlorophyll a (A), b (B) and carotenoid (C) contents over time for the three species combined.
The contents of these pigments remained relatively stable over time in wet *Sphagnum*, but decreased when subjected to desiccation. When the desiccated moss was rewatered however, the pigment contents recovered to pre-desiccation levels.

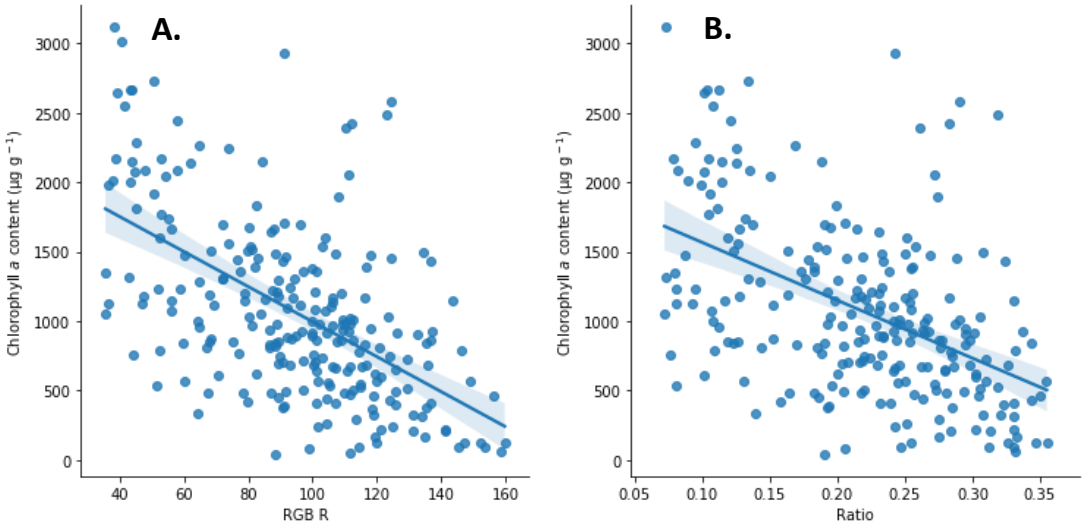

Supplementary Figure 5.7. Chlorophyll a content correlated with the R colour channel and the Ratio multispectral index.
While the R channel (A) was not the strongest correlating RGB variable with capitulum water content, it was the strongest correlating variable for each of the pigments. The multispectral index Ratio (B), which was designed to quantify photochemistry contents, was the strongest correlating multispectral variable for each of the pigments and capitulum water content.

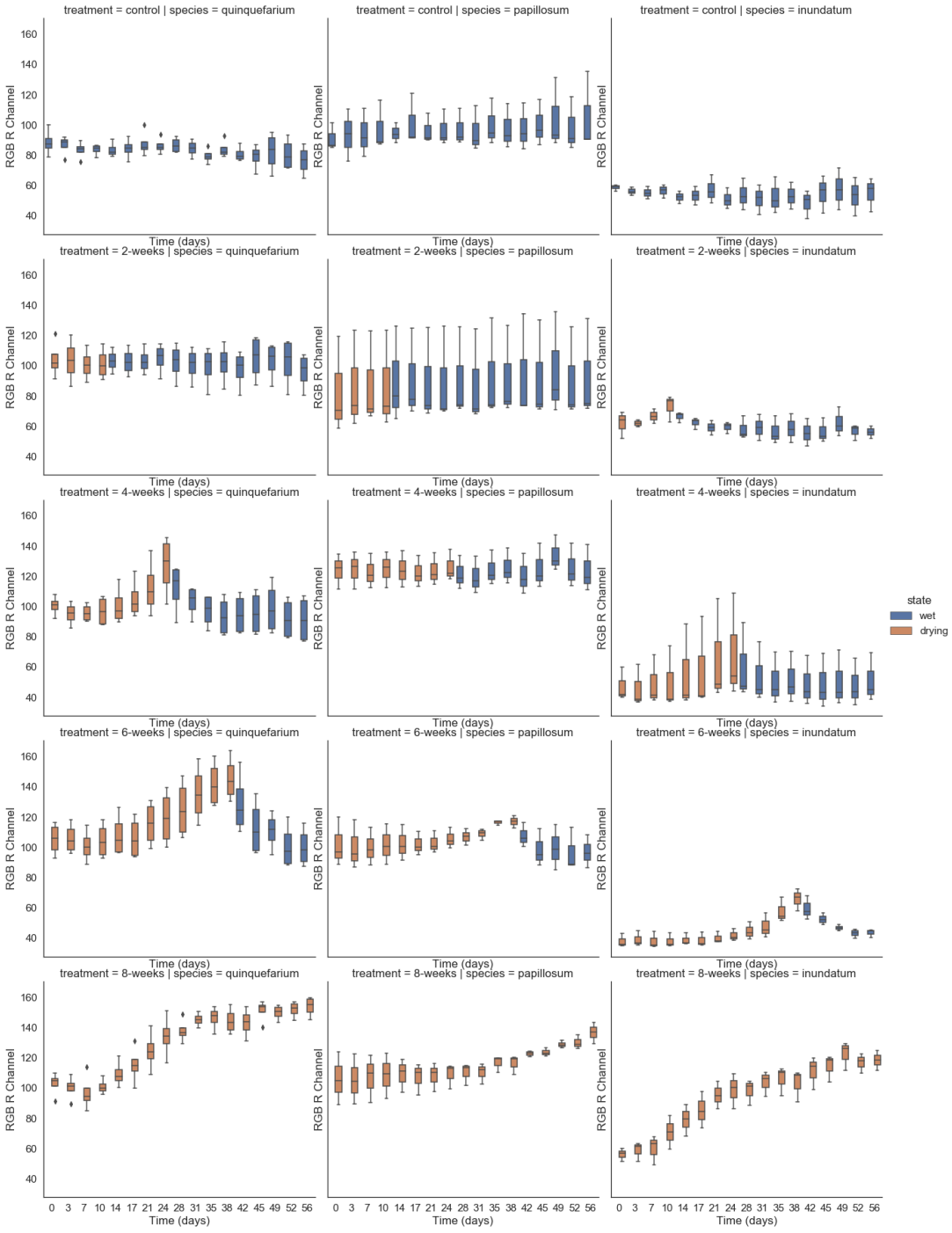

Supplementary Figure 5.8. Progression of the RGB R channel over time.
Columns represent the species *S. quinquefarium*, *S. papillosum* and *S. inundatum*. The rows indicate the treatments, namely control, 2-weeks, 4-weeks, 6-weeks and 8-weeks drought. Colours represent wet (blue) and dry (orange) states.

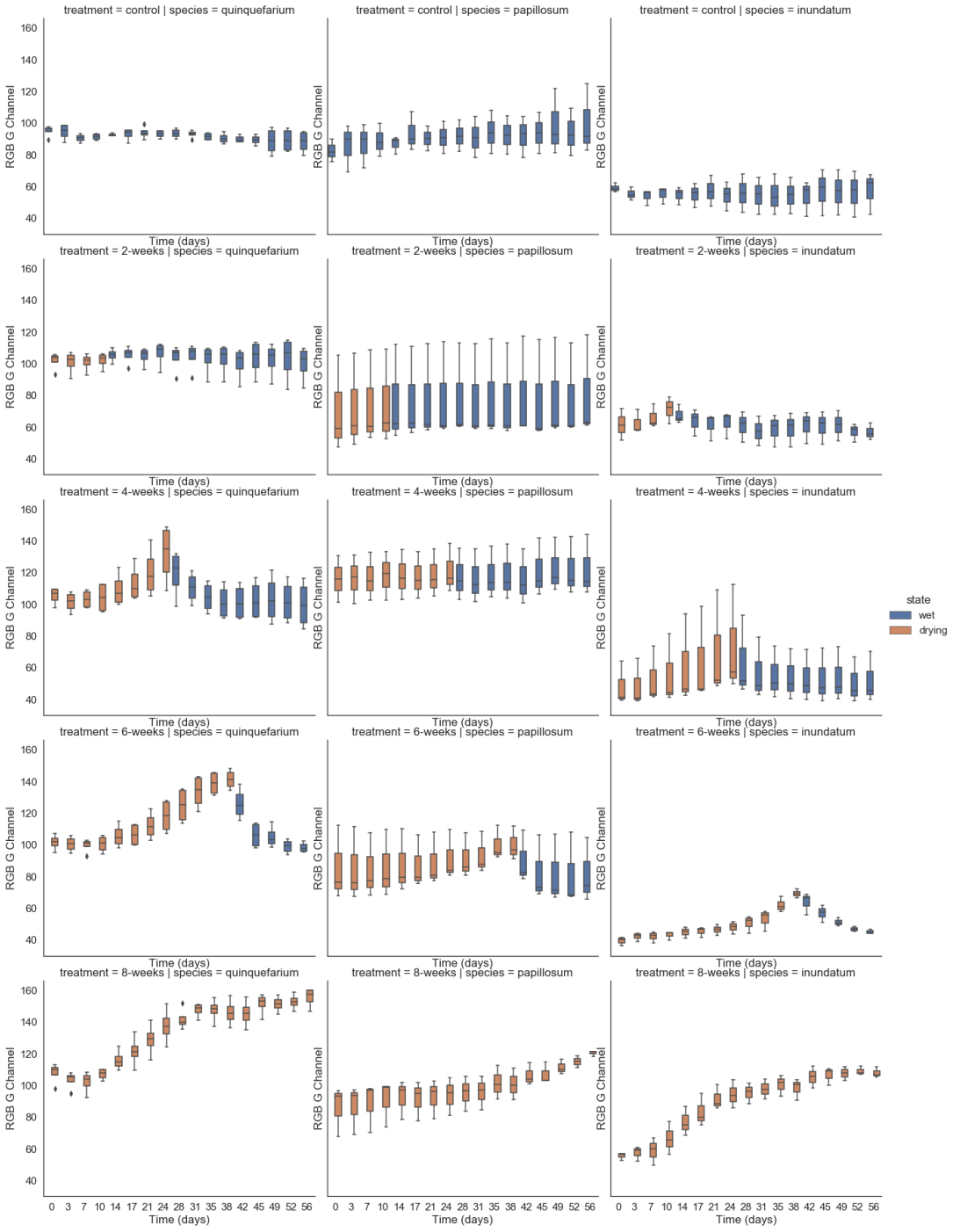

Supplementary Figure 5.9. Progression of the RGB G channel over time.

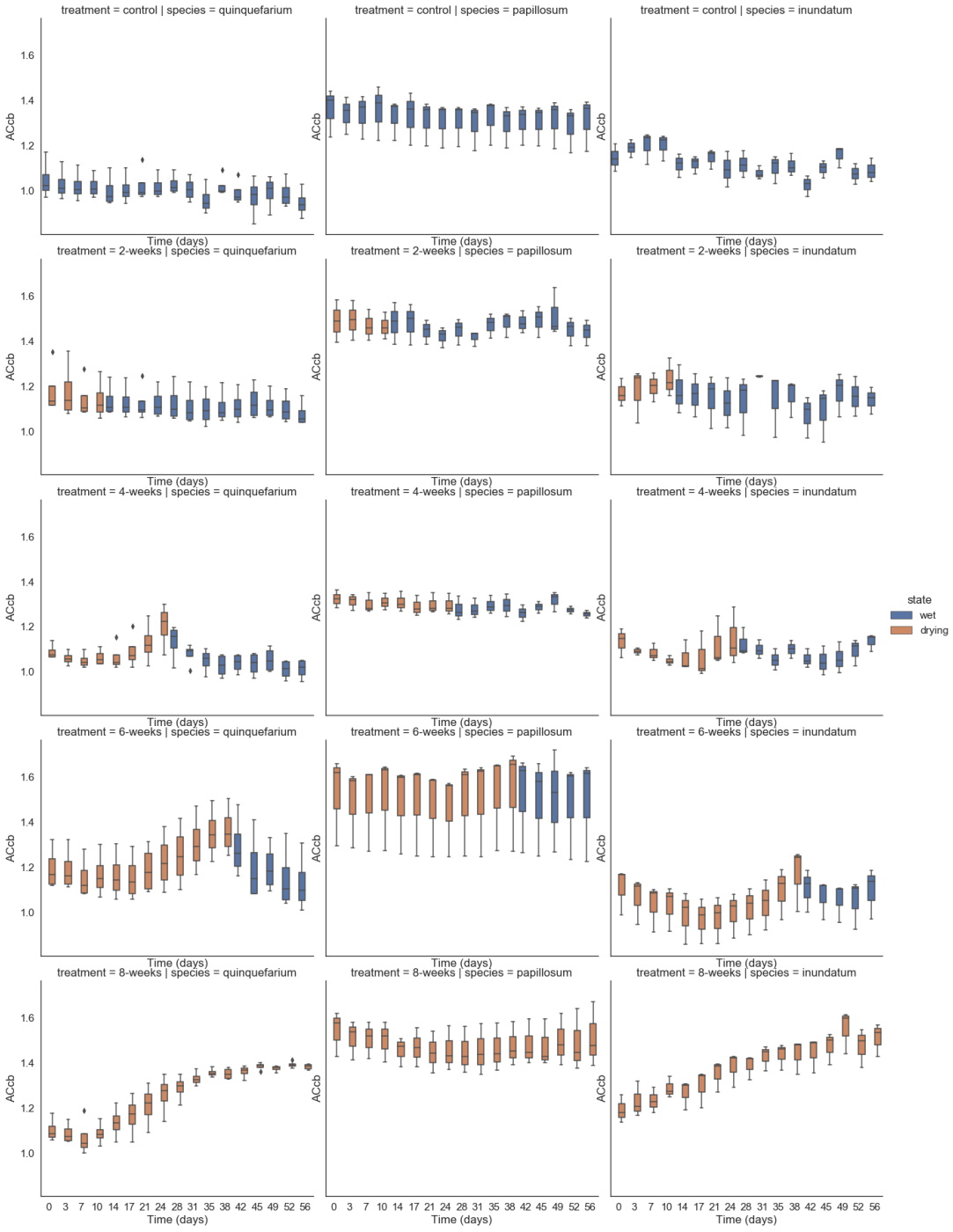

Supplementary Figure 5.10. Progression of the AC_{cb} index over time.

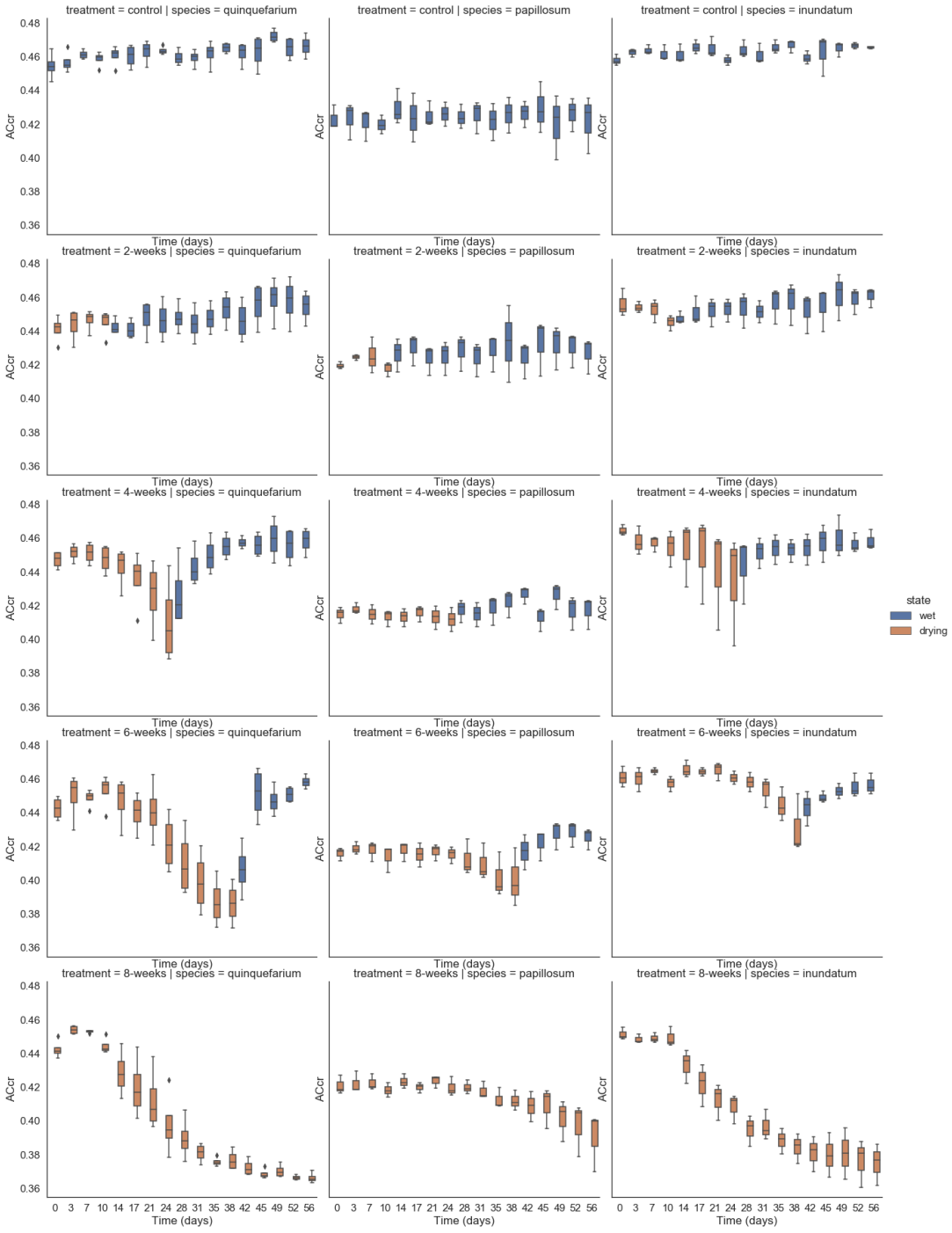

Supplementary Figure 5.11. Progression of the AC_{cr} index over time.

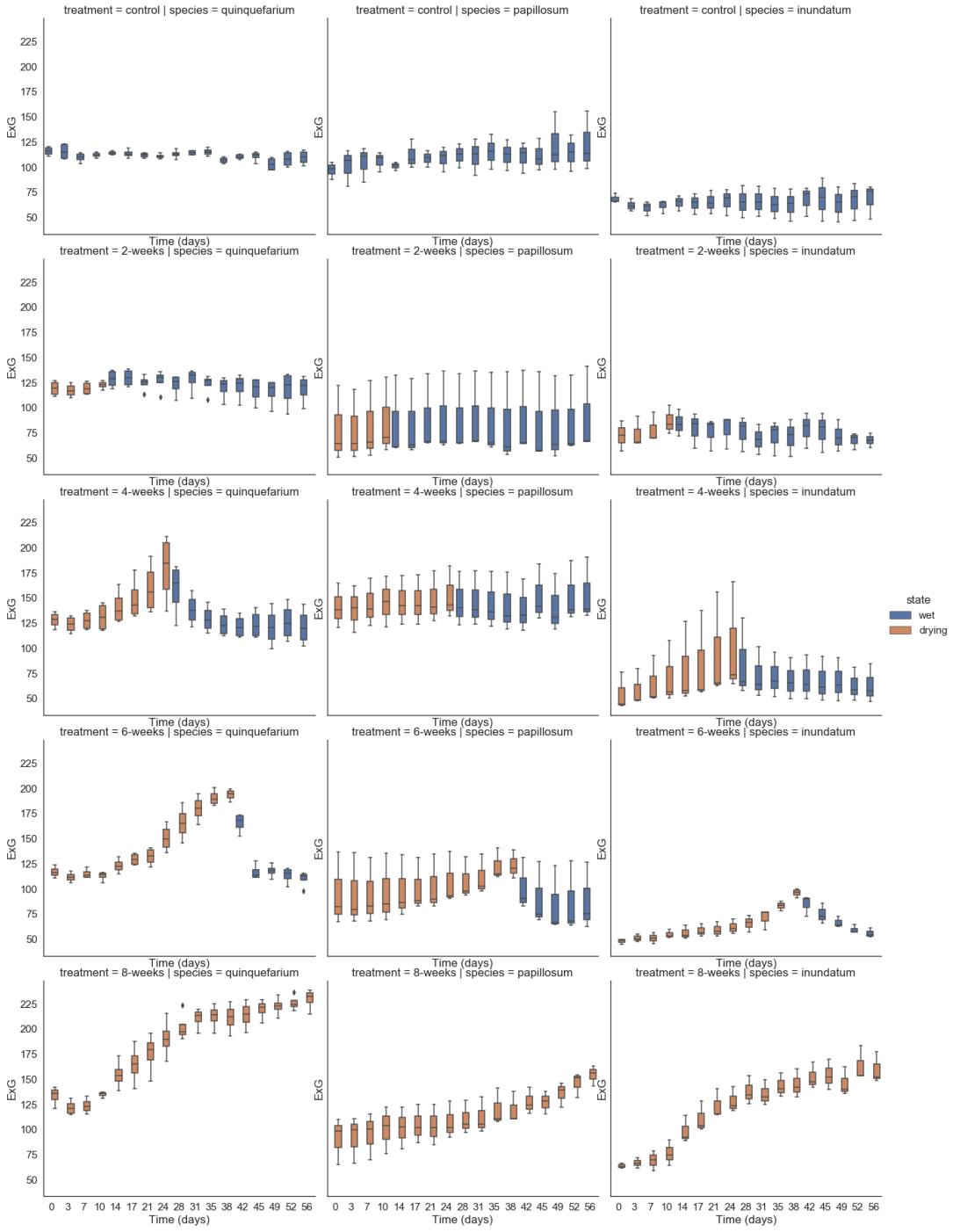

Supplementary Figure 5.12. Progression of the EXG index over time.

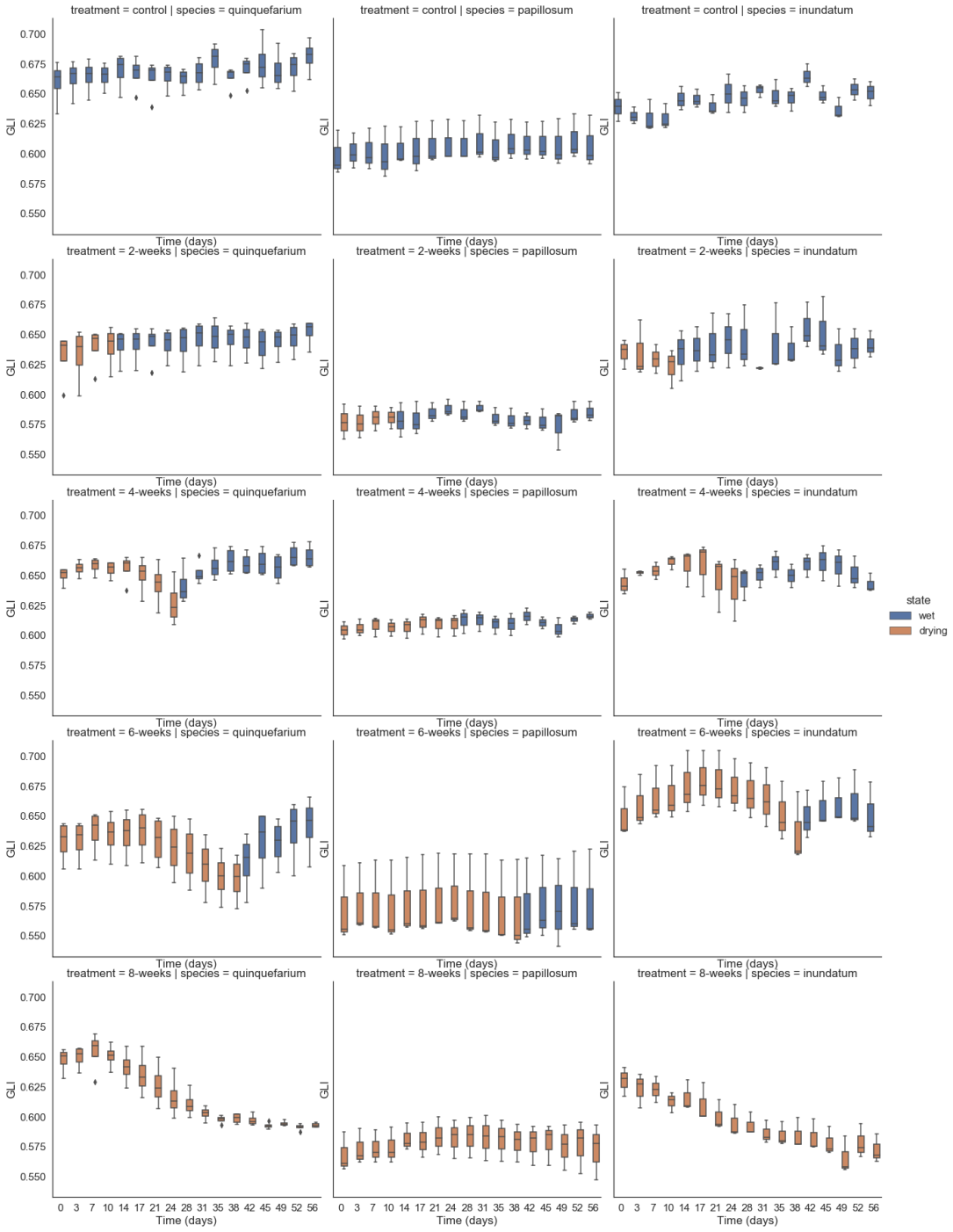

Supplementary Figure 5.13. Progression of the GLI index over time.

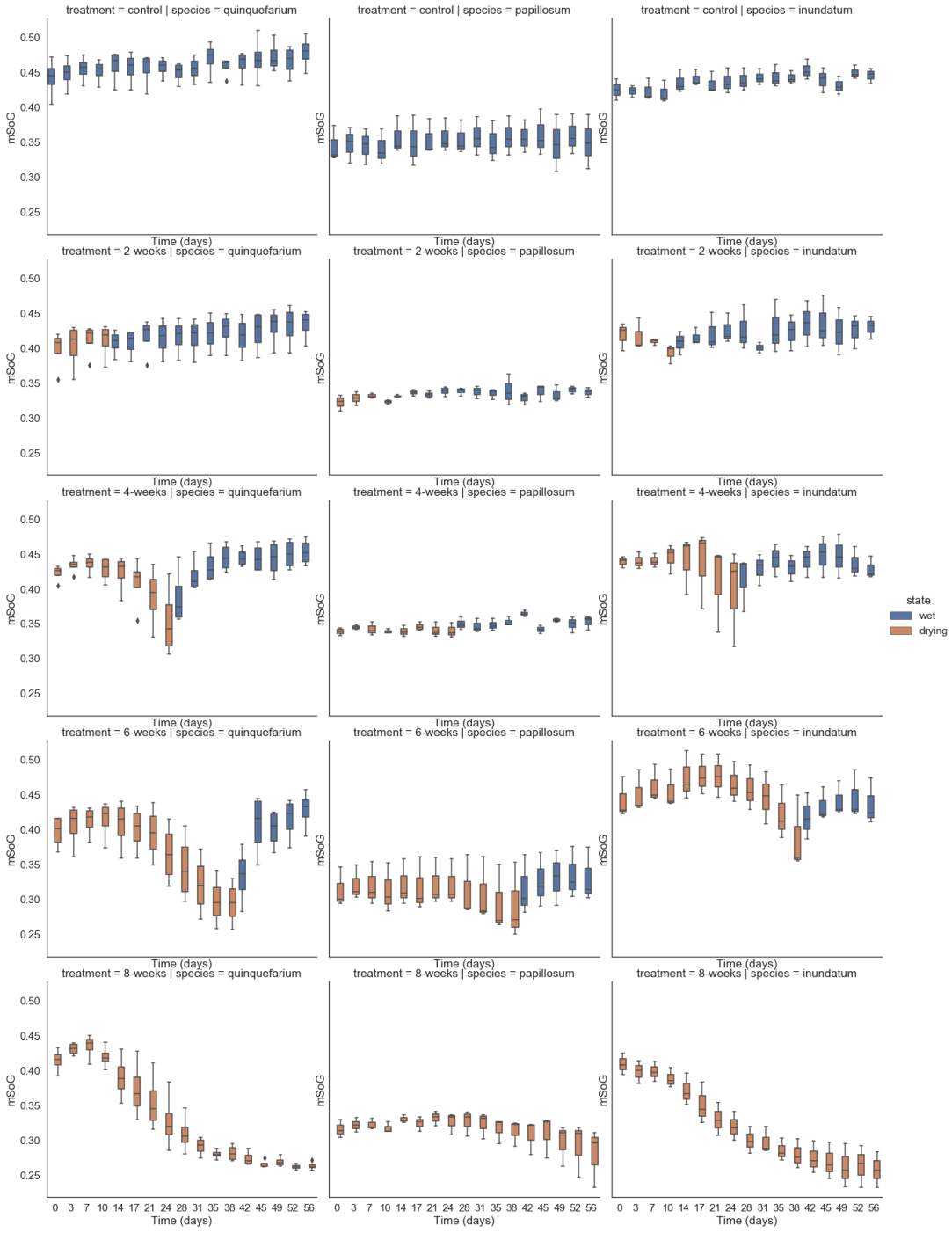

Supplementary Figure 5.14. Progression of the mSoG index over time.

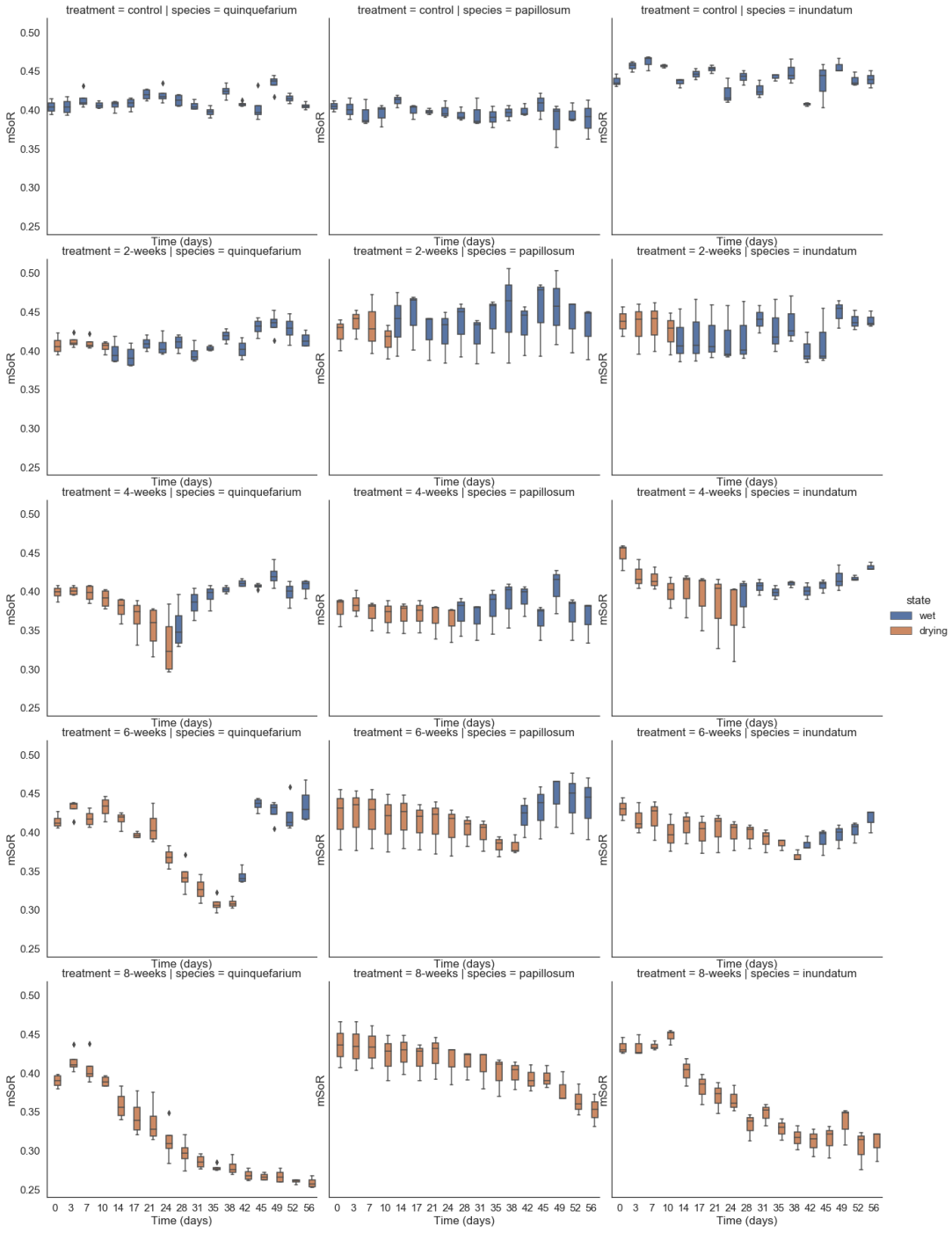

Supplementary Figure 5.15. Progression of the mSoR index over time.

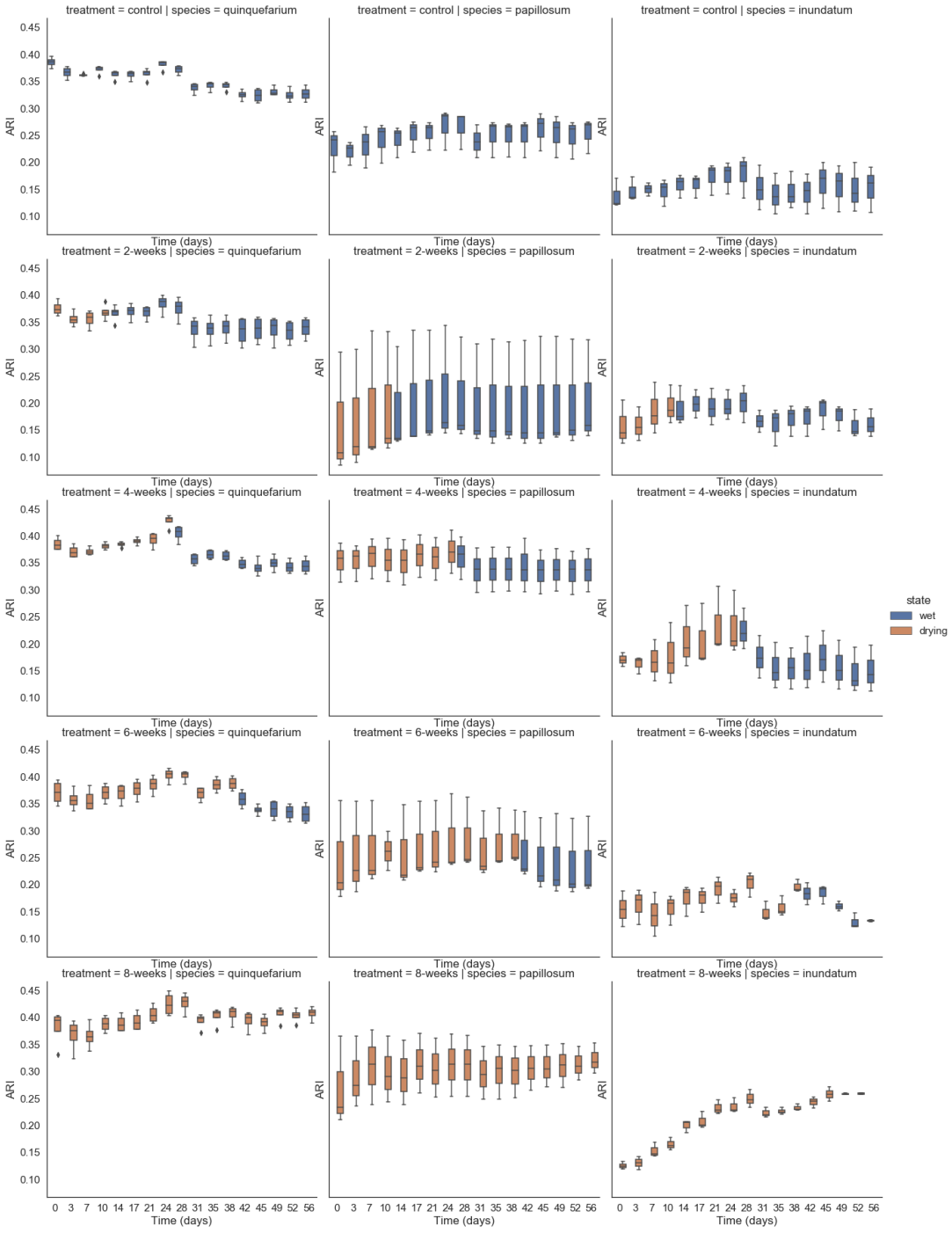

Supplementary Figure 5.16. Progression of the ARI index over time.

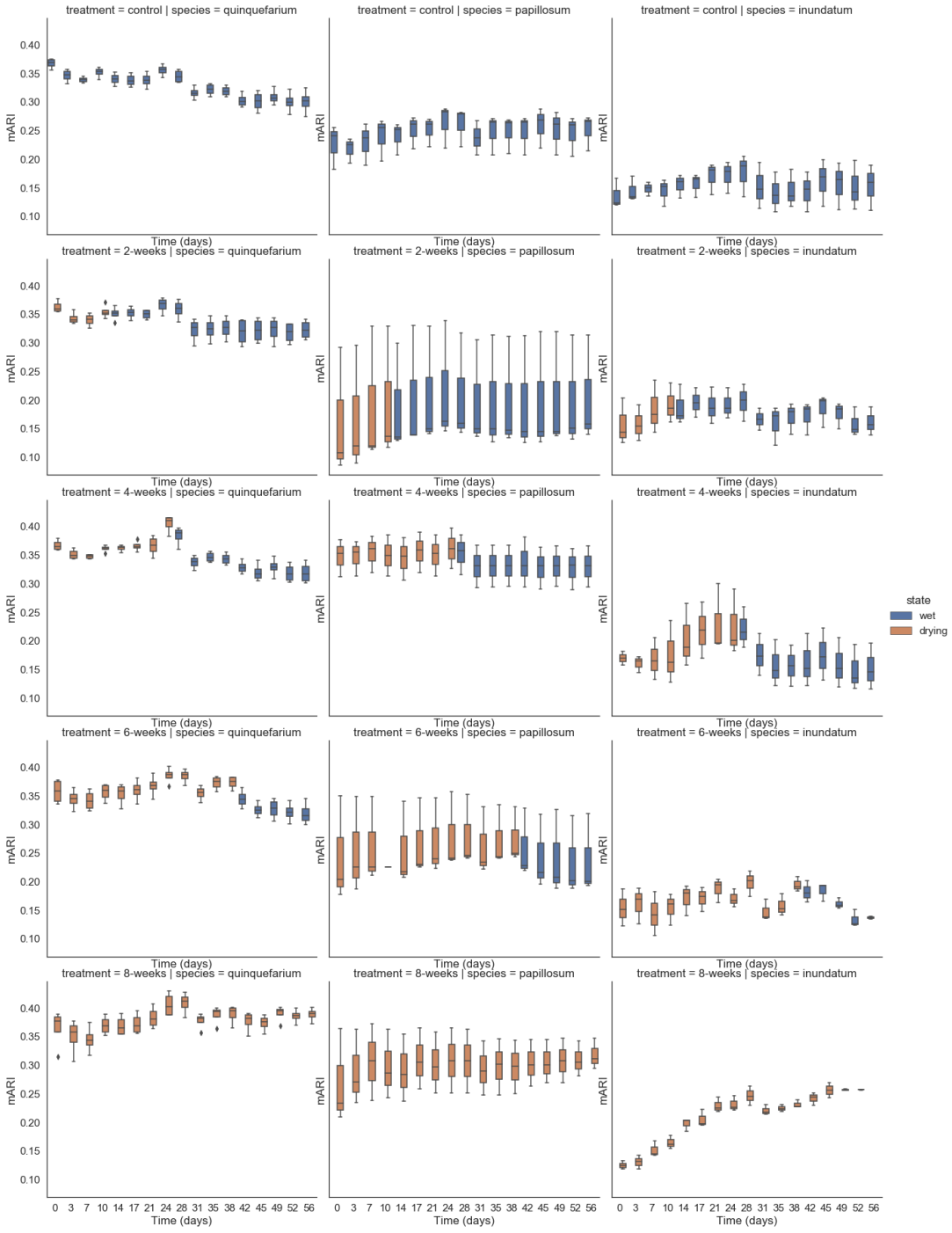

Supplementary Figure 5.17. Progression of the mARI index over time.

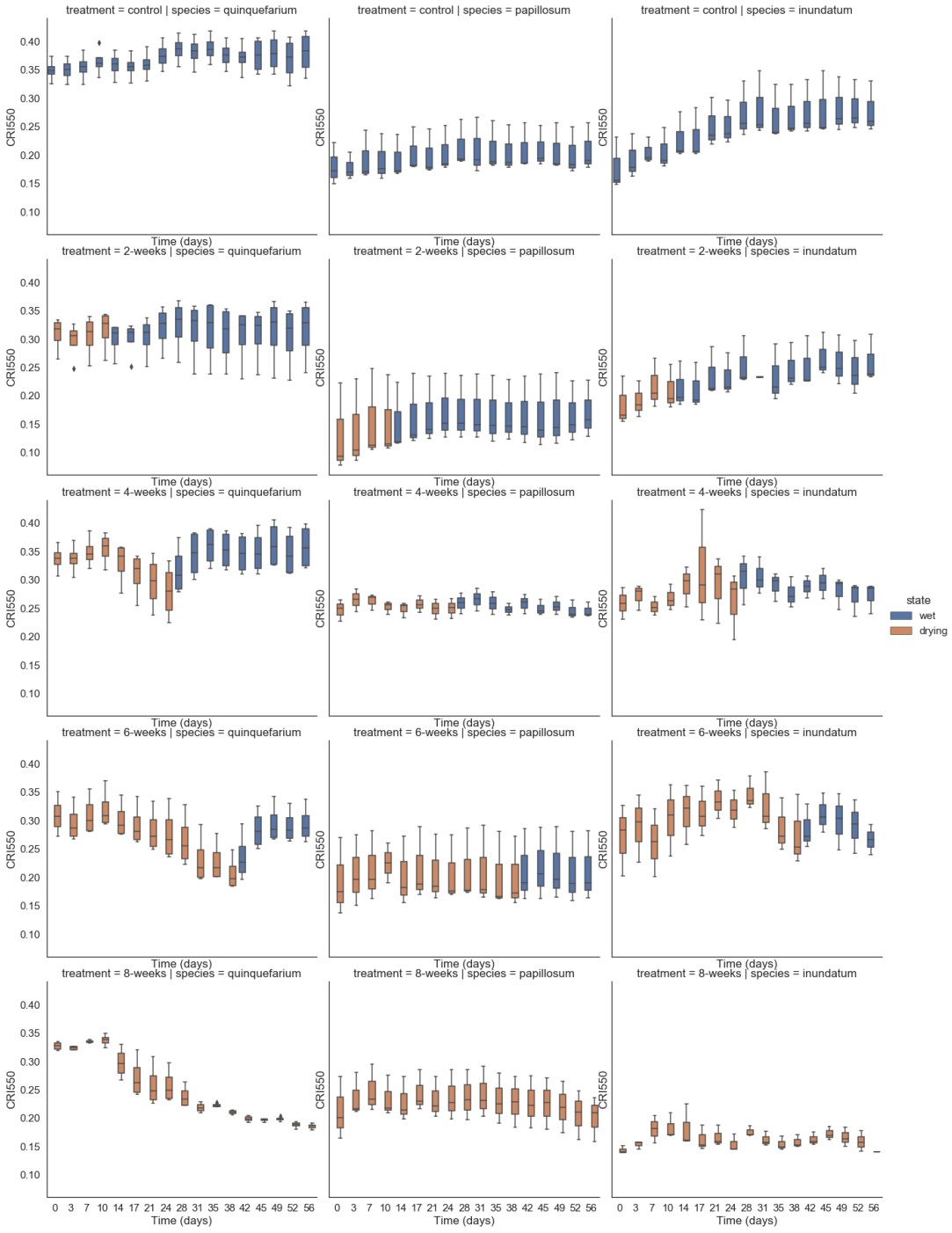

Supplementary Figure 5.18. Progression of the CRI550 index over time.

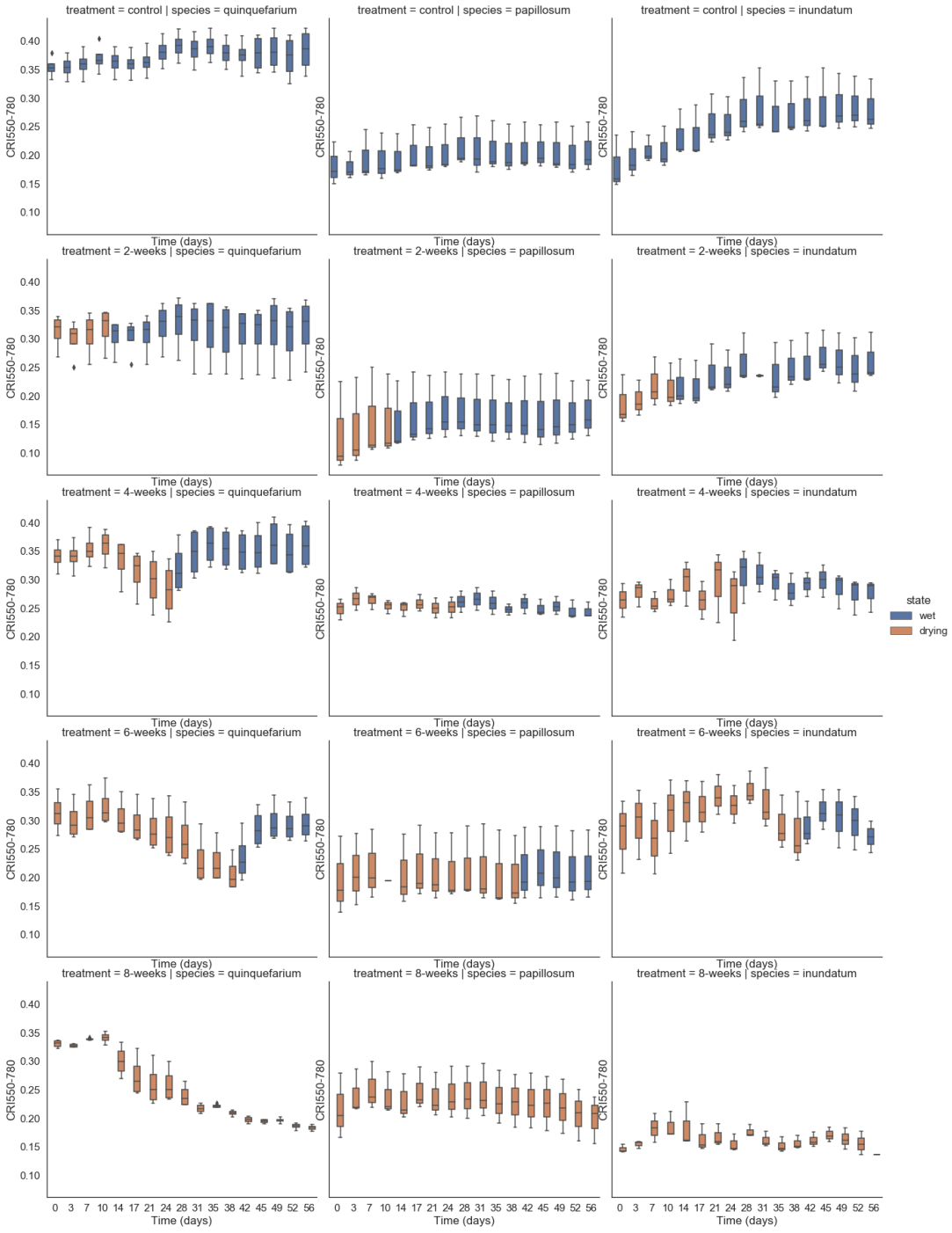

Supplementary Figure 5.19. Progression of the CRI550-780 index over time.

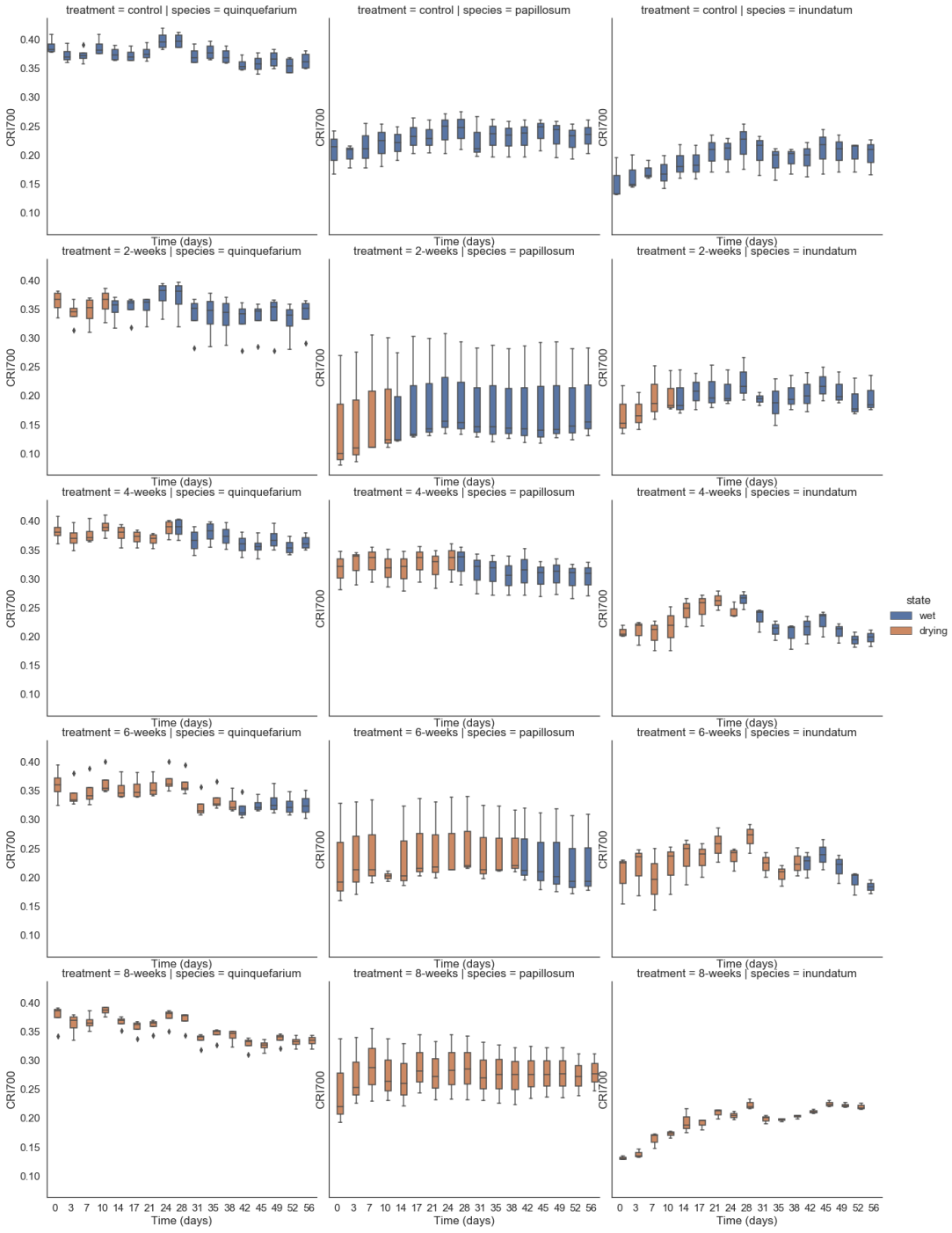

Supplementary Figure 5.20. Progression of the CRI700 index over time.

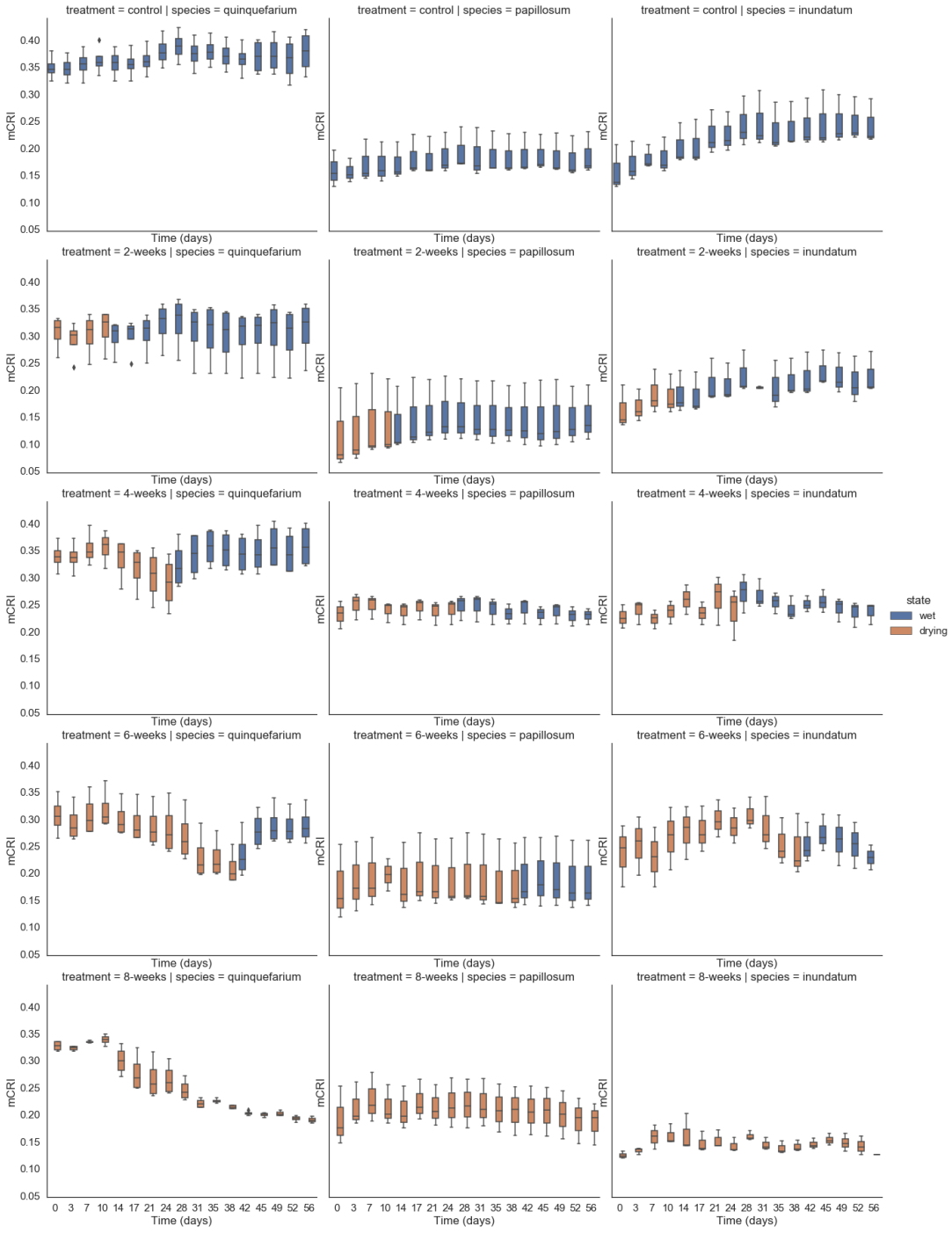

Supplementary Figure 5.21. Progression of the mCRI index over time.

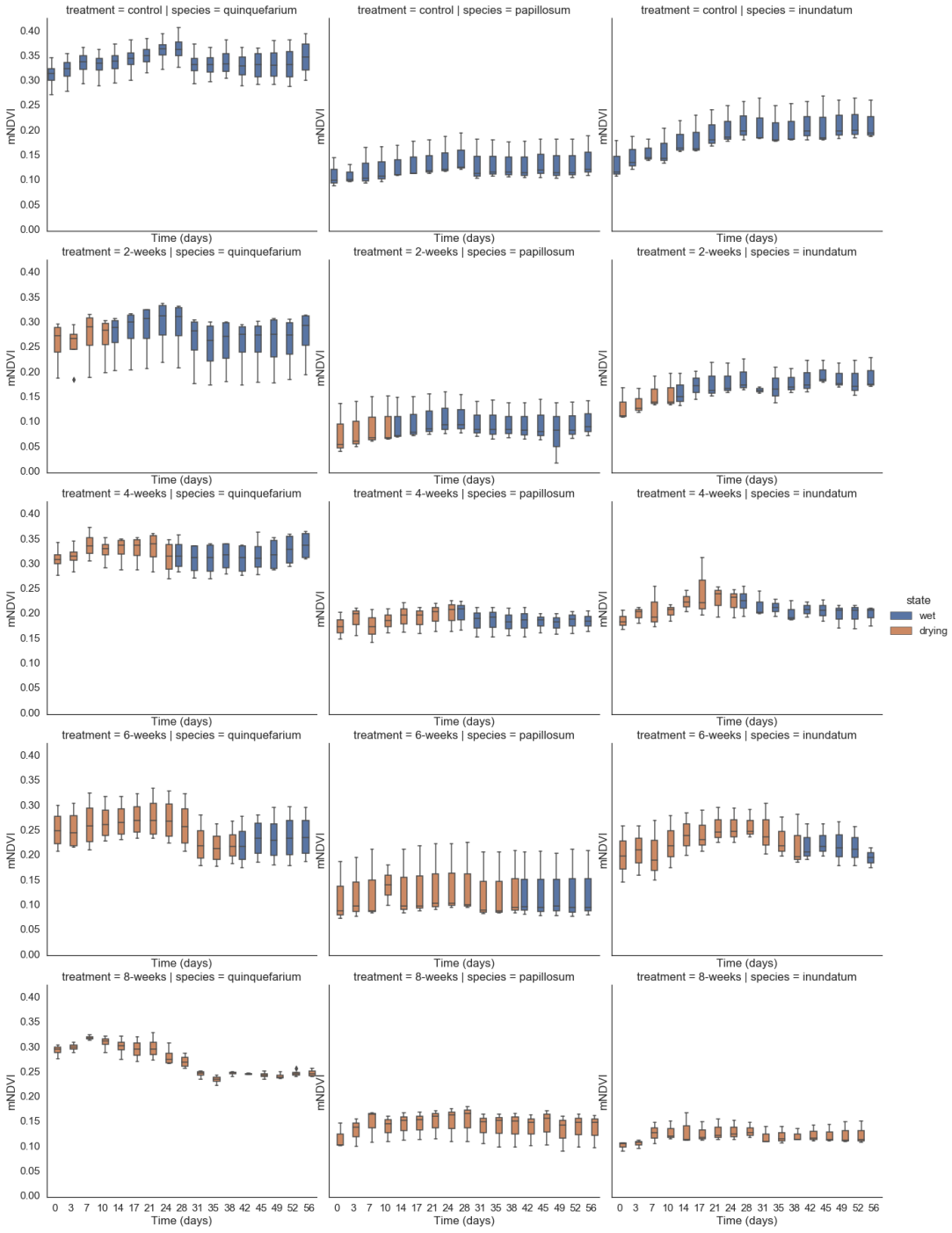

Supplementary Figure 5.22. Progression of the mNDVI index over time.

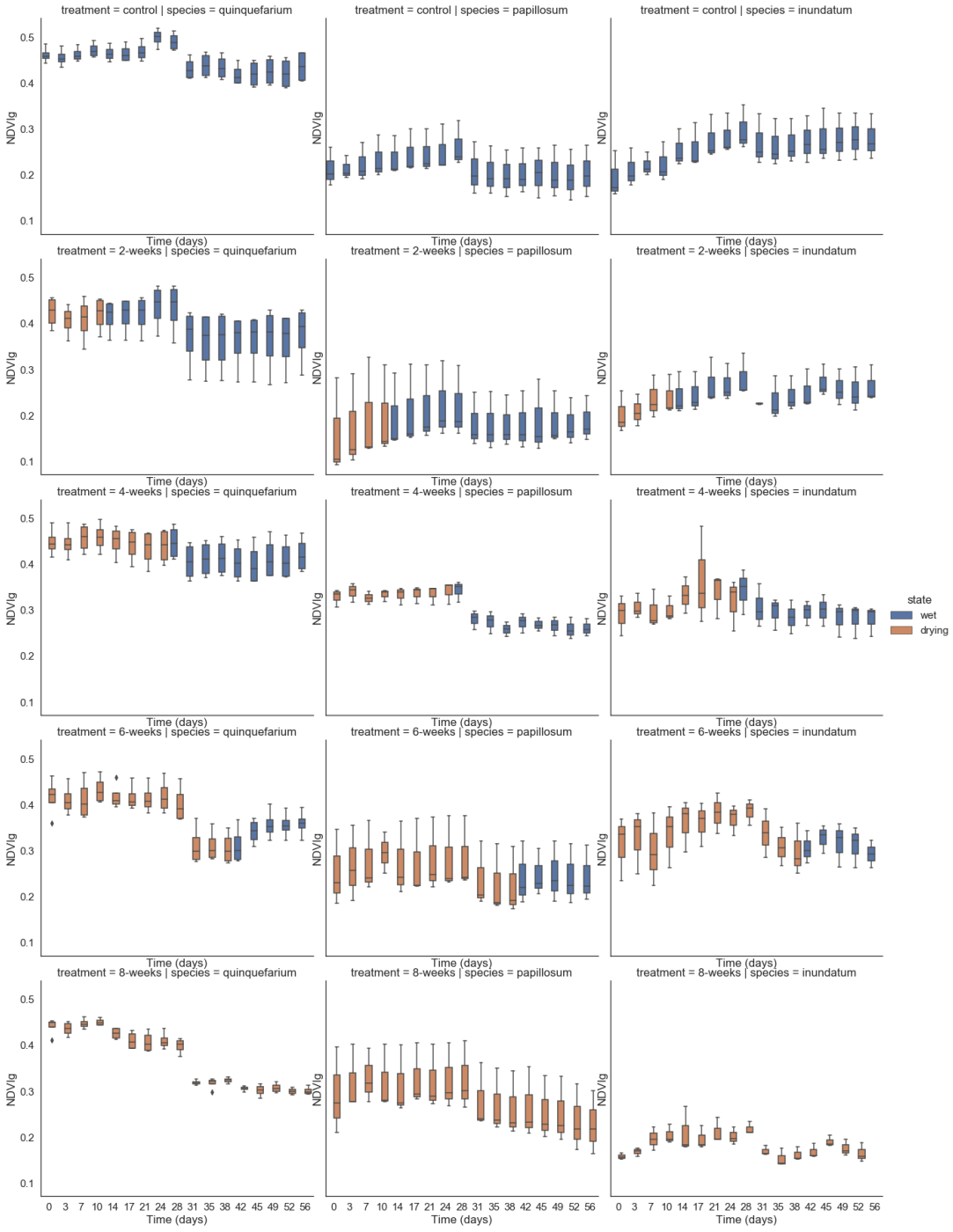

Supplementary Figure 5.23. Progression of the NDVIg index over time.

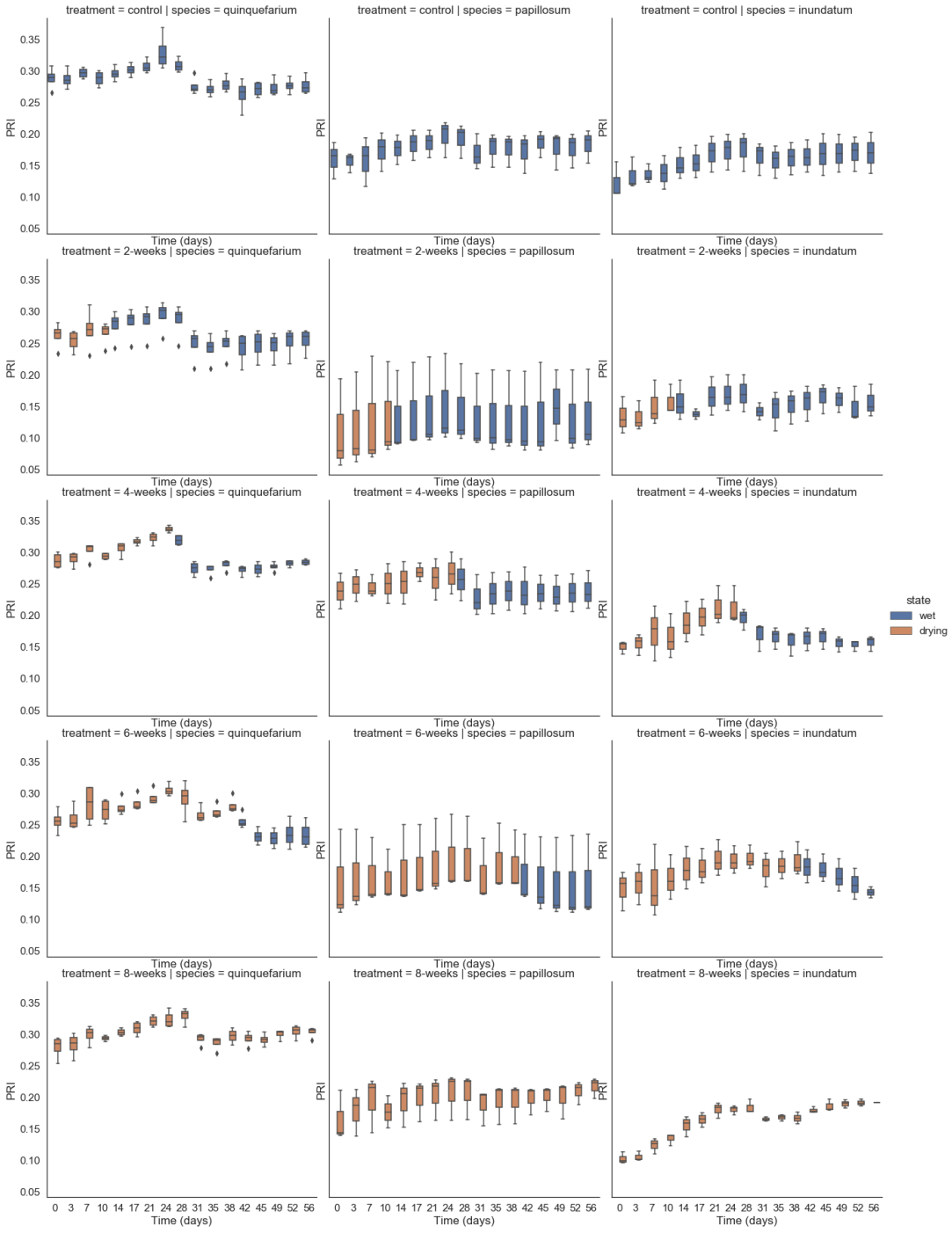

Supplementary Figure 5.24. Progression of the PRI index over time.

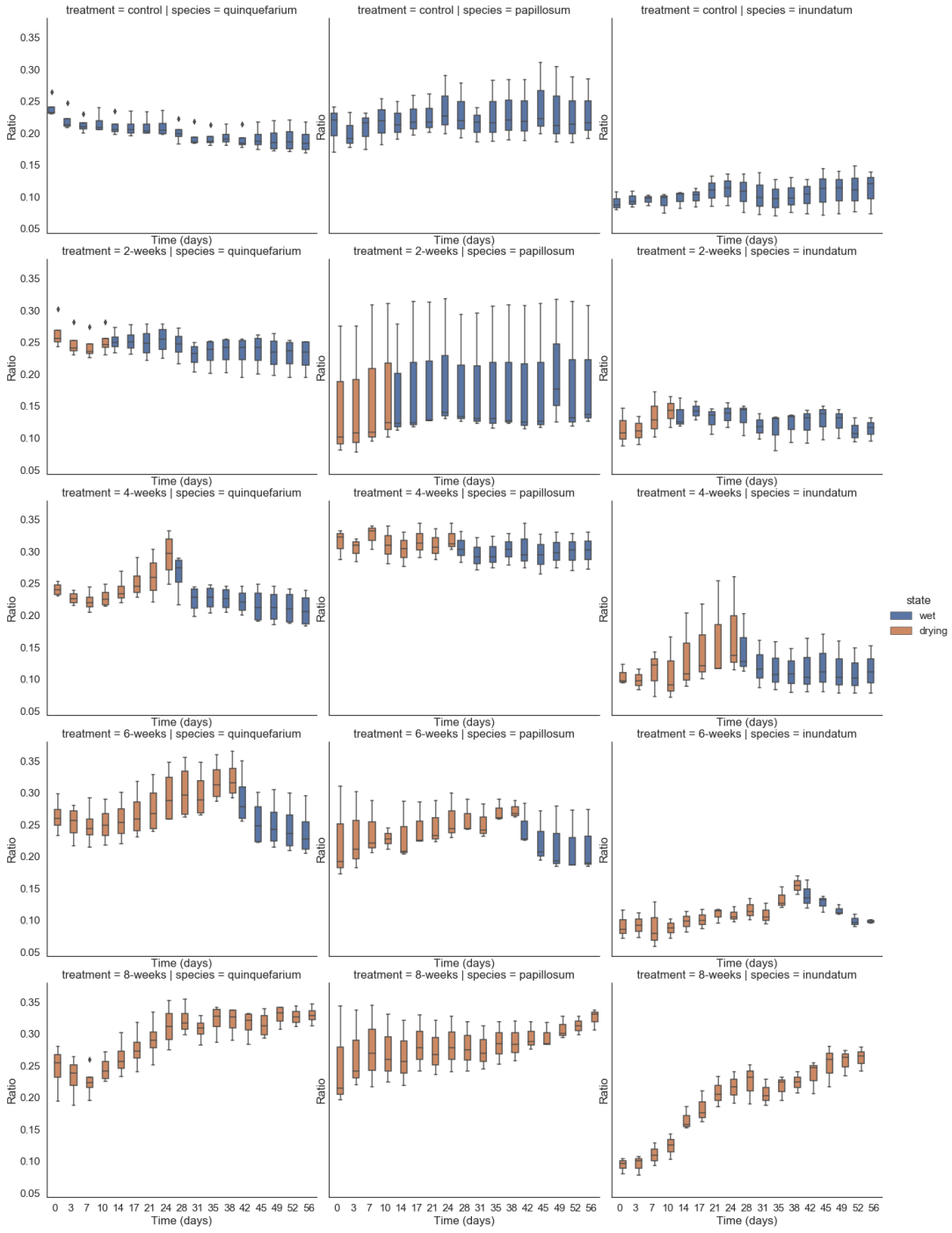

Supplementary Figure 5.25. Progression of the Ratio index over time.

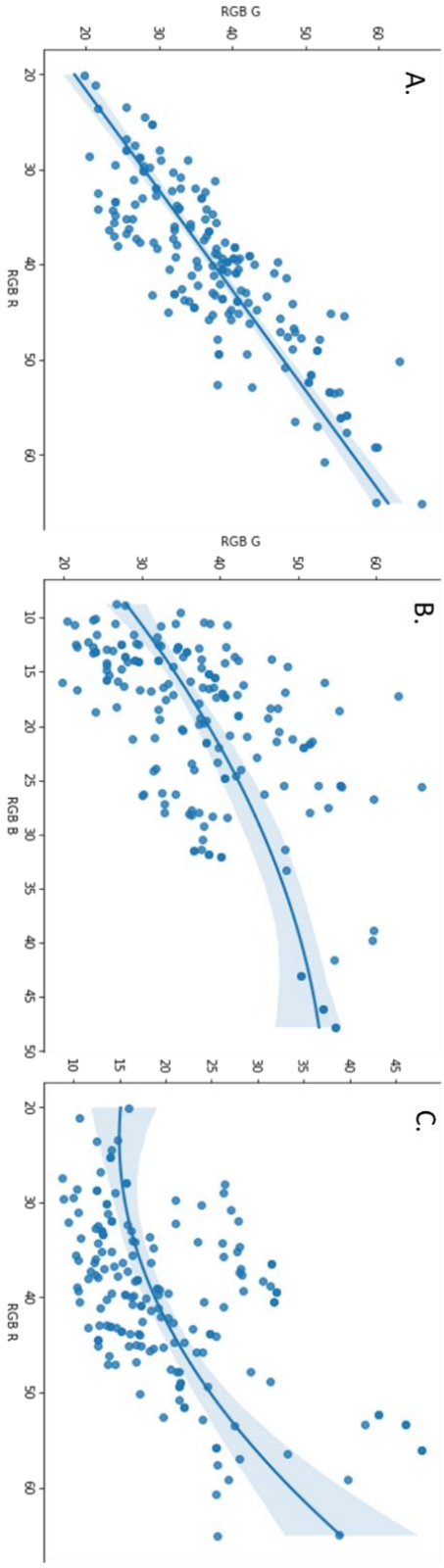

Supplementary Figure 5.26. Correlations between the three RGB colour channels for the field-collected image data.
While the R and G channels correlated linearly (A), these two channels were both non-linearly correlated with the B channel (B,C). Its exponential nature makes it more sensitive to lighting artefacts, and may influence the functionality of indices that rely on the B channel.

Chapter 6 Supplementary Figures

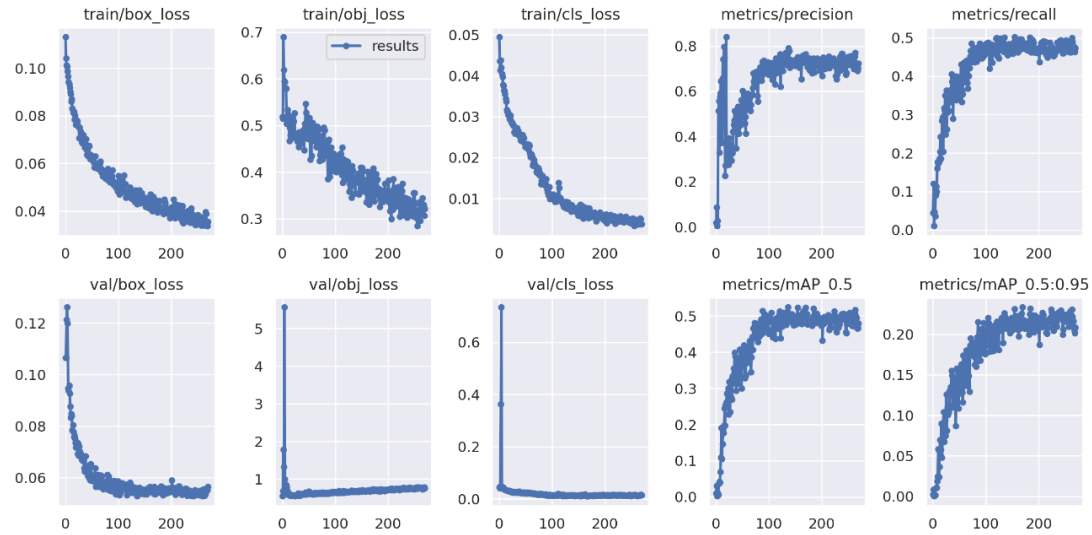

Supplementary Figure 6.1. Model parameter change during training per epoch.
The model has been trained for 269 epochs ended with precision at 0.72 and recall at 0.47. The testing set consisted of at least one image from each class except the MossR class, since the image quality of MossR class is not ideal. The resulting mean average precision (mAP_0.5) for the 15 validation images was 0.48.

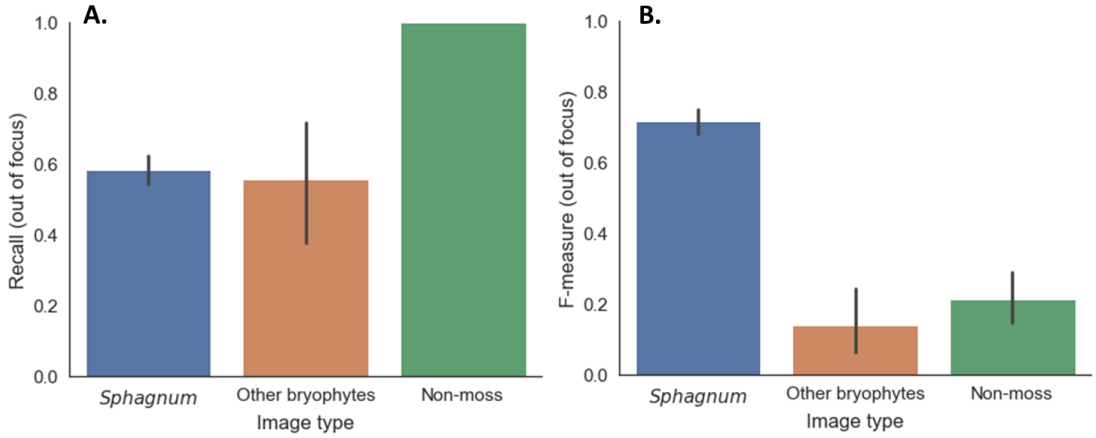

Supplementary Figure 6.2. Recall and F-measure when out of focus false negatives were considered.
A. As recall was generally a bit lower due to the larger number of false negatives, it still reached a value of almost 0.6 for *Sphagnum*, compared to 0.732 when they were not considered. B. The lower recall consequently also reduced the F-measure of the dataset, although it was still outperforming the testing dataset.

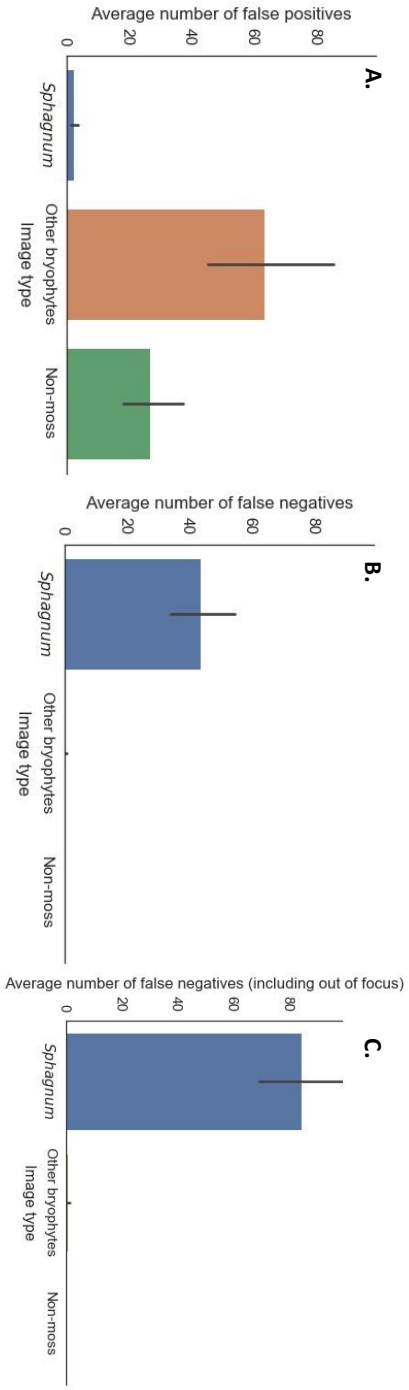

Supplementary Figure 6.3. Counts of false positives, negatives and out of focus false negatives.
A. *Sphagnum* had very few false positives, resulting in a very high precision score for the model. The other two image types, other bryophytes and non-moss, did get large numbers of false positives. As the other bryophyte category generally had more false positives than other moss, this suggests that the model may picking up other signals those images had in common with *Sphagnum*.
B. The number of false negatives for the *Sphagnum* class was relatively low, resulting in an average recall of 0.732.
C. When the out of focus false negatives were considered, this lowered to 0.583.

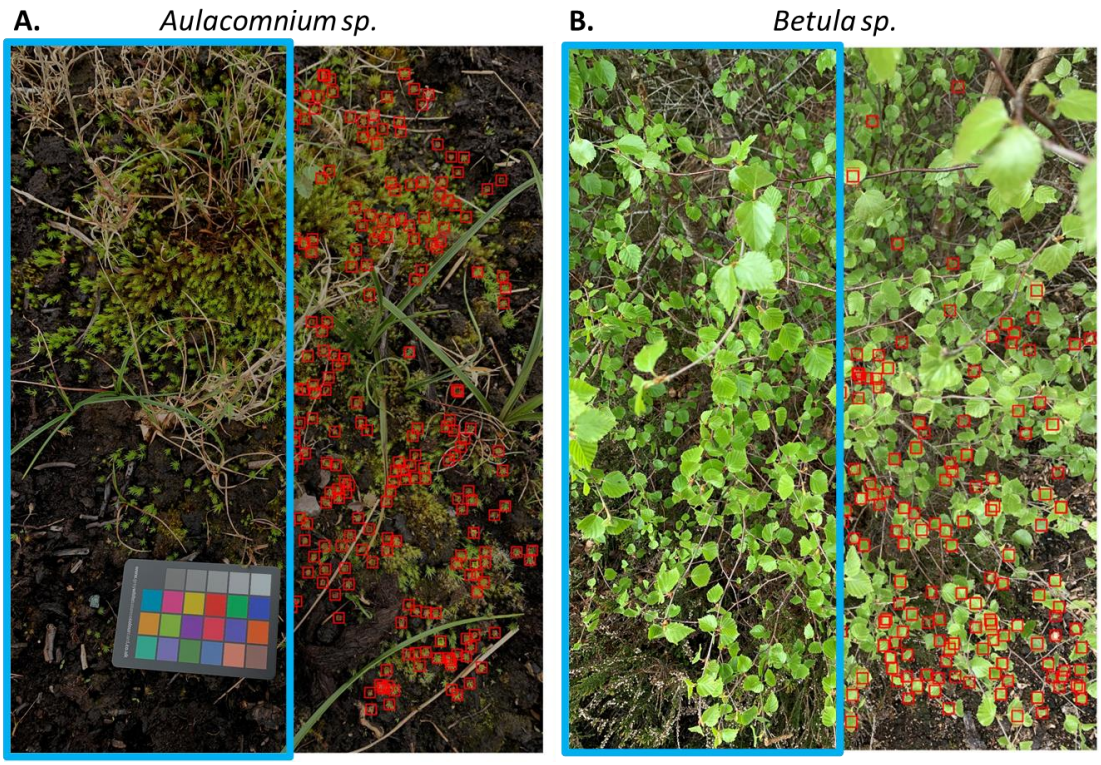

Supplementary Figure 6.4. Images with a large number of false positives from the non-*Sphagnum* classes.
A. This image of *Aulacomnium* sp. had the largest number of false positives of any image. Superficially, *Aulacomnium* plants resemble individual *Sphagnum* spreading branches.
B. False positives on a *Betula* sapling. The most obvious reason why these leaflets were detected is colour.
On both these images, the majority of annotations are in the MossG category, which is the most common category for false positives. This class was designed for wet green plants close to the water table, which may lack much of the typical Sphagnum morphological characteristics.

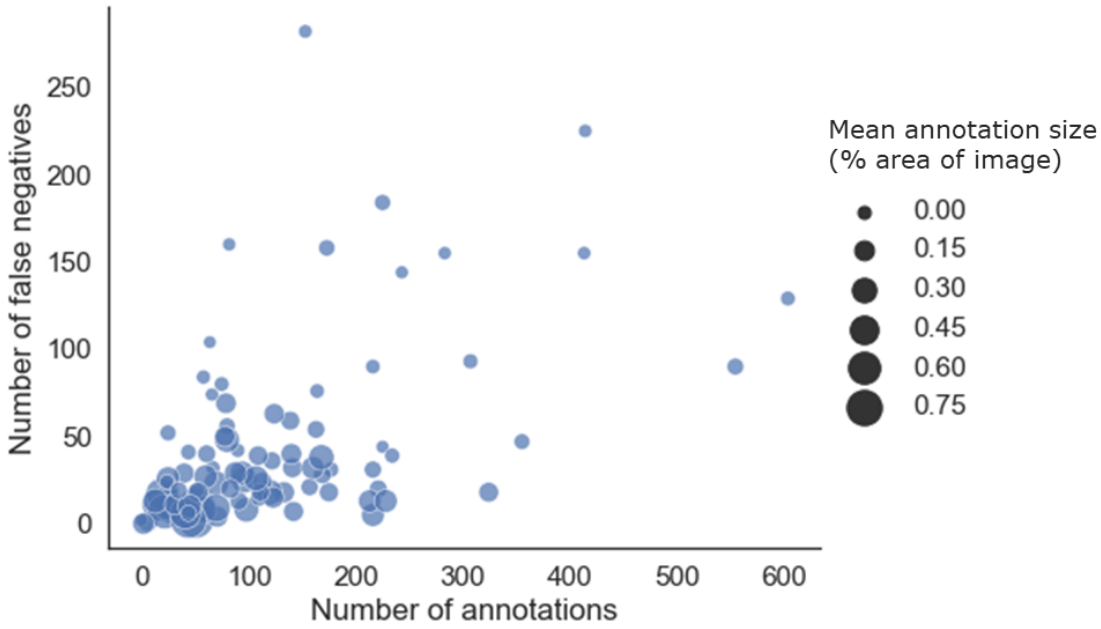

Supplementary Figure 6.5. Spatial dstribution of the number of false negatives against the total number of annotations.
Marker size corresponds to the mean relative annotation size (% of image size). The majority of false negatives corresponded to smaller marker sizes, signifying that images with smaller plants were more prone to miss annotations.

Appendix 2 - Supplementary Tables

Chapter 2 Supplementary Tables

Supplementary Table 2.1. List of the primers used in this study

Primer Name	Sequence	Purpose	(Physcomitrium patens v3.3, DOE-JGI, https://phytozome-	Gene (Sphagnum fallax v0.5, DOE-JGI, http://phytozome.jgi.doe.gov/info/Sfallax_v0_5)	Gene (Sphagnum fallax v1.1, DOE-JGI, http://phytozome.jgi.doe.gov/info/Sfallax_v1_1)	Reference
EF1α_Fw	TTGCGCTGTTCTCATCATCG	qPCR reference gene		Sphfalx0026s0086	Sphfalx03G087000	doi.org/10.1016/j.ppees.2019.02.004
EF1α_Rv	ATCTGGTCCAAGGCTTCCAA	qPCR reference gene		Sphfalx0026s0086	Sphfalx03G087000	doi.org/10.1016/j.ppees.2019.02.004
GAPDH_Fw	GCAGTGACGTGTCTTCCACT	qPCR reference gene		Sphfalx0068s0064	Sphfalx16G076000	doi.org/10.1016/j.ppees.2019.02.004
GAPDH_Rv	CCAGGCTACAACCTTGACCA	qPCR reference gene		Sphfalx0068s0064	Sphfalx16G076000	doi.org/10.1016/j.ppees.2019.02.004
AWPM19_domain_Fw	GACTTGGGAGAGGGTTGTCT	qPCR	Pp3c4_30620V3.1	Sphfalx0106s0009	Sphfalx10G088400	doi.org/10.1111/j.1469-8137.2007.02187.x
AWPM19_domain_Rv	CGCTCGCTATCAGTGCAATT	qPCR	Pp3c4_30620V3.1	Sphfalx0106s009	Sphfalx10G088400	doi.org/10.1111/j.1469-8137.2007.02187.x
Synaptotagmin_Fw	ATGTGTTGGGTGGGGATCTT	qPCR	Pp3c20_8650V3.1	Sphfalx0162s0043	Sphfalx05G060600	doi.org/10.1111/j.1469-8137.2007.02187.x
Synaptotagmin_Rv	AGTTCTTTGCACGGACAACC	qPCR	Pp3c20_8650V3.1	Sphfalx0162s0043	Sphfalx05G060600	doi.org/10.1111/j.1469-8137.2007.02187.x
LEA_Fw	CGATGTCGCAGTATACGCAG	qPCR	Pp3c12_22320V3	Sphfalx0198s0014	Sphfalx15G002200	doi.org/10.1111/j.1469-8137.2007.02187.x
LEA_Rv	GTGGAATCTGCAGCTTGGTC	qPCR	Pp3c12_22320V3	Sphfalx0198s0014	Sphfalx15G002200	doi.org/10.1111/j.1469-8137.2007.02187.x
SfABI3_16_Fw	TGACAGACATCAGGCCAACT	qPCR		Sphfalx0016s0174	Sphfalx01G102500	
SfABI3_16_Rv	CCCTTCTTTCAGCGTGAGAC	qPCR		Sphfalx0016s0174	Sphfalx01G102500	
SfABI3_16_attB1	GGGGACAAGTTTGTACAAAAAAGCAGGCTCG ATGGCTGGGGGAAGAGGAAAGG	cloning		Sphfalx0016s0174	Sphfalx01G102500	
SfABI3_16_attB2	GGGGACCACTTTGTACAAGAAAGCTGGGTTT CAACTTGCTGGCTCAATCTTTG	cloning		Sphfalx0016s0174	Sphfalx01G102500	
Primer Name	**Sequence**	**Purpose**				**Reference**
PpABI3A_F1cacc	CACCATGGTGCTCCTATCGAGTGT	cloning	Pp3c2_3370V3			
PpABI3A_R1	TCATCCTGCGGGCTCGGT	cloning	Pp3c2_3370V3			
PpEF1aFw	AATCATACATTTCACCTCGCC	qPCR reference gene	Pp3c2_10310V3			doi: 10.1371/journal.pone.0070998
PpEF1aRv	GATCAGTGGGTAGAAGTGAC	qPCR reference gene	Pp3c2_10310V3			doi: 10.1371/journal.pone.0070998
pTA1cF1	TGAGAAGCCACAACTTTTGGAA	insertion check				
pTA1-3F1	TACAAACCTGTGGACCGCCACGATGCGGT	insertion check				
pTA1cR1	TGCACCCGCTTAAGATGTTC	insertion check				
PpEF1aR1	AATTGATATTGCATGTGTTTTGA	insertion check				
n-F2	AGGAGGAAGACAAGGAAGGATAAGGTTGCA	insertion check				
nat1-atg	ATCACCACTCTTGACGACACGGCT	insertion check				
nat1-tga	GGGGCAGGGCATGCTCATGTA	insertion check				

Chapter 4 Supplementary Tables

Supplementary Table 4.1. Equations used to obtain colour channel image representations, Chromatic difference, HSV difference and Green difference.

Constructed colour channels	Equation
Chromatic difference	$\left(\frac{\text{RGB blue}+\text{RGB red}}{2}\right) - \text{RGB green}$
HSV difference	$\frac{(\text{HSV H} * 2) + \text{HSV V}}{2} - \text{HSV S}$
Green difference	$\left(\frac{(\text{RGB green} * 2) + \text{RGB blue}}{2}\right) - \text{RGB red}$

Supplementary Table 4.2. General ranges of lower threshold values for channel HSV S. Threshold values are mostly dependent on the amount of non-moss material in an image, lighting and the colouration of the *Sphagnum*.

Image characterisation	Lower threshold range	Lower threshold mean	Upper threshold
Pale discoloured *Sphagnum*, bright image	80-140	107	256
Wet saturated, dark image	50-200	157	256
Intermediates	50-180	110	256
		125	256

Supplementary Table 4.3. Location and species distribution of the 68 images that have been thresholded in HSV S and annotated in YCrCb Cb.

Location	Species	n images
Coed y Darren	*S. quinquefarium*	12
Pen y Garn	*S. fallax*	8
	S. inundatum	4
	S. papillosum	11
	S. fallax & S. papillosum (mix)	4
Llyn Pendam	*S. auriculatum*	11
	S. fallax	10
	S. papillosum	8
Total		68

Supplementary Table 4.4.Linear model showing the relationship between the automated counts and the manual counts.
This relationship was highly significant and there was no significant effect of species.

Model	Estimate	Std. Error	t-value	p-value	R^2	Df	AIC	Residual standard error
Intercept (*S. quinquefarium*)	69.88	8.33	8.39	1.38E-11***	0.63	58	513.3	12.57
Manual count	0.483	0.064	7.53	3.81E-10***				
S. fallax	-2.55	4.71	-0.542	0.590 ns				
S. papillosum	9.26	5.34	1.73	0.088 ns				
S. inundatum	-10.69	7.91	-1.35	0.182 ns				
S. auriculatum	-9.56	5.68	-1.68	0.098 ns				

Supplementary Table 4.5. Log model showing the relationship between the automated counts and the manual counts.
This relationship was highly significant and there was no significant effect of species except for *S. auriculatum*.

Model	Estimate	Std. Error	t-value	p-value	R^2	Df	AIC	Residual standard error
Intercept (*S. quinquefarium*)	-80.47	26.32	-3.06	0.00337**	0.65	58	509.92	12.24
Log Manual count	100.39	12.66	7.93	8.04E-11***				
S. fallax	-2.31	4.59	-0.50	0.616 ns				
S. papillosum	10.29	5.24	1.97	0.054 ns				
S. inundatum	-10.12	7.70	-1.32	0.194 ns				
S. auriculatum	-11.59	5.42	-2.14	0.037*				

Supplementary Table 4.6. The mean value per species of the automated count and the manual count and the resulting correction factor calculated from those values. These correction factors can be used to adjust the automated count to match those of human counters.

Species	Mean automated count (grid)	Mean manual count (grid)	Resulting correction factor
S. quinquefarium	126.3	117.0	0.93
S. fallax	120.0	109.2	0.91
S. papillosum	115.6	75.5	0.65
S. inundatum	92.0	68.0	0.74
S. auriculatum	100.5	83.2	0.83

Chapter 5 Supplementary Tables

Supplementary Table 5.1. The Spearman rho correlation values for capitulum water content, chlorophyll *a*, *b* and carotenoids with each of the RGB variables and multispectral indices of all species combined.
The strongest correlation in each row has been highlighted in bold and blue.

Variable	Subject	RGB G	RGB R	Ac_{cb}	Ac_{cr}	BGR	ExG	GLI	MSoG	MSoR
Capitulum	all species	-0.45	-0.45	-0.2	0.45	-0.45	**-0.51**	0.21	0.36	0.49
water content	*S. quinquefarium*	**-0.65**	-0.6	-0.52	0.6	-0.6	**-0.65**	0.52	0.58	0.59
	S. papillosum	-0.27	-0.4	-0.31	0.53	**-0.55**	-0.25	0.31	0.47	0.16
	S. inundatum	-0.59	-0.57	-0.43	0.66	**-0.67**	-0.63	0.43	0.54	0.59
Chlorophyll *a*	all species	-0.47	**-0.53**	-0.4	0.51	-0.49	-0.46	0.41	0.48	0.3
	S. quinquefarium	-0.48	**-0.5**	-0.46	0.46	-0.45	-0.43	0.45	0.45	0.28
	S. papillosum	-0.36	**-0.42**	0.09	0.35	-0.33	-0.34	-0.08	0.08	0.26
	S. inundatum	-0.63	**-0.66**	-0.58	0.47	-0.46	-0.56	0.6	0.58	0.19
Chlorophyll *b*	all species	-0.45	**-0.49**	-0.34	0.46	-0.44	-0.45	0.35	0.43	0.29
	S. quinquefarium	-0.45	**-0.48**	-0.44	0.44	-0.44	-0.41	0.44	0.44	0.26
	S. papillosum	-0.32	**-0.36**	0.1	0.32	-0.29	-0.29	-0.09	0.06	0.23
	S. inundatum	-0.62	**-0.63**	-0.52	0.42	-0.41	-0.55	0.54	0.53	0.2
Carotenoids	all species	-0.37	-0.44	-0.39	**0.46**	-0.45	-0.37	0.4	0.45	0.23
	S. quinquefarium	-0.42	**-0.43**	-0.39	0.4	-0.4	-0.39	0.39	0.39	0.27
	S. papillosum	-0.29	**-0.34**	0.06	0.31	-0.29	-0.26	-0.05	0.09	0.18
	S. inundatum	-0.55	**-0.59**	-0.57	0.43	-0.42	-0.48	0.58	0.55	0.15

Variable	Subject	ARI	mARI	CRI550	CRI550-780	CRI700	mCRI	mNDVI	NDVIg	PRI	Ratio
Capitulum	all species	-0.38	-0.38	0.07	0.07	-0.24	0	-0.13	-0.09	-0.32	**-0.42**
water	*S. quinquefarium*	-0.44	-0.46	0.55	0.55	0.28	0.53	0.33	0.47	-0.22	**-0.56**
content	*S. papillosum*	-0.27	-0.27	-0.13	-0.13	-0.25	-0.15	-0.07	-0.23	-0.19	**-0.37**
	S. inundatum	-0.56	-0.58	0.21	0.22	-0.27	0.2	0.19	0.21	-0.36	**-0.67**
Chlorophyll *a*	all species	-0.32	-0.34	0.31	0.31	-0.1	0.23	0.16	0.12	-0.16	**-0.48**
	S. quinquefarium	-0.34	-0.36	0.43	0.43	0.21	0.41	0.32	0.29	-0.1	**-0.47**
	S. papillosum	-0.36	-0.36	-0.18	-0.19	-0.33	-0.24	-0.23	-0.27	-0.32	**-0.39**
	S. inundatum	-0.4	-0.4	0.62	**0.63**	0.14	0.6	0.61	0.62	0.04	0.51
Chlorophyll *b*	all species	-0.34	-0.35	0.25	0.26	-0.13	0.18	0.1	0.06	-0.2	**-0.45**
	S. quinquefarium	-0.35	-0.37	0.4	0.4	0.16	0.38	0.3	0.25	-0.11	**-0.46**
	S. papillosum	-0.31	-0.31	-0.15	-0.16	-0.29	-0.2	-0.21	-0.24	-0.28	**-0.33**
	S. inundatum	-0.41	-0.41	**0.59**	**0.59**	0.1	0.57	0.58	0.58	0.01	-0.49
Carotenoids	all species	-0.23	-0.25	0.33	0.33	-0.02	0.27	0.2	0.16	-0.08	**-0.39**
	S. quinquefarium	-0.32	-0.34	0.38	0.38	0.18	0.36	0.27	0.25	-0.09	**-0.41**
	S. papillosum	-0.31	-0.31	-0.15	-0.16	-0.28	-0.19	-0.18	-0.24	-0.26	**-0.33**
	S. inundatum	-0.33	-0.34	**0.58**	**0.58**	0.16	0.57	0.57	**0.58**	0.07	0

Appendix 3 – Capitulum Counter Pipeline code

The code associated with Chapter 3

```
#########################################################################
#Install any
packages are
not already
available on
your
computer
                #You can copy paste the names of the packages below into the
                install line on numpy's position
                #These include:
                # numpy, pandas, matplotlib, opencv-python, plantcv, scikit-
                image, glob3 (if it does not work while importing)
                import sys
                get_ipython().system('{sys.executable} -m pip install numpy')


                #1
                #Load libraries
                import numpy as np
                import pandas as pd
                import matplotlib.pyplot as plt
                import cv2
                from plantcv import plantcv as pcv
                import glob
                from skimage import exposure, feature
                import json
                import os
                import sys
                import PySimpleGUI as sg
                from PIL import Image


                #2
                #Set the source folder to the folder that contains your image
                ('C:/abc/dfg/')
                #Set filename to the name of the image ('image.jpg')
                #Set the destination folder to the folder where you want the
                results to be saved
                #Set the lower limit of the threshold. You can find a table with
                ranges in the guide
                source_folder = 'C:/Users/abc/def/' #Use / in the file path,
                otherwise Python does not understand
```

```
fileformat = '.jpg' #The format of your images. the format
(.jpg) will help to load in the correct images
destination_folder = 'C:/Users/abc/def/ghi/' #making a separate
folder for your data makes it easier to find



#2
#Define functions for every step of the pipeline. You do not
have to change anything here!
#order_points will find the corners of the box
def order_points(pts):
    # initialise a list of coordinates that will be ordered such
that the first entry in the list is the top-left,
    # the second entry is the top-right, the third is the
bottom-right, and the fourth is the bottom-left
    rect = np.zeros((4, 2), dtype = "float32")
    # the top-left point will have the smallest sum, whereas the
bottom-right point will have the largest sum
    s = pts.sum(axis = 1)
    rect[0] = pts[np.argmin(s)]
    rect[2] = pts[np.argmax(s)]
    # now, compute the difference between the points, the top-
right point will have the smallest difference,
    # whereas the bottom-left will have the largest difference
    diff = np.diff(pts, axis = 1)
    rect[1] = pts[np.argmin(diff)]
    rect[3] = pts[np.argmax(diff)]
    # return the ordered coordinates
    return rect

#cropouter performs multiple steps to automatically crop the
image to the box edges
def cropouter(image):
    #First it will blur the image, convert it to HSV colour
space after which the blue colour of the box is defined,
    #which will be used to mask everything but the blue box
    blur = cv2.blur(image, (50,50))
    hsv = cv2.cvtColor(blur, cv2.COLOR_BGR2HSV)
    lower_blue = np.array([100,100,40])
    upper_blue = np.array([130,255,255])

    mask = cv2.inRange(hsv, lower_blue,
upper_blue).astype('uint8')
    newmask = cv2.erode(mask, kernel = (1,1), iterations = 10)
    dfmask = pd.DataFrame(newmask != 0)
```

```
    #The mask is used to determine the coordinations of the box
and find the corners
    coord = np.where(dfmask)
    x = coord[0].reshape(1,coord[0].shape[0])
    y = coord[1].reshape(1,coord[1].shape[0])
    box = np.concatenate([y,x])
    box1 = np.swapaxes(box, 0,1).reshape(box.shape[1], 2)
    rect = order_points(box1)
    lu, ru, rb, lb = rect

    #Some of the images that were used to develop the pipeline
had a blue demarcation in the lower right corner (was later
removed)
    #with the pythagorean theorem you can always find the true
corner when there is an artifact such as this
    #This code finds the right lower corner this way
    w = np.diff([lu[0], ru[0]])
    diffy = np.diff([lu[1], ru[1]])
    h = np.diff([lu[1], lb[1]])
    diffx = np.diff([lu[0], lb[0]])
    if diffy < 0:
        if diffx < 0:
            diffx = -diffx
        else:
            diffx = diffx
        widthbox = np.sqrt(w **2 + diffy ** 2)
        heightbox = np.sqrt(h ** 2 + diffx **2)
    else:
        if diffx > 0:
            diffx = -diffx
        else:
            diffx = diffx
        widthbox = np.sqrt(w **2 + diffy ** 2)
        heightbox = np.sqrt(h ** 2 + diffx **2)

    #The corners are then used to alter the perspective such
that it is always a topview and crops the image
    #to the edges of the blue box
    lu = [lu[0], lu[1]]
    ru = [ru[0], ru[1]]
    lb = [lb[0], lb[1]]
    rb = [ru[0] + diffx, ru[1] + h]
    rect = np.array([lu, ru, rb, lb], dtype = "float32")
    dst = np.array([
            [0, 0],
```

```
            [int(widthbox) - 1, 0],
            [int(widthbox) - 1, int(heightbox) - 1],
            [0, int(heightbox) - 1]], dtype = "float32")
    M2 = cv2.getPerspectiveTransform(rect, dst)
    cropout = cv2.warpPerspective(image, M2, (int(widthbox),
int(heightbox)))
    return cropout

#3
#Import the image you want to annotate
filenames = [f for f in sorted(os.listdir(source_folder)) if
((str(f))[-4:] == fileformat.lower()) or ((str(f))[-4:] ==
fileformat.upper())]
images=[]
for file in filenames:
    filepath = source_folder + file
    image = cv2.imread(filepath)
    images.append(image)

#4
#This part will crop the images to the edges of the box
interface=True
upper_threshold = 256
lower_threshold = 125

layout = [[sg.Text('Select version'), sg.Text('')],
              [sg.Radio('Use UI Version', 1, default= True,
key='UI_Version')],
              [sg.Radio('Use Automated Version', 1,
key='Automated_Version'),
              sg.InputText(upper_threshold, size=(8, 1),
key='input_upper_threshold'), sg.Text('Upper Threshold'),
              sg.InputText(lower_threshold, size=(8, 1),
key='input_lower_threshold'), sg.Text('Lower Threshold')],
              [sg.B('OK',key='okay button')]]

window = sg.Window('Select Version', layout)

    # Event loop
while True:
    event, values = window.read()
    if event == sg.WIN_CLOSED or event == 'Exit':
        break
    if event == 'input_upper_threshold':
        window['input_upper_threshold'].update('')
    if event == 'input_lower_threshold':
```

```
        window['input_lower_threshold'].update('')
    if event == 'okay button':
        if values['UI_Version']:
            interface=True
        else:
            interface=False

        upper_threshold = int(values['input_upper_threshold'])
        lower_threshold = int(values['input_lower_threshold'])
        break


    #This deletes the used preview image and therefore exits the
GUI section
window.close()

i = 0
regioncounts = []
files = []
for im in images:
    cropout = cropouter(im)

    #5
    #This part standardizes the crop to a certain width and
height
    stnd = cv2.resize(cropout, (1100,1350), interpolation =
cv2.INTER_LINEAR)

    #6
    #This part corrects the image using the white balance
correction
    roi = (390, 250, 40, 40)
    corrected_img = pcv.white_balance(stnd, mode='hist', roi=
roi)

    #7
    #This part crops the edges of the box off
    y1 = 351
    x1 = 121
    fcrop = corrected_img[y1:y1+800, x1:x1+800, :]
    filenamecrop = destination_folder + 'crop_' + filenames[i]
    cv2.imwrite(filenamecrop, fcrop)

     #8
    if interface:
```

```
       #This is the part where you mask all the non-moss
material
        preview_image_size=500
        #This creates an initial preview image for the GUI
        im1 = Image.open(filenamecrop)
        im1.thumbnail((preview_image_size, preview_image_size),
Image.ANTIALIAS)
        im1.save('preview_threshold.png')

        #This resizes the fcrop and hsv for preview images
        preview_fcrop = cv2.resize(fcrop, (preview_image_size,
preview_image_size), interpolation = cv2.INTER_LINEAR)
        preview_hsv = cv2.cvtColor(preview_fcrop,
cv2.COLOR_BGR2HSV)
        (preview_h, preview_s, preview_v) = (preview_hsv[:,:,0],
preview_hsv[:,:,1], preview_hsv[:,:,2])

        #Layout of the interactive GUI
        layout = [[sg.Text('Select Threshold'), sg.Text('')],
                  [sg.T('upper threshold'),
                   sg.B('<', key='decrease_ut'),
                   sg.Slider(range=(0,256),
default_value=upper_threshold, key = 'upper threshold',
enable_events= True,
                             size=(20,15), orientation='horizontal',
font=('Helvetica', 12)),
                   sg.B('>', key='increase_ut')],
                  [sg.T('lower threshold'),
                   sg.Button('<', key='decrease_lt'),
                   sg.Slider(range=(0,256),
default_value=lower_threshold, key = 'lower threshold',
enable_events= True,
                             size=(20,15), orientation='horizontal',
font=('Helvetica', 12)),
                   sg.B('>', key='increase_lt')],
                  [sg.B('OK',key='okay button')],
                  [sg.Image('preview_threshold.png', key =
'image')]]

        window = sg.Window('Image Preview', layout)

        # Event loop
        while True:
            event, values = window.read()
            if event == sg.WIN_CLOSED or event == 'Exit':
                break
```

```
            if event == 'okay button':
                lower_threshold = int(values['lower threshold'])
                upper_threshold = int(values['upper threshold'])
                break
            if event == 'decrease_ut':
                window['upper threshold'].update(values['upper
threshold'] - 1)
            if event == 'increase_ut':
                window['upper threshold'].update(values['upper
threshold'] + 1)
            if event == 'decrease_lt':
                window['lower threshold'].update(values['lower
threshold'] - 1)
            if event == 'increase_lt':
                window['lower threshold'].update(values['lower
threshold'] + 1)

            #This creates and updates the preview image for the
GUI
            preview_mask = cv2.inRange(preview_s,
int(values['lower threshold']), int(values['upper threshold']))
            preview_noleaves = cv2.bitwise_and(preview_fcrop,
preview_fcrop, mask = preview_mask)
            cv2.imwrite('preview_threshold.png',
preview_noleaves)

            window['image'].update('preview_threshold.png')

        #This deletes the used preview image and therefore exits
the GUI section
        window.close()
        os.remove('preview_threshold.png')


    #This is the part where you continue with masking all the
non-moss material
    hsv = cv2.cvtColor(fcrop, cv2.COLOR_BGR2HSV)
    (h, s, v) = (hsv[:,:,0], hsv[:,:,1], hsv[:,:,2])
    mask = cv2.inRange(s, lower_threshold, upper_threshold)
    noleaves = cv2.bitwise_and(fcrop, fcrop, mask = mask)



    #13
    #This is the part that does the annotating
    #The original image is converted from BGR to RGB
```

```
    #The thresholded image is converted to the colour space for
annotating
    rgb = cv2.cvtColor(fcrop, cv2.COLOR_BGR2RGB)
    ycrcb = cv2.cvtColor(noleaves, cv2.COLOR_BGR2YCrCb)
    (y, cr, cb) =(ycrcb[:,:, 0], ycrcb[:,:, 1], ycrcb[:,:, 2])
    #Add correct channel to find capitula
    inv= np.subtract(255, cb)
    #This is the function that will perform the annotation
    blobs_dog = feature.blob_dog(inv, min_sigma = 8, max_sigma =
11, threshold = 0.002, overlap = 0.5, sigma_ratio=1.1)

    #Then the annotations are plotted on the original image and
saved
    fig, axes = plt.subplots(figsize=(10, 10))
    axes.imshow(rgb)
    for blob in blobs_dog:
        y, x, r = blob
        c = plt.Circle((x, y), r, color='yellow', linewidth=1,
fill=False)
        axes.add_patch(c)
    plt.axis('off')
    plt.tight_layout()
    newfile = destination_folder + 'anno_' + filenames[i]
    fig.savefig(newfile)
    plt.close('all')

    #Then the count and individual annotations are extracted
    region_count = len(blobs_dog)
    regioncounts.append(region_count)
    filesize = os.stat(filenamecrop).st_size
    regions = []
    for idx, (blob) in enumerate(blobs_dog):
        region_id = idx
        y, x, r = blob
        region_shape_attributes =
json.dumps({"name":"circle","cx":int(x),"cy":int(y),"r":"{:.2f}"
.format(round(r, 3))})
        regions.append((region_id, region_shape_attributes))
    regionid = []
    regionshape = []
    for region, shape in regions:
        regionid.append(region)
        regionshape.append(shape)
    fileattributes = ({})
    regionattributes = ({})
```

```
    #then the file with annotations is made and saved
    split = '.' + filenames[i].split('.')[-1]
    file = filenames[i].replace(split, '')
    files.append(file)
    anno = {'filename': file, 'file_size': filesize,
'file_attributes': fileattributes, 'region_count' :
region_count,
            'region_id' : regionid, 'region_shape_attributes' :
regionshape, 'region_attributes': regionattributes}
    annotations = pd.DataFrame(pd.DataFrame(dict([
(k,pd.Series(v)) for k,v in anno.items() ])))
    annotations = annotations.ffill()
    annotations['file_attributes'] = '{}'
    annotations['region_attributes'] = '{}'
    annotations['file_size'] =
annotations['file_size'].astype('int64')
    annotations['region_count'] =
annotations['region_count'].astype('int64')
    newfile = destination_folder + 'anno_' + file + '.csv'
    annotations.to_csv(newfile, index=False, header = True)
    i += 1

#Then a file is made with all the automated and corrected counts
and is saved with the correct filenames
newfilenames = pd.Series(files)
regioncounts = pd.Series(regioncounts)
correctedcount = round(np.multiply(regioncounts, 0.81))
count = pd.concat([newfilenames, regioncounts, correctedcount],
axis = 'columns')
count = count.rename(columns = {0:'Filename',
1:'Automated_count', 2: 'Corrected_count'})
count.to_csv(destination_folder + 'All_counts.csv', header =
True, index = False)
```

##